IMPROVEMENTS OF BCU-BASED DIRECT METHODS AND APPLICATIONS OF BCU TO LINE SWITCHING DESIGNS FOR ENHANCING ONLINE TRANSIENT STABILITY OF LOOK-AHEAD POWER SYSTEMS

A Dissertation

Presented to the Faculty of the Graduate School

of Cornell University

In Partial Fulfillment of the Requirements for the Degree of

Doctor of Philosophy

by

Robert Owusu-Mireku

December 2018

IMPROVEMENTS OF BCU-BASED DIRECT METHODS AND APPLICATIONS OF BCU TO LINE SWITCHING DESIGNS FOR ENHANCING ONLINE TRANSIENT STABILITY OF LOOK-AHEAD POWER SYSTEMS

Robert Owusu-Mireku, Ph.D.

Cornell University 2018

The structure, layout, and components of the electric power grid are changing rapidly leading to new components, models, and power system static and dynamic behaviors that existing power system analysis tools cannot accommodate. Since electricity is an integral part of our daily lives, it is important that power system analysis and control tools keep up with the changes in the power grid. An existing methodology/tool with the potential to help the power industry keep up with the changing needs for dynamic stability and control of the power system, due to its strong theoretical basis, is the boundary of the stability region based controlling unstable equilibrium point (BCU) method.

This thesis develops tools for the online transient stability analysis and control of modern power systems using the BCU method. Towards this goal we first propose a method for improving the robustness of unstable equilibrium point computations using a combination of quotient gradient transformation and the pseudo-transient continuation method. We also extend the application of the BCU method to the assessment of the transient stability of power systems with nonlinear excitation system models. The thesis also studies the dynamics of transmission line switching events under changing loading conditions and proposes and implements a novel BCU-based method for the direct transient stability assessment of transmission switching events. A method based on a three-stage strategy is also proposed for the fast determination of transmission line switching candidates that can be used to enhance the transient stability of multiple contingencies

for look-ahead loading conditions of a power system. Finally, a three-stage, fast scenario-based tool for the online transient stability assessments of power systems with load or generation uncertainties under look-ahead load conditions is proposed and implemented.

BIOGRAPHICAL SKETCH

Robert Owusu-Mireku was born in Accra, Ghana on June 15, 1983. He graduated from Kwame Nkrumah University of Science and Technology in 2005 with a Bachelor of Science degree in electrical and electronic engineering and then worked as a teaching assistant at the same institution for a year. In June 2006 he joined Maersk Ghana Ltd, a subsidiary of A. P. Moller Maersk Group Inc., as a management trainee until January 2009 when he expatriated to the United States of America to work for APM Terminals North America Inc. as an operations specialist. Robert Owusu-Mireku attended Cornell University, Ithaca, NY, in 2010 earning a Master of Engineering degree in electrical and computer engineering in 2011. He joined Bigwood Systems Inc. in July 2011 as a research engineer until August 2013 when he went back to Cornell University to pursue his doctoral studies. Robert's primary research interests include dynamic system theory, nonlinear systems, power system transient stability assessment and control, energy-based direct methods for transient stability assessment of power systems, artificial neural networks, integration of intermittent energy source into power systems, and generator parameter validation and calibration.

Dedicated to my family and friends in appreciation of their unconditional love.

ACKNOWLEDGMENTS

I would first like to express my profound gratitude to my advisor, Prof. Hsiao-Dong Chiang, for the energy and time he has devoted to me and my education over the years. His intellectual, moral, financial support, and guidance throughout my years as a graduate student were key to the successful completion of this research work. I would also like to thank my other committee members, Prof. David Delchamps and Prof. Eilyan Bitar, for their patience, insightful comments, and thought-provoking questions.

Special thanks to my friend and fellow graduate student, Mr. Matt Hin, for his technical help and friendship. Working with Matt all these years has taught me the importance of mathematical rigor in the analysis of physical systems.

My sincere thanks to Mr. Scott Coldren for all the administrative support and guidance he has given me as I navigated the complexities of graduate school. I would also like to thank my colleagues at Bigwood Systems, Inc. for their friendship, advice, and help throughout my years in graduate school: Dr. Hua Li, Dr. Bin Wang, Dr. Tao Wang, Mr. Mohamed Hassanudeen Bin Abdul Samad, Mr. Gilburt Chiang, Mr. Patrick Causgrove, Mr. Benjamin Wu, and Ms. Laurie Shelton.

I would like to express my deepest appreciation to all the friends who made Ithaca feel like home these past years, notably, Miss Betsy Boatemaa Ampofo, Mr. David Agyeman-Budu, and Mr. Kobby Mensa.

Finally, I would like to express my profound thanks to my family and loved ones: Mr. and Mrs. Owusu-Mireku, Mrs. Rose Frimpong, Miss. Rosemond Owusu-Mireku, Mrs. Evelyn Tuffour, Mr. Joseph Owusu-Mireku, Mrs. Regina Sofo, Mr. Mahama Seidu Alhassan, and Miss Ernestina Adwoa Afriyie for their love, support, care, and encouragement during these challenging years in graduate school.

TABLE OF CONTENTS

BIOGRAPHICAL SKETCH iii
DEDICATION iv
ACKNOWLEDGMENTS v
TABLE OF CONTENTS vi
LIST OF FIGURES xi
LIST OF TABLES xiii

1 Introduction and Outline 1

1.1 Motivation 1
1.2 Scope of the Thesis 5
1.3 Contributions 8
1.4 Mathematical Preliminaries 11
1.5 Organization 16

2 Robust Methods for Computation of Unstable Equilibrium Points: Theory 17

2.1 Introduction 17
2.2 Problem Formulation 22
2.3 Quotient Gradient System Transformation 24
2.4 The Pseudo-Transient Continuation Method 28
2.5 The QGS-based Pseudo-Transient Continuation Method 30
2.6 Convergence of QGS-based Pseudo-Transient Continuation Method 33
2.7 Conclusion 39

3 Robust Methods for Computation of Unstable Equilibrium Points: Numerical Computations 40

3.1 Introduction 40
3.2 Nonlinear Equations for Unstable Equilibrium Points 41
3.2.1 Dynamic Equations 42
3.2.2 Equilibrium Equations 46
3.3 Convergence Region 47
3.4 Numerical Studies 48
3.4.1 The WSCC 9-Bus 3-Machine System with a Classical Generator Model 49
3.4.2 The IEEE 145-Bus 50-Machine System with the Classical Generator Model 59

3.5 Integrated Solution Algorithm 62
3.6 Conclusion....65
4 Application of the BCU Method to Power Systems with Nonlinear Excitation System Models 67
4.1 Introduction 67
4.2 Problem Formulation....69
4.3 Excitation System Model 71
4.4 The BCU Method 72
4.5 Construction of a Numerical Energy Function 76
4.5.1 Lossy Structure-Preserving Model with a Detailed Nonlinear Excitation System..76
4.5.2 A Numerical Energy Function for the q^{th} Order Nonlinear Excitation Model 79
4.6 Derivation of the BCU Dimension Reduced-State Model....80
4.7 BCU Method for Detailed Model....81
4.7.1 Application of the Seven-step Process to Detailed Model....82
4.7.2 Discussion of Static and Dynamic Properties....90
4.7.3 Application of BCU Method to Detailed Model....91
4.8 Numerical Example....95
4.9 Conclusions 104
5 Dynamics and Transient Stability of Power Systems Post Transmission Switching....105
5.1 Introduction 105
5.2 Preliminaries....108
5.3 Dynamic Model of Transmission Switching Events....109
5.4 Transient Stability of Switching Events....111
5.4.1 Numerical Example I 113
5.4.2 Numerical Example II....118
5.5 Occurrence of Counter-Examples and Nonlinear Analysis 119
5.5.1 The Effect of Loading Conditions on the Stability Region 121
5.5.2 The Effect of the Closest UEP on the Size of the Stability Region....122
5.6 Conclusion....124
6 A Direct Method for Transient Stability Analysis of Transmission Switching Events 126
6.1 Introduction 126
6.2 Problem Formulation....129

6.3 Direct Methods 130
6.4 Direct Methods for Transmission Switching Events 132
6.4.1 Proposed Method 133
6.5 Numerical Simulations and Discussions 137
6.5.1 Numerical Example for the WSCC 9-Bus 3-Machine System 137
6.5.2 Numerical Example for the IEEE 145-Bus 50-Machine System 139
6.6 Scheme for Online Transient Stability Analysis of Transmission Switching Events 140
6.7 Conclusion 142
7 Towards Online Line Switching for Transient Stability Enhancement of Look-ahead Power Systems 143
7.1 Introduction 143
7.2 Problem Formulation 146
7.2.1 Objective Function with Constraints 152
7.3 Proposed Architecture 154
7.3.1 Total Weighted Changes 156
7.3.2 Stage 1 (Screening Stage) 158
7.3.3 Stage 2 (Ranking Stage) 162
7.3.4 Stage 3 (Detailed Analysis and Identification) 165
7.4 Online Line Switching Control Methodology 168
7.5 Numerical Studies 170
7.5.1 Numerical Example I 171
7.5.2 Numerical Example II 176
7.5.3 Computational Performance 180
7.6 Conclusion 182
8 A Method for Online Transient Stability Analysis of Look-Ahead Power Systems with Uncertainty 183
8.1 Introduction 183
8.2 Problem Formulation 188
8.3 Architecture and Numerical Scheme for Proposed Method 194
8.3.1 Stage 1 (Scenario Creation) 195
8.3.2 Stage 2 (Scenario Reduction) 200
8.3.3 Stage 3 (Contingency Screening, Ranking and Detailed Analysis) 204
8.4 Implementation of the Proposed Method 206

8.5 Numerical Studies 210
8.5.1 Numerical Example I 211
8.5.2 Numerical Example II 219
8.5.3 Computational Performance 223
8.6 Conclusion 224
9 Conclusion and Future Work 226
9.1 Conclusion 226
9.2 Future Work 229
Line Switching Candidates 231
Scenario Contingency Analysis Results 236
Bibliography 248

LIST OF FIGURES

Figure 1.1 Layout of this thesis. The chapters can be grouped into three main sections: analysis, improvements & extensions, and applications. 16

Figure 2.1 An attempt at constructing the stability region of a UEP for the network-reduction model of the WSCC 9-bus 3-machine system after a Newton-Raphson transformation. After the transformation, the UEP should be an SEP, and hence, should have a stability region in the new system. But it does not because the resulting system does not have unique solutions. The result is a disconnected region of convergence around the SEP. 24

Figure 2.2 The WSCC 9-bus 3-machine system. The value of Y is half the line charging. 25

Figure 2.3 An illustration of the Quotient Gradient System Transformation. 25

Figure 2.4 The stability region of a UEP, now an SEP for the network-reduction model of the WSCC 9-bus 3-machine system after QGS transformation. After the transformation, the UEP is an SEP and has a stability region in the new system. The stability region of the new system is connected. 27

Figure 3.1 The NR method convergence region of a UEP for the network-reduction model (contingency 2) of a post-fault WSCC 9-bus 3-machine system. 50

Figure 3.2 The QGS-based $\boldsymbol{\psi}$tc method convergence region of a UEP for the network-reduction model (contingency 2) of a post-fault WSCC 9-bus 3-machine system ... 51

Figure 3.3 The NR convergence region of a UEP for the network-reduction model (contingency 2) of a post-fault WSCC 9-bus 3-machine system superimposed on the QGS-based $\boldsymbol{\psi}$tc convergence region. 51

Figure 3.4 The continuous NR method convergence region of a UEP for the network-reduction model (contingency 2) of a post-fault WSCC 9-bus 3-machine system. 52

Figure 3.5 The continuous NR convergence region of a UEP for the network-reduction model (contingency 2) of a post-fault WSCC 9-bus 3-machine system superimposed on the QGS-based $\boldsymbol{\psi}$tc convergence region. 52

Figure 3.6 The NR method convergence region of a UEP for the structure-preserving model (contingency 1) of the post-fault WSCC 9-bus 3-machine system. 54

Figure 3.7 The QGS-based $\boldsymbol{\psi}$tc method convergence region of a UEP for the structure-preserving model (contingency 1) of a post-fault WSCC 9-bus 3-machine system. 54

Figure 3.8 The NR convergence region of a UEP for the structure-preserving model (contingency 1) of a post-fault WSCC 9-bus 3-machine system superimposed on the QGS-based $\boldsymbol{\psi}$tc convergence region. 55

Figure 3.9 The continuous NR method convergence region of a UEP for the structure-preserving model (contingency 1) of a post-fault WSCC 9-bus 3-machine system. 55

Figure 3.10 The continuous NR convergence region of a UEP for the structure-preserving model (contingency 1) of a post-fault WSCC 9-bus 3-machine system superimposed on the QGS-based $\boldsymbol{\psi}$tc convergence region. 56

Figure 3.11 An example of an initial point that is in the convergence region of the QGS-based ψtc for a UEP for the structure-preserving model (contingency 1) of a WSCC 9-bus 3-machine system, but not in the convergence region of the NR method. 56

Figure 3.12 Comparison of the CUEP computation time (secs) for the structure- preserving model of the WSCC 9-bus 3-machine system for Fsolve (F(x)=0), Newton's method (F(x)=0), the Continuous Newton method, the exact $\boldsymbol{\psi}$tc method (Q(x)), the QGS-based $\boldsymbol{\psi}$tc method, and the QGS-based $\boldsymbol{\psi tc}$ method combined with the NR method.....58
Figure 3.13 Comparison of the number of iterations for CUEP computation for the structure-preserving model of the WSCC 9-bus 3-machine system for Fsolve (F(x)=0), Newton's method (F(x)=0), the Continuous Newton method, the $\boldsymbol{\psi}$tc method (Q(x)), the QGS-based $\boldsymbol{\psi tc}$ method, and the QGS-based $\boldsymbol{\psi tc}$ method combined with the NR method. 58
Figure 3.14 Comparison of the CUEP computation time (secs) for the structure-preserving model of the IEEE 145-bus 50-machine system for Fsolve (F(x)=0), Newton's method (F(x)=0), the Continuous Newton method, the exact $\boldsymbol{\psi}$tc method (Q(x)), the QGS-based $\boldsymbol{\psi}$tc method, and the QGS-based $\boldsymbol{\psi tc}$ method combined with the NR method.....61
Figure 3.15 Comparison of the CUEP computation time (secs) for the structure-preserving model of the IEEE 145-bus 50-machine system for Fsolve (F(x)=0), Newton's method (F(x)=0), the Continuous Newton method, the QGS-based $\boldsymbol{\psi tc}$ method, and the QGS-based $\boldsymbol{\psi tc}$ method combined with the NR method. 61
Figure 3.16 Comparison of the number of iterations for the CUEP computation for the structure-preserving model of the IEEE 145-bus 50-machine system for Fsolve (F(x)=0), Newton's method (F(x)=0), the Continuous Newton method, the exact $\boldsymbol{\psi tc}$ method (Q(x)), the QGS-based $\boldsymbol{\psi tc}$ method, and the QGS-based $\boldsymbol{\psi tc}$ method combined with the NR method. 62
Figure 3.17 Flowchart for the implementation of the proposed integrated Algorithm. 64
Figure 4.1 Block diagram of IEEE Type I Exciter model [108].....72
Figure 4.2 A seven-step procedure to show static properties S(1) and S(2) and dynamic properties D(1) and D(2) between system (4.20) and system (4.21). 89
Figure 4.3 Swing curves of a stable trajectory for a WSCC 9-bus 3-machine system with a third order IEEE Type I exciter model. 93
Figure 4.4 Energy function value along a stable trajectory for a WSCC 9-bus 3-machine system with a third order IEEE Type I exciter model.....93
Figure 4.5 Swing curve for the verification of the boundary property of the CUEPs computed for contingencies 1 and 2. The verification applies to the two contingencies since the two contingencies share the same SEP and CUEP. $d1, d2,$ and $d3$ represents the machine angles of machine 1, 2 and 3, respectively. The test trajectory converges to the SEP, hence, the computed CUEP is on the stability boundary of the SEP. 100
Figure 4.6 Swing curve for the verification of the boundary property of the CUEPs computed for contingencies 3 and 4. The verification applies to the two contingencies since the two contingencies share the same SEP and CUEP. $d1, d2,$ and $d3$ represents the machine angles of machine 1, 2 and 3, respectively. The test trajectory converges to the SEP, hence, the computed CUEP is on the stability boundary of the SEP. 101
Figure 4.7 Swing curve for the verification of the boundary property of the CUEPs computed for contingency 5. $d1, d2,$ and $d3$ represents the machine angles of machine 1, 2

and 3, respectively. The test trajectory converges to the SEP, hence, the computed CUEP is on the stability boundary of the SEP.....101
Figure 4.8 Swing curve for the verification of the boundary property of the CUEPs computed for contingency 6. $d1, d2,$ and $d3$ represents the machine angles of machine 1, 2 and 3, respectively. The test trajectory converges to the SEP, hence, the computed CUEP is on the stability boundary of the SEP.....102
Figure 4.9 Swing curve for the verification of the boundary property of the CUEPs computed for contingency 7. $d1, d2,$ and $d3$ represents the machine angles of machine 1, 2 and 3, respectively. The test trajectory converges to the SEP, hence, the computed CUEP is on the stability boundary of the SEP.....102
Figure 4.10 Swing curve for the verification of the boundary property of the CUEPs computed for contingency 9. $d1, d2,$ and $d3$ represents the machine angles of machine 1, 2 and 3, respectively. The test trajectory converges to the SEP, hence, the computed CUEP is on the stability boundary of the SEP.....103
Figure 4.11 Swing curve for the verification of the boundary property of the CUEPs computed for contingencies 11 and 12. $d1, d2,$ and $d3$ represents the machine angles of machine 1, 2 and 3, respectively. The test trajectory converges to the SEP, hence, the computed CUEP is on the stability boundary of the SEP.....103
Figure 5.1 An illustration of the stability region A(Xs) and convergence region N(Xs) for a numerical method N of a stable equilibrium point Xs.....109
Figure 5.2 Depiction of a stable (a) and an unstable (b) transmission switching event. 111
Figure 5.3 Comparison of the bus voltage magnitudes of the pre-switching system, the bus voltage magnitude from the power flow solution of the post-switching system and the bus voltage magnitude from the post-switching SEP after switching open the line between buses 5 and 7.....115
Figure 5.4 The post-switching swing curve for the WSCC 9-bus 3-machine system (branch 5-7 opened).....117
Figure 5.5 A plot of the stability region of the post-switching SEP and post-switching initial point (pre-switching SEP) of the WSCC 9-bus 3-machine system after opening the line between buses 7 and 5. The MATLAB fsolve solver converges to the SEP along the blue line, even though the initial post-switching point is outside the stability region. 117
Figure 5.6 The post-switching swing curve for the IEEE 145-bus 50-machine system (branch 137-145 opened). 119
Figure 5.7 A plot showing the change in the stability region of the post-switching SEP under increasing real power loading conditions for switching event 6.....121
Figure 5.8 Plot of the SEP and the closest UEP path with increasing loading conditions for switching contingency 6. 124
Figure 6.1 Comparison of Fault-on trajectories, starting from the post-switching SEP and the post-switching initial point for switching event 1 of the WSCC 9-bus 3-machine system. The fault was applied to bus 5. 135
Figure 6.2 Numerical example of the proposed method applied to the WSCC 9-bus 3-machine system for a switching event, opening of line between buses 4 and 5, under two

loading conditions. (a) Stable case, the system is under uniform loading condition of 200 MW. (b) Unstable case, the system is under uniform loading condition of 270.5 MW. 136
Figure 7.1 Illustration of transient stability enhancement by transmission line switching of a look-ahead system. (a) Depicts the difference in the stability region of a base case system and a look-ahead system. (b) Depicts the change in the stability region of the look-ahead system post-switching. The goal is to enlarge the stability margin of the look-ahead system for a fault by switching open a selected transmission line before the fault occurs. Thus, select a switching action that will make $EMPS > EMLA$. 151
Figure 7.2 Architecture of the proposed online switching for transient stability enhancement of look-ahead power systems. 156
Figure 7.3 Comparison of the energy margins of the base case and the top-1 post-switching case (Line 24 -76) for the top 7 critical contingencies.....175
Figure 7.4 Comparison of the energy margins of the look-ahead base case and the top-1 post-switching case (line 24-76) for the top 7 critical contingencies. 180
Figure 8.1 Architecture of the proposed online transient stability assessment of look-ahead power systems with load and renewable uncertainty.....195
Figure 8.2 Application of AP cluster to scenarios created from the forecast error of two random parameters (renewable energy generation or load). (a) Shows the original data points. (b) Shows the clusters after applying the AP cluster algorithm to the data in (a). 202
Figure 8.3 Application of AP cluster to scenarios created from the forecast error of two random parameters (renewable energy generation or load). This graph shows the clusters after applying the AP cluster method to the data points in Figure 8.2 (a) and also highlights the exemplars and outliers which are used as cluster representatives with circles. 204
Figure 8.4 Flowchart for the implementation of the probabilistic online transient stability analysis of look-ahead power systems with uncertainty.....209
Figure 8.5 The WSCC 9-bus 3-machine system with wind generation units. The value of Y is half the line charging. 211

LIST OF TABLES

Table 3.1 Contingency List of the WSCC 9-bus 3-machine System....49
Table 3.2 Contingency List of the IEEE 145-bus 50-machine System....60
Table 4.1 Contingency List for the WSCC 9-bus 3-machine System....96
Table 4.2 Post-fault SEPs for the WSCC 9-Bus 3-Machine System with a Third Order Nonlinear Excitation System Model....97
Table 4.3 CUEPs for the WSCC 9-Bus 3-Machine System with a Third Order Nonlinear Excitation System Model....98
Table 4.4 CCT Comparison (Time-domain vs. BCU) for the WSCC 9-Bus 3-Machine System with a Third Order Nonlinear Excitation System Model....99
Table 5.1 List of Line Switching Events for the WSCC 9-bus 3-machine System....113
Table 5.2 Power Flow Results of the Pre-Switching System – The WSCC 3-machine 9-bus System....114
Table 5.3 Power Flow Results of the Post-Switching System – The WSCC 3-machine 9-bus System....114
Table 5.4 Post-Switching Equilibrium Point – The WSCC 3-machine 9-bus System....115
Table 5.5 List of Line Switching Examples for the IEEE 145-bus 50-machine System with Post-Switching SEPs that are Dynamically Unstable....118
Table 5.6 Occurrence of Counter-Examples After Switching Events Under Increasing Loading Conditions: The WSCC 9-bus 3-machine System....120
Table 6.1 List of Line Switching Events for the WSCC 9-bus 3-machine System....137
Table 6.2 Stability Results for the WSCC 9-bus 3-machine System....138
Table 6.3 Stability Results for the IEEE 145-bus 50-machine System....139
Table 7.1 List of Fault based Contingencies for the IEEE 145-bus 50-machine System....172
Table 7.2 Ranking of Contingencies for the IEEE 145-bus 50-machine System Base Case ...173
Table 7.3 Top 20 Line Switching Candidates and their weighted changes in energy margin for the IEEE 145-bus System based on Stage 2....174
Table 7.4 Top 10 Line Switching Candidates and their weighted changes in energy margin for the IEEE 145-bus System based on Stage 3....175
Table 7.5 Comparison of Critical Clearing Times of the Top 7 Critical Contingencies after Opening the Top-1 Line Switching Candidate (Line 24 -76) for the IEEE 145-bus 50-machine System Base Case....176
Table 7.6 Real Load and Generation Variation....177
Table 7.7 Ranking of Contingencies for the IEEE 145-bus 50-machine System for the Look-ahead Loading Condition....177
Table 7.8 Top 20 Line Switching Candidates and their weighted changes in energy margin for the IEEE 145-bus System based on Stage 2 under the Look-ahead Loading Condition....178

Table 7.9 Top 10 Line Switching Candidates and their weighted changes in energy margin for the IEEE 145-bus System based on Stage 3 under the Look-ahead Loading Condition.....179
Table 7.10 Comparison of Critical Clearing Time for the Top 7 Critical Contingencies After Opening the Top-1 Line Switching Candidate (Line 24 -76) for the IEEE 145-bus 50-machine System.....180
Table 7.11 Average CPU Time in Minutes for the Two Numerical Examples.....181
Table 8.1 List of Network Contingencies for the WSCC 9-bus 3-machine System.....210
Table 8.2 Look-ahead Variation Data – Numerical Example I.....213
Table 8.3 Ranking of Contingencies for the WSCC 9-Bus 3-Machine System for Look-ahead Operating Condition without Uncertainty for Fault Duration of 0.1 Seconds.....213
Table 8.4 List of Scenario Contingencies for Contingency 3 After First Two Stages – Numerical Example I.....215
Table 8.5 Ranking of Scenario Contingencies for Contingency 3 – Numerical Example I.....216
Table 8.6 List of Scenario Contingencies for Contingency 8 After First Two Stages - Numerical Example I.....217
Table 8.7 Ranking of Scenario Contingencies for Contingency 8 – Numerical Example I.....218
Table 8.8 Look-ahead Variation Data – Numerical Example II.....219
Table 8.9 Ranking of Contingencies for the WSCC 9-Bus 3-Machine System for Look-ahead Operating Condition without Uncertainty for Fault Duration of 0.35 Seconds.....220
Table 8.10 List of Scenario Contingencies for Contingency 8 – Numerical Example II.....221
Table 8.11 Ranking of Scenario Contingencies for Contingency 8 – Numerical Example II...222
Table 8.12 Average CPU Time in Seconds for the Two Numerical Examples.....223

CHAPTER 1

Introduction and Outline

1.1 Motivation

The goal of this thesis is to extend the capabilities of the BCU method for fast online transient stability analysis and control of modern power systems. By developing algorithms that: 1) make it effective to compute the unstable equilibrium points required in the implementation of the BCU method, 2) extend the BCU method to the transient stability assessment of more detailed power system dynamic models, 3) apply the BCU method in the transient stability assessment of switching events, 4) apply the BCU method in the online transient stability assessment of look-ahead power systems with uncertainties, and 5) also apply the BCU method in the development of a transmission line switching-based online transient stability enhancement control for look-ahead power systems.

This is important because the electric power sector forms an integral part of our modern way of life. In 2016, 39% of primary energy consumed in the United States of America [102] and 18% of primary energy consumed in the world was in the electric power sector [105]. From 1997 to 2016, the total global primary energy consumption increased by 40.8% [104] and it is projected to grow by 28% in 2040 compared to the energy consumption in 2015[103]. According to the EIA, renewables and nuclear energy, both consumed mainly as electricity, are expected to be the fastest growing source of energy during this period. Meanwhile, investment in the electricity infrastructure in deregulated markets like the United States of America is not growing at the same

pace as the growth in electricity demand, especially the transmission system. This has led to the power system operating conditions reaching their operating limits. In addition, the increase in the percentage of intermittent renewable energy sources in the global electricity generation portfolio has led to more uncertainty in the electric power grid. The combination of growth, constrained transmission infrastructure, uncertainty due to intermittent energy source, natural disasters, and potential terrorist attacks makes fast online electric power grid stability assessment and control a very important subject for power system security and reliability.

Power system stability assessment, which is the assessment of an electric power grid's ability to operate at an acceptable steady state before and after a disturbance, is an integral part of the daily operation and planning of electric power grids. A large disturbance could be a fault, a switching event, or large changes in generation or load. Power system stability is assessed in the form of rotor angle stability and voltage stability. Each of these classes of stability can be further classified in terms of time scales, and the size of disturbances being considered [4]. In this work, we focus on the assessment and enhancement of transient stability, which is rotor angle stability under large disturbances.

Two major transient security assessment (TSA) tools are currently used for transient stability analysis in the electric power industry: the conventional time domain simulation method, and the controlling unstable equilibrium point-based direct methods which belongs to group called the energy-based methods [1, 78]. The time domain simulation method is the most robust method available for dynamic stability assessment. However, it is numerically demanding and consequently, time consuming for its online transient stability analysis. At present, only a small set of contingencies are assessed in online TSA. There has been some work to improve the speed using parallel processing [71–73] and semi-analytic integration methods [74–76]. However, in

some applications, the results from the former are still not fast enough for online transient stability analysis and control. Also lacking is a concrete measure of the degree of stability without having to run repeated time domain simulations. We note that the semi-analytic integration methods are also not able to accommodate the effect of the hard limits on exciters and governors. The energy function-based methods, particularly the controlling unstable equilibrium point (CUEP) method, are faster because they make the transient stability assessments of post-event systems without integrating the post-event trajectory. Transient stability assessment with direct methods also give a measure of the degree of stability, which is important for control actions. The energy-based direct methods can be fully implemented using parallel processing and can also employ the semi-analytic integration methods for the integration of the fault-on trajectory required in some implementations [77]. Hence, energy-based direct methods can benefit from any computational advantages offered by these techniques. Over the years the theory for extending energy-based direct methods, like the CUEP method, to detailed power system models has been developed [1]. However, it has not been extended to cover all physical power system models, a subject that is covered in this thesis. It has been demonstrated on the industrial scale that CUEP-based direct methods, like BCU method, produce accurate stability assessment of physical power systems [1, 8]. Like any method the energy-based direct method has some challenges like robustness in the computation of critical points needed for energy-based direct methods, and the construction of an energy function for detailed power systems. Each of which are integral components in the reliable and efficient assessment and control of future power systems' transient stability when using the energy-based direct method. As highlighted in [1] time domain simulation and direct method complement each other and can be used together for effective online transient stability analysis of power systems. This has been demonstrated in current hybrid methods used in the industry for online transient

stability analysis. Other hybrid and machine learning-based methods have been proposed in various literature works [78].

This thesis focuses on the most powerful direct method, CUEP-based direct method, whose CUEP is computed by the boundary of stability region based controlling unstable equilibrium (BCU) method, and its application in the online transient stability assessment and control of modern power systems. To that end we perform the following tasks:

- Propose and implement a new method for the robust computation of unstable equilibrium points. Unstable equilibrium points (UEP) are important in the implementation of the CUEP-based direct method and the closest UEP method.
- Extend the BCU method to the transient stability assessment of power systems with nonlinear excitation system models.
- Propose and implement a novel energy-based direct method for the transient stability assessment of line switching events.
- Propose and implement a fast tool for the determination of transmission line switching candidates that can be used to enhance the transient stability of multiple critical contingencies for a look-ahead loading condition.
- Propose and implement a fast scenario-based tool for online transient stability assessment of a power system with uncertainty under look-ahead loading conditions.

The thesis also studies the dynamics of post-switching systems and its behavior under increasing loading conditions.

To this end, the thesis combines dynamic system theory, optimization, sensitivity analysis, statistics, and power system analysis and computation. The remainder of this chapter elaborates

on the scope of the thesis, summarizes contributions of this work, and presents some definitions and background theorems that are used in this thesis.

1.2 Scope of the Thesis

The thesis addresses the problem of developing power system tools for fast online transient stability assessment and control with BCU-based methods. Performing this task will require that the underlying BCU method is robust, fast, reliable, and applicable to detailed power system models. With these conditions satisfied reliable and fast BCU-based methods can then be developed for online transient stability assessment and control. Thus, we address the stated goal by: 1) proposing a technique for the robustness computation of unstable equilibrium points; 2) extending the BCU-based controlling UEP method to more detailed exciter models; and 3) implementing novel transient stability assessment and control tools based on the BCU method.

The general steps for the transient stability analysis of a power system event using an energy-based direct method, like the BCU method, can be listed as follows [1]:

1. Compute the initial point of the post-event system.
2. Construct an energy function for the post-event system.
3. Compute the energy function value at the post-event initial point.
4. Determine the critical point, and then compute the corresponding critical energy.
5. Compare the energy at the post-event initial state with the critical energy. If the post-event initial state energy is smaller, then the post-event trajectory will be stable; otherwise, it may be unstable.

The critical point computation is one of the most important steps in implementing the energy-based direct method. It is also the most challenging aspect of the direct method and it is NP-hard. Depending on the intended applications of direct method, the critical point can be a closest unstable equilibrium point or a controlling unstable equilibrium point [1]. These two all require the determination of an unstable equilibrium point(s). Currently, the methods for computing unstable equilibrium points are not very robust, especially when the initial guesses are far from the intended unstable equilibrium point. In this thesis, as the first effort towards creating tools for online transient stability analysis and control of power systems, the development of a theoretical-based robust method for computing unstable equilibrium points is investigated. The potential of developing a numerical method with an expanded convergence region of unstable equilibrium points through a combination of the quotient gradient transformation and the pseudo-transient continuation method is explored.

The second effort towards addressing the problem of creating tools for online transient stability analysis and control of modern power systems with BCU-based method involves the extension of the model capabilities of the BCU method. We explore the possibility of extending the BCU method to handle lossy detailed power system models (4^{th} order generator models) with detailed nonlinear excitation system. We start by constructing a numerical energy function for lossy power systems with detailed nonlinear excitation system models. The resulting energy function is then used to extend the BCU method to transient stability assessment of lossy power systems with detailed nonlinear excitation system models.

The third and final group of efforts, in this thesis, comprises the development of novel tools for fast transient stability assessment and control of modern power systems.

Power system contingencies can be fault triggered, changes in network topology, changes in power injection (load or generation changes) or a combination. The CUEP-based or other direct methods all focus on fault related contingencies. In this thesis, the electromechanical dynamics of a post-switching system is studied and the applicability of direct methods to the transient stability assessment of a non-fault triggered event such as line switching is considered. The potential of using the CUEP of a closely related fault event to define the stability boundary of a switching event is evaluated in a novel direct method for transient stability assessment of post-switching systems.

Power system enhancement control will be an integral part of daily power system operations. These control actions need to be fast and accurate for online applications. This thesis explores combining CUEP-based direct methods, and sensitivity analysis to quickly determine transmission line switching candidates that can be used to enhance the transient stability of multiple contingencies for look-ahead loading conditions of a power system.

The proliferation of intermittent renewable energy has introduced more uncertainty in the power grid. The question then is, are there fast and accurate ways to assess the transient stability of power systems with uncertainty using the CUEP-based direct methods? In this thesis, we explore the implementation of a fast, scenario-based, solution to this problem using scenario generation, scenario reduction, and scenario contingency analysis (screening, ranking and detailed analysis).

1.3 Contributions

- **Chapter 2 & Chapter 3** focus on the robust computation of unstable equilibrium points:
    - We use the quotient gradient transformation to transform the unstable equilibrium point into a stable equilibrium point and effectively enlarge the convergence region of the point/state corresponding to the unstable equilibrium point. We then solve for the unstable equilibrium point by using the pseudo-transient continuation method to solve for the stable equilibrium point resulting from the quotient gradient transformation. It improves the speed of the UEP computation and expands the convergence region of the UEP compared to the convergence region of the same UEP for the Newton-Raphson method and other continuous Newton methods.
    - We improve the speed of the new method, which combines quotient gradient transformation and the pseudo-transient continuation method, by approximating the Jacobian in the pseudo-transient continuation steps. The Jacobian approximation is chosen such that it exploits the structure of the quotient gradient transformation. The approximation of Jacobian eliminates the construction of a second Jacobian for each step and ensure that the proposed method only converges to solutions that are equilibrium points of the original dynamic system.
    - We study the convergence properties of the method resulting from the proposed combination of the quotient gradient transformation and the inexact pseudo-transient continuation method. We show that the proposed method will only converge to solutions of the original system.
- **Chapter 4** explores the extension of the BCU method to power system models with detailed nonlinear excitation systems:

- We construct a numerical energy function for a lossy detailed power system model with a nonlinear excitation system using the first integral scheme.
- We use the constructed numerical energy function, and the theoretical work in [1] to extend the BCU method to detailed power system models with nonlinear excitation systems.

- **Chapter 5 & Chapter 6** investigates the dynamics and stability of post-switching power systems, and develops a novel controlling unstable equilibrium point-based direct method for the transient stability analysis of switching events:
  - We study the dynamics of the post-switching power system and numerically and theoretically show that the static stability of a post-switching power system does not imply dynamic stability. Thus, the existence of a post-switching equilibrium point does not imply the post-switching system is stable. We also show that the frequency of occurrence of the mismatch between static and dynamic stability assessments increases with increasing loading conditions, and this increase in frequency of static and dynamic stability mismatches can be attributed to the decrease in the size of the stability region of the post-switching equilibrium point as the loading condition increases.
  - Based on work done in [114] we show that the decrease in the size of the stability region of the post-switching power system with increase in loading condition can be attributed to the changes in the locations of the stable post-switching equilibrium point and the unstable equilibrium points on the stability boundary of the post-switching power system. We also show that beyond a threshold, loading condition, close to the saddle node bifurcation point of a post-switching power system the changes in the size of the stability region of the post-switching power system due to changes in loading condition

can be attributed to the movement of the closest UEP towards or away from the post-switching stable equilibrium point.

- In Chapter 6, we propose and implement a novel BCU-based direct method for assessing the transient stability of switching events. The proposed method uses the controlling unstable equilibrium point of a fault event, closely related to the switching event being assessed, to define the stability region of the post-switching system. A scheme, based on the proposed direct method, comprising screening, ranking and detailed analysis for the transient stability assessment of switching events is proposed.

- **Chapter 7** proposes and implements a tool for the fast and online determination of transmission line switching candidates that can be used to enhance the transient stability of multiple contingencies for look-ahead operating conditions of a power system:
  - We formulate the look-ahead line switching for transient stability enhancement of multiple critical contingencies optimization problem.
  - We propose and implement a novel weighting scheme to help compare the impact of various line switching actions on the transient stability of multiple contingencies.
  - We implement a three-stage strategy for the fast and online determination of line switching candidates that can be used to enhance the transient stability of multiple critical contingencies for a look-ahead operating condition of a power system. The three-stage strategy comprises a screening stage using energy margin sensitivity, a ranking stage using a minimum gradient point approximation technique, and an identification stage using the BCU method.
- **Chapter 8** proposes and implements a scenario contingency-based method for online look-ahead transient stability assessment of power systems with uncertainty:

- We formulate the electromechanical dynamics of a look-ahead power system before, during, and after a fault-disturbance.
- We implement a three-stage strategy for the online transient stability assessment of a look-ahead power system with uncertainty and automatic governor control using a three-stage scenario-based approach. The three-stage strategy comprises a scenario creation stage using the Latin hypercube sampling method, a scenario reduction stage using the affinity propagation clustering algorithm, and a scenario contingency analysis stage using a combination of an energy-based direct method like the BCU method and time domain simulations.

- **Chapter 9** summarizes the work presented in the thesis and outlines some directions for future work.

1.4 Mathematical Preliminaries

Considering a nonlinear dynamical system represented by a system of (autonomous) ordinary differential equations (ODEs) of the form:

$$\dot{x} = f(x)$$

$$x \in R^n,\ f(x): R^n \to R^n. \tag{1.1}$$

- If f is C^1 in a set $\Omega \in R^n$, then for all initial points $x_0 \in \Omega$ at time $t = 0$, a unique solution starting from the initial point exists within Ω. The solution curve $\varphi(x,.): R^n \to R^n$ of (1.1) with initial condition $\varphi(x_0, t_0) = x_0$ is called a system trajectory.
- A state vector $\bar{x}$ is called a hyperbolic equilibrium point of (1.1) if $f(\bar{x}) = 0$ and the Jacobian matrix of $f(.)$ at $\bar{x}$ has no purely imaginary eigenvalues.

- An equilibrium point $\bar{x}$ is Lyapunov stable if nearby trajectories stay nearby.
- An equilibrium point $\bar{x}$ is asymptotically stable if nearby trajectories stay nearby and converge to $\bar{x}$.
- A point p is the ω- limit set of x if there is a sequence $\{t_i\}$ in R, $t_i \to \infty$, with the property that $p = \lim_{i\to\infty} \varphi(x, t_i)$[1]. Thus, p is a limit of the trajectory of x in forward time.
- A hyperbolic equilibrium point is asymptotically stable if all the eigenvalues of its corresponding Jacobian have negative real parts; otherwise, it is unstable.
- The stability region or region of attraction $A(x_s)$ of an asymptotically stable equilibrium point (SEP) x_s is defined as [1]:

$$A(x_s) := \left\{x \in R^n : \lim_{t\to\infty} \varphi(t, x) = x_s\right\}. \tag{1.2}$$

- Characterization of the Stability Boundary of ODEs [1]:

Assumptions:

1. All equilibrium points on the stability boundary of (1.1) are hyperbolic.
2. The stable and unstable manifolds of equilibrium points on the stability boundary of the (1.1) satisfy the transversality condition.
3. The ω-limit set of every trajectory on the stability boundary of the dynamic system is an equilibrium point on the stability boundary.

Theorem 1.1[118]: For a nonlinear system of the form (1.1) which satisfies the assumptions above, let x_i $i = 1,2 \cdots$ *be the equilibrium points on the stability boundary* $\partial A(x_s)$ *of the SEP* x_s*. If the stable and unstable manifolds of* x_i *are defined as* $W^s(x_i)$ *and* $W^u(x_i)$*, respectively. Then,*

1. $x_i \in \partial A(x_s)$ *if and only if* $W^u(x_i) \cap A \neq \emptyset$
2. $\partial A(x_s) = \cup_i W^s(x_i)$

- Characterization of the Stability Boundary of Differential Algebraic Equations [1, 107]:

Considering a nonlinear dynamical system represented by a system of differential algebraic equations:

$$\dot{x} = f(x, y, u)$$

$$0 = g(x, y, u)$$

$$x \in R^n, y \in R^m \tag{1.3}$$

where $f: R^n \times R^m, g: R^n \times R^m \to R^m$ are smooth functions. The system trajectories $\varphi(x, y)$, of (1.4) are constrained to the manifold:

$$\Gamma = \{(x, y) \in R^{n+m} | g(x, y) = 0\}. \tag{1.4}$$

The constraint manifold Γ may contain singular surfaces at points where the corresponding Jacobians are singular. If singular surfaces exist, they decompose Γ into several disjoint stable (Γ_s) and unstable (Γ_u) components.

Definition: Let Γ_s *be a component of* Γ *and* $(x_s, y_s) \in \Gamma_s$ *be an asymptotically stable equilibrium point of the system of differential algebraic equation in (1.3). The stability region of* (x_s, y_s) *is*

defined as

$$A(x_s, y_s) = \left\{(x, y) \in \Gamma_s : \lim_{t \to \infty} \varphi(x, y) = (x_s, y_s)\right\}. \tag{1.5}$$

The stability boundary of (1.3) is characterized in [1,107] as comprising of two parts: the union of the stable manifold of the unstable equilibrium points on the stability boundary, and a collection of trajectories reaching the singular surfaces in Γ. The complicated nature of the DAE stability region $A(x_s, y_s)$ and boundary makes a numerical construction of $A(x_s, y_s)$ very challenging, to overcome this challenge equation (1.3) is sometimes approximated by a two-time scale differential equation model using the singular perturbation approach [1, 107].

- Singular Perturbation Approach [1,107]:

In the singular perturbation approach, equation (1.3) is replaced with a two-time scale system with a slow variable x and a fast variable y of the form:

$$\dot{x} = f(x, y)$$

$$\varepsilon \dot{y} = g(x, y) \tag{1.6}$$

where ε is a sufficiently small positive scalar. The basic idea behind the SPA is to treat $0 = g(x, y)$ as a limit to $\varepsilon \dot{y} = g(x, y)$ as $\varepsilon \to 0$ [1].

Thereon 1.2 [1]: Let (x_s, y_s) and (x_u, y_u) be the SEP and unstable equilibrium point (UEP) of the DAE system (1.3) on the stable component Γ_s, respectively. Suppose that, for each $\varepsilon > 0$, the associated singularly perturbed system (1.6) has an energy function and its equilibrium points are isolated. Then there exists an $\varepsilon > 0$ such that for all $\varepsilon \in (0, \varepsilon), (x_u, y_u)$lies on the stability boundary of $\partial A(x_s, y_s)$ of the DAE (1.3) if and only (x_u, y_u) lies on the stability boundary of $\partial_\varepsilon A(x_s, y_s)$ of the singularly perturbed system (1.6).

Thus, we can use the stability boundary and stability region of the singular perturbed system as an approximation of the stability boundary and region of the DAE system [1, 107].

- Energy Function [117]:

The function $V: R^n \rightarrow R$ is an energy function for the system (1.1), (1.3) or (1.6), if the following conditions are satisfied:

1. Along any nontrivial trajectory $\varphi(t, x_0)$, $\dot{V}\big(\varphi(t, x_0)\big) \leq 0$ and the set $\big\{t \in R: \dot{V}\big(\varphi(t, x_0)\big) = 0\big\}$ has a measure of zero in R.
2. If $\big\{V\big(\varphi(t, x_0)\big): t \geq 0\big\}$ is bounded, then $\{\varphi(t, x_0): t \geq 0\}$ is bounded.

- Direct Methods:

If an energy function $V(.)$ exist in the neighborhood of a SEP x_s of (1.1), (1.3) or (1.6) then the stability region of the SEP can be approximated via the inequality $V(x) < V_{cr}$, where $V_{cr}$is the energy function value at a critical point, the point at which the corresponding energy function value/constant energy surface approximates the stability boundary. Depending on the intended application of the UEP-based direct method either the closest UEP (closest UEP method) or the controlling UEP (controlling UEP method) is computed [1,108].

- Energy Margin:

The energy margin is defined as $E_M = V_{cr} - V(x)$. Where V_{cr} is critical energy and $V(x)$ is the energy at the initial post-event state of a dynamic system. For power system transient stability analysis of a fault event E_M is the difference between the energy at the CUEP and the energy at the post-fault initial state. A positive energy margin implies transient stability, and a negative energy margin can imply transient instability.

These definitions and properties are used in the coming chapters and forms the bedrock of the BCU method which is the foundation upon which this thesis is built.

1.5 Organization

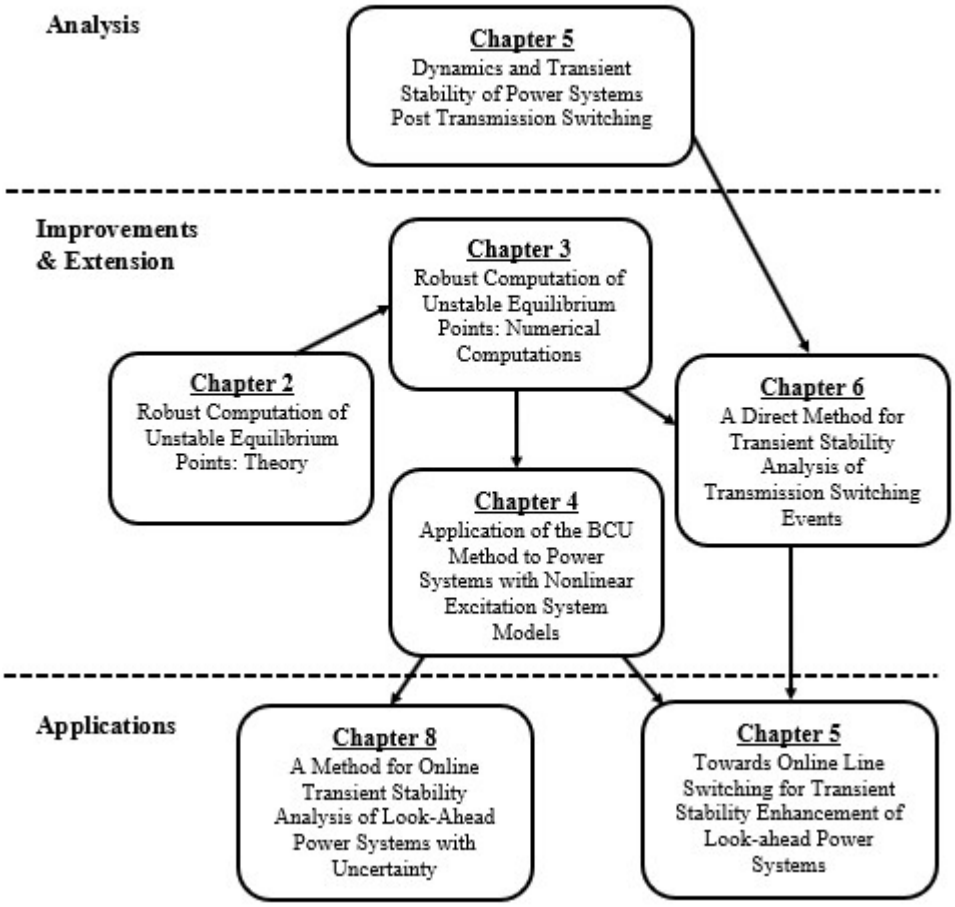

Figure 1.1 Layout of this thesis. The chapters can be grouped into three main sections: analysis, improvements & extensions, and applications.

CHAPTER 2

Robust Methods for Computation of Unstable Equilibrium Points: Theory

2.1 Introduction

One way to achieve the goal of online stability analysis of power systems is to use direct or energy-based methods for transient [1, 2] and voltage security assessments [3-6]. The authors in [1, 2] have shown how to use energy-based techniques like the closest unstable equilibrium point (UEP) and controlling UEP methods to assess and enhance the transient stability of power systems. In [5-7], the authors presented the potential application of energy methods to voltage stability assessment and enhancement. In [7, 8], the authors also demonstrated how a direct method for voltage stability and transient stability assessment can be used online. Fast and accurate methods for computation of UEPs are important in all the direct method applications proposed in [1, 2, 5-8]. In the closest and controlling UEP methods for transient stability assessment, the computation of type-1 UEPs is required to determine the relevant critical energy level needed for stability assessment [1, 2, 8]. The computation of a UEP is also required in assessing the proximity of an operating point to a system's voltage collapse limit [5-7]. UEPs are also computed in power flow analysis [4] when all the possible solutions of a power system are required [9–13]. However, the computation of UEPs with algebraic solvers like Newton-Raphson's method are inherently difficult due to the generally small size of their convergence regions [1, 30], and the difficulty in finding an initial point that is in the solver's convergence region. The difficulty associated with

the computation of UEPs and the key role that UEPs will play in the future operation and planning of power systems make fast and robust computations of UEPs an important research area.

In many research work publications, various methods have been proposed for computing UEPs. These methods can be grouped into those based on algebraic solvers [1, 14-17], methods based on continuation and homotopy [9–13, 18, 20, 22, 23], those based on dynamic transformation [19, 21, 24, 25], and optimization methods [28]. Most of the methods based on algebraic solvers focus on finding efficient and robust ways of determining the correct initial point for the UEP solution [1, 14-17]. They then solve for the exact UEP using algebraic solvers like the Newton-Raphson method. The corrected corner and the ray point approximation methods [16, 17] are two of the early methods that focused on finding the correct initial point of the controlling UEPs. Despite some theoretical explanation in [27] on why the methods in [16, 17] sometimes work, they lacked a strong theoretical foundation and failed most of the time in practical applications. The MOD method, which is based on how the power system separates after a disturbance, uses the corrected corner or the ray point approximation method to generate the initial guess of a controlling UEP [15]. The MOD, like the corrected corner method, does not have a strong theoretical foundation, leading to inexplicable failures when applied to real systems. The BCU method [1] is another example of a method that focused on finding initial points for algebraic solvers. The BCU method works by tracing a path along a stability boundary toward a controlling UEP. Even though the BCU method has a strong theoretical foundation, its success still depends on the convergence characteristics of the algebraic solver used to compute the exact controlling UEP and the successful numerical tracing of the stability boundary [1]. The continuation and homotopy-based methods have been studied and employed extensively in the computation of controlling UEPs [18, 20], closest UEPs [20, 22, 23], and in the computation of all the equilibrium

points in the power system [9-13]. In all of these applications, they have been found to either fail in some instances [9, 12, 18, 20, 26] due to theoretical and numerical challenges or found to be intractable for large-scale systems [10–13, 18, 20, 22, 23]. In [19, 21, 25], the authors addressed the challenge that accompanies computing UEPs by proposing methods that transformed the problem into the computation of SEPs, an approach generally called dynamic methods. The transformation method proposed in [19] focused on the challenge of finding multiple UEPs on the stability boundary of a power system SEP by combining a system transformation, like the one proposed in this chapter, with related minus systems to determine initial guesses sufficiently close to the UEPs on the stability boundary of an SEP of a power system. The methods proposed in [21, 25] used a spectral decomposition of the original system Jacobian to construct a new gradient system with similar equilibrium points to that of the original system and turn UEPs into SEPs. In [21], the authors used the transformation method to compute the closest UEP, while the authors in [25] used the method for controlling UEP (CUEP) computations. The closest UEP application in [21] can find only two type-1 UEPs, even when there are more type-1 UEPs. Hence, it fails in most practical applications. The author in [26] has shown that generally, transformation techniques like the one in [21] do not work properly when used to compute the closest UEPs on a stability boundary. The proposed methods in [21, 25] are only applicable to power system network-reduction models. The author in [28] proposes an optimization-based technique for computation of the controlling UEP. Even though this method has a theoretical basis, it is intractable in large systems.

In this chapter, a new trajectory-based algebraic solver for the computation of UEPs is proposed and implemented. The proposed solver generally has better convergence regions as compared to the Newton-Raphson (NR) method when applied to computing UEPs. The proposed method is to

be used in tandem with existing methods, like the BCU method or any of the other methods that require an algebraic solver for UEP computations. The method comprises two main parts: (1) transformation of the relevant UEP of a given system into a stable equilibrium point (SEP) of a related dynamical system, called the quotient gradient system (QGS) [29]; and (2) computation of the resulting SEP of the QGS using a trajectory-unified method (TJU), exploiting the exact or the in-exact/quasi Pseudo-transient continuation (ψtc) method [34].

The QGS transformation converts the UEP into an SEP, which has a stability region, and hence, can be solved with a TJU method. Also, pairing the transformation with the $\boldsymbol{\psi tc}$ expands the resulting convergence region of the UEP, since the $\boldsymbol{\psi tc}$ has a more continuous (connected and smooth) convergence region, unlike NR, where the convergence region is a fractal [30]. The major difference between our proposed method and the method in [21, 25] is that our method uses a fast transformation technique and combines it with a fast, quasi-Newton method to solve for the UEP after the transformation. The proposed method does not require eigenvalue computations like in [21, 25] and it is applicable to UEP computations in general. The transformation method used in [19] is similar to the transformation method used in our work, but the authors in [19] focus on determining initial points close to UEPs, and also exploiting the periodic structure and Lyapunov function of the resulting system to validate the calculated UEPs. In this work, we focus on exploiting the structure of the QGS, resulting from the transformation, to speed up the computation of the UEP and to ensure convergence to the desired solution of the original system given an initial guess.

The use of this specific QGS structure dependent in-exact/quasi method to speed up computation and avoid convergence to points that are not solutions to the original system is also

new in this kind of power system application. In effect, this proposed method will improve the robustness of UEP computations for large power systems, such as real power grids, by converting the UEP into an SEP and enlarging its convergence region. The method is also independent of the network model and can be applied to problems that are unrelated to power systems. Under certain conditions, the proposed method can have local q-superlinear or local quadratic convergence.

The main contributions of this work are: 1) the combination of QGS transformation and the pseudo-transient continuation method to create a UEP computation method with a generally larger convergence region compared to the Newton-Raphson method, 2) the use of a quasi-Newton pseudo-transient continuation method that exploits the structure of the QGS system to improve the speed of the UEP computation and also ensures the convergence of the method to only solutions of the original system, and 3) analysis of the convergence of the proposed method and proof that the proposed method will only converge to solutions of the original system.

This chapter is organized as follows. Section 2.2 presents the original algebraic problem where the zero, for a given initial point, corresponds to the UEP being computed for a dynamic system. Section 2.3 presents the transformation of the original system into the QGS system. Section 2.4 reviews the pseudo-transient continuation ($\boldsymbol{\psi tc}$) method for ODE systems. Section 2.5 proposes the QGS-based pseudo-transient continuation ($\boldsymbol{\psi tc}$) method, and section 2.6 conducts analysis of the convergence of the proposed method.

2.2 Problem Formulation

Without loss of generality, we consider the following system of algebraic equations:

$$F(x) = 0 \tag{2.1}$$

where $F: R^n \rightarrow R^n$, F is assumed to be C^2, $x \in R^n$ is a vector of equilibrium states, and $n \geq 1$.

In most power system applications where the computation of UEPs is required, (2.1) is either the vector field of a system of differential equations or a system of the vector field and the algebraic manifold of a system of differential algebraic equations. Regardless of what (2.1) represents, UEPs are inherently very difficult to compute because appropriate initial guesses are difficult to determine, and UEPs generally have a small convergence region with respect to a numerical method, say, the Newton-Raphson [1, 30]. Numerical simulations performed by the authors in [30] demonstrated that the convergence region of the Newton-Raphson load flow is fractal. The results also showed that the Newton-Raphson convergence region for UEPs are generally smaller than that of stable equilibrium points. However, like any equilibrium point or zero of a function, UEPs can be computed using algebraic solvers when an initial point sufficiently close to the UEP is provided. The size and continuity/compactness of the convergence region of an algebraic solver determines how close an initial guess must be for the solver to successfully converge to the UEP. The purpose of this work is to provide a fast algebraic solver that has a large connected convergence region, implying that the initial guesses can be further away from a UEP. One common solver used for UEP computations is the NR method.

$$\dot{x} = f(x) = -DF(x)^{-1}F(x) \tag{2.2}$$

Each step in the NR algorithm can also be viewed as a forward Euler step of the dynamic system (2.2) with a time step of 1, where $DF(x)$ is the Jacobian matrix of $F(x)$ and $-DF(x)^{-1}F(x)$ is the vector field $f(x)$ of the ordinary differential equation (ODE) (2.2) [31].

Thus, the NR method and some of its variants—for example, Iwamoto's method—are basically the forward Euler integration of the new dynamic system (2.2) [31]. This new system (2.2) is stable at all equilibrium points where $DF(x)$ is nonsingular. Consequently, in terms of the computation of UEPs, the NR method and some of its variants can be considered as a numerical technique that involves the transformation of a UEP of the original system (2.1) into an SEP of (2.2), and an application of an explicit integration method like the Euler method, to solve for the new system's SEP, which is the UEP of the system of differential equations corresponding to (2.1) for a given initial point. The transformation, (2.2), will be called the Newton-Raphson transformation.

Some variants of the NR method, like the Continuous Newton-Raphson method (Continuous NR) presented in [31], propose the use of a much more stable explicit integration technique, such as the fourth order Runge-Kutta (RK4) method over the forward Euler method, for the integration of the dynamic system in (2.2).

Unlike the transformation used in this work, the transformation used in the NR method employs the inverse of a Jacobian $DF(x)$ which can be singular somewhere in the neighborhood of the resulting SEP. Implying that (2.2) does not always satisfy the requirements for existence and uniqueness of solution. Figure 2.1 demonstrate an attempt to plot the stability region of the WSCC 9-bus 3-machine system after a Newton-Raphson transformation. The magenta points correspond to initial points that converge to the UEP when (2.2) is integrated with an ODE solver. The region was computed using a classical fourth order Runge-Kutta method. The diagram with data for the WSCC 9-bus 3-machine system used in this simulation is as shown in Figure 2.2. The complete power flow and dynamic data can be found in [1,108].

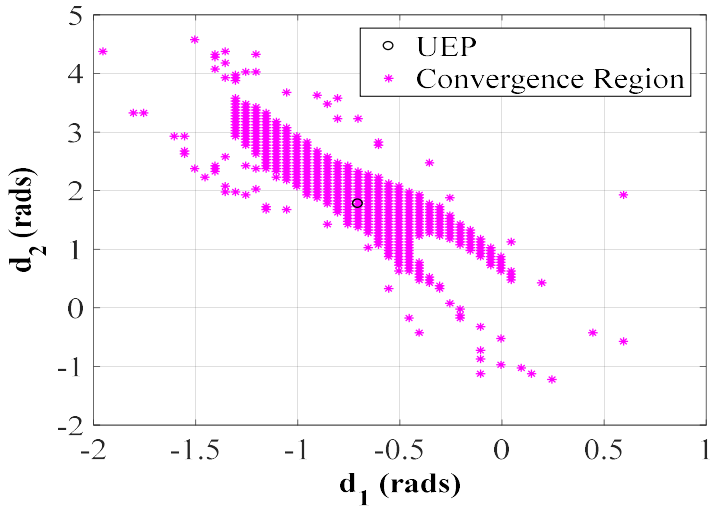

Figure 2.1 An attempt at constructing the stability region of a UEP for the network-reduction model of the WSCC 9-bus 3-machine system after a Newton-Raphson transformation. After the transformation, the UEP should be an SEP, and hence, should have a stability region in the new system. But it does not because the resulting system does not have unique solutions. The result is a disconnected region of convergence around the SEP.

2.3 Quotient Gradient System Transformation

The proposed method first transforms the UEP into an SEP of a new system and then solves for the UEP by solving for the SEP using a trajectory-unified method (TJU) [32]. The transformation step in the method is illustrated in Figure 2.3. The transformation used in this work is called the Quotient Gradient System (QGS) [29] transformation, and has the following form:

$$\dot{x} = Q(x) = \ -DF(x)^T F(x). \tag{2.3}$$

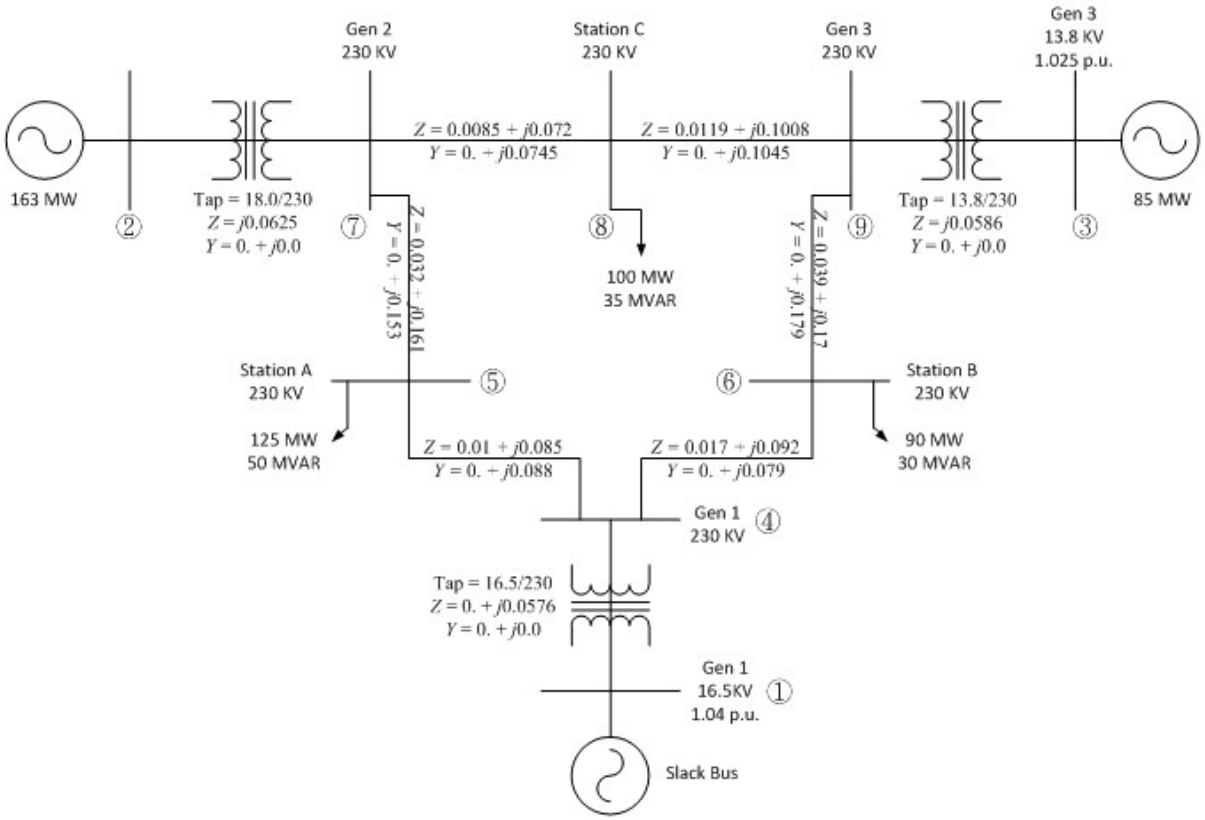

Figure 2.2 The WSCC 9-bus 3-machine system. The value of Y is half the line charging.

Figure 2.3 An illustration of the Quotient Gradient System Transformation.

Proposition 2.1: Let all the equilibrium points of (2.3) be hyperbolic and finite in number. If $\hat{x}$ is the solution of (2.1), then $\hat{x}$ is an SEP of (2.3).

Proof:

It is obvious that if $\hat{x}$ is a solution of (2.1), then it is an equilibrium point of (2.3). For $\hat{x}$ to be an SEP of (2.3), the Jacobian ($DQ(x)$) of (2.3) at the equilibrium point $\hat{x}$ should be negative definite.

Thus, for any nonzero vector, $y \in R^n$, $y^T DQ(\hat{x})y < 0$. The Jacobian of (2.3) at a point x is given by (2.4):

$$DQ(x) = -\sum_{k=1}^{n} f_k H^T(f_k) - DF(x)^T DF(x) \tag{2.4}$$

where f_k is the k[th] function in $F(\hat{x})$ and $H^T(f_k)$ is the Hessian of f_k. At $\hat{x}$, $f_k = 0$ and hence,

$$DQ(\hat{x}) = -DF(\hat{x})^T DF(\hat{x}). \tag{2.5}$$

The Jacobian matrix (2.5) is negative semi-definite. Since all the equilibrium points of (2.3) are assumed to be hyperbolic, it implies that none of the equilibrium points have eigenvalues with a zero real part, and hence, none of the equilibrium points have zero eigenvalues. That is, all the eigenvalues of the equilibrium points of (2.3) have negative real parts, which implies that (2.5) is negative definite.

The advantage of the proposed method over the NR method is that the stability region of the SEP resulting from the transformation exist and is path-connected if the underlying assumptions are satisfied, while there is no stability region for the SEP from the NR transformation (since the resulting system does not have unique solutions). The UEP and consequently, its corresponding stability region in the new system (2.3) can also be efficiently computed by solving for the SEP

using implicit integration techniques, which are more stable compared to explicit ones like the Euler method.

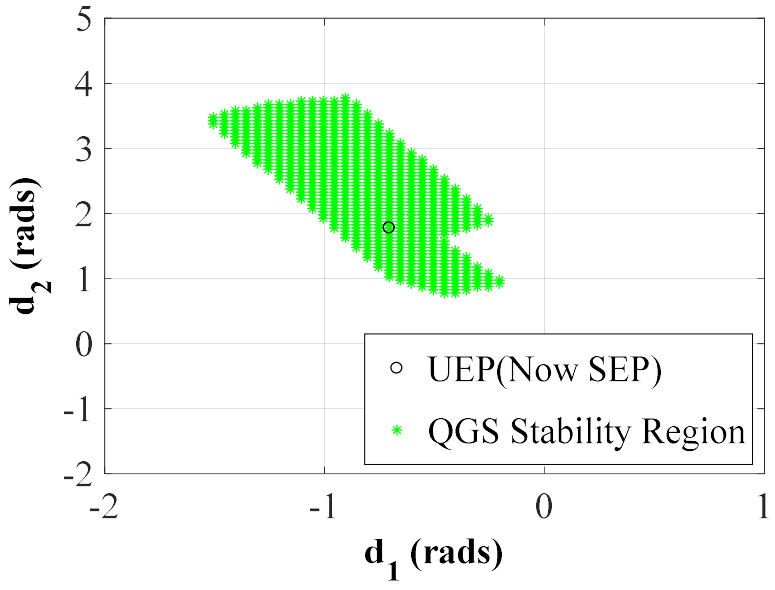

Figure 2.4 The stability region of a UEP, now an SEP for the network-reduction model of the WSCC 9-bus 3-machine system after QGS transformation. After the transformation, the UEP is an SEP and has a stability region in the new system. The stability region of the new system is connected.

Figure 2.4 shows the stability region of the SEP corresponding to the same UEP in Figure 2.1 after a QGS transformation of the WSCC 9-bus 3-machine system. We can see that the UEP is now an SEP of (2.3), since it now has a stability region. We observed that the SEP has a connected stability region in (2.3). This implies that initial points don't have to be as close as the NR method requires to converge to the original UEP when the QGS transformation is used for a UEP computation. It also implies that it is less likely for an initial point to converge to a wrong UEP when the QGS transformation is used.

2.4 The Pseudo-Transient Continuation Method

After transforming the algebraic problem into computation of an SEP of a dynamic system (2.3), the most efficient way to solve for the equilibrium point is to use the TJU method. Since we are only interested in the steady state solution, we need a TJU method that will converge quickly to the right steady state solution. The TJU method can be explicit (Euler or Runge-Kutta) or implicit (the trapezoidal method). One such implicit method is the pseudo-transient continuation ($\boldsymbol{\psi tc}$) method. The $\boldsymbol{\psi tc}$ is an implicit TJU that employs adaptive time-stepping for the computation of steady state solutions for partial differential equations, differential equations (ODEs), and semi-explicit index-one differential algebraic equations (DAEs) [33-35]. It is analogous to an implicit integration of a dynamic system with increasing time steps as the system trajectory approaches the steady state solution.

The trajectory-based nature of $\boldsymbol{\psi tc}$ makes its convergence region a better approximation of an SEP's stability region compared to the convergence region of other algebraic solvers. This characteristic of $\boldsymbol{\psi tc}$ implies that the initial points don't have to be as close as the NR method requires. It also means trajectories are more likely to converge to the correct physical SEP and not to other SEPs or non-physical local minima [34]. The adaptive nature of the $\boldsymbol{\psi tc}$ method makes it faster than conventional fixed-step integration methods, since larger time steps are taken as the trajectory gets closer to the EP. The $\boldsymbol{\psi tc}$ method is an implicit method, making it numerically more stable than explicit methods like the Euler and Runge-Kutta methods.

Given an initial value problem of the form (2.6):

$$\dot{x} = -G(x), \qquad x(0) = x_0 \tag{2.6}$$

The steady state solution can be found by integrating (2.6) with $\boldsymbol{\psi tc}$. Each step in the $\boldsymbol{\psi tc}$ method is given by (2.7):

$$x_{i+1} = x_i - \left(h_i^{-1} I + DG(x_i)\right)^{-1} G(x_i) \tag{2.7}$$

where I is an identity matrix of appropriate size, and h_i is a variable time step systematically adjusted to improve speed of convergence to steady state. The time step can be adjusted using the "switch evolution relaxation" (SER) (2.8) or the norm of the steps (2.9) [34]:

$$h_i = min\left(h_{i-1}\frac{\|G(x_{i-1})\|}{\|G(x_i)\|}, h_{max}\right) \tag{2.8}$$

$$h_i = min(h_{i-1}\|x_i - x_{i-1}\|, h_{max}) \tag{2.9}$$

where h_{max} is a large upper bound of h_i. For the results in this work, equation (2.8) was used for the time step adjustments and h_{max} was set to ∞. h can be a vector of different time steps if the system of equations in (2.6) is stiff or has an ill-conditioned Jacobian.

$\boldsymbol{\psi tc}$ Algorithm [34]:

1. Set $x = x_0$ and $h = h_0$. Evaluate $G(x)$.
2. While $\|G(x)\|$ is larger than a threshold:
    a. Solve $(h^{-1}I + DG(x))s = -G(x)$.
    b. Set $x = x + s$.
    c. Evaluate $G(x)$.
    d. Update h.

For very large time steps h_i, the variant of the $\boldsymbol{\psi tc}$ method used in this work approximates the NR method, since when h_i is very large, then $h_i^{-1}I \approx 0$ and consequently, (2.7) is equivalent to an NR step like in (2.2). $\boldsymbol{\psi tc}$ in general requires more iterations as compared to NR. In [34], the authors prove that if a steady state solution exists, then $\boldsymbol{\psi tc}$ for ODEs of the form (2.6) has a local q-superlinear or quadratic convergence if some assumptions are satisfied. To improve the computational performance of the application of the $\boldsymbol{\psi tc}$ to (2.3) and guarantee convergence to solutions of (2.1), we proposed the Quotient Gradient System-based Pseudo-Transient Continuation method (QGS-based $\boldsymbol{\psi tc}$), which is presented in the next section.

2.5 The QGS-based Pseudo-Transient Continuation Method

In this section, we present the QGS-based $\boldsymbol{\psi tc}$ method for UEP computations. If we apply the $\boldsymbol{\psi tc}$ method to (2.3), each step of the $\boldsymbol{\psi tc}$ method, (2.7), can be rewritten, as shown in (2.10). We can then simply solve (2.10) at step (2a) for each iteration of the $\boldsymbol{\psi tc}$ algorithm without any further modifications, since the UEP is now an SEP due to the QGS transformation. However, this approach requires the construction of two Jacobians at each iteration, one for the QGS transformation and another for step (2a) of the $\boldsymbol{\psi tc}$ algorithm. This can be computationally expensive if the Jacobians are constructed numerically. Also, the analytical Jacobian for step (2a) can be complex and error-prone. The use of automatic differentiation for a Jacobian construction in step (2a) can also be quite challenging for complex functions or systems of equations like (2.3).

$$x_{i+1} = x_i - \left(\begin{matrix} h_i^{-1}I + \sum_{k=1}^{n} f_k H^T(f_k) \\ + \\ DF(x_i)^T DF(x_i) \end{matrix} \right)^{-1} DF(x_i)^T F(x_i) \tag{2.10}$$

If we assume that $\|-\sum_{k=1}^{n} f_k H^T(f_k)\|$ is sufficiently small, which is true as we approach the equilibrium point of (2.3), then we can use a quasi-Newton method approach and approximate the Jacobian of (2.3) with (2.11):

$$D\tilde{Q}(x) \approx -DF(x)^T DF(x) \tag{2.11}$$

$$\left(h^{-1}I + DF(x)^T DF(x)\right)s \;\approx\; -DF(x)^T F(x) \tag{2.12}$$

$$\min_s \left\| \begin{bmatrix} DF(x) \\ h^{-\frac{1}{2}}I \end{bmatrix} s + \begin{bmatrix} F(x) \\ 0 \end{bmatrix} \right\| \tag{2.13}$$

$$\left\| \left(h^{-1}I + DF(x)^T DF(x)\right)s + DF(x)^T F(x) \right\| \leq \xi \|DF(x)^T F(x)\| \tag{2.14}$$

$$x_{i+1} = x_i + s. \tag{2.15}$$

Step (2a) in the $\boldsymbol{\psi tc}$ algorithm can then be replaced by either (2.12) or (2.13). For small systems with dense Jacobians and function vectors, it might be more efficient to solve (2.12) using QR factorization. In larger sparse systems, solving (2.13) using Cholesky decomposition or iterative methods like the conjugate gradient methods (precondition conjugate gradient methods) might be more efficient [36]. Generically, (2.12) and (2.13) can be represented by (2.14) where ξ could be related to the difference between the exact Jacobian of (2.3) and the approximate Jacobian (2.11) if (2.12) or (2.13) are solved using QR factorization or Cholesky decomposition, or ξ could be related to the Jacobian approximation and the inexact steps involved when iterative methods are used to solve the Newton step.

The solutions/equilibrium points of the QGS system (3) can be of three types:

1. A solution x^* such that $F(x^*) = 0$, and $-DF(x^*)^T F(x^*) = 0$.
2. A solution x^* such that $F(x^*) \neq 0$, and $-DF(x^*)^T F(x^*) = 0$.
3. A x^* such that $F(x^*) = 0,\ -DF(x^*)^T F(x^*) = 0$, and $DF(x^*)^T$ is singular.

The QGS-based $\boldsymbol{\psi tc}$ method converges only to solutions of type 1 because of the QGS structure-dependent Jacobian approximation. This implies that approximating the QGS Jacobian guarantees that if the method converges, it will only converge to solutions of (2.1). The proof will be presented in the next section.

The proposed QGS-based $\boldsymbol{\psi tc}$ method can be summarized by the following steps.

1. Transform the original algebraic problem (2.1) into a dynamic system (2.3) using the QGS transformation.

2. Starting at the given initial guess, apply the $\boldsymbol{\psi tc}$ method to the original system's (2.1) surrogate QGS system, (2.3), solving either (2.12) or (2.13) at step (2a) of the $\boldsymbol{\psi tc}$ algorithm.

In comparison to the NR method, the QGS-based $\boldsymbol{\psi tc}$ method will, in most cases, require more iterations since it does not always converge quadratically to the equilibrium point. Since it will also require more computations per iteration compared to the NR method, we propose that the QGS-based $\boldsymbol{\psi tc}$ be used as a re-starting algorithm after the NR method fails. The idea is to re-start the UEP computation with the QGS-based $\boldsymbol{\psi tc}$ method and then switch back to the NR method when the convergence criterion for the QGS-based $\boldsymbol{\psi tc}$ method is below a defined threshold.

2.6 Convergence of QGS-based Pseudo-Transient Continuation Method

In this section we present the type of convergence and the conditions necessary for the convergence of the QGS-based $\boldsymbol{\psi tc}$ method. We show that the QGS-based $\boldsymbol{\psi tc}$ can have local q-superlinear or even local quadratic convergence if certain assumptions and conditions are satisfied. We also show that the Jacobian approximation used in the QGS-based $\boldsymbol{\psi tc}$ method guarantees that if the QGS-based $\boldsymbol{\psi tc}$ method convergences it will only converge to solutions of the original system (2.1). Let x^* be a UEP of the dynamic system with equilibrium equations represented by equation (2.1).

Proposition 2.2:

Let $F(x^*) = 0$. *Let Assumptions 1,2,3 and 4 hold. The QGS-based* $\boldsymbol{\psi tc}$ *method will have a local q-superlinear convergence to* x^* *from an initial point* x_0 *if* x^* *is a stable hyperbolic equilibrium point of the QGS system (2.3),* x_0 *is in the stability region of* x^* *for the QGS system (2.3),* $\{h_i\}$ *is of the form (2.8),* $h_{max} = \infty$, $\xi_i \leq \hat{\xi}$, $h_i \to h_{max}$, *and* $\xi_i \to 0$. *The convergence to* x^* *will be q-linear if* $h_{max} < \infty$.

Assumptions:

1. $DF(x)^T F(x)$ is everywhere defined and Lipschitz continuously Fréchet differentiable (the norm of the changes in the Jacobian of $DF(x)^T F(x)$ is bounded), and $\|DF(x)^T F(x)\| \leq M$, $M > 0$ for all x.

2. There are $\epsilon_2, \beta > 0$ such that if $\|x - x^*\| < \epsilon_2$, then $\left\|\left(h^{-1}I + D\left(DF(x)^T F(x)\right)\right)^{-1}\right\| \leq (1 + \beta h)^{-1}$ for all $h \geq 0$.
3. Equation (2.3) has unique hyperbolic equilibrium points.
4. $\underset{i}{Inf}\, h_i > 0$. This assumption must be satisfied to prevent the QGS-based $\boldsymbol{\psi}$tc method from stalling.

Proof:

From proposition 2.1, if $F(x^*) = 0$ and Assumption 3 holds, then x^* is a hyperbolic stable equilibrium point of (2.3). Consequently, x^* has a stability region in (2.3). We also know that the portion of ξ_i that is due to the approximation of the Jacobian in the QGS-based $\boldsymbol{\psi tc}$ method is directly proportional to $\|-\sum_{k=1}^{n} f_k H^T(f_k)\|_i$, and that $\|-\sum_{k=1}^{n} f_k H^T(f_k)\|_i \to 0$ since $f_{k_i} \to 0$ as you get closer to x^*. This implies that $\xi_i \to 0$ as $x \to x^*$. Now, since x^* has a stability region in the quotient gradient system, equation (2.3), the convergence of the QGS-based $\boldsymbol{\psi tc}$ method to x^* can be analyzed using the analysis in [34]. As in [34], the QGS-based $\boldsymbol{\psi tc}$ can be viewed as comprising three phases after the initial transformation of the system from the form of equation (2.1) to equation (2.3): an initial phase where x is far from the UEP/SEP and h is small, a midrange phase where the QGS-based $\boldsymbol{\psi tc}$ must produce an accurate x and a large h to ensure convergence in the terminal phase, and a terminal phase where the trajectory is close to the UEP and h is large.

If the initial value for the terminal phase is in the stability region of x^* for system (2.3), then for the terminal phase of the QGS-based $\boldsymbol{\psi tc}$ method, the local convergence can be analyzed with the following Lemma. The detailed proof can be found in [34].

Lemma 2.1. [34]: Let $\{h_i\}$ *be of the form (2.8). Let Assumption 1 hold. Let* $DF(x^*)^T F(x^*) = Q(x^*) = 0$, $DQ(x^*)$ *be nonsingular, and* $DQ(x)$ *be Lipschitz continuous with Lipschitz constant* γ *in a ball of radius* ϵ *about* x^*. *Then there are* $\epsilon_1 > 0$, $\hat{\xi} > 0$, *and* $\Delta_0 > 0$ *such that if* $h_{max}, h_0 > \Delta_0, \xi_i \leq \hat{\xi}$ *for all i, and* $\|x_0 - x^*\| < \epsilon_1$, *then the sequence of values generated by the QGS-based* $\boldsymbol{\psi tc}$ *method satisfies* $h_i \to h_{max}$, $x_i \to x^*$ *q-superlinearly if* $h_{max} = \infty$ *and* $\xi_i \to 0$, *and* $x_i \to x^*$ *q-linearly if* $h_{max} < \infty$.

Lemma 2.1 is based on Lemma 3.1 in [34], which shows that if the listed assumptions/conditions are satisfied, then for every current iteration in the inexact $\boldsymbol{\psi tc}$ algorithm, the norm of the error for the next iterate $\|e_+\| = \|x_+ - x^*\|$ will be smaller than the norm of the current error $\|e_c\| = \|x_c - x^*\|$, and every h_+ will be greater than h_c where x_+ and x_c are the next and current values of x, respectively, and h_+ and h_c are the next and current values of h_i, respectively. The convergence of x to x^* in the terminal phase of the inexact $\boldsymbol{\psi tc}$ is shown to be q-superlinear if $h_{max} = \infty$ and $\xi_i \to 0$, and q-linear if $h_{max} < \infty$.

Since the QGS-based $\boldsymbol{\psi tc}$ is a special case of the inexact $\boldsymbol{\psi tc}$ and $\xi_i \to 0$ as $x \to x^*$ for the QGS-based $\boldsymbol{\psi tc}$, this implies that the QGS-based $\boldsymbol{\psi tc}$ will converge to x^*, at least q-linearly, if Assumption 1 is satisfied, the upper limit of h_i is sufficiently large, the approximation errors for the Jacobian and the inexact iterative steps at this phase of the method are sufficiently small, and the midrange phase of the QGS-based $\boldsymbol{\psi tc}$ produces an x_i value sufficiently close to the UEP/SEP and a sufficiently large h_i for the initial step of the terminal phase. The magnitude of the upper limit of h_i, which is h_{max}, can be chosen such that it is sufficiently large or ∞. At the terminal phase, the trajectory of the x_i values leading to the UEP/SEP should be close to the UEP/SEP if the midrange phase is accurate, so the error due to the Jacobian approximations

$\|-\sum_{k=1}^{n} f_k H^T(f_k)\|_i$ should be small since $\|-\sum_{k=1}^{n} f_k H^T(f_k)\|_i \to 0$. The error due to iterative steps will depend on the inexact or iterative technique used and hence can be chosen to ensure it has minimal effect on ξ_i. With $\|-\sum_{k=1}^{n} f_k H^T(f_k)\|_i \to 0$ by the time the QGS-based $\boldsymbol{\psi tc}$ is in the terminal phase, we can assume that ξ_i will be sufficiently small. Thus, if Assumption 1 holds and the midrange phase of the QGS-based $\boldsymbol{\psi tc}$ performs as required, then the terminal phase of the QGS-based $\boldsymbol{\psi tc}$ will converge either q-linearly or q-superlinearly, depending on the upper limit of h_i. From [34] it can be shown that the terminal phase QGS-based $\boldsymbol{\psi tc}$ will have local quadratic convergence if $h_{max} = \infty$ and $\xi_i = O\|Q(x_i)\|$.

Lemma 2.2. [34]: Let $\{h_i\}$ be of the form (2.8). Let $\{x_i\}$ be given by (2.15) and (2.14). Let Assumptions 1, 2, and 4 hold if h_{max} is large enough for Lemma 2.1. to hold. Then there are $\epsilon_3 > 0$, $\hat{\xi} > 0$ such that if $\xi_i \leq \hat{\xi}$, $\|x_0 - x^*\| < \epsilon_3$, and $h_0 > 0$, then the sequence generated by the QGS-based $\boldsymbol{\psi tc}$ in the midrange phase is $x_i \to x^*$ and $h_i \to h_{max}$.

Lemma 2.2 is based on the proof in [34] that if the listed assumptions are satisfied, then x_i converges to x^* q-linearly and $Q(x_n)$ converges to 0 with $h_i \to h_{max}$.

This implies that the QGS-based $\boldsymbol{\psi tc}$ will converge to x^* q-linearly and $h_i \to h_{max}$ if Assumptions 1, 2, and 4 hold; the upper limit of h_i is sufficiently large; the approximation errors for the Jacobian and the inexact/iterative steps at the midrange phase of the method are sufficiently small; and the initial phase of the QGS-based $\boldsymbol{\psi tc}$ produces an x_i value sufficiently close to the UEP/SEP and a sufficiently large h_i for the initial step of the midrange phase. h_{max} the magnitude of the upper limit of h_i can be chosen to be sufficiently large or ∞. If the initial phase of the QGS-based $\boldsymbol{\psi tc}$ is accurate, then again it can be assumed that the error of the Jacobian approximations

and the approximations in any inexact/iterative steps in the midrange phase should be sufficiently small. If, and once Assumptions 1, 2, and 4 hold, then the midrange phase of the QGS-based $\boldsymbol{\psi tc}$ should approach the UEP/SEP as h_i increases. If Assumption 4 does not always hold, then the QGS-based $\boldsymbol{\psi tc}$ can stall as h_i gets smaller, also if the error of the Jacobian approximations and the approximations in any inexact/iterative steps are not sufficiently small, then as with Gauss-Newton method used for least square problems the convergence of the midrange phase will be slow.

Lemma 2.3. [34]: Let $\{h_i\}$ *be of the form (2.8). Let* $\{x_i\}$ *be given by (2.16) and (2.15). If Assumptions 1 and 2 hold, the initial guess* x_0 *is in the stability region of* x^* *for (2.3) and the operators* $\left(h_i^{-1}I + D\left(DF(x_i)^T F(x_i)\right)\right)^{-1}$ *in the* QGS-based $\boldsymbol{\psi tc}$ *are uniformly bounded in* i*, then given any* $\epsilon > 0$*, there exist* $\hat{\xi} > 0$ *and* $\hat{h} > 0$ *such that if* $\xi_i \leq \hat{\xi}$ *and* $h_0 \leq \hat{h}$*, then there is an* i *such that* $\|x_i - x^*\| < \epsilon$ *for the initial phase of the QGS-based* $\boldsymbol{\psi tc}$ *.*

Lemma 2.3, based on Lemma 3.4 in [34], shows that the steps in the initial phase of the QGS-based $\boldsymbol{\psi tc}$ method will be a good approximation of the trajectory of an initial value problem of the form (2.3) with an initial guess x_0 if Assumptions 1 and 2 hold, none of the linear solver steps $\left(h_i^{-1}I + D\left(DF(x_i)^T F(x_i)\right)\right)^{-1}$ are singular, the initial time step h_0 is sufficiently small, $\{h_i\}$ is of the form (2.9), and the error of the Jacobian and any iterative step approximations is sufficiently small. If x_0 is in the stability region of x^* for (2.3) then the approximated trajectory will have a steady state solution equivalent to x^*. The uniform boundedness of the linear solver steps, like the other two assumptions, will depend on the nature of the function, equation (2.1), being solved.

Additionally, to ensure a good approximation of the equation (2.3) trajectory to the UEP in the initial phase, a sufficiently small h_0 should be selected. The error of the Jacobian and inexact/iterative step approximations can be kept sufficiently small if the initial guess for the solver is adequately chosen. The error related to the Jacobian can be rather large if the initial guess is far from the steady state solution. However, as in the midrange phase the main challenge associated with a big error in the Jacobian approximation is a slow rate of convergence of the initial phase.

In summary, subject to the above assumptions and conditions discussed for each phase, the QGS-based $\boldsymbol{\psi tc}$ with $h_{max} = \infty$ will at least have a local q-superliner convergence if ξ_i is sufficiently small and $\xi_i \to 0$ as $x_i \to x^*$. The convergence of the QGS-based $\boldsymbol{\psi tc}$ method to x^* is locally q-quadratic if $\xi_i = O\|Q(x_i)\|$, Corollary 3.2 of [34].

Theorem 2.3: If the QGS-based $\boldsymbol{\psi tc}$ method converges to x^*, then x^* is a solution of type 1 and hence, a solution of the original system (2.1).

Proof:

If the QGS-based $\boldsymbol{\psi}$tc method converges, then it implies that $DF(x^*)^T F(x^*) = 0$ and the inverse $\left(h_{x^*}^{-1} I + DF(x^*)^T DF(x^*)\right)^{-1}$ exists where h_{x^*} is the final value of the time step.

If x^* is of type 3, then $DF(x^*)^T DF(x^*)$ is singular. Since the function $\lambda_{min}\big(DF(x)^T DF(x)\big)$, the minimum eigenvalue of $DF(x)^T DF(x)$, is continuous in x, the sequence

$$\left\{\lambda_{i,min} = \lambda_{min}\big(DF(x_i)^T DF(x_i)\big)\right\}$$

converges to zero as $x_i \to x^*$. Thus, there exists a value of $i < \infty$ where $DF(x_i)^T DF(x_i)$ is singular and h_i is very large such that $\left(h_i^{-1} I + DF(x_i)^T DF(x_i)\right) \approx DF(x_i)^T DF(x_i)$, which is a contradiction since $\left(DF(x_i)^T DF(x_i)\right)^{-1}$ must exist. Hence, the QGS-based $\boldsymbol{\psi}$tc method cannot converge to solutions of type 3.

If x^* is of type 2, then the $Null(DF(x^*)^T) \neq \emptyset$, and $F(x^*) \in Null(DF(x^*)^T)$. This implies that $DF(x^*)^T DF(x^*)$ is singular, which implies that the QGS-based $\boldsymbol{\psi}$tc method cannot converge to solutions of type 2, since it will be a contradiction. Thus, if the QGS-based $\boldsymbol{\psi}$tc method converges, the solution can only be of type 1 and hence, the solution will be a solution of (2.1).

2.7 Conclusion

A new robust method that combines a QGS transformation with a dynamic trajectory-based integration method for the computation of a UEP, given an initial point, was proposed. The method converts the UEP to an SEP by changing the problem into a quotient gradient system. It then applies a quasi-Newton form of the pseudo-transient continuation method by exploiting the structure of the proposed QGS's Jacobian to speed up computations and avoid convergence to zeros that are not solutions to the original problem. The convergence and the conditions for the convergence of the proposed method have been presented and discussed. We have also shown that the proposed method will only converge to solutions of the original problem. Thus, the proposed method will not converge to a UEP that is not a solution of (2.1). In the next chapter, the proposed method will be evaluated on the WSCC 9-bus 3-machine system and the IEEE 145-bus 50-machine system.

CHAPTER 3

Robust Methods for Computation of Unstable Equilibrium Points: Numerical Computations

3.1 Introduction

It is well recognized that the computation of unstable equilibrium points (UEP) is important for online applications that will rely on energy-based direct methods. It was shown in Chapter 2 that a QGS transformation of a system of algebraic/equilibrium equations being solved for zeros corresponding to a UEP can convert a UEP to an SEP. This implies that after the QGS transformation, the UEP will be an SEP in the new system and consequently, we can solve the new system for the resulting SEP using TJU methods.

From a theoretical viewpoint, the applicability and convergence of the QGS-based $\boldsymbol{\psi tc}$ method in the computation of UEPs after the QGS transformations has been established in Chapter 2. In this chapter, the numerical evaluation of the proposed method, the QGS-based $\boldsymbol{\psi tc}$ method, will be conducted on three test systems: a network-reduction power system model and two structure-preserving power system models. In addition, a comparison between the QGS-based $\boldsymbol{\psi tc}$ method and other algebraic solvers will be made, and an integrated numerical method that combines the proposed method with the NR method for UEP computations will be proposed.

The numerical simulations were performed on a computer with an Intel® Core™ i7-3630QM CPU @2.40GHz processor and 16GB memory. All the simulations were performed with Matlab 7.11. Matlab's Fsolve is used as a check for accuracy.

The chapter is organized as follows. In section 3.2, the form of the nonlinear equations for power system UEP computation is presented. The numerical technique used for the construction of the convergence region of the algebraic solvers is presented in section 3.3. Section 3.4 presents the numerical simulation results. Section 3.5 discusses the findings from the numerical simulations and proposes the integrated method for UEP computation. The conclusions are then stated in Section 3.6.

3.2 Nonlinear Equations for Unstable Equilibrium Points

Generally, the electromechanical dynamics of a power system can be modeled by a system of differential algebraic equations (DAEs) (3.1).

$$\begin{aligned} \dot{x} &= f(x, y) \\ 0 &= g(x, y) \end{aligned} \tag{3.1}$$

where x and y are vectors of the dynamic state and algebraic variables, respectively. The system of differential equations describes the electromechanical and electrical dynamics of components like generators, dynamic loads, and their associated control systems. The algebraic system of equations in (3.1) represent the transmission system and the internal static behaviors of passive devices [1].

Solving for the equilibrium points of (3.1) translates into solving for the roots of the algebraic equation (3.2).

$$0 = f(x, y)$$

$$0 = g(x, y) \tag{3.2}$$

Power system dynamic models of the form (3.1) are referred to as structure-preserving models. Alternatively, the power system can be modeled by a network-reduction model that takes the form of an ODE (3.3) [1, 37].

$$\dot{x} = f(x) \tag{3.3}$$

Solving for the equilibrium points of (3.3) translates to solving for the roots of the algebraic equation (3.4).

$$0 = f(x) \tag{3.4}$$

In this chapter, the numerical simulations are performed with the following network-reduction and structure-preserving power system dynamic equations.

3.2.1 Dynamic Equations

The Network-Reduction Model:

For n generators, the swing equation for generator i in the center of inertia (COI) reference frame is as shown below [1]:

$$\dot{\tilde{\delta}}_i = \tilde{\omega}_i \tag{3.5}$$

$$M_i \dot{\tilde{\omega}}_i = -D_i \tilde{\omega}_i + P_{m_i} - P_{e_i}\left(\tilde{\delta}_1, \tilde{\delta}_2, \dots, \tilde{\delta}_n\right) - \frac{M_i}{M_T} P_{COI} \tag{3.6}$$

$$P_{e_i}(\tilde{\delta}_1, \tilde{\delta}_2, \dots, \tilde{\delta}_n) = \sum_{j=1, j\neq i}^{n} E_i E_j \left(B_{ij}^I \sin(\tilde{\delta}_i - \tilde{\delta}_j) + G_{ij}^I \cos(\tilde{\delta}_i - \tilde{\delta}_j)\right). \quad (3.7)$$

where δ_i is the rotor angle of machine i, ω_i is the angular velocity of machine i, M_i is the moment of inertia of machine i, D_i is the damping coefficient of machine i, P_{m_i} is the mechanical power of machine i, E_i is the internal voltage of machine i, and $G_{ik}^I + jB_{ik}^I$ is the internal admittances.

For both network-reduction and the subsequent structure-preserving models, δ_0, ω_0, M_T, $\tilde{\delta}_i$, $\widetilde{\omega}_i$, $\tilde{\theta}_i$, P_{COI} are defined as follows:

$$\delta_0 = \frac{1}{M_T} \sum_{i=1}^{n} M_i \delta_i \quad (3.8)$$

$$\omega_0 = \frac{1}{M_T} \sum_{i=1}^{n} M_i \omega_i \quad (3.9)$$

$$M_T = \sum_{i=1}^{n} M_i \quad (3.10)$$

$$\tilde{\delta}_i = \delta_i - \delta_0 \quad (3.11)$$

$$\widetilde{\omega}_i = \omega_i - \omega_0 \quad (3.12)$$

$$\tilde{\theta}_i = \theta_i - \theta_0 \quad (3.13)$$

$$P_{COI} = \sum_{i=1}^{n} P_{m_i} - \sum_{i=1}^{n} P_{e_i}(\tilde{\delta}_1, \tilde{\delta}_2, \dots, \tilde{\delta}_n) \tag{3.14}$$

The Structure-Preserving Model:

The classical generation model, with constant voltage behind a reactance, is used for the structure-preserving numerical simulations in this chapter. The loads for the simulations are modeled as constant impedance loads. For n generators and m buses, the swing equations for generator i in the center of the inertia (COI) reference frame is as shown below [1]:

$$\dot{\tilde{\delta}}_i = \tilde{\omega}_i \tag{3.15}$$

$$M_i \dot{\tilde{\omega}}_i = -D_i \tilde{\omega}_i + P_{m_i} - P_{e_i}(\tilde{\delta}_1, \tilde{\delta}_2, \dots, \tilde{\delta}_n) - \frac{M_i}{M_T} P_{COI} \tag{3.16}$$

$$P_{e_i}(\tilde{\delta}_1, \tilde{\delta}_2, \dots, \tilde{\delta}_n) = P_{G_i}(\tilde{\delta}_i, \tilde{\theta}_i, V_i) \tag{3.17}$$

where δ_i is the rotor angle of machine i, ω_i is the angular velocity of machine i, M_i is the moment of inertia of machine i, D_i is the damping coefficient of machine i, and P_{m_i} is the mechanical power of machine i.

The network equations for the structure-preserving model are as shown below.

For generator buses:

$$0 = P_{G_i}(\tilde{\delta}_i, \tilde{\theta}_i, V_i) - \sum_{j=1}^{m} V_i V_j (B_{ij} \sin(\tilde{\theta}_i - \tilde{\theta}_j) + G_{ij} \cos(\tilde{\theta}_i - \tilde{\theta}_j)) \tag{3.18}$$

$$0 = Q_{G_i}(\tilde{\delta}_i, \tilde{\theta}_i, V_i) - \sum_{j=1}^{m} V_i V_j \left(G_{ij} \sin(\tilde{\theta}_i - \tilde{\theta}_j) + B_{ij} \cos(\tilde{\theta}_i - \tilde{\theta}_j)\right) \tag{3.19}$$

$$P_{G_i}(\tilde{\delta}_i, \tilde{\theta}_i, V_i) = \frac{E'_{qi} V_i \sin(\tilde{\delta}_i - \tilde{\theta}_i)}{X'_{di}} \tag{3.20}$$

$$Q_{G_i}(\tilde{\delta}_i, \tilde{\theta}_i, V_i) = -\frac{V_i^2}{X'_{di}} + \frac{E'_{qi} V_i \sin(\tilde{\delta}_i - \tilde{\theta}_i)}{X'_{di}} \tag{3.21}$$

For load buses:

$$0 = \sum_{j=1}^{m} V_i V_j \left(B_{ij} \sin(\tilde{\theta}_i - \tilde{\theta}_j) + G_{ij} \cos(\tilde{\theta}_i - \tilde{\theta}_j)\right) \tag{3.22}$$

$$0 = \sum_{j=1}^{m} V_i V_j \left(G_{ij} \sin(\tilde{\theta}_i - \tilde{\theta}_j) + B_{ij} \cos(\tilde{\theta}_i - \tilde{\theta}_j)\right) \tag{3.23}$$

where E'_{qi} is the equivalent transient quadrature internal voltage of machine i, X'_{di} is the equivalent transient reactance of machine i, G_{ij} is the conductance of the transmission line between buses i and j, B_{ij} is the susceptance of the transmission line between buses i and j. If $i = j$, then $G_{ii} + jB_{ii}$ is the self-admittance of bus i, which includes the constant impedance representation of the load, V_i is the voltage magnitude at bus i, and θ_i is the voltage angle at bus i.

3.2.2 Equilibrium Equations

The Network-Reduction Model:

At an equilibrium point, the right-hand side of (3.5) and (3.6) is zero. Thus, for n generators, the equilibrium equation for generator i in the center of inertia (COI) reference frame is as shown below (3.24):

$$0 = P_{m_i} - P_{e_i}(\tilde{\delta}_1, \tilde{\delta}_2, \dots, \tilde{\delta}_n) - \frac{M_i}{M_T} P_{COI} \tag{3.24}$$

The Structure-Preserving Model:

At an equilibrium point, the right-hand side of (3.18) and (3.19) is zero and the algebraic constraints (3.20, 3.21, 3.22, 3.23) are satisfied. For *n* generators and *m* buses, the equilibrium equation for generator i in the center of inertia (COI) reference frame is as shown below:

$$0 = P_{m_i} - P_{e_i}(\tilde{\delta}_1, \tilde{\delta}_2, \dots, \tilde{\delta}_n) - \frac{M_i}{M_T} P_{COI} \tag{3.25}$$

$$0 = P_{G_i}(\tilde{\delta}_i, \tilde{\theta}_i, V_i) - \sum_{j=1}^{m} V_i V_j (B_{ij} \sin(\tilde{\theta}_i - \tilde{\theta}_j) + G_{ij} \cos(\tilde{\theta}_i - \tilde{\theta}_j)) \tag{3.26}$$

$$0 = Q_{G_i}(\tilde{\delta}_i, \tilde{\theta}_i, V_i) - \sum_{j=1}^{m} V_i V_j (G_{ij} \sin(\tilde{\theta}_i - \tilde{\theta}_j) + B_{ij} \cos(\tilde{\theta}_i - \tilde{\theta}_j)) \tag{3.27}$$

$$0 = \sum_{j=1}^{m} V_i V_j \left(B_{ij} \sin\left(\tilde{\theta}_i - \tilde{\theta}_j\right) + G_{ij} \cos\left(\tilde{\theta}_i - \tilde{\theta}_j\right) \right) \tag{3.28}$$

$$0 = \sum_{j=1}^{m} V_i V_j \left(G_{ij} \sin\left(\tilde{\theta}_i - \tilde{\theta}_j\right) + B_{ij} \cos\left(\tilde{\theta}_i - \tilde{\theta}_j\right) \right) \tag{3.29}$$

3.3 Convergence Region

The convergence region of a UEP of a dynamic system for a numerical algebraic solver N is defined as the set of initial points that converge to the UEP for the numerical algebraic solver [1].

The size and connectedness of the convergence region of the QGS-based $\boldsymbol{\psi tc}$ method will be one of the metrics used in our evaluation of the proposed method's performance in comparison to other algebraic solvers. Obviously, a large and connected convergence region implies that the initial point for the UEP computation does not have to be very close to the UEP for the algebraic solver to converge.

By observing equilibrium equations (3.24) – (3.29), it is obvious that the convergence region of a UEP for a classical generator model can be constructed using a dimension-reduced model in which ω is a zero vector. This construction is implemented by first creating a grid of initial points around the UEP in the machine angle space less the reference machine angle variable. Thus, the grid of initial points will have values representing the initial values of all the machine angles except

the reference machine angle. The reference machine angle and the algebraic variables corresponding to the initial points on the grid are then updated by using the COI equation for machine angles (3.17), and the solutions of the network algebraic equations at the grid points, respectively. For a system with n generators, the dimension of a point in the grid is thus equal to $n-1$. For the convergence region of the network-reduction model, only the machine angle of the reference generator must be updated for the initial points.

The solutions of the equilibrium equations for the dynamic system starting at these initial points is then computed using the algebraic solver for which a convergence region of a UEP is being constructed. The computed equilibrium point is then compared to the UEP for which a convergence region is being constructed. If the L2 norm of the difference between the computed equilibrium point and the UEP is below a defined threshold, then the initial point is in the convergence region of the UEP for that algebraic solver. A similar approach was used for the construction of the stability regions. However, in the case of the stability region, the equilibrium points were computed using ODE solvers instead of algebraic solvers.

3.4 Numerical Studies

To illustrate the performance of the proposed QGS-based $\boldsymbol{\psi tc}$ method, we compare its performance with the Newton-Raphson method, the continuous Newton-Raphson method, Matlab's fsolve, and the QGS system solved with exact $\boldsymbol{\psi tc}$. The performance of our proposed integrated method that combines the Newton-Raphson method with the QGS-based $\boldsymbol{\psi tc}$ is also evaluated. The numerical studies are performed with the network-reduction and structure-preserving models of the WSCC 9-bus 3-machine system with classical generator models and the

structure-preserving model of the IEEE 145-bus 50-machine system, also with classical generator models. The load was modeled as constant impedances.

3.4.1 The WSCC 9-Bus 3-Machine System with a Classical Generator Model

The QGS-based $\boldsymbol{\psi tc}$ method is tested on the WSCC 9-bus 3-machine system [1] (see Figure 2.2) to compute a UEP on the stability boundary of a post-fault system. A uniform damping of $\lambda = 0.1$ is assumed, and the simulation is done in the Center of Inertia (COI) reference framework. Initial time step h_0 of the exact $\boldsymbol{\psi tc}$ and QGS-based $\boldsymbol{\psi tc}$ methods are set to 0.01 for the network-reduction model and 0.1 for the structure-preserving model. Table 2.1 shows the list of contingencies used in our simulations of this system.

Table 3.1 Contingency List of the WSCC 9-bus 3-machine System

Contingency Number	Fault Bus	Trip Branch	
		From Bus	To Bus
1	7	7	5
2	7	8	7
3	6	4	6
4	6	6	9
5	9	9	8

We first look at simulation results on the network-reduction model. Figures 3.1-3.5 show the projections of the convergence regions of the NR method in Figure 3.1, the Continuous NR method in Figure 3.4, and the QGS-based $\boldsymbol{\psi tc}$ in Figure 3.2 into the δ_1-δ_2 space for a specific type-1 UEP on the stability boundary of the post-fault system after contingency 2. We can observe that, among the three methods, the QGS-based $\boldsymbol{\psi tc}$ method has the largest connected convergence region in the closest neighborhood of the UEP. The QGS-based $\boldsymbol{\psi tc}$ convergence region is much more

compact and connected while that of the NR is fractal and disconnected. Figure 3.3 shows a detailed comparison between the NR convergence region and the QGS-based $\boldsymbol{\psi tc}$ convergence region. The green region is the QGS-based $\boldsymbol{\psi tc}$ convergence region while the magenta region is the NR convergence region. The convergence region of the continuous NR method is disconnected and fractal like the NR method, shown in Figure 3.4. However, the connected portions of the convergence region of the continuous NR method are larger than those of the NR method. The connected portion of the convergence region of the continuous NR method is also smaller than the connected portion of the convergence region QGS-based $\boldsymbol{\psi tc}$ method, as shown in Figure 3.5.

This result shows that the QGS-based $\boldsymbol{\psi tc}$ method expands the connected portion of the convergence region of the UEP as compared with the NR and the continuous NR methods by enjoying the gain in the stability region from the QGS transformation. Consequently, the QGS-based $\boldsymbol{\psi tc}$ is a more robust method for UEP computations.

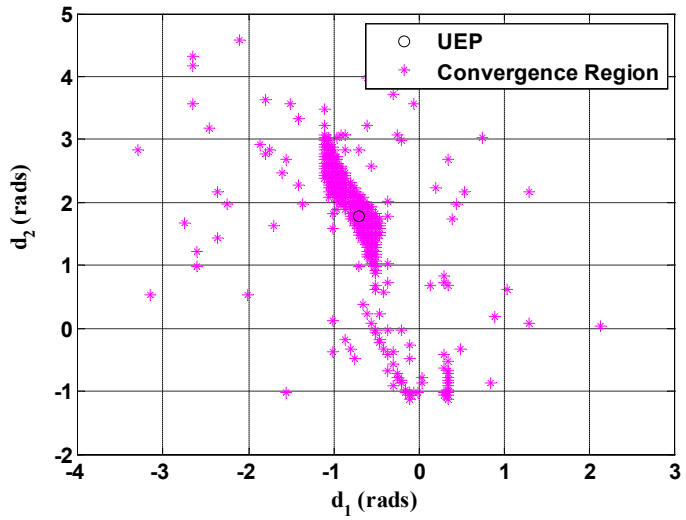

Figure 3.1 The NR method convergence region of a UEP for the network-reduction model (contingency 2) of a post-fault WSCC 9-bus 3-machine system.

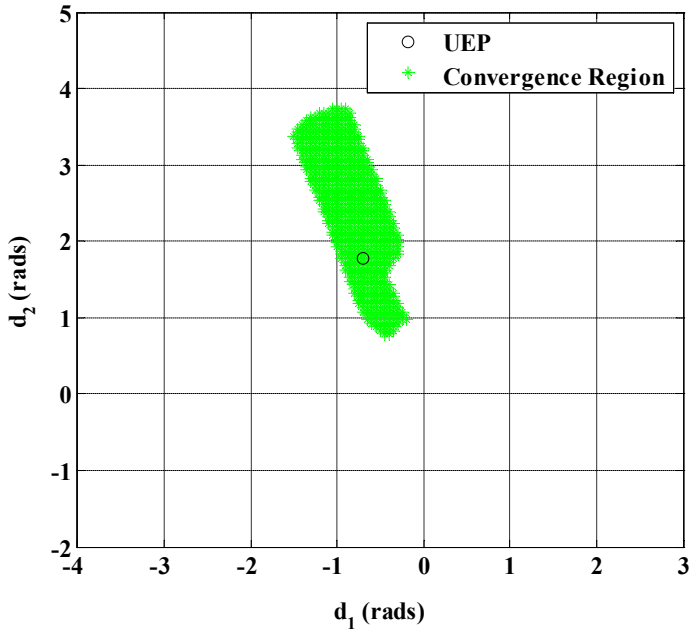

Figure 3.2 The QGS-based ψtc method convergence region of a UEP for the network-reduction model (contingency 2) of a post-fault WSCC 9-bus 3-machine system.

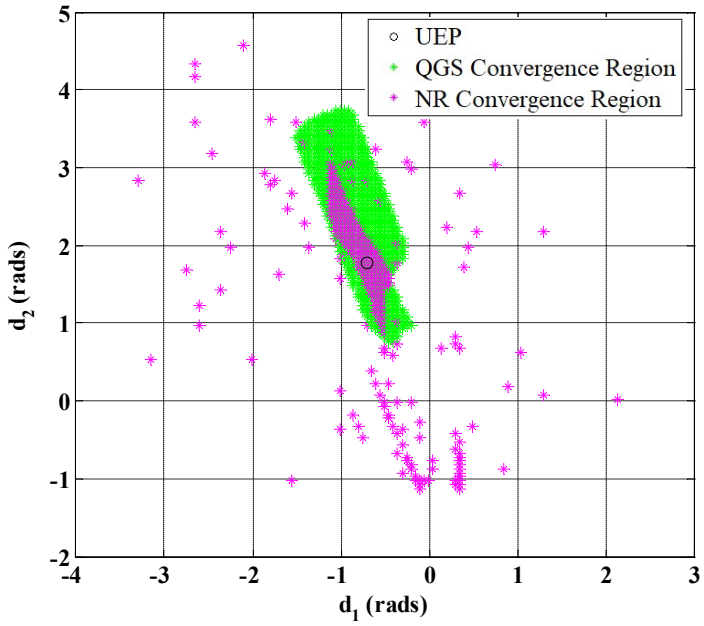

Figure 3.3 The NR convergence region of a UEP for the network-reduction model (contingency 2) of a post-fault WSCC 9-bus 3-machine system superimposed on the QGS-based ψtc convergence region.

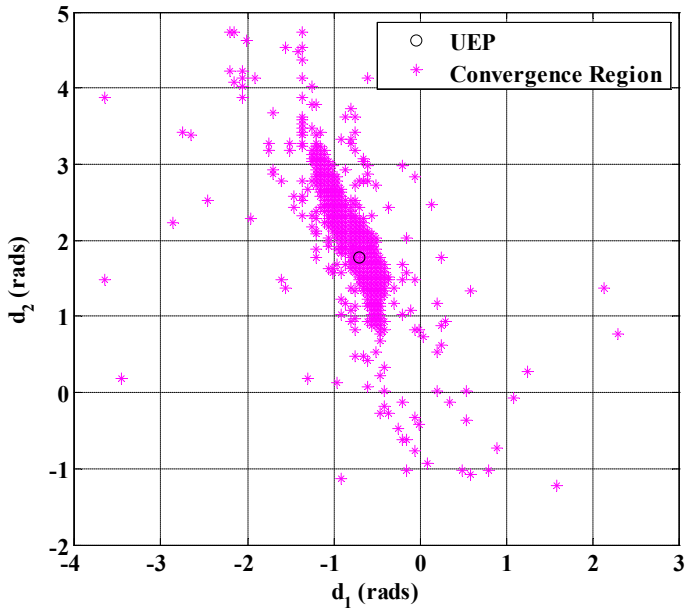

Figure 3.4 The continuous NR method convergence region of a UEP for the network-reduction model (contingency 2) of a post-fault WSCC 9-bus 3-machine system.

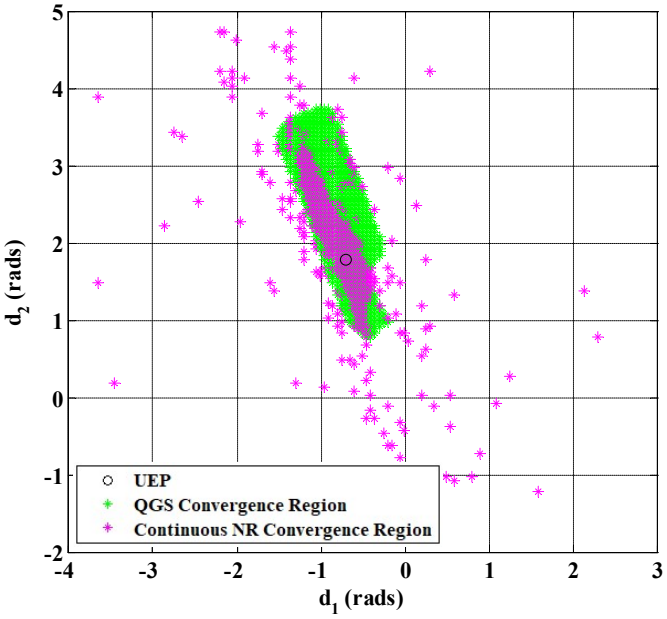

Figure 3.5 The continuous NR convergence region of a UEP for the network-reduction model (contingency 2) of a post-fault WSCC 9-bus 3-machine system superimposed on the QGS-based ψtc convergence region.

For the structure-preserving model of the WSCC 9-bus 3-machine system, we first study the convergence regions for a specific type-1 UEP on the stability boundary of the post-fault system after contingency 1. We also compare the computational performance of the NR method, the exact $\boldsymbol{\psi tc}$ method, the QGS-based $\boldsymbol{\psi tc}$, the QGS-based $\boldsymbol{\psi tc}$ coupled with the NR method, the Continuous NR method, and Matlab's Fsolve function. Figure 3.6, Figure 3.7, and Figure 3.9 show the projected convergence regions of the NR method, the QGS-based $\boldsymbol{\psi tc}$ method, and the Continuous NR method, respectively. It can be seen that the QGS-based $\boldsymbol{\psi tc}$ method has the largest connected portion of convergence region in the closest neighborhood of the UEP. Figure 3.8 shows a comparison of the convergence region of the QGS-based $\boldsymbol{\psi tc}$ method with the convergence region of the NR method. Figures 3.9-3.10 present the convergence region of the Continuous NR method and its comparison to the convergence region of the QGS-based $\boldsymbol{\psi tc}$ method. We observe that the Continuous NR method's convergence region is also disconnected and fractal, as in the NR method. The connected portion of the convergence region of the Continuous NR method is again larger than that of the NR method, but still smaller than that of the QGS-based $\boldsymbol{\psi tc}$ method, as previously observed in the network-reduction case. Figure 3.11 shows an example of an initial point, depicted by the black asterisk that falls within the convergence region of the QGS-based $\boldsymbol{\psi tc}$ method for the CUEP of contingency 1 but outside the convergence region of the NR method. Hence, the proposed QGS-based $\boldsymbol{\psi tc}$ method can converge to the CUEP of contingency 1 while the NR method diverges. The divergence of the NR method, despite the proximity of the initial point to the CUEP, points out the advantage of using the QGS-based $\boldsymbol{\psi tc}$ method over the NR method when computing UEPs. The initial point represented by the black star was obtained from the stability boundary following the procedure used in the BCU method [1] for CUEP computations.

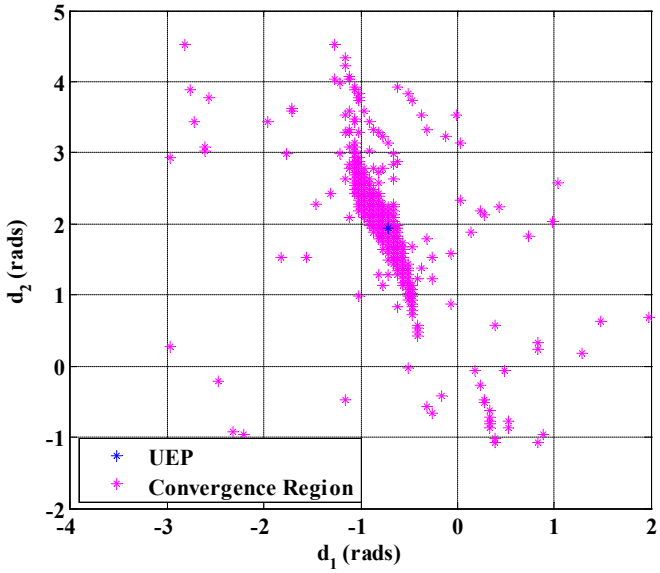

Figure 3.6 The NR method convergence region of a UEP for the structure-preserving model (contingency 1) of the post-fault WSCC 9-bus 3-machine system.

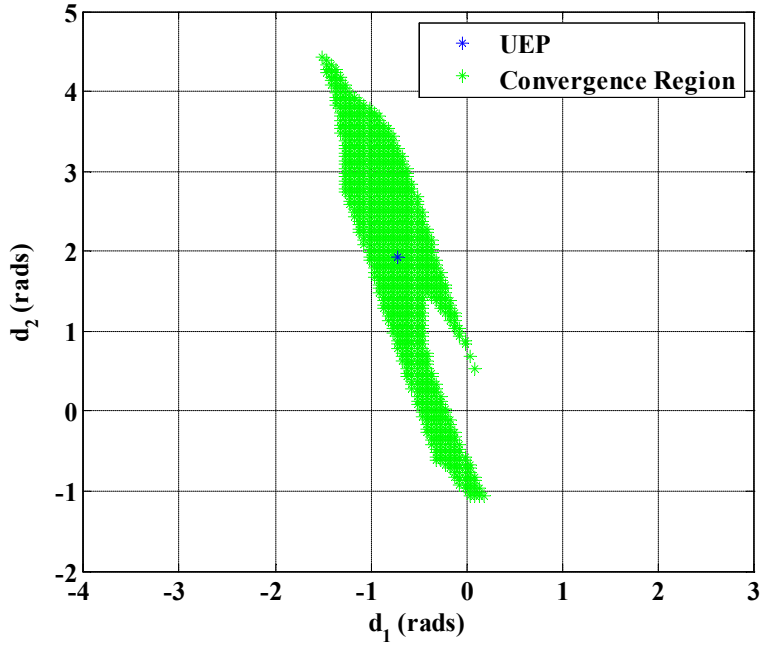

Figure 3.7 The QGS-based ψtc method convergence region of a UEP for the structure-preserving model (contingency 1) of a post-fault WSCC 9-bus 3-machine system.

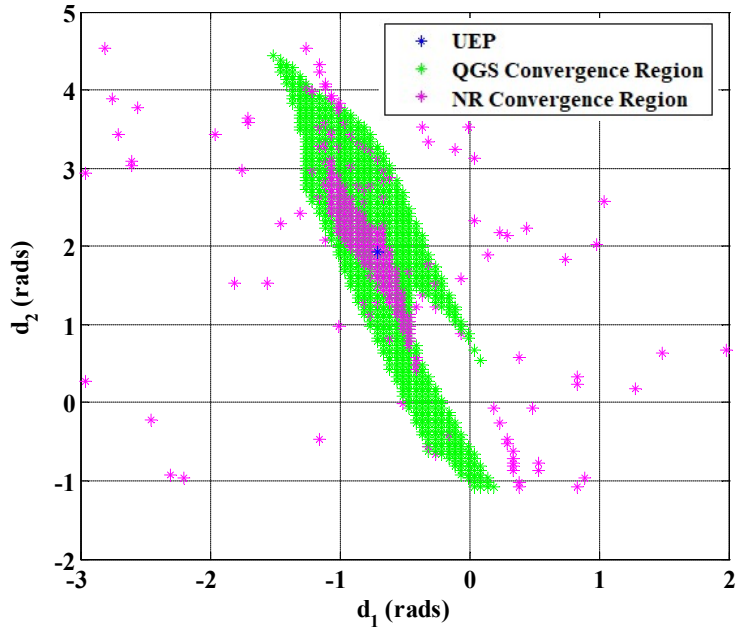

Figure 3.8 The NR convergence region of a UEP for the structure-preserving model (contingency 1) of a post-fault WSCC 9-bus 3-machine system superimposed on the QGS-based ψtc convergence region.

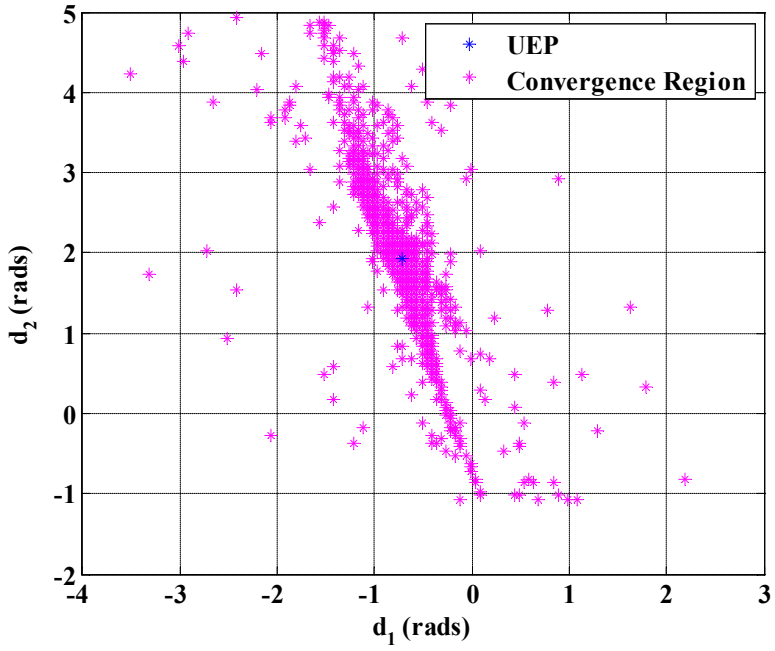

Figure 3.9 The continuous NR method convergence region of a UEP for the structure-preserving model (contingency 1) of a post-fault WSCC 9-bus 3-machine system.

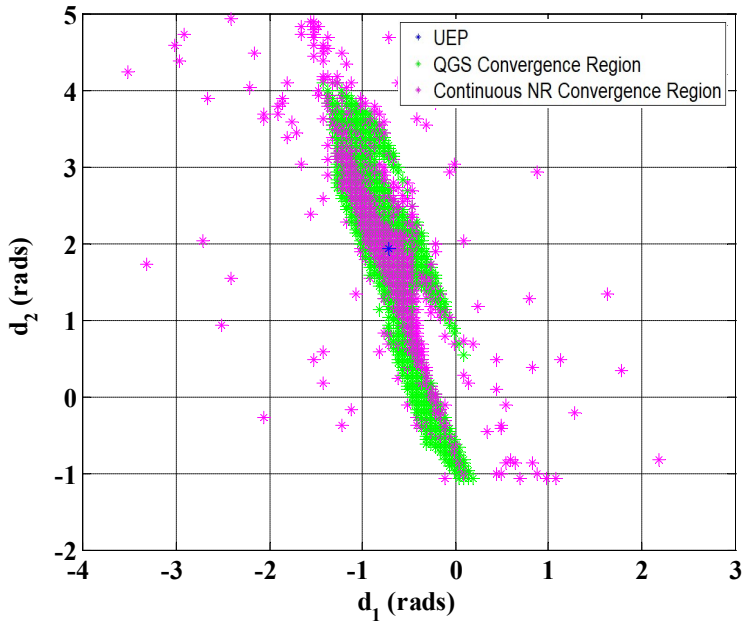

Figure 3.10 The continuous NR convergence region of a UEP for the structure-preserving model (contingency 1) of a post-fault WSCC 9-bus 3-machine system superimposed on the QGS-based ψtc convergence region.

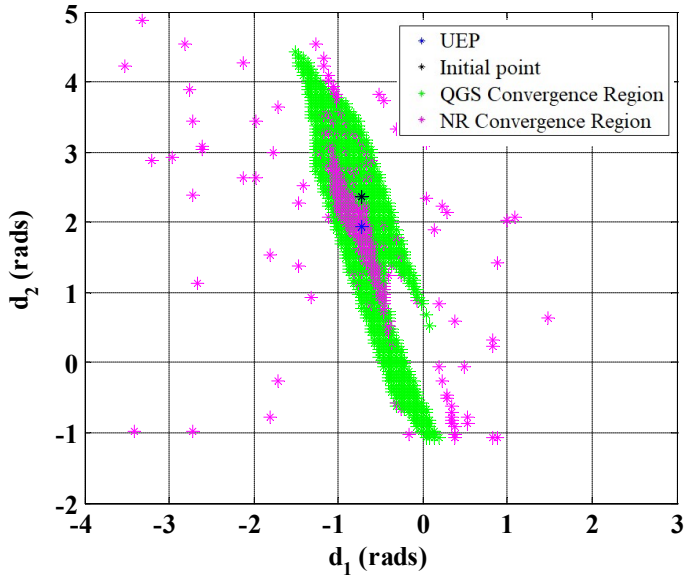

Figure 3.11 An example of an initial point that is in the convergence region of the QGS-based ψtc for a UEP for the structure-preserving model (contingency 1) of a WSCC 9-bus 3-machine system, but not in the convergence region of the NR method.

Figure 3.12 shows a comparison of the computation time in seconds for CUEP evaluations for all 5 contingencies, using Matlab's Fsolve, the NR method, the Continuous NR method, the exact $\boldsymbol{\psi tc}$ method, the QGS-based $\boldsymbol{\psi tc}$ method, and the QGS-based $\boldsymbol{\psi tc}$ method combined with the NR method (where the computation of the UEP is started using the QGS-based $\boldsymbol{\psi tc}$ method and then, after the convergence criteria reaches a threshold, the computation method is switched to the NR method). The initial points used in these simulations were computed using the stability boundary, following procedure [1]. The chart indicates that the exact $\boldsymbol{\psi tc}$ method is significantly slower than the other three methods. A closer look at the graph shows that, by using the QGS-based $\boldsymbol{\psi tc}$ method or its combination with the NR method, we improve the UEP computational speed by 7.5 times on average as compared to the exact $\boldsymbol{\psi tc}$ method. Figure 3.12 also shows that the UEP computation time for the QGS-based $\boldsymbol{\psi tc}$ method is almost equivalent to the computation time of the NR method and less than Matlab's Fsolve and the Continuous NR method, as implemented in [31]. It is also observed that combining the QGS-based $\boldsymbol{\psi tc}$ method with the NR method does not speed up the UEP computation time significantly when compared to just computing the UEP with the QGS-based $\boldsymbol{\psi tc}$ method. The insignificant difference in speed between the NR method and the QGS-based $\boldsymbol{\psi tc}$ method in this numerical example can be attributed to the small size of the test system. The graph in Figure 3.12 suggests that the speed of the QGS-based $\boldsymbol{\psi tc}$ is comparable to the NR method but faster than Matlab's Fsolve and the Continuous NR method for a system of this size. Figure 3.13 shows that the QGS-based $\boldsymbol{\psi tc}$ method requires more iterations compared to the NR method and Matlab's Fsolve for UEP computation, as expected. Figure 3.13 also indicates that the QGS-based $\boldsymbol{\psi tc}$ method usually requires more iterations compared to the exact $\boldsymbol{\psi tc}$ method. The number of iterations is slightly reduced when the QGS-based $\boldsymbol{\psi tc}$ method is used as a starter for the NR method. The Continuous NR method requires the largest number of iterations

for all the contingencies.

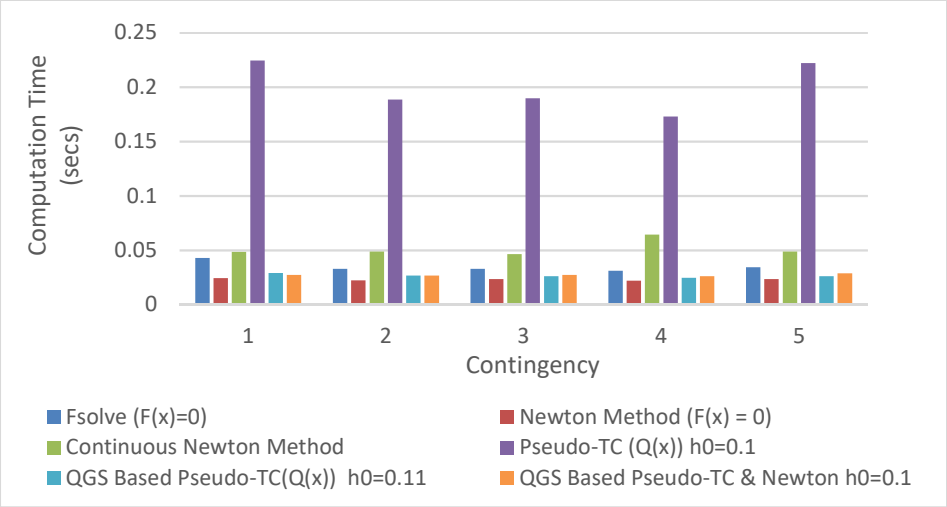

Figure 3.12 Comparison of the CUEP computation time (secs) for the structure- preserving model of the WSCC 9-bus 3-machine system for Fsolve (F(x)=0), Newton's method (F(x)=0), the Continuous Newton method, the exact $\boldsymbol{\psi}$tc method (Q(x)), the QGS-based $\boldsymbol{\psi}$tc method, and the QGS-based $\boldsymbol{\psi tc}$ method combined with the NR method.

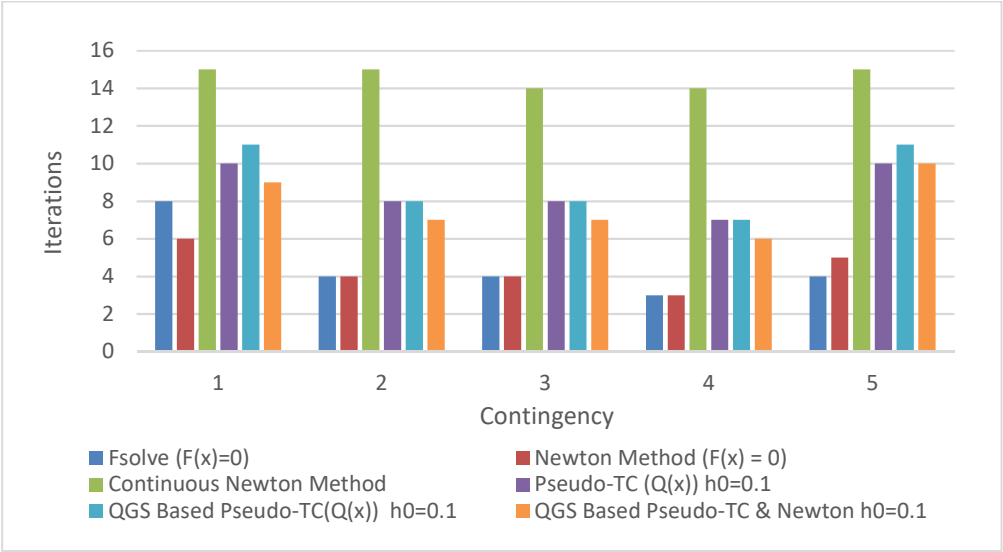

Figure 3.13 Comparison of the number of iterations for CUEP computation for the structure-preserving model of the WSCC 9-bus 3-machine system for Fsolve (F(x)=0), Newton's method (F(x)=0), the Continuous Newton method, the $\boldsymbol{\psi}$tc method (Q(x)), the QGS-based $\boldsymbol{\psi tc}$ method, and the QGS-based $\boldsymbol{\psi tc}$ method combined with the NR method.

3.4.2 The IEEE 145-Bus 50-Machine System with the Classical Generator Model

The proposed method is also tested on the IEEE 145-bus 50-machine system for CUEP computations. The test is done for the structure-preserving power system model with the classical generator model and constant impedance load model. A uniform damping of $\lambda = 0.5$ is assumed and the simulation is done in the Center of Inertia (COI) reference framework. The resulting system of equations is as shown in (3.15) – (3.23). An initial time step, the same as in the previous study, is used. Table 3.2 shows the list of 9 contingencies used in the test.

Figure 3.14 compares the computation time needed in CUEP evaluations for all 9 contingencies using Matlab's Fsolve, the NR method, the Continuous NR method, the exact $\boldsymbol{\psi tc}$ method, the QGS-based $\boldsymbol{\psi tc}$, and the QGS-based $\boldsymbol{\psi tc}$ combined with the NR method. The chart shows that the computational speed advantage of the QGS-based $\boldsymbol{\psi tc}$ over the exact $\boldsymbol{\psi tc}$ method and the Continuous NR method increases significantly for a larger system. A closer look at the graph shows that, by using the QGS-based $\boldsymbol{\psi tc}$ method, we improve the UEP computational speed by 136 times on average compared to the exact $\boldsymbol{\psi tc}$ method. We can achieve a better average computational speed at 155 times the speed of the exact $\boldsymbol{\psi tc}$ method when the QGS-based $\boldsymbol{\psi tc}$ method is combined with the NR method. Figure 3.15 shows that the QGS-based $\boldsymbol{\psi tc}$ method is about 4 times faster compared to the Continuous NR method and 2 times slower than the NR method. Figure 3.15 show that the computational speed of the Matlab's Fsolve is on the average faster than the QGS-based $\boldsymbol{\psi tc}$ method but slower than the combination of the QGS-based $\boldsymbol{\psi tc}$ method and the NR method for this numerical example.

Table 3.2 Contingency List of the IEEE 145-bus 50-machine System

Contingency Number	Fault Bus	Tripped Branch	
		From Bus	To Bus
1	6	7	6
2	72	59	72
3	116	115	116
4	100	100	72
5	91	91	75
6	112	112	69
7	101	101	73
8	6	6	1
9	59	59	103

Figure 3.16 show that combining the QGS-based $\boldsymbol{\psi tc}$ and the NR methods generally leads to a decrease in the number of iterations required for a UEP computation. The number of iterations required by the QGS-based $\boldsymbol{\psi tc}$ method is either the same or less than that required by the exact $\boldsymbol{\psi tc}$ method. The chart also shows that the Continuous NR method requires the greatest number of iterations for all the contingencies in this study, as was the case in the WSCC 9-bus 3-machine system case study.

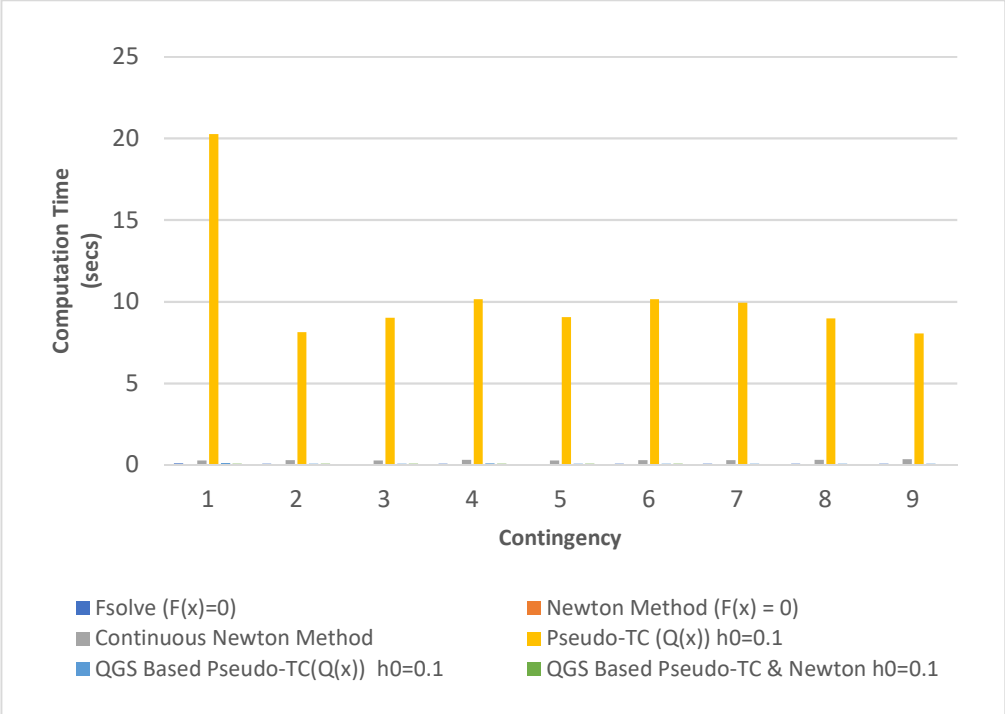

Figure 3.14 Comparison of the CUEP computation time (secs) for the structure-preserving model of the IEEE 145-bus 50-machine system for Fsolve (F(x)=0), Newton's method (F(x)=0), the Continuous Newton method, the exact $\boldsymbol{\psi}$tc method (Q(x)), the QGS-based $\boldsymbol{\psi}$tc method, and the QGS-based $\boldsymbol{\psi tc}$ method combined with the NR method.

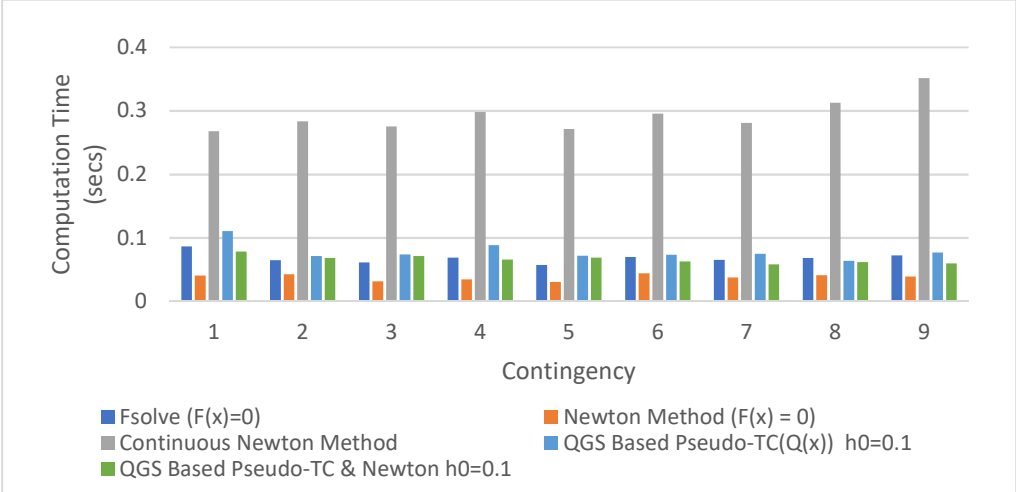

Figure 3.15 Comparison of the CUEP computation time (secs) for the structure-preserving model of the IEEE 145-bus 50-machine system for Fsolve (F(x)=0), Newton's method (F(x)=0), the Continuous Newton method, the QGS-based $\boldsymbol{\psi tc}$ method, and the QGS-based $\boldsymbol{\psi tc}$ method combined with the NR method.

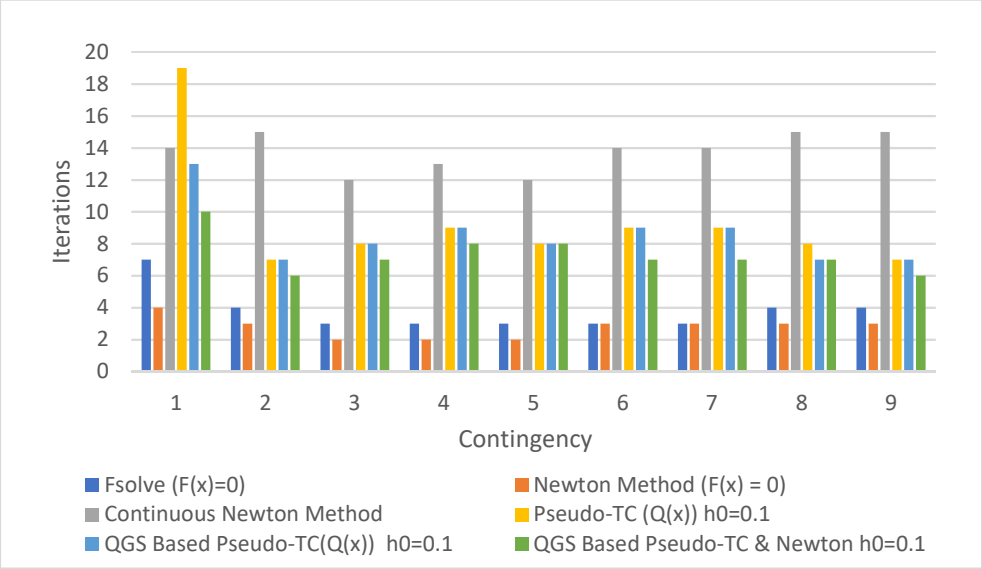

Figure 3.16 Comparison of the number of iterations for the CUEP computation for the structure-preserving model of the IEEE 145-bus 50-machine system for Fsolve (F(x)=0), Newton's method (F(x)=0), the Continuous Newton method, the exact ψtc method (Q(x)), the QGS-based ψtc method, and the QGS-based ψtc method combined with the NR method.

3.5 Integrated Solution Algorithm

The numerical studies show that the proposed method improves the robustness and accuracy of UEP computations at the expense of speed. The computation time required by the exact form of the ψtc method is significantly larger than that of the NR method, especially for a large system due to increases in the number of iterations required for convergence, the QGS transformation, and the need to construct two Jacobians in each iteration. From the results in Figures 3.1-3.16, it is observed that exploiting the structure of the QGS system (2.3) by using an appropriate approximation of the Jacobian (2.11) can improve the speed of the QGS-based ψtc method significantly while preserving most of the expansion of the UEP convergence region gained from the QGS transformation. The gain in speed from the approximation of the Jacobian increases

significantly with an increase in system size, as shown by the results in Figure 3.12 and Figures 3.14-3.15. Even though the difference in computation times of the QGS-based $\boldsymbol{\psi tc}$ method and the NR method increases with an increase in system size, the computational performance of the proposed method can be improved by combining it with the NR method.

Figures 3.1-3.11 also show the expansion of the convergence region by the QGS transformation, making it possible for the initial guesses to be farther away from the UEP compared to the NR method or the Continuous NR method. Hence, less computational work is required to determine an appropriate initial guess.

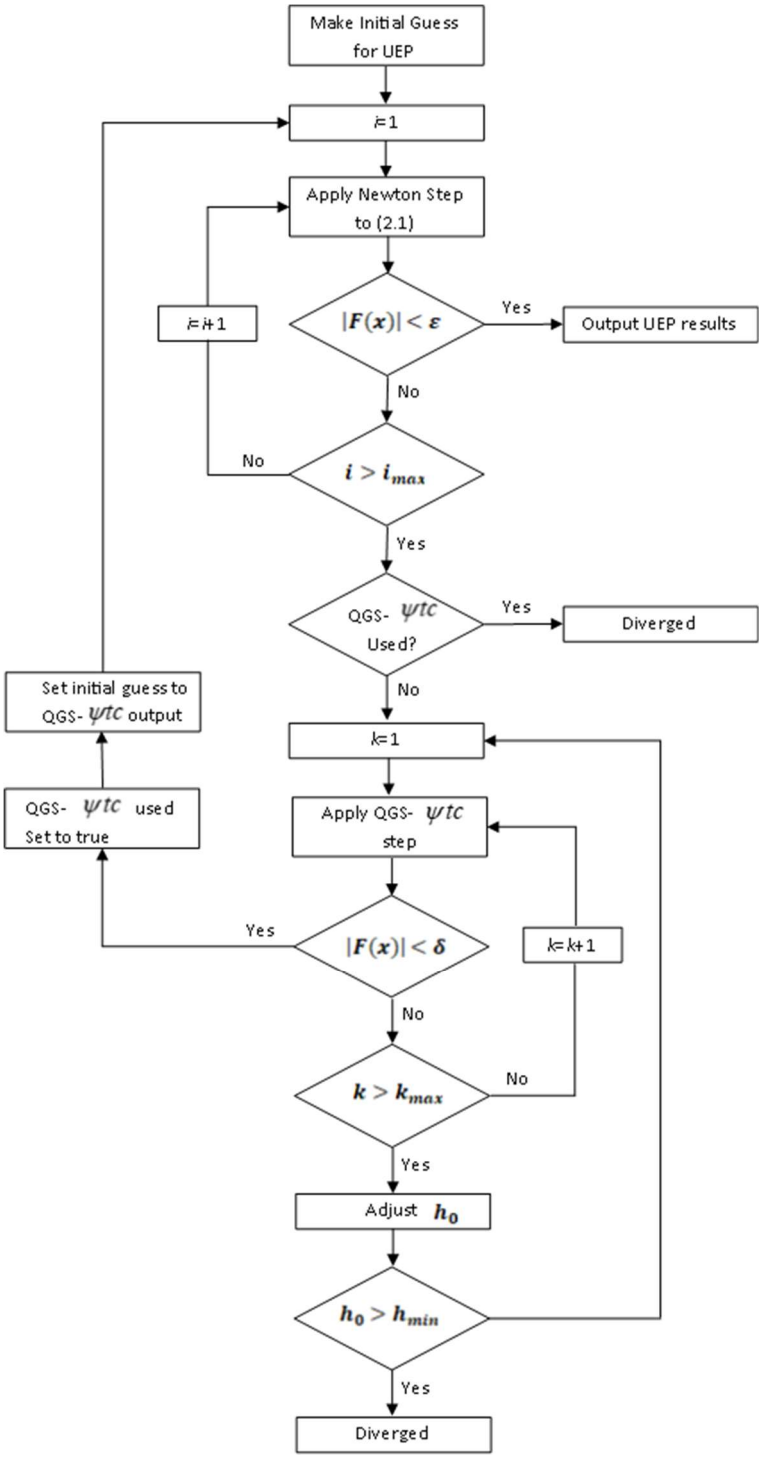

Figure 3.17 Flowchart for the implementation of the proposed integrated Algorithm.

As the QGS-based $\boldsymbol{\psi tc}$ method is slower than the NR method, we recommend using the QGS-based $\boldsymbol{\psi tc}$ method when the NR method fails. We therefore propose the algorithm illustrated in Figure 3.17. Given an initial point the proposed algorithm can be described as follows:

Step 1: Starting from the initial point, we apply Newton's method to (2.1) for UEP computation.

Step 2: If Newton's method does not converge, say after 6 to 10 iterations, we terminate Newton's method and move to step 3. In a direct method for a transient stability application, we can check for accuracy of the UEP by numerically checking whether the UEP is on the stability boundary of an SEP [1].

Step 3: Starting from the initial point, we apply the QGS-based $\boldsymbol{\psi tc}$ method until we reach a pre-defined convergence threshold, δ, after which we switch back to the Newton method. If the QGS-based $\boldsymbol{\psi tc}$ fails, exceeds max iteration k_{max}, start over with a smaller initial step size, h_0. If, after several attempts, the QGS-based $\boldsymbol{\psi tc}$ does not converge to a reasonable UEP, use the Continuous NR method or the original $\boldsymbol{\psi tc}$ method.

3.6 Conclusion

The proposed QGS-based $\boldsymbol{\psi tc}$ method has been tested on three systems, network-reduction model of the WSCC 9-Bus 3-Machine system, the structure-preserving model of the WSCC 9-Bus 3-Machine system, and the structure-preserving model of the IEEE 145-Bus 50-Machine system. The main advantages of this method are: 1) the method has a larger connected convergence region than the NR method and thus, the initial guess does not have to be as close to the equilibrium point as the NR method requires; 2) the method is more stable and hence, more robust than the Newton's method for UEP computations since the convergence region is connected; 3) it is faster than simply applying the exact pseudo-transient continuation method to the QGS; and 4) the proposed inexact

pseudo-transient continuation method can only converge to solutions of the original system, unlike the exact pseudo-transient continuation method. The applicability of the proposed method to improving the robustness of CUEP computations in the direct method for transient stability analysis of power systems will be investigated in future work.

CHAPTER 4

Application of the BCU Method to Power Systems with Nonlinear Excitation System Models

4.1 Introduction

In previous work, the BCU method has been developed and implemented for the following power system models: network-reduction power system models, represented by ordinary differential equations (ODE) [1,117]; structure-preserving models with classical generators [1]; and structure-preserving detailed generators with first order linear excitation systems and ZIPM load models [39]. Thus, there is no BCU implementation for power system models with detailed nonlinear or higher order linearized excitation system models.

With the limiting effect of the existing transmission infrastructure and the increase in uncertainty due to the proliferation of intermittent renewable energy sources, it is important that the transient stability analysis and control of power systems be performed with speed and accuracy. The celerity, degree of stability, and control information provided by the BCU method makes it an ideal candidate for online power system transient stability assessment and control. It is therefore important to extend the capabilities of the BCU method to more detailed power system models. The strong theoretical foundation of the BCU method makes it readily applicable to any power system model when the static and dynamic properties are satisfied. The work by [40] on lossless numerical energy functions for structure-preserving power systems with detailed generator

models, including exciters, and by [1] on numerical energy functions for lossy structure-preserving power system models, provides a good foundation for an extension of the BCU method to detailed power systems with nonlinear or higher order linear exciter models.

The development of energy-based direct methods for the transient stability analysis of power systems has been ongoing since the late 1940s [1-2,8,14-28,37-44,46,47,48]. Most of the effort has been focused on the construction of analytical energy functions and the fast and robust determination of critical points. Over these past decades, huge progress has been made in the construction of analytical energy functions for lossless, network-reduction [37,45], and structure-preserving power system models [1,40,43,44]. There has also been good progress on the construction of numerical energy functions for lossy structure-preserving models [1,46].

Work on the fast and robust computation of the controlling UEP [1,14,18,10,25,28] has progressed significantly, leading to practical commercial applications like the TEPCO-BCU software package [1,8]. Progress has also been made on extending the direct method to dynamic load models [39], among others. Despite the significant amount of effort and the progress made in this area, there has not been much effort in extending the direct method to detailed power system models with detailed high order excitation system models except for the work done by the authors in [40], where the author applies the PEBS method to a lossless structure-preserving power system model with detailed generators and excitation systems, and the energy function work done with power systems using linear excitation models [38]. The work done by [40], although similar to the work in this chapter, focuses on lossless structure-preserving power system models and uses the PEBS method, which is known to fail frequently due to its heuristic nature.

In this chapter, we focus on extending the capability of the BCU method to lossy structure-preserving power system models with detailed nonlinear or higher order linear excitation system models.

The main contributions of this work are:

1) the construction of a numerical energy function for lossy structure-preserving power system models with detailed nonlinear excitation system, and

2) the extension and implementation of the BCU method for lossy structure-preserving power system models with detailed nonlinear or higher order linear excitation system models.

In section 4.2, we present a generic problem formulation for power systems under contingencies. We then present a general form of the excitation system model in section 4.3 followed by a brief overview of the BCU method in section 4.4. Section 4.5 presents the construction of a numerical energy function for a lossy structure-preserving power system model with detailed fourth order generator models and high order nonlinear excitation system models. In section 4.6, we present a compact representation of the original power system dynamic model and the artificial dimension reduced-state model based on the constructed energy function and then present a numerical example in section 4.7. The conclusions on the work in this chapter are then presented in section 4.8.

4.2 Problem Formulation

In this chapter, we work with disturbances or events that include a fault. The power system transient stability problem due to a fault disturbance can be represented mathematically as follows:

Pre-Fault System:

$$\left(x_s^{pre}, y_s^{pre}\right), t < t_f \tag{4.1}$$

Fault System:

$$\dot{x} = f_F(x, y)$$

$$0 = g_F(x, y)$$

$$t_f \leq t < t_{cl} \tag{4.2}$$

Post-Fault System:

$$\dot{x} = f(x, y)$$

$$0 = g(x, y)$$

$$t \geq t_{cl} \tag{4.3}$$

where the variables x and y are vectors of the dynamic and static variables of the system, respectively, and u is a vector of control variables like bus voltage magnitudes [1]. In the pre-fault system, the system is operating at a known stable state (x_s^{pre}, y_s^{pre}). When a fault occurs at time t_f, there is a structural change in the power system, leading to a new system represented mathematically by the DAE in (4.2). This system is called the fault-on system. During the fault on period, the structure of the network topology can change many times as the system reacts to the fault with switching actions. When the fault is finally cleared at time t_{cl}, we get the new system represented by (4.3), the post-fault system. The differential equations in (4.2) and (4.3) correspond

to electromechanical dynamics, like generator dynamics, and electrical dynamics, like excitation system dynamics. The algebraic equations correspond to the power balance equations. If (4.3) has an asymptotically stable equilibrium point $\left(x_s(t), y_s(t)\right)$, then the transient stability problem is whether or not a trajectory starting at the post-fault initial state denoted as $(x(t), y(t))$, the point at which the fault is cleared, will converge to the post-fault SEP $\left(x_s(t), y_s(t)\right)$.

4.3 Excitation System Model

The excitation system is an important component of synchronous generators that provides the needed field current. The excitation system also performs voltage control by varying the magnitude of the field current supplied to the generator.

A generic qth order excitation system model can be represented by the system of differential equations in (4.4):

$$T\dot{E_x} = A_E E_x + bV + l$$

$$T \in R^{q\times q}, \quad E_x \in R^{q\times 1}, \quad A_E \in R^{q\times q}, \quad b \in R^{q\times 1}, \quad l \in R^{q\times 1}. \tag{4.4}$$

where E_x is a vector of the excitation system variables, T is a positive definite diagonal matrix of time constants, A_E is a matrix function of the excitation system variables, V is also a vector of the terminal voltage of the attached synchronous generator, and b and l are constant vectors. The system of equations is purely electrical, with feedback loops, and limiters for some of the excitation system variables. The excitation system model is mostly a linear model, except for the saturation component, which can be modeled as an exponential or quadratic function. Some of the variables of the excitation system such as the field voltage are bounded because of the effects of upper and

lower limiters. The EXAC3 and IEEE Type I exciter models are examples of 5th and 3rd order exciter models, respectively [119, 108]. For more details about the excitation system models, see [4, 119]. Figure 4.1 shows a block diagram of the IEEE Type I excitation system.

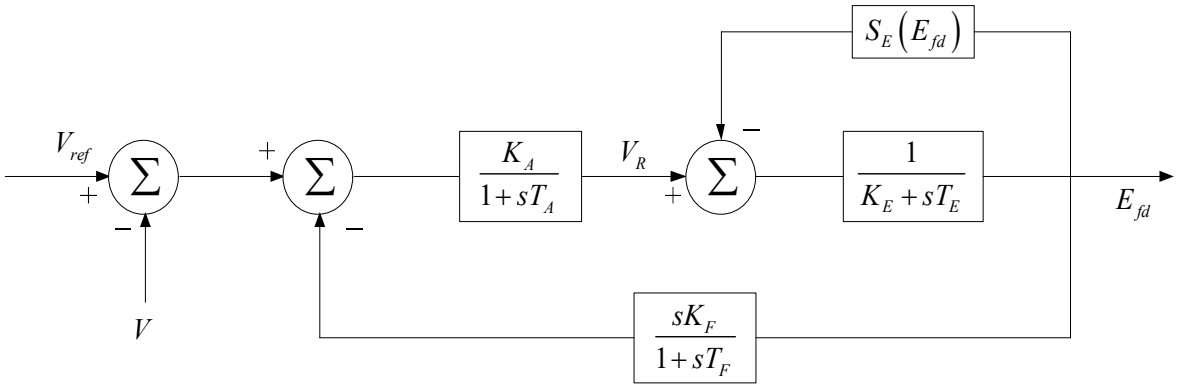

Figure 4.1 Block diagram of IEEE Type I Exciter model [108]

where E_x, A_E, b and l are defined as shown below and $S_E(E_{fd})$ is an exponential function of E_{fd} [108].

$$E_x = \begin{bmatrix} E_{fd} \\ R_f \\ V_R \end{bmatrix},\ A_E = \begin{bmatrix} K_E + S_E(E_{fd}) & 0 & 1 \\ \frac{K_F}{T_F} & -1 & 0 \\ \frac{-K_A K_F}{T_F} & K_A & -1 \end{bmatrix},\ T = \begin{bmatrix} T_E \\ T_F \\ T_A \end{bmatrix},\ b = \begin{bmatrix} 0 \\ 0 \\ -K_A \end{bmatrix}, \text{ and } l = \begin{bmatrix} 0 \\ 0 \\ K_A V_{ref} \end{bmatrix}$$

4.4 The BCU Method

The boundary of the stability region-based controlling unstable equilibrium method (BCU) is a theory-based methodology for computing the controlling unstable equilibrium point (CUEP) of a post-fault system. It was proposed and developed by the authors in [117].

A lossy structure-preserving power system model can be represented by the generalized DAE system shown in (4.5). U is a function that corresponds to the potential energy component of the energy function of system (4.5), and g represents the network conductance. The variables u and w are instantaneous variables, and the variables x, y, and z are state variables. In this work, it is assumed that the network conductance is sufficiently small to ensure the existence of a numerical energy function [1].

$$0 = -\frac{\partial U}{\partial u}(u, w, x, y) + g_1(u, w, x, y)$$

$$0 = -\frac{\partial U}{\partial w}(u, w, x, y) + g_2(u, w, x, y)$$

$$T\dot{x} = -\frac{\partial U}{\partial x}(u, w, x, y) + g_3(u, w, x, y)$$

$$\dot{y} = z$$

$$M\dot{z} = -Dz - \frac{\partial U}{\partial y}(u, w, x, y) + g_4(u, w, x, y) \tag{4.5}$$

If all the equilibrium points of (4.5) are hyperbolic, an energy function (analytical or numerical) exists for (4.5), and (4.5) satisfies the transversality conditions [1], then the artificial dimension reduced-state system in (4.6) can be constructed such that it satisfies the following static and dynamic properties [1].

$$0 = -\frac{\partial U}{\partial u}(u, w, x, y) + g_1(u, w, x, y)$$

$$0 = -\frac{\partial U}{\partial w}(u, w, x, y) + g_2(u, w, x, y)$$

$$T\dot{x} = -\frac{\partial U}{\partial x}(u, w, x, y) + g_3(u, w, x, y)$$

$$M\dot{y} = -\frac{\partial U}{\partial y}(u, w, x, y) + g_4(u, w, x, y) \tag{4.6}$$

Static Properties [1,39]:

(S1): The equilibrium points of the dimension reduced-state model (4.6) and the equilibrium points of the original model (4.5) share the same locations.

(S2): The equilibrium points of the dimension reduced-state model (4.6) and the equilibrium points of the original model (4.5) are of the same type.

Dynamic Properties [1,39]:

(D1): An energy function U exists for the artificial dimension reduced-state model (4.6).

(D2): An equilibrium point $(\bar{u}, \bar{w}, \bar{x}, \bar{y})$ is on the stability boundary $\partial A(u_s, w_s, x_s, y_s)$ of the SEP (u_s, w_s, x_s, y_s) of the dimension reduced-state model (4.5) if and only if the equilibrium point $(\bar{u}, \bar{w}, \bar{x}, \bar{y}, 0)$ is on the stability boundary $\partial A(u_s, w_s, x_s, y_s, 0)$ of the SEP $(u_s, w_s, x_s, y_s, 0)$ of the original model (4.5).

(D3): It is computationally easier to detect the exit-point of the projection of the fault-on trajectory $\big(u(t), w(t), x(t), y(t)\big)$. Thus, the point at which a projection of the fault-on

trajectory $\big(u(t), w(t), x(t), y(t)\big)$ intersects the stability boundary $\partial A(u_s, w_s, x_s, y_s)$ of the SEP (u_s, w_s, x_s, y_s) of the dimension reduced-state model (4.6).

With a dimension reduced-state model that satisfies these conditions, the CUEP for a fault of the original system (4.5) can be computed by computing the CUEP of an associated dimension reduced-state system (4.6) [1].

Implementation of the BCU Method [1,39]

Step 1: Construct an energy function for the original system (4.5). The energy function can be analytic $E(u, w, x, y, z)$ in the case of a lossless network reduction model or numerical $E_{num}(u, w, x, y, z)$ in the case of lossy network-reduction and structure-preserving models. For the work in this thesis, we use numerical energy functions.

Step 2: Compute the post-fault SEP of the original system (4.5).

Step 3: Find the exit point of the projected sustained fault-on trajectory in the post-fault system. This point corresponds to the point of first maximum potential energy along the projected sustained fault-on trajectory.

Step 4: Using the stability boundary following procedure, find the initial guess of the CUEP, the minimum gradient point [1], in the dimension reduced-state system (4.6). See [1] for details on the minimum gradient point and the stability boundary following procedure.

Step 5: Starting from the minimum gradient point in the dimension reduced-state system (4.6), compute the CUEP using the integrated solutions algorithm proposed in section 3.5 of Chapter 3.

Step 6: Compute the critical energy value at the CUEP and the energy at the time the fault is cleared for the fault contingency understudy using the constructed numerical energy function.

Step 7: Compare the critical energy to the energy at the time the fault is cleared. If the critical energy is greater, the post-fault system is stable; otherwise, the post-fault system might be unstable.

4.5 Construction of a Numerical Energy Function

In this section, we are going to construct a numerical energy function for a lossy structure-preserving power system model with a detailed generator and nonlinear excitation system. The first integral principle [1] will be used in the construction of the numerical energy function. We will start by defining the DAE system with which we will be working.

4.5.1 Lossy Structure-Preserving Model with a Detailed Nonlinear Excitation System

The lossy structure-preserving model with a detailed non-linear excitation system is a DAE system comprised of swing equations, rotor dynamics equations, excitation system dynamic equations, and network balance algebraic equations. We are going to work with the following notations: We have a total of m buses, with buses $1,\ldots,n$ being generator buses, and buses $n+1,\ldots,m$ being load buses. The generator model used in this work will be the two-axis 4^{th} order generator dynamic model. We will neglect the dynamics of the governor control system, which will be considered in future research work. We also assume there are no limiters on the excitation system variables.

Two-axis 4th order generator dynamics for $i = 1, \ldots . n$ generators.

$$\dot{\delta}_i = \omega_i$$

$$M_i \dot{\omega}_i = P_{mi} - D_i \omega_i - E'_{di} I_{di} - E'_{qi} I_{qi} - \left(X'_{qi} - X'_{di}\right) I_{di} I_{qi}$$

$$T'_{doi} \dot{E}'_{qi} = -E'_{qi} - (X_{di} - X'_{di}) I_{di} + E_{fdi}$$

$$T'_{qoi} \dot{E}'_{di} = -E'_{di} + \left(X_{qi} - X'_{qi}\right) I_{qi} \tag{4.7}$$

where

$$I_{di} = \frac{E'_{qi} - V_i \cos(\delta_i - \theta_i)}{X'_{di}}$$

$$I_{qi} = \frac{-E'_{di} + V_i \sin(\delta_i - \theta_i)}{X'_{qi}}$$

qth order excitation system dynamics for $i = 1, \ldots . n$ generators

$$T \dot{E_x} = A_E E_x + bV + l$$

$$T \in R^{q \times q}, \qquad E_x \in R^{q \times 1}, \qquad A_E \in R^{q \times q}, \qquad b \in R^{q \times 1}, \qquad l \in R^{q \times 1}. \tag{4.8}$$

For generator buses for $i = 1, \ldots . n$

$$V_i e^{j\theta_i} \left(I_{di} - j I_{qi}\right) e^{-j\left(\delta_i - \frac{\pi}{2}\right)} + P_{Li}(V_i) + j Q_{Li}(V_i) = \sum_{k=1}^{m} V_i V_k Y_{ik} e^{j(\theta_i - \theta_k - \alpha_{ik})} \tag{4.9}$$

For load buses for $i = n + 1, \ldots . m$

$$P_{Li}(V_i) + j Q_{Li}(V_i) = \sum_{k=1}^{m} V_i V_k Y_{ik} e^{j(\theta_i - \theta_k - \alpha_{ik})} \tag{4.10}$$

δ_i is the rotor angle of machine i, ω_i is the angular velocity of machine i, M_i is the moment of inertia of machine i, D_i is the damping coefficient of machine i, P_{m_i} is the mechanical power of machine i, E'_{di} is the direct axis internal voltage of machine i, E'_{qi} is the quadrature axis internal voltage of machine i, X'_{di} is the direct axis transient reactance of machine i, X'_{qi} is the quadrature axis transient reactance of machine i, X_{di} is the direct axis synchronous reactance of machine i, X_{qi} is the quadrature axis synchronous reactance of machine i, T'_{doi} is the direct axis transient open-circuit time constant of machine i, T'_{qoi} is the quadrature axis transient open-circuit time constant of machine i, P_{Li} is the real load demand at bus i, Q_{Li} is the reactive load demand at bus i, $Y_{ik}e^{j\alpha_{ik}} = G_{ik} + jB_{ik}$ is the network admittance, V_i is the voltage magnitude at bus i, and θ_i is the voltage angle at bus i.

The construction of an energy function for the system of equations above, (4.7) – (4.10), involves the derivation of a function that is monotonically decreasing along trajectories of the system. To construct this function, we will decompose the energy function into five components (4.11). A component relating to the kinetic energy of the machine swing equations W_k, a component relating to the potential energy of the machine swing equations U_{Swing}, a component for the potential energy of the rotor equations U_{Rotor}, a component related to the potential energy of the network equations U_{PF}, and finally, a component for representing the potential energy of the excitation system equations $U_{Exciter}$. The first three components have already been derived in [1, 43]. In the next section, we will focus on the derivation of the exciter component using the first integral method.

$$E_{Total} = W_k + U_{Swing} + U_{PF} + U_{Rotor} + U_{Exciter} \tag{4.11}$$

4.5.2 A Numerical Energy Function for the q[th] Order Nonlinear Excitation Model

In the application of the first integral method to the construction of the exciter component of the energy function for (4.7) – (4.10), we start by taking the dot product of (4.8) and $\dot{E}_{x_i}$ for $i = 1, \ldots . n$. where $\dot{E}_{x_i}$ is the vector of the time derivative of the excitation system variables.

$$T_i \dot{E}_{x_i} . \dot{E}_{x_i} = A_E E_{x_i} . \dot{E}_{x_i} + b_i V_i . \dot{E}_{x_i} + l_i . \dot{E}_{x_i} \tag{4.12}$$

By taking the summation over *n* of the path integral of (4.12), the first integral terms of the excitation system dynamics can be obtained.

$$\sum_{i=1}^{n} \int \left(T \dot{E}_{x_i} . \dot{E}_{x_i} \right) dt = \sum_{i=0}^{n} \int \left(A_E E_{x_i} . \dot{E}_{x_i} + bV . \dot{E}_{x_i} + l . \dot{E}_{x_i} \right) dt \tag{4.13}$$

$$\sum_{i=1}^{n} \int \left(T \dot{E}_{x_i} . \dot{E}_{x_i} \right) dt - \sum_{i=0}^{n} \int \left(A_E E_{x_i} . \dot{E}_{x_i} + bV . \dot{E}_{x_i} + l . \dot{E}_{x_i} \right) dt = 0 \tag{4.14}$$

From (4.14), we now have these two new energy terms, which are analytical and path-dependent terms.

$$U_{new1}^{Exciter} = \sum_{i=1}^{k} \int \left(T \dot{E}_{x_i} . \dot{E}_{x_i} \right) dt \tag{4.15}$$

$$U_{new2}^{Exciter} = - \sum_{i=0}^{k} \int \left(A_E E_{x_i} . \, dE_{x_i} + bV . dE_{x_i} + l . dE_{x_i} \right) \tag{4.16}$$

$$U_{Exciter} = U_{new1}^{Exciter} + U_{new2}^{Exciter} \tag{4.17}$$

With these new energy function terms, we have our $U_{Exciter}$ component of the energy function for the lossy structure-preserving energy function with a detailed excitation system model. We can now express the energy function as shown in (4.11) [1].

4.6 Derivation of the BCU Dimension Reduced-State Model

The DAE system for the lossy structure-preserving power system with a nonlinear excitation model can be represented in the canonical form as shown in (4.18).

$$0 = -\frac{\partial}{\partial \theta_i} \boldsymbol{U}_{Exciter}(\delta, \theta, V, E'_q, E'_d, E_x) + g_1(\delta, \theta, V, E'_q, E'_d, E_x)$$

$$0 = -\frac{1}{V_i}\frac{\partial}{\partial V_i} \boldsymbol{U}_{Exciter}(\delta, \theta, V, E'_q, E'_d, E_x) + g_2(\delta, \theta, V, E'_q, E'_d, E_x)$$

$$\dot{\delta}_i = \omega_i$$

$$M_i \dot{\omega}_i = -D\omega - \frac{\partial}{\partial \delta_i} \boldsymbol{U}_{Exciter}(\delta, \theta, V, E'_q, E'_d, E_x) + g_3(\delta, \theta, V, E'_q, E'_d, E_x)$$

$$0 = -\frac{\partial}{\partial E'_{qi}} \boldsymbol{U}_{Exciter}(\delta, \theta, V, E'_q, E'_d, E_x) + g_4(\delta, \theta, V, E'_q, E'_d, E_x)$$

$$0 = -\frac{\partial}{\partial E'_{di}} \boldsymbol{U}_{Exciter}(\delta, \theta, V, E'_q, E'_d, E_x) + g_5(\delta, \theta, V, E'_q, E'_d, E_x)$$

$$0 = -\frac{\partial}{\partial E_{x_i}} \boldsymbol{U}_{Exciter}(\delta, \theta, V, E'_q, E'_d, E_x) + g_6(\delta, \theta, V, E'_q, E'_d, E_x) \tag{4.18}$$

Equation (4.19) shows the dimension reduced-state system for the system in (4.18). If (4.18) has only hyperbolic equilibrium points, satisfies the transversality condition, and the transfer conductance is sufficiently small, then the artificial dimension reduced-state system will satisfy the static and dynamic properties presented in section 4.4. Thus, with the energy function and the dimension reduced-state model, we can now apply the BCU method to the lossy structure-preserving power system model with a detailed excitation system for transient stability analysis.

$$0 = -\frac{\partial}{\partial \theta_i}\boldsymbol{U}_{Exciter}\left(\delta, \theta, V, E'_q, E'_d, E_x\right) + g_1\left(\delta, \theta, V, E'_q, E'_d, E_x\right)$$

$$0 = -\frac{1}{V_i}\frac{\partial}{\partial V_i}\boldsymbol{U}_{Exciter}\left(\delta, \theta, V, E'_q, E'_d, E_x\right) + g_2\left(\delta, \theta, V, E'_q, E'_d, E_x\right)$$

$$\dot{\delta}_i = -\frac{\partial}{\partial \delta_i}\boldsymbol{U}_{Exciter}\left(\delta, \theta, V, E'_q, E'_d, E_x\right) + g_3\left(\delta, \theta, V, E'_q, E'_d, E_x\right)$$

$$0 = -\frac{\partial}{\partial E'_{qi}}\boldsymbol{U}_{Exciter}\left(\delta, \theta, V, E'_q, E'_d, E_x\right) + g_4\left(\delta, \theta, V, E'_q, E'_d, E_x\right)$$

$$0 = -\frac{\partial}{\partial E'_{di}}\boldsymbol{U}_{Exciter}\left(\delta, \theta, V, E'_q, E'_d, E_x\right) + g_5\left(\delta, \theta, V, E'_q, E'_d, E_x\right)$$

$$0 = -\frac{\partial}{\partial E_{x_i}}\boldsymbol{U}_{Exciter}\left(\delta, \theta, V, E'_q, E'_d, E_x\right) + g_6\left(\delta, \theta, V, E'_q, E'_d, E_x\right) \tag{4.19}$$

4.7 BCU Method for Detailed Model

In this section, we apply the BCU method to the detailed lossy power system model with nonlinear excitation models. To do that, we must show that equations (4.18) and (4.19) satisfy the static and dynamic properties presented in section 4.4.

We adopt the seven-step process proposed in [1] to show that equations (4.18) and (4.19) satisfy the static properties (S1) and (S2), and the dynamic properties (D1) and (D2). Figure 4.2 shows a pictorial illustration of the seven-step process. In this section we will present how the seven-step process applies to the detailed lossy power system model with nonlinear excitation system models and refer readers to [1] for the details of the seven-step process. The seven-step process establishes that for a generic structure-preserving power system model if the equilibrium points are hyperbolic, the transversality condition is satisfied, and the transfer conductance are sufficiently small then (4.18) and (4.19) will satisfy static properties (S1) and (S2), and dynamic properties (D1) and (D2).

4.7.1 Application of the Seven-step Process to Detailed Model

If the detailed lossy power system model with nonlinear excitation models has hyperbolic equilibrium points, satisfies the transversality condition, and has a sufficiently small transfer conductance, then we can show that (4.18) and (4.19) will satisfy static properties (S1) and (S2) and dynamic properties (D1) and (D2) using the following steps.

Step 1 and 7: In these two steps based on the static property and dynamic property theorems in [1, page 291 - 292], we can prove that for sufficiently small values of $\varepsilon_1, \varepsilon_2, \varepsilon_3, \varepsilon_4$, and ε_5, the system pairs (4.27) and (4.26), and (4.20) and (4.21) satisfy static and dynamic properties like (S1), (S2), and (D2), respectively. That is, in each system pair the systems share the same equilibrium points, the shared equilibrium points are of the same types, and the systems have the same equilibrium points defining their stability boundaries.

Step 2 and 6: In these two steps based on the persistence property theorems in [1, page 290] we can prove that for sufficiently small transfer conductance the system pairs (4.26) and (4.25), and

(4.21) and (4.22) satisfy static and dynamic properties (S1), (S2), and (D2), respectively. That is in each system pair the systems share the same equilibrium points, the shared equilibrium points are of the same types, and the systems have the same equilibrium points defining their stability boundaries.

$$0 = -\frac{\partial}{\partial \theta_i}\boldsymbol{U}_{Exciter}\left(\delta, \theta, V, E'_q, E'_d, E_x\right) + g_1\left(\delta, \theta, V, E'_q, E'_d, E_x\right)$$

$$0 = -\frac{1}{V_i}\frac{\partial}{\partial V_i}\boldsymbol{U}_{Exciter}\left(\delta, \theta, V, E'_q, E'_d, E_x\right) + g_2\left(\delta, \theta, V, E'_q, E'_d, E_x\right)$$

$$\dot{\delta}_i = \omega_i$$

$$M_i\dot{\omega}_i = -D\omega - \frac{\partial}{\partial \delta_i}\boldsymbol{U}_{Exciter}\left(\delta, \theta, V, E'_q, E'_d, E_x\right) + g_3\left(\delta, \theta, V, E'_q, E'_d, E_x\right)$$

$$0 = -\frac{\partial}{\partial E'_{qi}}\boldsymbol{U}_{Exciter}\left(\delta, \theta, V, E'_q, E'_d, E_x\right) + g_4\left(\delta, \theta, V, E'_q, E'_d, E_x\right)$$

$$0 = -\frac{\partial}{\partial E'_{di}}\boldsymbol{U}_{Exciter}\left(\delta, \theta, V, E'_q, E'_d, E_x\right) + g_5\left(\delta, \theta, V, E'_q, E'_d, E_x\right)$$

$$0 = -\frac{\partial}{\partial E_{x_i}}\boldsymbol{U}_{Exciter}\left(\delta, \theta, V, E'_q, E'_d, E_x\right) + g_6\left(\delta, \theta, V, E'_q, E'_d, E_x\right) \qquad (4.20)$$

Step 3: In this step since the machine speed variable ω is completely decoupled from the rest of the system and based on the static and dynamic properties theorems in [1, page 290] we can prove that the system pair (4.25) and (4.24), satisfy static and dynamic properties like (S1), (S2), and (D2) respectively. That is the systems share the same equilibrium points, the shared equilibrium points are of the same types, and the systems have the same equilibrium points defining their stability boundaries.

$$\varepsilon_1\dot{\theta}_i = -\frac{\partial}{\partial\theta_i}\boldsymbol{U}_{Exciter}\left(\delta,\theta,V,E'_q,E'_d,E_x\right) + g_1\left(\delta,\theta,V,E'_q,E'_d,E_x\right)$$

$$\varepsilon_2\dot{V}_i = -\frac{1}{V_i}\frac{\partial}{\partial V_i}\boldsymbol{U}_{Exciter}\left(\delta,\theta,V,E'_q,E'_d,E_x\right) + g_2\left(\delta,\theta,V,E'_q,E'_d,E_x\right)$$

$$\dot{\delta}_i = \omega_i$$

$$M_i\dot{\omega}_i = -D\omega - \frac{\partial}{\partial\delta_i}\boldsymbol{U}_{Exciter}\left(\delta,\theta,V,E'_q,E'_d,E_x\right) + g_3\left(\delta,\theta,V,E'_q,E'_d,E_x\right)$$

$$\varepsilon_3\dot{E}'_{qi} = -\frac{\partial}{\partial E'_{qi}}\boldsymbol{U}_{Exciter}\left(\delta,\theta,V,E'_q,E'_d,E_x\right) + g_4\left(\delta,\theta,V,E'_q,E'_d,E_x\right)$$

$$\varepsilon_4\dot{E}'_{di} = -\frac{\partial}{\partial E'_{di}}\boldsymbol{U}_{Exciter}\left(\delta,\theta,V,E'_q,E'_d,E_x\right) + g_5\left(\delta,\theta,V,E'_q,E'_d,E_x\right)$$

$$\varepsilon_5\dot{E}_{x_i} = -\frac{\partial}{\partial E_i}\boldsymbol{U}_{Exciter}\left(\delta,\theta,V,E'_q,E'_d,E_x\right) + g_6\left(\delta,\theta,V,E'_q,E'_d,E_x\right) \qquad (4.21)$$

Step 4 and 5: In these two steps based on the static properties and dynamic properties theorems in [1, page 288-289] we can prove that if $\boldsymbol{U}_{Exciter}$ is constant at all equilibrium points, that is $\boldsymbol{U}_{Exciter}$ is the potential energy component of an energy function for (4.22), (4.23), and (4.24), and all the equilibrium points on the stability boundary of (4.23) satisfy the transversality condition, then the system pair (4.22) and (4.24) satisfy static and dynamic properties (S1), (S2), and (D2) respectively. That is the systems (4.22) and (4.24) share the same equilibrium points, the shared equilibrium points are of the same types, and the systems have the same equilibrium points defining their stability boundaries.

$$\varepsilon_1\dot{\theta}_i = -\frac{\partial}{\partial\theta_i}\boldsymbol{U}_{Exciter}\left(\delta,\theta,V,E'_q,E'_d,E_x\right)$$

$$\varepsilon_2\dot{V}_i = -\frac{1}{V_i}\frac{\partial}{\partial V_i}\boldsymbol{U}_{Exciter}\left(\delta,\theta,V,E'_q,E'_d,E_x\right)$$

$$\dot{\delta}_i = \omega_i$$

$$M_i\dot{\omega}_i = -D\omega - \frac{\partial}{\partial\delta_i}\boldsymbol{U}_{Ex} \qquad \left(\delta,\theta,V,E'_q,E'_d,E_x\right)$$

$$\varepsilon_3 E'_{qi} = -\frac{\partial}{\partial E'_{qi}}\boldsymbol{U}_{Exciter}\left(\delta,\theta,V,E'_q,E'_d,E_x\right)$$

$$\varepsilon_4 E'_{qi} = -\frac{\partial}{\partial E'_{di}}\boldsymbol{U}_{Exciter}\left(\delta,\theta,V,E'_q,E'_d,E_x\right)$$

$$\varepsilon_5\dot{E}_{x_i} = -\frac{\partial}{\partial E_i}\boldsymbol{U}_{Exciter}\left(\delta,\theta,V,E'_q,E'_d,E_x\right) \tag{4.22}$$

From the seven-step process summarized above and the static and dynamic relationship theorems in [1, page 293 – 294] we can conclude that system (4.18) and (4.19) satisfy the static conditions (S1), (S2), and (D2). The system (4.18) and (4.19) also satisfy the dynamic condition (D2) based on the seven-step process since $\boldsymbol{U}_{Exciter}$ will be the energy function of (4.19) if all the required assumptions for the seven-step process are satisfied.

$$\varepsilon_1\dot{\theta}_i = -\frac{\partial}{\partial\theta_i}\boldsymbol{U}_{Exciter}\left(\delta,\theta,V,E'_q,E'_d,E_x\right) + g_1\left(\delta,\theta,V,E'_q,E'_d,E_x\right)$$

$$\varepsilon_2\dot{V}_i = -\frac{1}{V_i}\frac{\partial}{\partial V_i}\boldsymbol{U}_{Exciter}\left(\delta,\theta,V,E'_q,E'_d,E_x\right) + g_2\left(\delta,\theta,V,E'_q,E'_d,E_x\right)$$

$$\dot{\delta}_i = (1-\lambda)\omega_i - \lambda \frac{\partial}{\partial \delta_i} \boldsymbol{U}_{Exciter}\left(\delta, \theta, V, E'_q, E'_d, E_x\right)$$

$$M_i \dot{\omega}_i = -D\omega - (1-\lambda) \frac{\partial}{\partial \delta_i} \boldsymbol{U}_{Exciter}\left(\delta, \theta, V, E'_q, E'_d, E_x\right)$$

$$\varepsilon_3 E'_{qi} = -\frac{\partial}{\partial E'_{qi}} \boldsymbol{U}_{Exciter}\left(\delta, \theta, V, E'_q, E'_d, E_x\right) + g_4\left(\delta, \theta, V, E'_q, E'_d, E_x\right)$$

$$\varepsilon_4 E'_{qi} = -\frac{\partial}{\partial E'_{di}} \boldsymbol{U}_{Exciter}\left(\delta, \theta, V, E'_q, E'_d, E_x\right) + g_5\left(\delta, \theta, V, E'_q, E'_d, E_x\right)$$

$$\varepsilon_5 \dot{E}_{x_i} = -\frac{\partial}{\partial E_i} \boldsymbol{U}_{Exciter}\left(\delta, \theta, V, E'_q, E'_d, E_x\right) + g_6\left(\delta, \theta, V, E'_q, E'_d, E_x\right) \qquad (4.23)$$

$$\varepsilon_1 \dot{\theta}_i = -\frac{\partial}{\partial \theta_i} \boldsymbol{U}_{Exciter}\left(\delta, \theta, V, E'_q, E'_d, E_x\right)$$

$$\varepsilon_2 \dot{V}_i = -\frac{1}{V_i} \frac{\partial}{\partial V_i} \boldsymbol{U}_{Exciter}\left(\delta, \theta, V, E'_q, E'_d, E_x\right)$$

$$\dot{\delta}_i = -\frac{\partial}{\partial \delta_i} \boldsymbol{U}_{Exciter}\left(\delta, \theta, V, E'_q, E'_d, E_x\right)$$

$$M_i \dot{\omega}_i = -D\omega$$

$$\varepsilon_3 E'_{qi} = -\frac{\partial}{\partial E'_{qi}} \boldsymbol{U}_{Exc} \quad \left(\delta, \theta, V, E'_q, E'_d, E_x\right)$$

$$\varepsilon_4 E'_{qi} = -\frac{\partial}{\partial E'_{di}} \boldsymbol{U}_{Exciter}\left(\delta, \theta, V, E'_q, E'_d, E_x\right)$$

$$\varepsilon_5 \dot{E}_{x_i} = -\frac{\partial}{\partial E_i} \boldsymbol{U}_{Exciter}\left(\delta, \theta, V, E'_q, E'_d, E_x\right) \qquad (4.24)$$

$$\varepsilon_1 \dot{\theta}_i = -\frac{\partial}{\partial \theta_i} \boldsymbol{U}_{Exciter}\left(\delta, \theta, V, E'_q, E'_d, E_x\right)$$

$$\varepsilon_2 \dot{V}_i = -\frac{1}{V_i}\frac{\partial}{\partial V_i} \boldsymbol{U}_{Exciter}\left(\delta, \theta, V, E'_q, E'_d, E_x\right)$$

$$\dot{\delta}_i = -\frac{\partial}{\partial \delta_i} \boldsymbol{U}_{Exciter}\left(\delta, \theta, V, E'_q, E'_d, E_x\right)$$

$$\varepsilon_3 E'_{qi} = -\frac{\partial}{\partial E'_{qi}} \boldsymbol{U}_{Exciter}\left(\delta, \theta, V, E'_q, E'_d, E_x\right)$$

$$\varepsilon_4 E'_{qi} = -\frac{\partial}{\partial E'_{di}} \boldsymbol{U}_{Exciter}\left(\delta, \theta, V, E'_q, E'_d, E_x\right)$$

$$\varepsilon_5 \dot{E}_{x_i} = -\frac{\partial}{\partial E_i} \boldsymbol{U}_{Exciter}\left(\delta, \theta, V, E'_q, E'_d, E_x\right) \tag{4.25}$$

$$\varepsilon_1 \dot{\theta}_i = -\frac{\partial}{\partial \theta_i} \boldsymbol{U}_{Exciter}\left(\delta, \theta, V, E'_q, E'_d, E_x\right) + g_1\left(\delta, \theta, V, E'_q, E'_d, E_x\right)$$

$$\varepsilon_2 \dot{V}_i = -\frac{1}{V_i}\frac{\partial}{\partial V_i} \boldsymbol{U}_{Exciter}\left(\delta, \theta, V, E'_q, E'_d, E_x\right) + g_2\left(\delta, \theta, V, E'_q, E'_d, E_x\right)$$

$$\dot{\delta}_i = -\frac{\partial}{\partial \delta_i} \boldsymbol{U}_{Exciter}\left(\delta, \theta, V, E'_q, E'_d, E_x\right) + g_3\left(\delta, \theta, V, E'_q, E'_d, E_x\right)$$

$$\varepsilon_3 E'_{qi} = -\frac{\partial}{\partial E'_{qi}} \boldsymbol{U}_{Exciter}\left(\delta, \theta, V, E'_q, E'_d, E_x\right) + g_4\left(\delta, \theta, V, E'_q, E'_d, E_x\right)$$

$$\varepsilon_4 E'_{qi} = -\frac{\partial}{\partial E'_{di}} \boldsymbol{U}_{Exciter}\left(\delta, \theta, V, E'_q, E'_d, E_x\right) + g_5\left(\delta, \theta, V, E'_q, E'_d, E_x\right)$$

$$\varepsilon_5 \dot{E}_{x_i} = -\frac{\partial}{\partial E_i} \boldsymbol{U}_{Exciter}\left(\delta, \theta, V, E'_q, E'_d, E_x\right) + g_6\left(\delta, \theta, V, E'_q, E'_d, E_x\right) \tag{4.26}$$

$$0 = -\frac{\partial}{\partial \theta_i} \boldsymbol{U}_{Exciter}\left(\delta, \theta, V, E'_q, E'_d, E_x\right) + g_1\left(\delta, \theta, V, E'_q, E'_d, E_x\right)$$

$$0 = -\frac{1}{V_i}\frac{\partial}{\partial V_i} \boldsymbol{U}_{Exciter}\left(\delta, \theta, V, E'_q, E'_d, E_x\right) + g_2\left(\delta, \theta, V, E'_q, E'_d, E_x\right)$$

$$\dot{\delta}_i = -\frac{\partial}{\partial \delta_i} \boldsymbol{U}_{Exciter}\left(\delta, \theta, V, E'_q, E'_d, E_x\right) + g_3\left(\delta, \theta, V, E'_q, E'_d, E_x\right)$$

$$0 = -\frac{\partial}{\partial E'_{qi}} \boldsymbol{U}_{Exciter}\left(\delta, \theta, V, E'_q, E'_d, E_x\right) + g_4\left(\delta, \theta, V, E'_q, E'_d, E_x\right)$$

$$0 = -\frac{\partial}{\partial E'_{di}} \boldsymbol{U}_{Exciter}\left(\delta, \theta, V, E'_q, E'_d, E_x\right) + g_5\left(\delta, \theta, V, E'_q, E'_d, E_x\right)$$

$$0 = -\frac{\partial}{\partial E_{x_i}} \boldsymbol{U}_{Exciter}\left(\delta, \theta, V, E'_q, E'_d, E_x\right) + g_6\left(\delta, \theta, V, E'_q, E'_d, E_x\right) \tag{4.27}$$

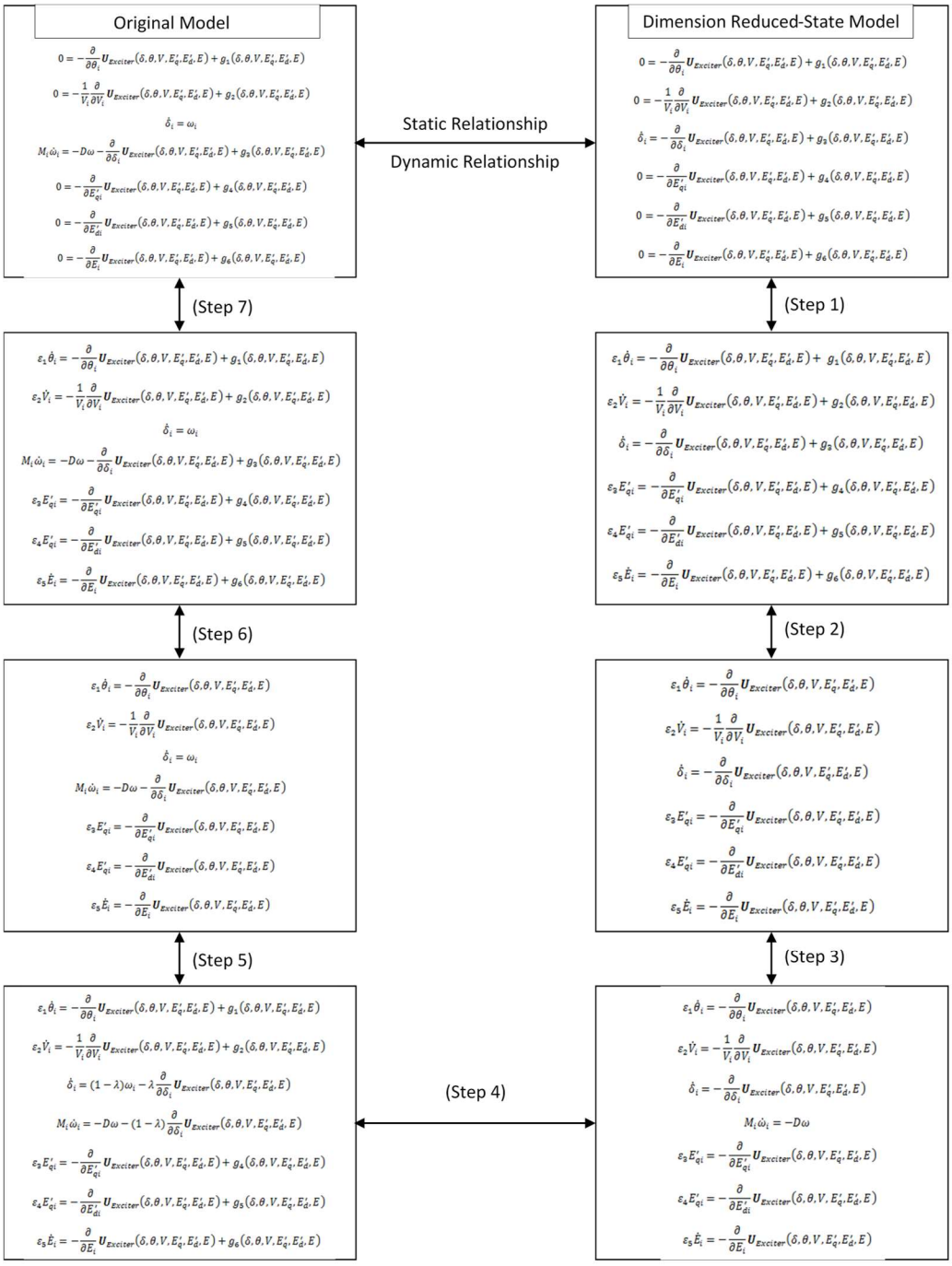

Figure 4.2 A seven-step procedure to show static properties S(1) and S(2) and dynamic properties D(1) and D(2) between system (4.20) and system (4.21).

4.7.2 Discussion of Static and Dynamic Properties

We will now discuss the conditions necessary for the satisfaction of the static and dynamic properties. We will first present arguments to support the satisfaction of hyperbolicity by the equilibrium points of the detailed lossy power system model with nonlinear excitation models based on the existence of an energy function and generally observations of power system dynamics. We will also present arguments to support the satisfaction of the transversality conditions and propose a technique to handle situations where the transversality condition is not satisfied. Finally, we will present an argument why the transfer conductance of the lossy power system model with nonlinear excitation models can be considered as being sufficiently small.

- Hyperbolicity of Equilibrium points: If an energy function exists for the power system model then limit cycles or any other types of strange attractors do not exist in the system since the energy function is monotonically decreasing along a trajectory. Thus, the existence of a limit cycle or strange attractor for a system with an energy function is a contradiction. If limit cycles or strange attractors do not exist, then it means that the equilibrium points for the power system model do not have purely imaginary eigenvalues and are hyperbolic. Coupled with the observation that, generally, in most practical power system dynamic models the condition for hyperbolicity of equilibrium points are satisfied for well damped power system cases, we can assume that in most cases the equilibrium points of the detailed lossy power system model with nonlinear excitation models will be hyperbolic if an energy function exist for the model.
- Transversality Condition: The satisfaction of the transversality condition by the power system dynamic model is difficult to prove, but it has been observed that the power system model generally satisfies the transversality condition [1]. However, in cases where the transversality condition is not satisfied for a contingency of the detailed lossy power system model with

nonlinear excitation models, the group-based BCU approach can be applied in its transient stability assessment [1].

- Transfer Conductance: The transfer conductance of the power system has been found to be sufficiently small in commercial applications of the TEPCO-BCU method to other structure-preserving models [1,8]. Since the transfer conductance values will not change for this detailed model, it is safe to assume that the transfer conductance will be sufficiently small for static properties (S1) and (S2), and dynamic properties (D1) and (D2) to hold for the detailed lossy power system model with nonlinear excitation models.

With the static properties (S1) and (S2), and dynamic properties (D1) and (D2) satisfied. We, must show that the dynamic property (D3) is true for equations (4.18) and (4.19). This can be proven by presenting the existence of a numerical scheme for finding the exit point in the dimension reduced-state model. Two numerical schemes described in [1] can be applied to the case of the detailed lossy power system model with nonlinear excitation system models. The exit point can be either approximated by the point where the projected fault-on trajectory reaches its first local maximum potential energy or approximated by the point where the vector field along projected fault-on trajectory changes direction. Since these numerical methods can find the point of intersection between the projected fault-on trajectory and the stability boundary of the post-fault system, dynamic property (D3) is satisfied.

4.7.3 Application of BCU Method to Detailed Model

If the static and dynamic properties are satisfied by (4.18) and (4.19), then the BCU implementation scheme presented in section 4.4 can be extended to detailed power systems with nonlinear excitation system models. The BCU implementation scheme for the detailed power systems with nonlinear excitation system models is as shown below.

Step 1: Construct the numerical energy function $E_{Total}(\omega, \delta, \theta, V, E'_q, E'_d, E_x)$ derived in section 4.5 for the original system (4.18). For a power system model using a fourth order generator model with a q[th] order exciter model as in (4.7) – (4.8) the numerical energy function will be the sum of (4.17), (4.28), (4.29), (4.30), and (4.31) as defined by (4.11) [43]. Since (4.17) adds up to zero, the numerical energy function for a power system comprising a fourth order generator model with a q[th] order exciter model is equivalent to the energy function of the power system without the exciter model.

For the case of the WSCC 9-bus 3-machine system with a third order IEEE type I excitation system represented by the system of equations (4.32) Figure 4.4 shows a plot of the numerical energy function values along the stable trajectory shown in Figure 4.3. We observe that the energy function value is monotonically decreasing along the trajectory.

$$W_k = \sum_{i=1}^{n} \frac{1}{2} M_i i \tag{4.28}$$

$$U_{Swing} = -\oint_{\delta_{0_i}}^{\delta_i} P_{m_i}\, d\delta_i \tag{4.29}$$

$$\begin{aligned} U_{PF} = \sum_{i}^{m} \left[-\frac{1}{2} B_{ii} V_i^2 - \frac{1}{2} \sum_{j \neq i}^{m} V_i V_j B_{ij} \cos\theta_{ij} \right] + \sum_{i=1}^{m} \oint_{\theta_{0_i}}^{\theta_i} G_{ii} V_i^2 \, d\theta_i \\ + \sum_{i=1}^{m} \sum_{j \neq i}^{m} G_{ij} \oint_{(V_{0_i}, \theta_{0_i})}^{(V_i, \theta_i)} \left[V_i V_j \cos\theta_{ij} d\theta_i + V_j \sin\theta_{ij}\, dV_i \right] \\ + \sum_{i=1}^{m} \left[\oint_{\theta_{0_i}}^{\theta_i} P_{L_i}\, d\theta_i + \oint_{V_{0_i}}^{V_i} \left(\frac{Q_{L_i}}{V_i} \right) dV_i \right] \end{aligned} \tag{4.30}$$

$$U_{Rotor} = -\oint_{V_{q0_i}}^{V_{q_i}} I_{di}\, dV_{q_i} + \oint_{V_{d0_i}}^{V_{d_i}} I_{qi}\, dV_{d_i} \tag{4.31}$$

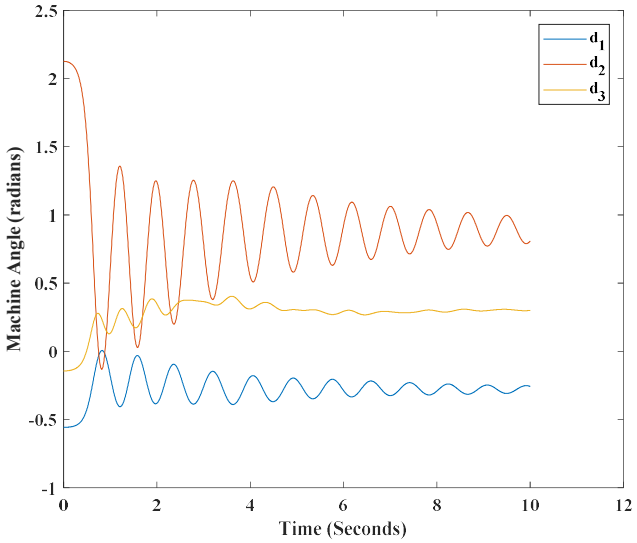

Figure 4.3 Swing curves of a stable trajectory for a WSCC 9-bus 3-machine system with a third order IEEE Type I exciter model.

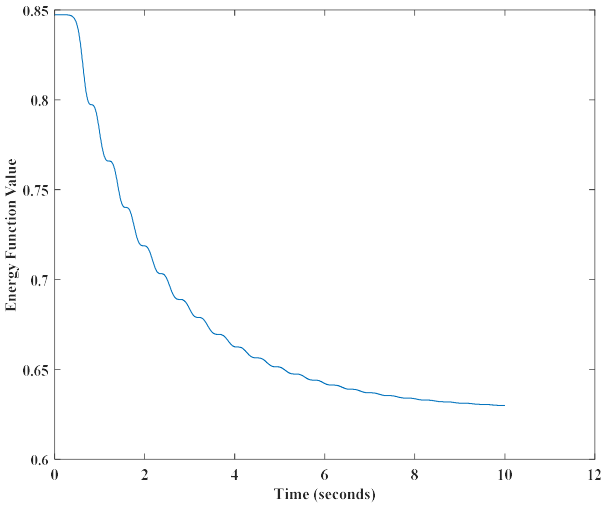

Figure 4.4 Energy function value along a stable trajectory for a WSCC 9-bus 3-machine system with a third order IEEE Type I exciter model.

Step 2: Compute the post-fault SEP $\left(0, \delta_s, \theta_s, V_s, E'_{q,s}, E'_{d,s}, E_{x,s}\right)$ of the original system (4.18) using an algebraic solver.

Step 3: Find the exit point $\left(\delta_e, \theta_e, V_e, E'_{q,e}, E'_{d,e}, E_{x,e}\right)$ of the projected sustained fault-on trajectory in the post-fault system which can be approximated by using the point corresponding to the first local maximum potential energy along the projected fault-on trajectory or by the point where the vector field along the projected fault-on trajectory changes sign.

Step 4: Using the stability boundary following procedure find the initial guess of the CUEP, known as the minimum gradient point (MGP) [1], in the dimension reduced-state system (4.19). In the implementation of stability boundary following procedure the post-fault system is integrated starting from the exit point $\left(\delta_e, \theta_e, V_e, E'_{q,e}, E'_{d,e}, E_{x,e}\right)$ for 4 to 5 time steps. If the resulting post-fault trajectory reaches a local minimum along the boundary, then that minimum is used as the MGP, otherwise the ray-adjustment method will be used to find a new initial point along the boundary and then the post-fault system will be integrated again in search of the MGP. This procedure will be repeated until a local minimum on the stability boundary is found. The ray-adjustment method comprise of drawing a ray between the current point on the post-fault trajectory and the SEP $\left(\delta_s, \theta_s, V_s, E'_{q,s}, E'_{d,s}, E_{x,s}\right)$ of the dimension reduced-state system, and then moving along the ray until a point corresponding to first local maximum of the system potential energy is found. This point is then set as the new initial point for the search of the MGP.

Step 5: Starting from the minimum gradient point in the dimension reduced-state system (4.19), compute the CUEP $\left(\delta_{cuep}, \theta_{cuep}, V_{cuep}, E'_{q,cuep}, E'_{d,cuep}, E_{x,cuep}\right)$ using the integrated solutions algorithm proposed in section 3.5 of Chapter 3.

Step 6: Compute the critical energy value $E_{cuep} = E\left(\delta_{cuep}, \theta_{cuep}, V_{cuep}, E'_{q,cuep}, E'_{d,cuep}, E_{x,cuep}\right)$ at the CUEP and the energy $E_{cl} = E\left(\omega_{cl}, \delta_{cl}, \theta_{cl}, V_{cl}, E'_{q,cl}, E'_{d,cl}, E_{x,cl}\right)$ at the post-fault initial state $\left(\omega_{cl}, \delta_{cl}, \theta_{cl}, V_{cl}, E'_{q,cl}, E'_{d,cl}, E_{x,cl}\right)$ for the contingency, understudy, using the constructed numerical energy function (4.11).

Step 7: If $E_{cuep} > E_{cl}$, the post-fault system is stable; otherwise, the post-fault system may be unstable.

Numerical examples of the application of the BCU method for detailed lossy power system models with a nonlinear excitation system is presented in the next section.

4.8 Numerical Example

In this section, we present numerical results for simulations performed on a list of 12 contingencies (see Table 4.1) for the lossy structure-preserving model of the WSCC 9-bus 3-machine system using the proposed BCU method for detailed lossy power system models with nonlinear excitation system models. Each generator is represented by the two-axis 4th order model (4.7), with a third order IEEE type I excitation system in (4.32) [108]. The loads are all modeled as constant impedance in these simulation studies.

Nonlinear Exciter models for *i=1,.,3*

$$T_{Ei}\dot{E}_{fdi} = -\left(K_{Ei} + S_{Ei}\left(E_{fdi}\right)\right)E_{fdi} + V_{Ri}$$

$$T_{Fi}\dot{R}_{fi} = -R_{fi} + \frac{K_{Fi}}{T_{Fi}}E_{fdi}$$

$$T_{Ai}\dot{V}_{Ri} = -V_{Ri} + K_{Ai}R_{fi} - \frac{K_{Ai}K_{Fi}}{T_{Fi}}E_{fdi} + K_{Ai}\left(V_{refi} - V_i\right) \tag{4.32}$$

Table 4.1 Contingency List for the WSCC 9-bus 3-machine System

Contingency Number	Fault Bus	Tripped Branch	
		From Bus	To Bus
1	7	8	7
2	8	8	7
3	4	4	6
4	6	4	6
5	8	9	8
6	9	9	8
7	5	7	5
8	7	7	5
9	6	6	9
10	9	6	9
11	4	5	4
12	5	5	4

Table 4.2 shows the list of post-fault SEPs for 6 out of the 12 contingencies where the proposed BCU method worked successfully. Table 4.3 shows the CUEPs computed with the proposed method, BCU method for lossy structure-preserving power system models with nonlinear excitation systems, for each of the 6 contingencies. In Table 4.4, we present a comparison of the CCT estimated with the proposed method and the actual CCT computed from repeated time-domain simulations for the 12 contingencies. The results show that the proposed BCU method is successful for 6 out of the 12 contingencies, giving a conservative estimation of the CCT for four and exact CCT estimations for two contingencies. However, the proposed method failed for the other 6 contingencies. The proposed method either gave optimistic estimations of the CCT, contingencies 7, 9, 11, and 12 or failed to find the CUEP.

Table 4.2 Post-fault SEPs for the WSCC 9-Bus 3-Machine System with a Third Order Nonlinear Excitation System Model

Variable	Contingency 1	Contingency 2	Contingency 3	Contingency 4	Contingency 5	Contingency 6
δ_1	-0.27831	-0.27831	-0.2445	-0.2445	-0.26203	-0.26203
δ_2	0.887233	0.887233	0.689458	0.689458	0.64061	0.64061
δ_3	0.299296	0.299296	0.454328	0.454328	0.69582	0.69582
ω_1	0	0	0	0	0	0
ω_2	0	0	0	0	0	0
ω_3	0	0	0	0	0	0
E'_{q1}	1.065086	1.065086	1.054608	1.054608	1.059449	1.059449
E'_{q2}	0.817774	0.817774	0.806642	0.806642	0.847724	0.847724
E'_{q3}	0.877568	0.877568	0.848382	0.848382	0.759677	0.759677
E'_{d1}	1.51E-21	1.51E-21	4.29E-22	4.29E-22	-2.44E-23	-2.44E-23
E'_{d2}	0.601915	0.601915	0.609378	0.609378	0.581113	0.581113
E'_{d3}	0.53697	0.53697	0.561476	0.561476	0.629397	0.629397
E_{fd1}	1.104092	1.104092	1.076974	1.076974	1.089587	1.089587
E_{fd2}	1.825938	1.825938	1.802746	1.802746	1.894393	1.894393
E_{fd3}	1.612871	1.612871	1.541332	1.541332	1.377526	1.377526
V_{R1}	1.128064	1.128064	1.099391	1.099391	1.112716	1.112716
V_{R2}	1.947741	1.947741	1.918743	1.918743	2.034956	2.034956
V_{R3}	1.690118	1.690118	1.607381	1.607381	1.423282	1.423282
R_{f1}	0.198737	0.198737	0.193855	0.193855	0.196126	0.196126
R_{f2}	0.328669	0.328669	0.324494	0.324494	0.340991	0.340991
R_{f3}	0.290317	0.290317	0.27744	0.27744	0.247955	0.247955
V_1	1.03884	1.03884	1.040273	1.040273	1.039607	1.039607
V_2	1.022717	1.022717	1.024167	1.024167	1.018356	1.018356
V_3	1.013068	1.013068	1.017205	1.017205	1.02641	1.02641
V_4	1.01502	1.01502	1.027715	1.027715	1.021879	1.021879
V_5	0.974497	0.974497	0.997437	0.997437	0.988201	0.988201
V_6	0.997913	0.997913	0.954298	0.954298	1.009065	1.009065
V_7	1.017858	1.017858	1.021709	1.021709	1.006633	1.006633
V_8	0.968073	0.968073	1.005899	1.005899	0.977782	0.977782
V_9	1.006332	1.006332	1.014831	1.014831	1.034933	1.034933
θ_1	-0.33363	-0.33363	-0.30041	-0.30041	-0.31863	-0.31863
θ_2	0.020638	0.020638	-0.19015	-0.19015	-0.19089	-0.19089
θ_3	-0.42356	-0.42356	-0.30565	-0.30565	-0.17571	-0.17571
θ_4	-0.36866	-0.36866	-0.3348	-0.3348	-0.35392	-0.35392
θ_5	-0.33515	-0.33515	-0.38477	-0.38477	-0.39867	-0.39867
θ_6	-0.45589	-0.45589	-0.48992	-0.48992	-0.35878	-0.35878
θ_7	-0.07615	-0.07615	-0.28639	-0.28639	-0.28934	-0.28934
θ_8	-0.56329	-0.56329	-0.35361	-0.35361	-0.35497	-0.35497
θ_9	-0.47189	-0.47189	-0.35336	-0.35336	-0.22216	-0.22216

Table 4.3 CUEPs for the WSCC 9-Bus 3-Machine System with a Third Order Nonlinear Excitation System Model

Variable	Contingency 1	Contingency 2	Contingency 3	Contingency 4	Contingency 5	Contingency 6
δ_1	-0.56006	-0.56006	-0.88002	-0.88002	-0.61873	-0.42078
δ_2	2.138571	2.138571	2.335001	2.335001	2.223858	0.392188
δ_3	-0.14855	-0.14855	1.946743	1.946743	0.130956	2.470837
ω_1	0	0	0	0	0	0
ω_2	0	0	0	0	0	0
ω_3	0	0	0	0	0	0
E'_{q1}	1.213309	1.213309	1.283383	1.283383	1.210407	1.18978
E'_{q2}	0.918612	0.918612	1.001626	1.001626	0.882145	0.957121
E'_{q3}	1.019575	1.019575	1.126208	1.126208	0.981253	0.717994
E'_{d1}	3.67E-23	3.67E-23	-8.69E-23	-8.69E-23	-1.23E-23	1.21E-29
E'_{d2}	0.260386	0.260386	0.250367	0.250367	0.230657	0.489718
E'_{d3}	0.394314	0.394314	0.240526	0.240526	0.420501	0.199027
E_{fd1}	1.487232	1.487232	1.670301	1.670301	1.479864	1.42621
E_{fd2}	3.952698	3.952698	3.804234	3.804234	4.042524	2.129903
E_{fd3}	2.059192	2.059192	3.176424	3.176424	1.76232	4.230271
V_{R1}	1.545821	1.545821	1.757771	1.757771	1.537499	1.477309
V_{R2}	11.15258	11.15258	9.305179	9.305179	12.50986	2.357836
V_{R3}	2.256612	2.256612	4.906762	4.906762	1.868806	16.09487
R_{f1}	0.267702	0.267702	0.300654	0.300654	0.266376	0.256718
R_{f2}	0.711486	0.711486	0.684762	0.684762	0.727654	0.383383
R_{f3}	0.370655	0.370655	0.571756	0.571756	0.317218	0.761449
V_1	1.017952	1.017952	1.007354	1.007354	1.018368	1.021377
V_2	0.562475	0.562475	0.654845	0.654845	0.494611	1.002212
V_3	0.984743	0.984743	0.852236	0.852236	1.004134	0.29283
V_4	0.833015	0.833015	0.745974	0.745974	0.836722	0.862175
V_5	0.526132	0.526132	0.363774	0.363774	0.531245	0.871151
V_6	0.861511	0.861511	0.714142	0.714142	0.873362	0.583514
V_7	0.416047	0.416047	0.488535	0.488535	0.349422	0.962804
V_8	0.91456	0.91456	0.594056	0.594056	0.339408	0.935209
V_9	0.950705	0.950705	0.759442	0.759442	0.983314	0.261357
θ_1	-0.57537	-0.57537	-0.86731	-0.86731	-0.59661	-0.44568
θ_2	1.49574	1.49574	1.817059	1.817059	1.575495	-0.29292
θ_3	-0.67186	-0.67186	1.586779	1.586779	-0.419	1.458129
θ_4	-0.5899	-0.5899	-0.85266	-0.85266	-0.57578	-0.46782
θ_5	-0.42077	-0.42077	-0.66518	-0.66518	-0.45031	-0.50433
θ_6	-0.68971	-0.68971	1.383673	1.383673	-0.58142	-0.38456
θ_7	1.085316	1.085316	1.543207	1.543207	1.064364	-0.39203
θ_8	-0.81248	-0.81248	1.491692	1.491692	0.998736	-0.45766
θ_9	-0.72108	-0.72108	1.520233	1.520233	-0.46172	0.79703

Table 4.4 CCT Comparison (Time-domain vs. BCU) for the WSCC 9-Bus 3-Machine System with a Third Order Nonlinear Excitation System Model

Contingency	Actual CCT Time Domain	Estimated CCT BCU	% Relative Error
1	0.130	0.070	-46.15
2	0.200	0.085	-57.50
3	0.220	0.220	0.00
4	0.295	0.295	0.00
5	0.220	0.120	-45.45
6	0.190	0.065	-65.79
7	0.16	0.23	43.75
8	-	-	-
9	0.23	0.27	18.18
10	-	-	
11	0.215	0.23	6.98
12	0.265	0.3	13.21

To confirm that the CUEP computed with the proposed method is on the stability boundary of the SEP for the 10 contingencies (contingencies 1-7, 9, 11, and 12) where a CUEP was successfully found, we employ the boundary property verification scheme proposed in [1]. The boundary property verification scheme is implemented as follows:

Step 1: Compute the initial point given by (4.33). Where:

- $X^{test} = \left(0, \delta_t, \theta_t, V_t, E'_{q,t}, E'_{d,\mathrm{t}}, E_{fd,\mathrm{t}}, R_{F,t}, V_{R,t}\right)$ is the initial point to be computed for the verification scheme.
- $X_s^{post} = \left(0, \delta_s, \theta_s, V_s, E'_{q,s}, E'_{d,\mathrm{s}}, E_{fd,\mathrm{s}}, R_{F,s}, V_{R,s}\right)$ is the post-fault SEP of the original system.
- $X^{UEP} = \left(0, \delta_{uep}, \theta_{uep}, V_{uep}, E'_{q,\mathrm{uep}}, E'_{d,\mathrm{uep}}, E_{fd,\mathrm{uep}}, R_{F,uep}, V_{R,uep}\right)$ is the UEP computed as the CUEP of the original system for a given contingency.

$$X^{test} = X_s^{post} + 0.99\left(X^{UEP} - X_s^{post}\right) \tag{4.33}$$

Step 2: starting from X^{test}, integrate the post-fault system. If the post-fault trajectory converges to the post-fault SEP, X_s^{post}, then it implies that the computed UEP, X^{UEP}, lies on the stability boundary of the post-fault system. Thus, the boundary property is satisfied.

The results from the boundary property verification scheme for the 10 contingencies are as shown in Figures. 4.5 – 4.11. The figures show that for each of the 10 contingencies a trajectory that starts from an initial point very close to the UEP and lying on a ray joining the computed UEP and the SEP converges to the SEP. Hence, the obtained UEP lies on the stability boundary of the original system.

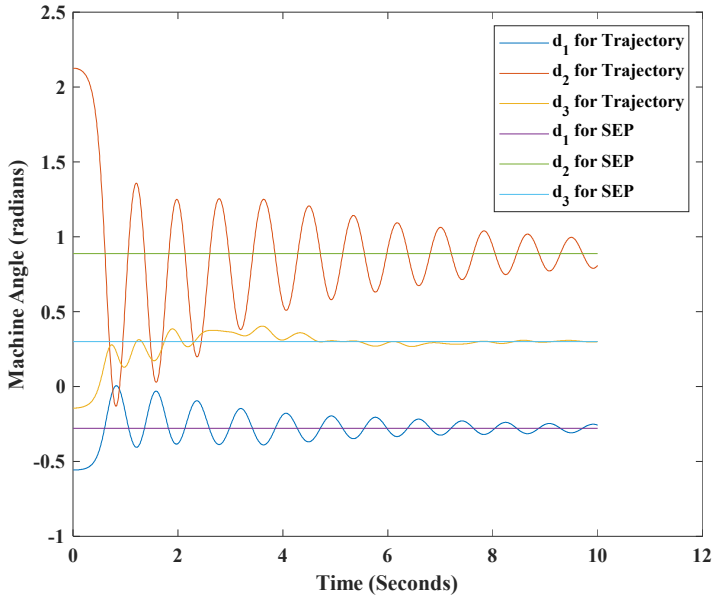

Figure 4.5 Swing curve for the verification of the boundary property of the CUEPs computed for contingencies 1 and 2. The verification applies to the two contingencies since the two contingencies share the same SEP and CUEP. $d_1, d_2,$ and d_3 represents the machine angles of machine 1, 2 and 3, respectively. The test trajectory converges to the SEP, hence, the computed CUEP is on the stability boundary of the SEP.

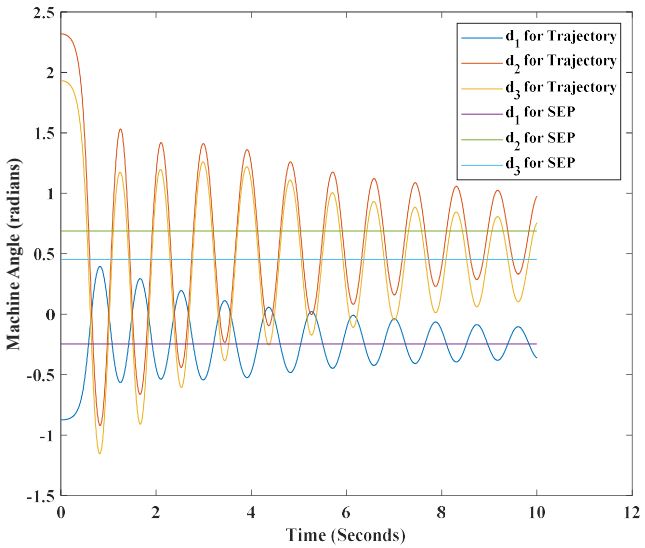

Figure 4.6 Swing curve for the verification of the boundary property of the CUEPs computed for contingencies 3 and 4. The verification applies to the two contingencies since the two contingencies share the same SEP and CUEP. $d_1, d_2,$ and d_3 represents the machine angles of machine 1, 2 and 3, respectively. The test trajectory converges to the SEP, hence, the computed CUEP is on the stability boundary of the SEP.

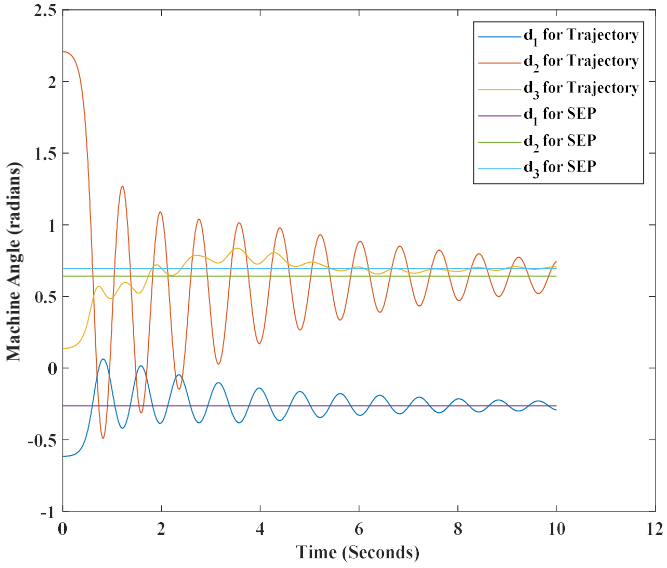

Figure 4.7 Swing curve for the verification of the boundary property of the CUEPs computed for contingency 5. $d_1, d_2,$ and d_3 represents the machine angles of machine 1, 2 and 3, respectively. The test trajectory converges to the SEP, hence, the computed CUEP is on the stability boundary of the SEP.

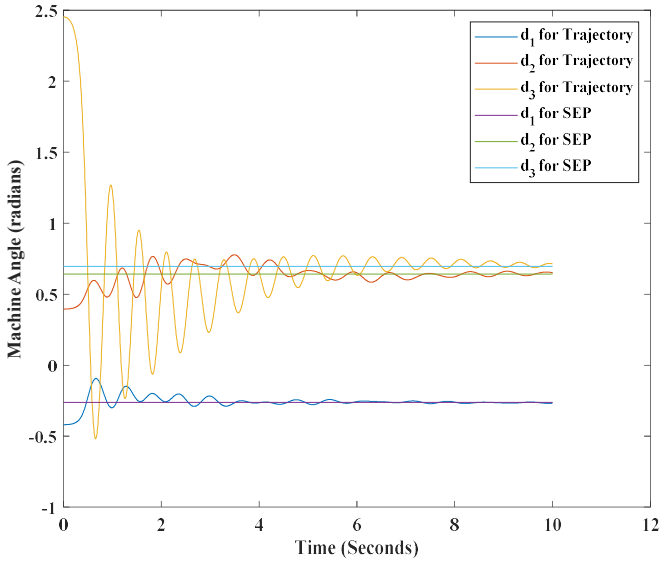

Figure 4.8 Swing curve for the verification of the boundary property of the CUEPs computed for contingency 6. $d_1, d_2,$ and d_3 represents the machine angles of machine 1, 2 and 3, respectively. The test trajectory converges to the SEP, hence, the computed CUEP is on the stability boundary of the SEP.

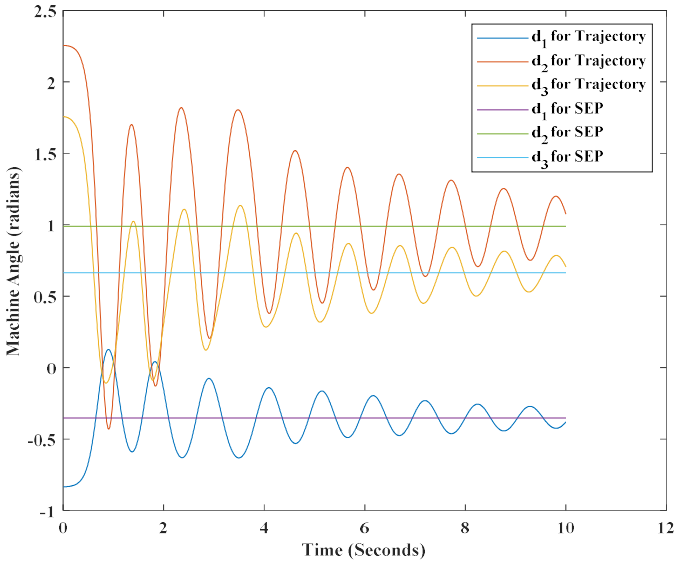

Figure 4.9 Swing curve for the verification of the boundary property of the CUEPs computed for contingency 7. $d_1, d_2,$ and d_3 represents the machine angles of machine 1, 2 and 3, respectively. The test trajectory converges to the SEP, hence, the computed CUEP is on the stability boundary of the SEP.

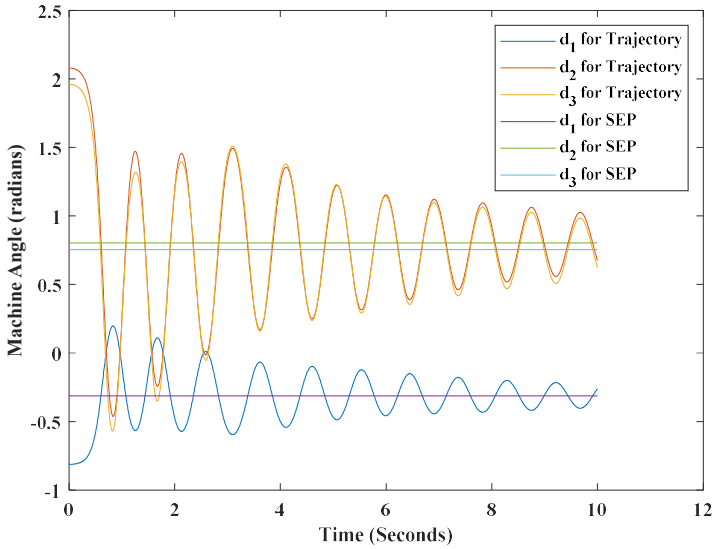

Figure 4.10 Swing curve for the verification of the boundary property of the CUEPs computed for contingency 9. $d_1, d_2,$ and d_3 represents the machine angles of machine 1, 2 and 3, respectively. The test trajectory converges to the SEP, hence, the computed CUEP is on the stability boundary of the SEP.

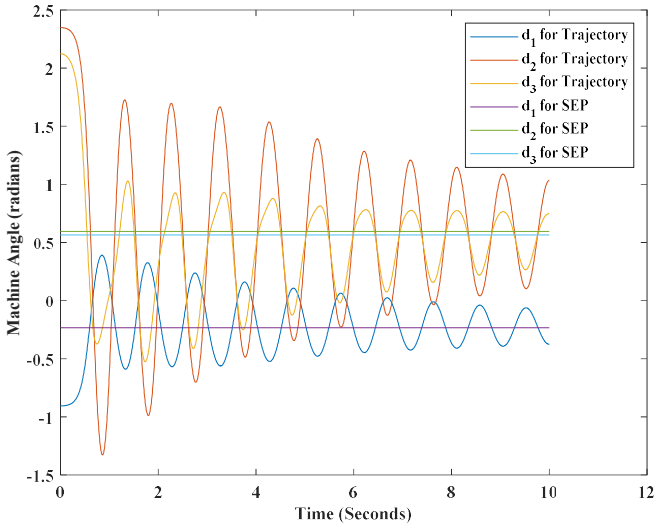

Figure 4.11 Swing curve for the verification of the boundary property of the CUEPs computed for contingencies 11 and 12. $d_1, d_2,$ and d_3 represents the machine angles of machine 1, 2 and 3, respectively. The test trajectory converges to the SEP, hence, the computed CUEP is on the stability boundary of the SEP.

4.9 Conclusions

In this chapter, the BCU method was extended to lossy structure-preserving power system models with nonlinear excitation system models. The general BCU method was presented. A numerical energy function for lossy structure-preserving power system models with detailed exciters was constructed using the first integral scheme. The proposed BCU extension was tested on the lossy structure-preserving model of the WSCC 9-bus 3-machine system with IEEE type I excitation systems. The results show that the extended BCU method gives conservative and accurate estimations of the CCT for some contingencies but also fails sometimes by overestimating the CCT or failing to find the CUEP. The CCT overestimation could be attributed to the fact that a large portion of the numerical energy function is path dependent making it difficult to find an accurate energy function value at the CUEP. The failure to find the CUEP for two contingencies can be attributed to numerical problems during the stability boundary following procedure [1]. Future, work will focus on making the implementation of the proposed method more robust to ensure a high level of accuracy and reliability of the BCU extension to lossy structure-preserving model with nonlinear excitation system models by focusing on constructing a better energy function, and also improving the stability boundary following procedure for lossy structure-preserving model with nonlinear excitation system models.

CHAPTER 5

Dynamics and Transient Stability of Power Systems Post Transmission Switching

5.1 Introduction

In the daily operation of a power systems, network topological changes, transmission switching, are performed either automatically or manually in the transmission network in response to faults or as enhancement control actions. Transmission switching (TS) is the alteration of a power network configuration or line impedance via the change of on/off status of circuit breakers (transmission line switching or bus splitting) or change of tap positions of transformers [106]. Despite the potential adverse static and dynamic effects of transmission switching, it can be used as a control tool to improve static and dynamic performance of a power systems [49, 50]. Transmission switching has also been used as an economic tool in [51–54] to help improve optimal power dispatch. These applications are possible because based on Kirchoff's current law (KVL) transmission switching/network topology changes lead to changes in the direction of power flow in the network, which can lead to improvements in: bus voltages, line currents, system frequency and the cost at which the load demand is met. Changes in network topology can also lead to reduction in line losses, and consequently economic gains for system operators. It should be noted that these changes in flows may have adverse impact on the performance of the transmission network.

Most of the literature work on switching and optimal switching for power system static control and optimization treat switching as a static phenomenon and do not include its transient stability implications in their models except when they are used for transient stability control [55]. This common practice assumes that the existence of an acceptable static solution post-switching implies stability of the post-switching power system. A power system is operating at an acceptable static condition if its power flow solution has voltage magnitudes and angles that are within an acceptable range. Static assessment could also include load margin and thermal limit checks. However, these static assessments alone might not be sufficient for ensuring the stability of a TS event which leads to topological changes altering power flow in the grid. The change in power flow can then change how the synchronous generators participate in the power generation, and hence, can change the generation units' synchronism to the system frequency. Thus, TS can lead to dynamic instability and so switching and optimal switching actions should be performed and properly modeled to reflect their impacts on the dynamic stability of power systems. This chapter studies the dynamics of TS and provides numerical examples of power system scenarios where the system is dynamically unstable, despite its "static stability" after a TS. It will be shown that the frequency of these numerical examples, called counter-examples, increases with increasing loading conditions. This phenomenon will be explained using numerical simulations of shrinking stability region of the post-switching system under heavy loading conditions.

The use of TS for power system control dates to the 1980s [56, 57]. Since then, numerous research studies have been focusing on the development of efficient algorithms for finding optimal TS configurations, and on extensions to more control applications [58]. In [49], TS was employed via a static model for corrective control actions. In [50], TS and generator rescheduling are used to solve steady state security-related problems. TS was used as a control action to reduce overload

and static voltage violations during contingencies in [59]. The authors in [60] also used TS for online voltage stability enhancement. Apart from these security enhancement and contingency analysis applications of TS, there are also economic applications. In [52], the authors introduced the economic concept of transmission capacity bidding under market rules. In [56], the optimal generation dispatch problem is extended to include TS for cost reduction. This study is extended in [53] for a contingency analysis. In [54], the use of TS for mitigating overloads in a security-constrained unit commitment is also investigated. In all of these studies and applications of TS, the models used were purely static with no transient or dynamic constraints except for [61]. In [61], Chen et al. proposed a theoretical method for optimal TS with a transient stability constraint. This general trend of research might suggest that there is a general belief that a static model for TS is sufficient for analyzing the stability of the post-switching system. This chapter provides a theoretical basis as to why it is important to include dynamic constraints in TS control and optimization models by presenting numerical examples of power system cases where a static secure solution after TS does not imply dynamic stability. It also provides numerical evidence of increases in the occurrence of counter-examples (i.e. dynamic instability despite "static stability") in the post-switching system with increasing loading conditions. An explanation for the increase in counter-examples during heavy loading conditions is presented.

In section 5.2, a brief description of the stability region and the convergence region (under a numerical method) of a stable equilibrium point and how they differ from each other is provided. The dynamic model for TS is then presented in section 5.3. Section 5.4 presents numerical simulation results demonstrating conflict between the static and dynamic stability on a modified WSCC 3-machine 9-bus model and the IEEE 145 bus system. In Section 5.5, the increase in the occurrence of disparity in the static and dynamic stability of post-TS systems with an increase in

the system loading condition is demonstrated. The link between the changes in the stability region of the post-switching power system and the increase in the occurrence frequency of the disparity between the static and dynamic stability of post-TS systems under load increase is also analyzed in section 5.5. Finally, we discuss our concluding remarks in section 5.6. The chapter is based on the work published in [115].

5.2 Preliminaries

The stability region or region of attraction $A(X_s)$ of an asymptotically stable equilibrium point (SEP) X_s is defined as $A(X_s) \coloneqq \{X \in R^n : \lim_{t\to\infty} \varphi(t, X) = X_s\}$, shown in equation (1.3).

When computing an equilibrium point, algebraic numerical root finders like the Newton-Raphson method are usually used for celerity instead of time domain simulations. However, these numerical root finders are based on approximations or transformations of the system, mostly linear, and thus, they do not have the same level of accuracy as the higher order time domain simulation. The convergence region of an SEP X_s of an ODE or DAE for a numerical algebraic solver N denoted by $N(X_s)$, defined as the set of initial points that converge to X_s for the numerical algebraic solver N, is not equivalent to the theoretical stability region $A(X_s)$ of X_s. While $A(X_s)$ is an open, invariant, and connected set, $N(X_s)$ is usually an open, disjoint set, and sometimes fractal in nature, e.g. the Newton-Raphson Method.

Figure 5.1 provides a graphical illustration of the difference between the $A(X_s)$ and the $N(X_s)$ of X_s. The whole region bounded by stability boundary $\partial A(X_s)$ is the stability region $A(X_s)$ of X_s, with the points, X_1, X_2, X_3, X_4, and X_5 on the boundary representing the type-1 UEPs whose stable manifold defines $\partial A(X_s)$. The shaded regions form the convergence region $N(X_s)$ of the

numerical algebraic method N for X_s. The difference in $A(X_s)$ and $N(X_s)$ implies that the numerical convergence of an initial point X_0 to X_s computed by N does not necessarily guarantee that X_0 is in the stability region $A(X_s)$ of X_s. This means that a trajectory starting from X_0 might diverge or converge to a different SEP, even though X_0 converged numerically to X_s under the numerical method N. The converse is also true. Applying such a numerical method for power flow studies or transient stability analysis might therefore provide inaccurate results.

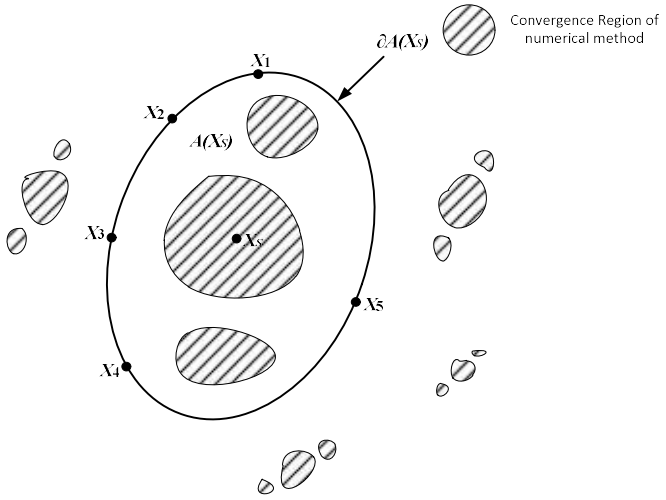

Figure 5.1 An illustration of the stability region A(X_s) and convergence region N(X_s) for a numerical method N of a stable equilibrium point X_s.

5.3 Dynamic Model of Transmission Switching Events

The major difference between the power system transient stability problem due to a TS event and the power system transient stability problem due to a fault event is that TS events do not involve faults. Thus, while fault events comprise of three periods, pre-fault, fault-on, and post-

fault, TS events comprise of two periods, a pre-switching period and a post-switching period. In terms of changes to the power system's Ybus, a single fault event without network adjustments involves a single change in the value of a diagonal element of the Ybus. On the other hand, a single TS event involves a change to a two-dimensional submatrix of the Ybus. However, in fault events where the fault clearing process involves TS then the number of changes to the pre-fault Ybus into post-fault Ybus will be as much as that in a TS event or more. Mathematically, the power system transient stability problem due to a TS event can be modeled as follows:

Pre-Switching System:

$$\left(x_s^{pre}, y_s^{pre}\right), t < t_s \tag{5.1}$$

Post-Switching System:

$$\dot{x} = f(x, y)$$

$$0 = g(x, y)$$

$$t \geq t_s \tag{5.2}$$

where the variables x and y are vectors of the dynamic and static variables of the system respectively. The differential equations in (5.2) represent the electromechanical dynamics, like generator dynamics, and the electrical dynamics, like the excitation system dynamics. The algebraic equations correspond to the power balance equations. In the pre-switching state, the system is operating at a known stable state (x_s^{pre}, y_s^{pre}). When a transmission element or line is switched at time t_s, there is a structural change in the power system, leading to a new system represented mathematically by the differential algebraic equations (DAE) in (5.2), called the post-switching system. The differential equations in (5.2) describe the electromechanical and electrical

dynamics of components like generators, dynamic loads, and their associated control systems. The algebraic system of equations in (5.2) represents the transmission system and the static behaviors of devices like static loads [1]. Representing the vector (x, y) by X, if (5.2) has an asymptotically stable equilibrium point $X_s(t)$, then the post-switching system is transiently stable if a trajectory, starting at the post-switching initial state denoted as $X(t)$, converges to $X_s(t)$. Thus, (5.2) is stable if $X(t)$ is in the stability region $A(X_s(t))$ of $X_s(t)$. If $X(t)$ is outside the stability region $A(X_s(t))$ of $X_s(t)$, then the post-switching system will be unstable. Figure 5.2(a) – 5.2(b) shows a pictorial illustration of a stable and an unstable post-switching system, respectively. The general form of the DAE model in (5.2) has been thoroughly analyzed in [1].

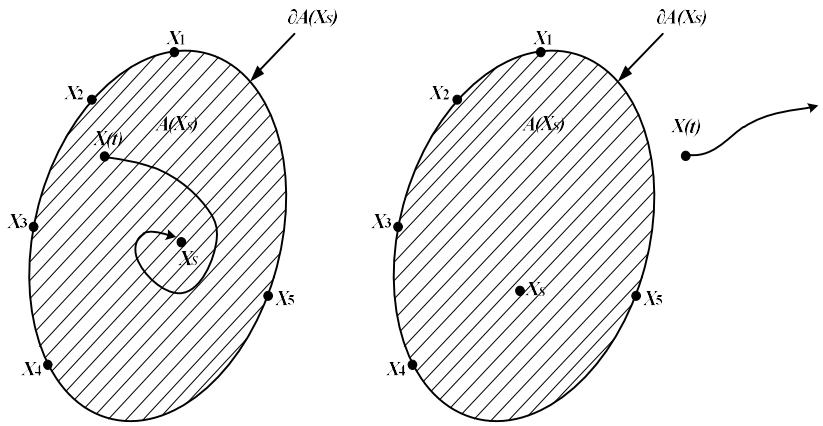

(a) (b)

Figure 5.2 Depiction of a stable (a) and an unstable (b) transmission switching event.

5.4 Transient Stability of Switching Events

Currently, the stability analysis of a transmission switching event can be conducted in two ways. The first and conventional approach is to numerically integrate the post-switching trajectory from the post-switching initial point. The second one solves for the post-switching SEP. Theoretically,

if an acceptable post-switching SEP exists, then the post-switching system can be stable; otherwise, it is unstable. Note that acceptable means voltage magnitudes and angles lie within a reasonable range. However, the existence of an acceptable post-switching SEP does not guarantee the stability of the post-switching system.

Depending on the relationship between the convergence region of a numerical technique used in the computation of the post-switching SEP and the stability region of the post-switching SEP, the initial point of the post-switching system used for the computation might be outside the stability region of the post-switching SEP, and therefore, the post-switching system is actually unstable, as explained in Section 5.2. The converse is also true. Even though the frequency of occurrence of this numerical problem is not high, it is however very important to capture and avoid them in the analysis and applications of TS, especially in control applications. In our numerical studies, we provide examples of power system cases where the post-switching SEP exists while the stability assessment of a post-TS system using time domain simulation is unstable (we call these examples counter-examples). All the TS examples used in the numerical studies are transmission line switching (TLS) cases. We also show that the occurrence frequency of this problem increases under heavy loading conditions. To show that an initial point is inside or outside the stability region of the post-switching SEP, we approximate the stability region of the post-switching SEP with trajectories of the singular perturbed equivalent system, equation (1.7), of the post-switching system for a sufficiently small ε. The structure-preserving model with a classical generator (the constant voltage behind reactance) and a constant impedance load model was used in the simulations. The numerical study was performed in MATLAB and the convergence threshold for trajectories used for the stability region approximation was defined as the L-2 norm of 0.5. To solve the singular perturbed system, the MATLAB ODE solvers, the Sundials CVODE solver, and

the implicit Euler method were used in the trajectory simulations, depending on the stiffness of the system equations. The trapezoidal method was used for the time domain simulation of the DAE system. The post-switching SEPs were computed with the MATLAB fsolve.

Table 5.1 List of Line Switching Events for the WSCC 9-bus 3-machine System

Event Number	Switched Line	
	From Bus	To Bus
1	7	5
2	8	7
3	4	6
4	6	9
5	9	8
6	5	4

5.4.1 Numerical Example I

The WSCC 9-bus 3-machine system is used in this example [1]. The list of TLS switching events used in the simulation is shown in Table 5.1. In the first case study, the transmission line between buses 5 and 7 is switched open under a uniform real power loading condition of 279.5 MW at each load bus, and the reactive component of the load was not changed in this simulation. The pre-switching and post-switching power flow solutions from MATPOWER are shown in Table 5.2 and Table 5.3. Table 5.4 shows the post-switching equilibrium point. The difference between the post-switching power flow solution in Table 5.3 and the post-switching equilibrium point in Table 5.4 is that the voltage magnitude and angle values in Table 5.3 only satisfy the power flow equations of the system, as it is a static approach, whereas the voltage magnitude and angle values in Table 5.4 satisfy both the dynamic and algebraic components of (5.2). Table 5.4 is a result of a dynamic simulation of the system, while Table 5.2 and 5.3 are the results from static

simulations. Hence, Table 5.4 is more accurate if static control actions are not ignored in the computation of the post-switching SEPs.

Table 5.2 Power Flow Results of the Pre-Switching System – The WSCC 3-machine 9-bus System

Bus	Voltage Magnitude	Voltage Angle	PG	QG	PL	QL
1	1.04	0	648.50	521.50	0	0
2	1.025	-49.29	163	143.70	0	0
3	1.025	-54.80	85	128.94	0	0
4	0.83	-25.55			0	0
5	0.77	-49.86			279.5	50
6	0.76	-52.46			279.5	30
7	0.94	-55.34			0	0
8	0.91	-64.07			279.5	35
9	0.95	-57.72			0	0

Table 5.3 Power Flow Results of the Post-Switching System – The WSCC 3-machine 9-bus System

Bus	Voltage Magnitude	Voltage Angle	PG	QG	PL	QL
1	1.04	0	601.61	375.30	0	0
2	1.025	-41.88	163	50.18	0	0
3	1.025	-44.31	85	73.81	0	0
4	0.9	-21.82			0	0
5	0.79	-38.53			279.5	50
6	0.86	-41.59			279.5	30
7	1.00	-47.59			0	0
8	0.96	-54.38			279.5	35
9	0.98	-47.14			0	0

Table 5.4 Post-Switching Equilibrium Point – The WSCC 3-machine 9-bus System

Bus	Voltage Magnitude	Voltage Angle
1	1.004	14.285
2	1.067	-76.742
3	0.970	-71.771
4	0.72	-9.891
5	0.619	-29.243
6	0.608	-49.247
7	1.001	-81.046
8	0.916	-86.248
9	0.880	-74.473

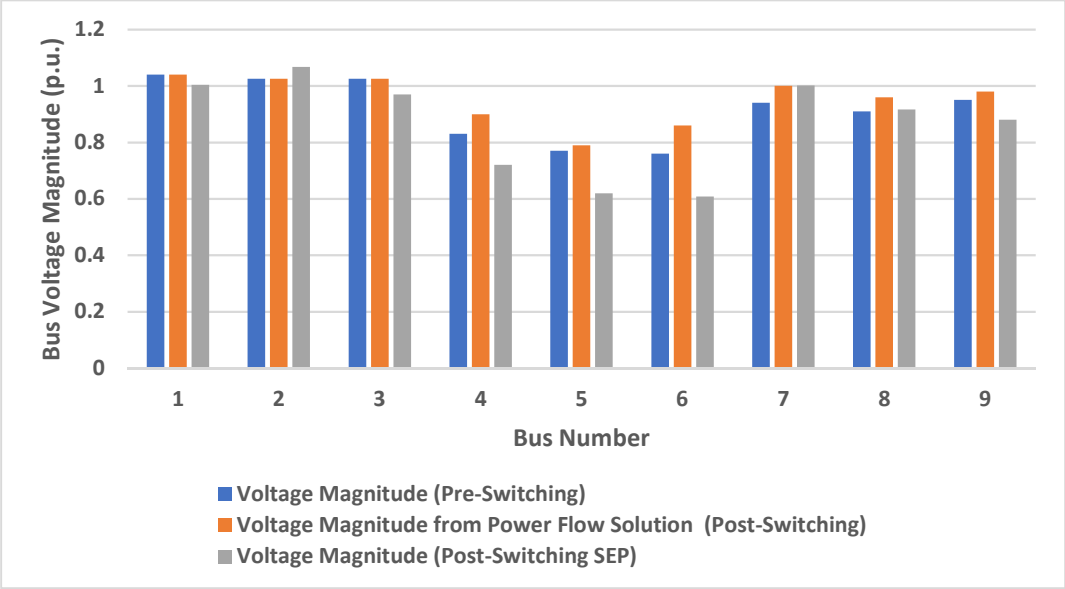

Figure 5.3 Comparison of the bus voltage magnitudes of the pre-switching system, the bus voltage magnitude from the power flow solution of the post-switching system and the bus voltage magnitude from the post-switching SEP after switching open the line between buses 5 and 7.

Comparing the voltage magnitudes from the pre-switching power flow solution, the post-switching power flow solution, and the post-switching SEP, in Figure 5.3, we observe that even though the post-switching power flow solution suggests that the bus voltage magnitudes of the system are improved by opening the line between buses 5 and 7 the results from a dynamic analysis

where the post-switching SEP is computed shows that the bus voltage magnitudes actually gets worse. The time domain simulation in Figure 5.4 shows that the post-switching system is unstable. Thus, switching open the line between buses 5 and 7 makes the system unstable instead of improving it as suggested by the static assessment using power flow. The machine angles of all three generators grow exponentially after the switching event. Figure 5.3 and Table 5.4 also show that the bus voltage magnitudes at buses 3, 4, 5, 6, and 9 would be worse in the post-switching system even if the post-switching system converged to the post-switching SEP.

The plot in Figure 5.5 shows an approximation of the stability region, in the δ_1-δ_2 machine angel space, of the post-switching system after branch 5-7 is opened. The green region is the stability region of the post-switching SEP. The black asterisk in the green region of the plot is the post-switching SEP and the blue asterisk represents the post-switching initial point/ pre-switching SEP. The blue trajectory connecting the post-switching initial point and the SEP is the trajectory of the fsolve solution for the post-switching SEP. Figure 5.5. shows that, even though fsolve converges to the SEP, the post–switching initial point is outside the stability region and hence, the post-switching system should be unstable. Thus, relying on a successful computation of the post-switching SEP by a numerical zero solver, for example, the MATLAB fsolve solver, as a proof of stability for a system, can lead to wrong stability assessments that can be detrimental to the safe operation of the power system. This counter-example was only observed in the system under heavy loading conditions for the WSCC 9-bus 3-machine system.

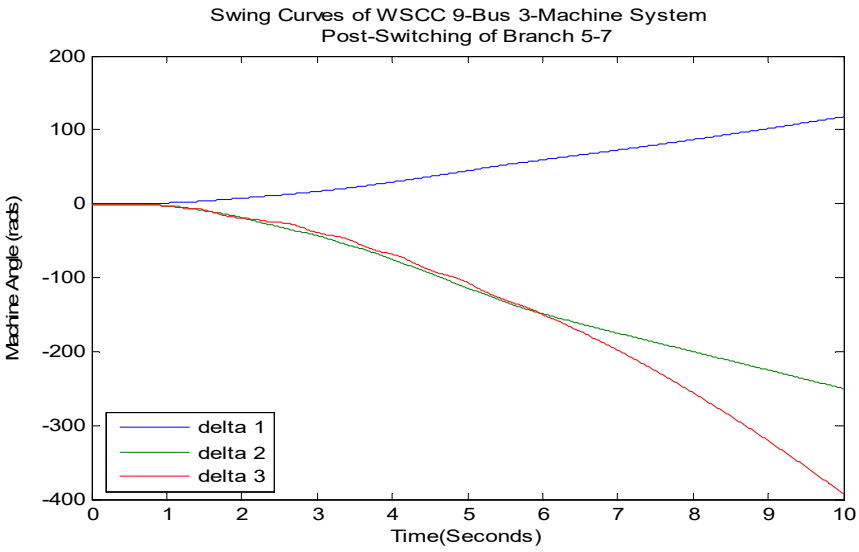

Figure 5.4 The post-switching swing curve for the WSCC 9-bus 3-machine system (branch 5-7 opened).

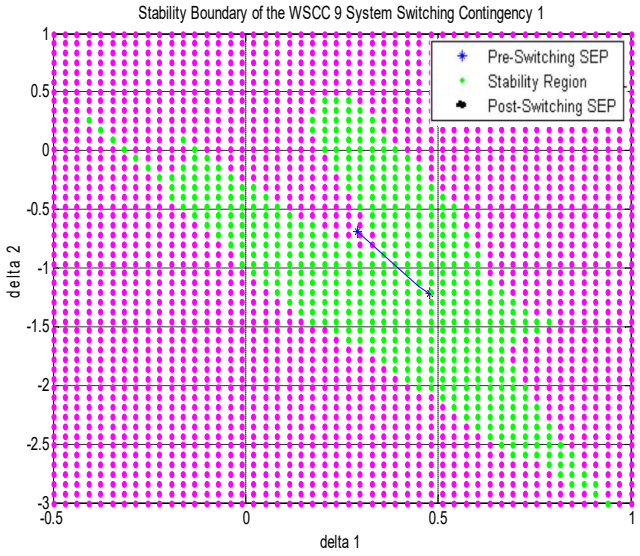

Figure 5.5 A plot of the stability region of the post-switching SEP and post-switching initial point (pre-switching SEP) of the WSCC 9-bus 3-machine system after opening the line between buses 7 and 5. The MATLAB fsolve solver converges to the SEP along the blue line, even though the initial post-switching point is outside the stability region.

5.4.2 Numerical Example II

With the IEEE-145 bus numerical example, the simulation was conducted by switching open each of the 453 branches and testing for static stability (power flow) and transient stability (time domain simulation and post-switching SEP computation). The results showed that three of the branches when switched open exhibited similar numerical discrepancies, a mismatch between dynamic stability and static security, to the case demonstrated in numerical example I. Table 5.5 shows the list of branches that had acceptable static stability solutions and post-switching SEPs but were dynamically unstable. Figure 5.6 shows a plot of the swing curves for a switching event where the branch between buses 137 and 145 is opened. It is observed that the post-switching system is unstable. Similar observations can be made from the time domain simulations of the other two switching events.

In the IEEE-145 bus system, the numerical discrepancies were observed in the base case, so there was no need for the heavy loading condition required in the WSCC 9-bus 3-machine system. This undesirable numerical behavior has also been observed in heavy loaded power systems in the United States where the power flow solution voltage magnitudes and angles are within normal operating range.

Table 5.5 List of Line Switching Examples for the IEEE 145-bus 50-machine System with Post-Switching SEPs that are Dynamically Unstable

Branch Number	Switched Line	
	From Bus	To Bus
1	14	17
2	137	145
3	139	145

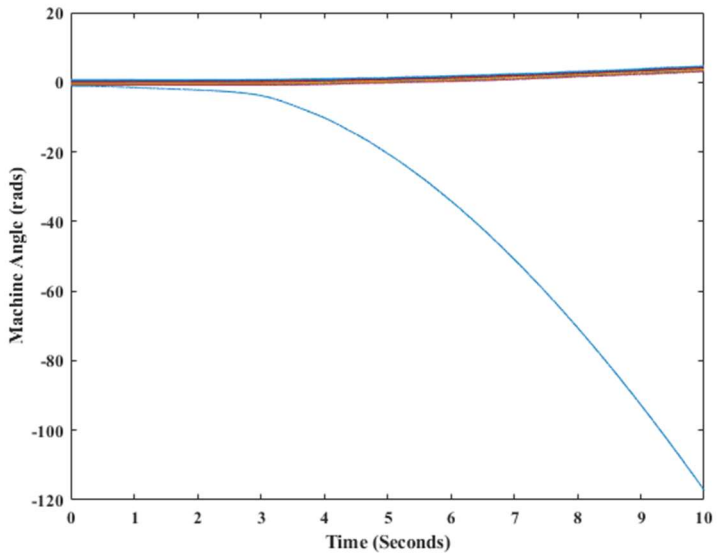

Figure 5.6 The post-switching swing curve for the IEEE 145-bus 50-machine system (branch 137-145 opened).

5.5 Occurrence of Counter-Examples and Nonlinear Analysis

To check the frequency of the occurrence of counter-examples under increasing loading conditions, the 6 events in Table 5.1 were simulated under increasing loading conditions from a uniform base real power load of 240MW at each load bus. Table 5.6 shows that initially, at the base real power load, there are no switching events exhibiting the counter-example behavior of secure static and dynamic stability mismatch. When the real power loading condition is increased to 259.5MW at each load bus, switching event 6 begins to exhibit the counter-example behavior. Event 6 continues to exhibit this post-switching behavior until at 275.5MW real power loading condition when the post-switching power flow diverges. At a real power loading condition of

275.5MW, switching event 3 also begins to exhibit the counter-example behavior. This numerical behavior of event 3 persists until the maximum loading condition of the pre-switching system is reached, where event 1 also shows similar numerical behavior alongside contingency 3. The secure static and dynamic stability discrepancy exhibited by the post-switching systems can be attributed to the difference between the stability region of their post-switching equilibrium point and the convergence region of the numerical method implemented.

Table 5.6 Occurrence of Counter-Examples After Switching Events Under Increasing Loading Conditions: The WSCC 9-bus 3-machine System

Loading Condition (Uniform, MW)	**Cumulative # of Counter Examples**	**Cumulative % of Counter Examples (Out of 6 Contingencies)**	**Events with a Numerical Problem**
240	0	0.00	-
259.5	1	16.67	6
275	1	16.67	6
275.5	2	33.33	3
279.5	3	50.00	1 & 3

We postulate that the frequency of the occurrence of the counter-examples increase with increasing loading conditions for some switching events because the stability region of the post-switching system shrinks with increasing loading conditions, leading to cases where we have the pre-switching equilibrium point or post-switching initial point outside the stability region of the post-switching system. Next, we present a numerical example demonstrating this hypothesis, and a theoretical explanation for the shrinking of the stability region under some specific scenarios.

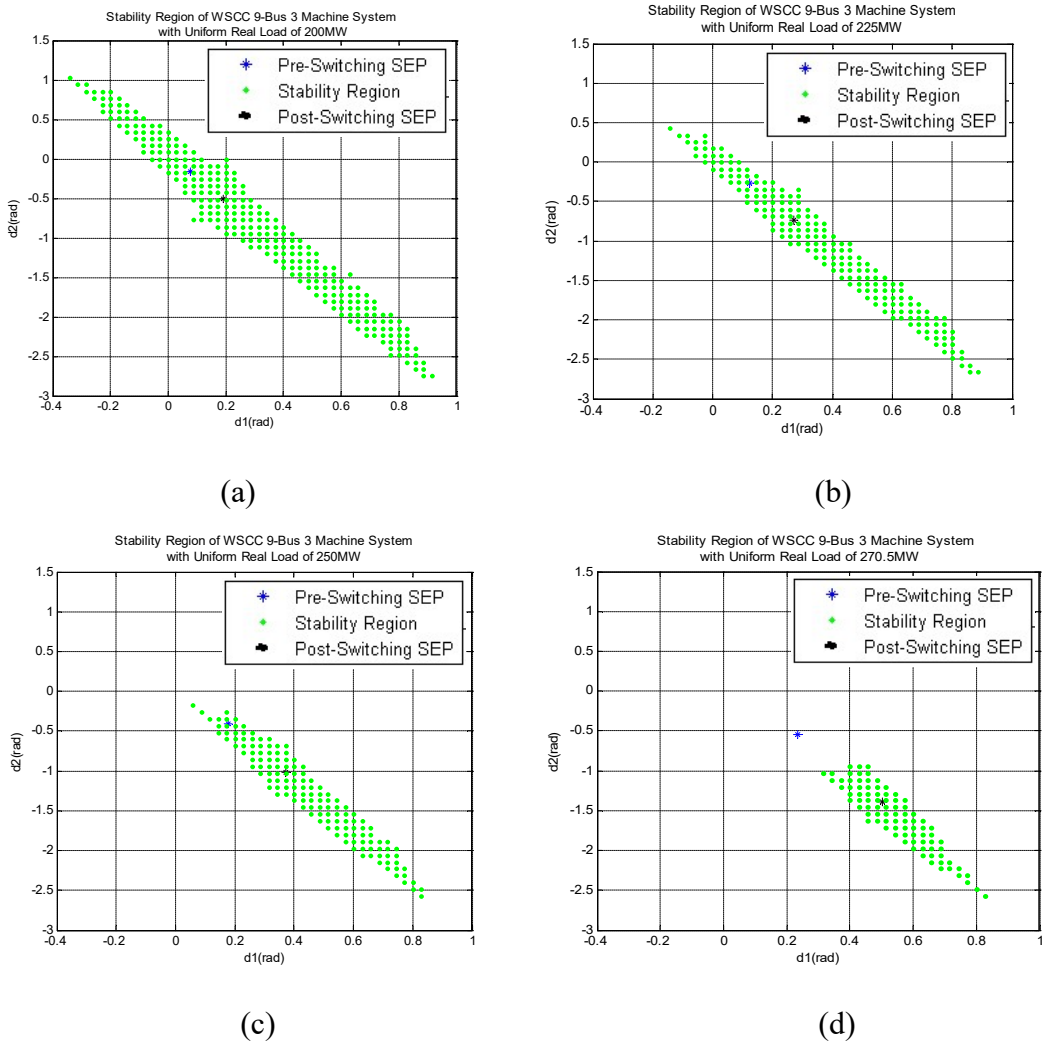

Figure 5.7 A plot showing the change in the stability region of the post-switching SEP under increasing real power loading conditions for switching event 6.

5.5.1 The Effect of Loading Conditions on the Stability Region

In this section, we investigate the reason for the increase in frequency of counter-examples with increasing loading conditions. We numerically examine the effect of increasing loading conditions on the size of the machine angle stability region. This study was conducted using the structure-preserving model of the WSCC 9-bus 3-machine system under uniform increasing loading conditions. The green region in the first graph in Figure 5.7(a) shows the projection of the

machine angle stability region of the post-switching system after switching event 6 when all load buses have the same real power loading condition of 200MW. The black star corresponds to the post-switching SEP and the blue star corresponds to the post-switching initial point. Figures 5.7(b) – 5.7(d) show the same results for real power loads of 225MW, 250MW, and 270.5MW, respectively. These figures show that the size of the stability region of the post-switching SEP changes monotonically decreases in with increasing loading conditions. Similar changes in the stability region with increasing loading conditions were observed with switching events 1 and 3, the same events that became unstable under heavy loading conditions.

5.5.2 The Effect of the Closest UEP on the Size of the Stability Region

These changes in the size of the stability region can be attributed to changes in the distance between the SEP and the UEPS on its stability boundary. From equation (1.3), we know that the stability boundary of an SEP is defined by the union of the stable manifolds of the UEPs on the boundary. Thus, any movement of the UEPs on the stability boundary and the SEP due to parameter changes, like changes in loading conditions, will effectively change the size and shape of the stability region of the SEP, since the stable manifolds of the UEPs on the stability boundary will change. If the UEPs on the stability boundary move away from the SEP with the parameter change, then the stability region will expand, and the converse is true if the UEPs move closer to the SEP. The distance is measured using an energy function value. The larger the energy function value of a UEP the farther it is from the SEP.

Since the closest UEP is the UEP that coincides with the SEP during a saddle node bifurcation [114], there exists a given loading condition, r, from the saddle node of a power system, beyond which any increase in loading condition for a given stress pattern will lead to the movement of the closest UEP closer to the SEP, which will lead to the shrinking of the stability region of the SEP

and vice versa. Figures 5.8(a)-5.8(d) show the paths of the SEP and closest UEP of the post-switching system of the WSCC 9-bus 3-machine system after switching event 6. It is observed that, as the real load demand is increased, the closest UEP and the SEP approach each other towards a saddle node. This behavior is observed in both the path of the machine angles in Figures 5.8(a)-5.8(c) and the voltage magnitude in Figure 5.8(d) at bus 1. The movement of the closest UEP and SEP towards each other is as expected just before a saddle node bifurcation, and it is the reason why the stability region is also shrinking in Figure 5.7. However, it should be noted that, at loading conditions before r, the effect of the movement of the closest UEP cannot be characterized in this generic manner.

From the theoretical explanations and numerical observations above, it is obvious that the shrinking of the stability region of the SEP with increasing loading conditions explains why more numerical counter-examples were observed under an increasing real power load in the WSCC 9-bus 3-machine case studies. Since as the stability region shrinks, it is more likely to have a post-switching initial point lie outside the stability region of the post-switching SEP, as shown in Figure 5.7(d).

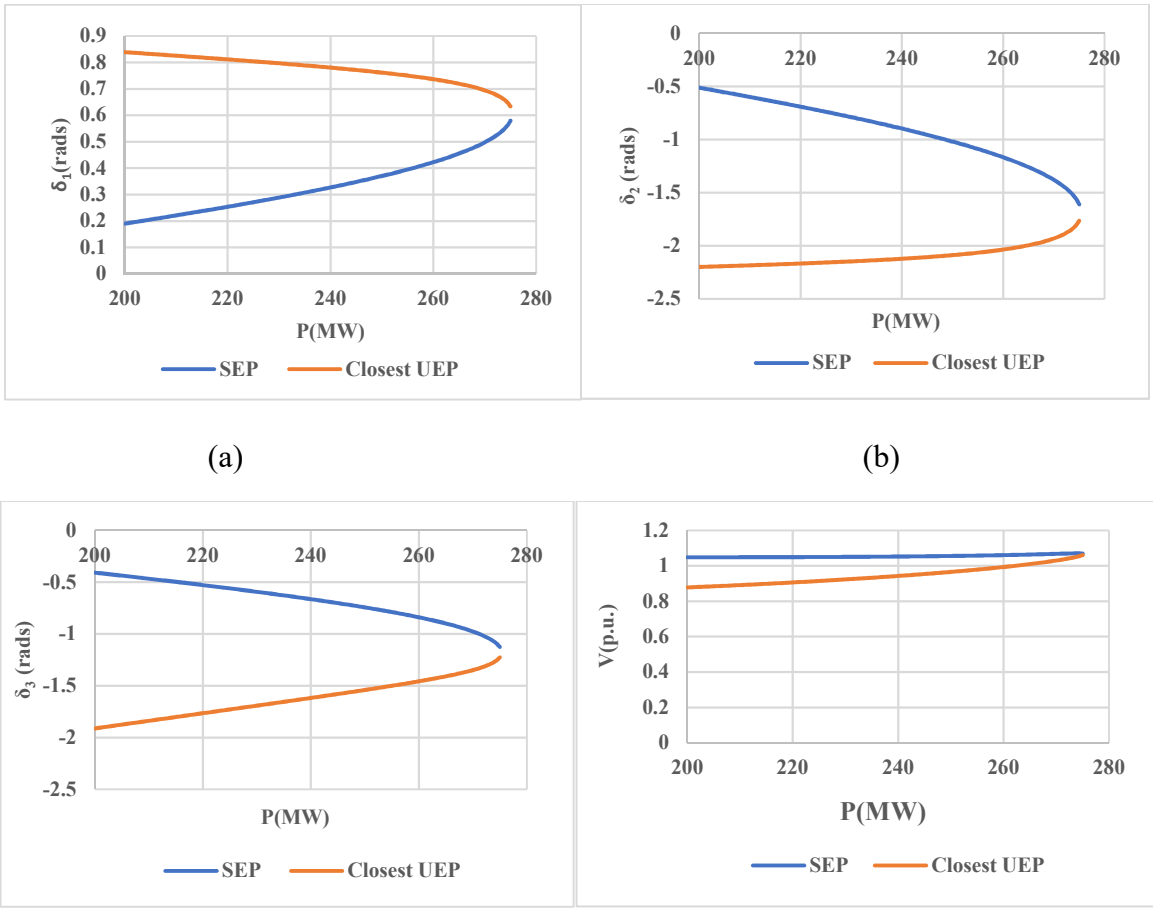

Figure 5.8 Plot of the SEP and the closest UEP path with increasing loading conditions for switching contingency 6.

5.6 Conclusion

An electromechanical model for transmission switching was presented. Numerical counter-examples showing the problem with excluding dynamic models in transmission switching analysis and applications were also presented. The increase in the frequency of the occurrence of counter-examples under increasing loading conditions was illustrated with numerical examples. The

analytical basis for the increase in the frequency of the occurrence of counter-examples with increasing load is also presented. The findings from the counter-examples and illustrations suggest that it is important to include dynamic models in transmission switching control applications to account for the potential dynamic instabilities, especially under heavy loading conditions. To this end, a new direct method for the online and look-ahead transient stability analysis of power system switching events will be presented in the next chapter.

CHAPTER 6

A Direct Method for Transient Stability Analysis of Transmission Switching Events

6.1 Introduction

Transmission switching (TS) is the alteration of a power network configuration via the change of on/off status of circuit breakers or change of tap positions. It could be in the form of opening or closing a transmission line (transmission line switching), transformer tap changes or bus splitting. Through automatic controls or operators, the configuration of the transmission system is changed in response to faults or to improve voltage profiles or the transfer capability of transmission interfaces [56]. In this chapter, a novel method for assessing the transient stability of transmission switching events is proposed and tested with numerical simulations performed on transmission line switching (TLS) events.

TS for power system control has been in use since the 1980s [56, 57]. Numerous research studies have been presented on efficient algorithms for finding optimal TS configurations and extensions to more control applications [58], like steady state security control [49, 50, 59, 60], and economic applications, such as in [51 – 53, 61]. In most of these applications of TS, the models used were purely static with no transient or dynamic constraints except for [11]. As highlighted in Chapter 5 this trend in research might suggest that there is a general belief that a static model for TS is sufficient for analyzing the stability of the post-switching system except in transient stability

control applications. The focus of most TS research topics on static models of the power system could also be attributed to the computational challenges that transient stability models present when incorporated in TS problems. Since currently the existing methods for the transient stability assessment of TS events, which are time domain simulations or the closest UEP method, require large computational efforts. However, as shown in Chapter 5 there are cases where acceptable steady state solutions exist after a TS event but the post-switching system are unstable. Thus, the dynamic security assessment of switching events needs to be factored into TS design and analysis. This chapter proposes a direct method designed for the transient stability assessment of TS events.

The power system dynamic stability analysis is focused on whether a post-event trajectory will settle to an acceptable condition. Currently, only three dynamic security assessment tools can be used for the transient stability analysis of TS events: the conventional time domain simulation method, the energy-based closest UEP method, and the energy margin sensitivity-based method [69, 70]. The time domain simulation method is currently the most common and robust method used for dynamic stability assessment. However, it is numerically demanding and consequently, time consuming. The energy function-based methods, direct methods, make transient stability assessments without integrating the post-event system by comparing the energy of the post-event initial state to a critical energy value. Energy function methods are based on Lyapunov function theory. For a dynamic system that has an energy function, an equilibrium point p is the closest UEP of an SEP X_s with respect to an energy function $V(.)$ if $V(p) = \min_{X \in \partial A(x_s)} V(X)$ where $\partial A(X_s)$ is the stability boundary of the SEP X_s. The closest UEP method has the problem of requiring the computation of all UEPs on the stability boundary of the post-event system, a requirement that is impractical. The energy level of the closest UEP method may also be too conservative if the post-switching initial point is not close to the relevant portion of the stability boundary defined by the

stable manifold of the closest UEP. The energy margin sensitivity method computes the sensitivity of an energy margin for a fault-based contingency to changes in network variables or parameters like network topology or loading conditions. This implies that the energy margin sensitivity method can be used to assess the stability of a network topology change event like transmission switching [69], but only if they occur after a fault-based event. In this chapter, a new energy-based method for the transient stability analysis of transmission switching events that does not require or depend on a previous fault-based event is proposed. The goal is to have a transient stability analysis tool that is fast and able to detect the counter-examples presented in Chapter 5.

In section 6.2, the problem formulation for transmission switching events is presented. A general description of the major energy-based direct methods and their applicability to transient stability analysis of transmission switching events are presented in section 6.3. In section 6.4, the newly proposed direct method for the transient stability analysis of TS events is presented, and numerical examples of the proposed method being applied to the structure-preserving model of the WSCC 9-bus 3-machine system and the IEEE 145-bus 50-machine system are presented in section 6.5. A scheme for the general transient stability analysis of TS events is presented in section 6.6, and then finally, the conclusion for this chapter is presented in section 6.7. The chapter is based on the work published in [116].

6.2 Problem Formulation

The mathematical representation of the power system transient stability problem due to a TS event comprises the following components, as presented in Chapter 5:

Pre-Switching System:

$$\left(x_s^{pre}, y_s^{pre}\right), t < t_s \tag{6.1}$$

Post-Switching System:

$$\dot{x} = f(x, y)$$

$$0 = g(x, y)$$

$$t \geq t_s \tag{6.2}$$

In the pre-switching state, the system is operating at a stable state (x_s^{pre}, y_s^{pre}). When a transmission element or line is switched at time t_s, there is a structural change in the power network, leading to a new system represented mathematically by the differential algebraic equations (DAE) in (6.2), called the post-switching system. If a system represented by equation (6.2) has an asymptotically stable equilibrium point $X_s(t)$, then the post-switching transient stability problem is whether or not a trajectory starting at the post-switching initial state denoted as $X(t)$ will converge to $X_s(t)$. In other words, is $X(t)$ in the stability region $A(X_s(t))$ of $X_s(t)$?

6.3 Direct Methods

The direct methods for transient stability analysis are composed of the following steps:

1. Compute the initial point, say (x^0, y^0), of the post-event system.
2. Construct an energy function for the post-event system, say $E(x, y)$.
3. Compute the energy function value at the post-event initial point, $E(x^0, y^0)$.
4. Determine the critical point, say (x^{cr}, y^{cr}), and then compute the corresponding critical energy, E_{cr}. The critical point is a point on the stability boundary of the post-event system. The energy function value at his point is used to approximate the stability boundary of the post-event system such that any point with energy less than the critical energy E_{cr} is in the approximated stability region.
5. Compare the system energy at the post-event initial state, $E(x^0, y^0)$ with the critical energy, E_{cr}. If the $E(x^0, y^0) < E_{cr}$, then the post-event trajectory will be stable; otherwise, it may be unstable.

The most challenging aspects of these steps are:

(i) construction of the energy function and

(ii) determination of the critical point (x^{cr}, y^{cr}) and critical energy E_{cr}.

There is currently no analytical energy function for structure-preserving power systems with detailed generator models, controls, and a large network resistance. However, numerical energy functions can be constructed for the detailed structure-preserving power system model [1] with a sufficiently small network resistance and nonlinear exciter models, Chapter 4. In this work, the numerical energy function derived by the author in [1] is used for the energy computations since the method has only been implemented for structure-preserving models with classical generators.

Currently, direct methods are applied to only fault-based events or disturbances. These direct methods can be classified mainly into three groups depending on the type of critical point used in the stability assessment [1]. The first is the potential energy surface (PEBS) method, which uses the energy at the point of maximum potential along the fault trajectory as the critical energy. The major challenge with the PEBS method is that the point of maximum potential is not always a conservative approximation of the stability boundary of the post-fault SEP [1]. The second direct method is the closest UEP method, which uses the energy at the closest UEP as the critical energy. The closest UEP is defined as the UEP on the stability boundary of the post-event SEP with the lowest energy value. The closest UEP method is known to be always conservative. However, the biggest challenge with the closest UEP method is the computational requirements. To find the closest UEP, all the UEPs on the stability boundary of the post-event SEP must be found, which, in most cases, is not an easy task. There has been much effort towards efficiently computing the closest UEP [21 - 23], but to no avail. The controlling UEP (CUEP) method is the third major energy-based direct method for fault-based disturbance direct stability analysis. The controlling UEP is defined as the UEP on the stability boundary of the post-event (post-fault) SEP whose stable manifold intersects with the fault trajectory. The advantage of the controlling UEP over the closest UEP method is its accuracy in stability assessment. However, finding the controlling UEP is also a challenging problem. Work in [1, 14] and others have provided a theoretical foundation and algorithmic solutions that have helped improve the computation of the controlling UEP. In this work, the BCU method presented in [1] will be used in the computation of a CUEP, which is required in our proposed direct method for transient stability analysis of switching events.

6.4 Direct Methods for Transmission Switching Events

The following assumptions are made in this section:

1. A numerical energy function exists for the system (6.2).
2. The pre-switching SEP is close to the post-switching SEP in terms of Euclidian distance and energy function value. This is usually true and has been observed in the application of the energy-based direct methods to the transient stability assessment of fault events.
3. The energy function value at an exit point is representative of the energy at the corresponding CUEP. In effect, CUEPs are close to their exit points. This is a weaker assumption, but it is important only if we want to prevent the need to compute two CUEPs.

The PEBS and the controlling UEP methods cannot be directly applied to transient stability analysis of a post-switching system since these methods require a fault trajectory, which is not present in switching events. The closest UEP method, on the other hand, does not require a fault-on trajectory and hence, it is directly applicable to the transient stability analysis of a switching event. However, the closest UEP method has the problem of requiring the computation of all UEPs on the stability boundary of the post-event system, a requirement that is impractical. The critical energy level of the closest UEP method may also be too conservative if the post-switching initial point is not close to the portion of the stability boundary defined by the stable manifold of the closest UEP. Ideally, a method that can characterize the relevant stability region with respect to both the post-switching SEP and the post-switching initial point is needed for direct stability assessment of the transient stability of a switching event. However, such a relevant stability boundary is very difficult to determine. Instead, a direct method based on the idea of the controlling UEP method, is proposed.

6.4.1 Proposed Method

The use of a pseudo-fault trajectory to determine the relevant portion of the stability boundary of the post-switching SEP is proposed. The idea is to use the energy at the CUEP of a pseudo-fault applied to one of the buses of the transmission switching event as the critical energy for the direct assessment of the post-switching system's stability. The proposal is as follows:

Step 1: For a given TS action, identify the two buses, say buses i and j.

Step 2: Apply a pseudo-fault to each of the buses of the branch/transformer that is being switched.

Step 3: Determine the exit points of the two sustained pseudo-fault trajectories in the post-switching system using the iterative method proposed in [1].

Step 4: From the two exit points compute the controlling UEP with the lowest energy in the post-switching system, using the BCU method.

Step 5: Compute the critical energy at the CUEP and the energy at the post-switching initial point.

Step 6: Evaluate the transient stability of the post-switching system by comparing the energy at the CUEP with the energy at the post-switching initial point. If the former is greater than the latter, the post-switching system is stable; otherwise, the post-switching system may be unstable.

Since there are two buses at a switching branch, and the CUEPs corresponding to faults at the two buses may differ, we propose using the bus corresponding to the CUEP with the lowest energy. Based on assumption 3, an educated estimation of the bus corresponding to the CUEP with the lowest energy can be made by comparing the energy of the two fault trajectories, for faults applied to the two buses, at their exit points. The fault trajectory with the lowest energy at the exit point

will most likely have the CUEP with the lowest energy. Since the exit point is in the stable manifold of the corresponding CUEP and the minimum value of the energy function in a CUEP's stable manifold is at the CUEP itself, the smaller the energy at the exit point, the more likely it is that the energy of the CUEP will be the smallest. Successfully identifying the CUEP with based on assumption 2 will improve the conservativeness of the proposed method and eliminate the need to check the stability of a switching event twice with two pseudo-fault trajectories. However, to ensure reliability we recommend that the two CUEPs should be calculated to determine the one with the lowest energy.

In an unstable post-switching case, applying a fault to one of the buses of the switched branch that starts from the projection of the post-switching initial point in the fault-on system will imply that the fault trajectory will start from outside the stability region of the post-switching system. In such a case, our proposed method will not work as expected. To overcome this challenge, it is proposed that the fault trajectory start from or close to the post-switching SEP in the fault-on system. Based on assumption 2, and since the path of fault trajectories is mostly influenced by the location of the fault, the network configuration and the unstable mode, the two fault trajectories, should be similar and close to each other, as demonstrated in Figure 6.1. Figure 6.1 shows a fault trajectory comparison for a fault applied to bus 5 of the first event in Table 5.1, starting from the post-switching initial point and the post-switching SEP in the fault-on system of the WSCC 9-bus 3-machine system. We observe that the two trajectories, swing curves, take the same path and are practically equal.

Since applying a fault to the power system is considered much more severe than most switching events, we expect the resulting transient stability analysis results to be conservative.

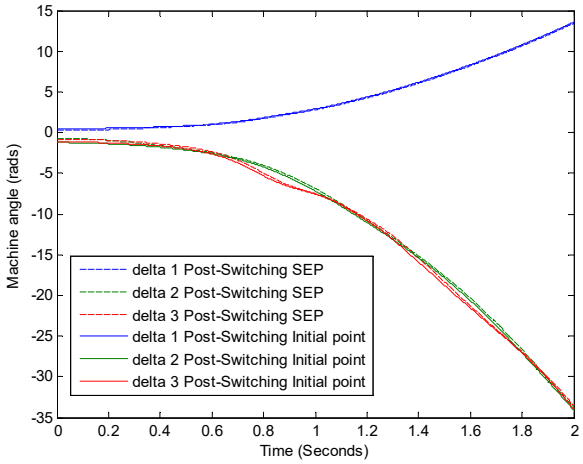

Figure 6.1 Comparison of Fault-on trajectories, starting from the post-switching SEP and the post-switching initial point for switching event 1 of the WSCC 9-bus 3-machine system. The fault was applied to bus *5*.

Figure 6.2(a) – (b) shows a numerical example of the proposed method applied to the WSCC 9-bus 3-machine system for a switching event, opening of line between buses 4 and 5, under two loading conditions. Figure 6.2 (a) shows the stable case where the system is under uniform loading condition of 200 MW and Figure 6.2(b) shows the unstable case where the system is under uniform loading condition of 270.5 MW. The projection of the stability region of the post-switching system in the machine angle plane is represented by the green area. In both figures the pseudo-fault trajectory intersects the stable manifold of the controlling UEP, type-1 UEPs, highlighted in the Figures 6.2(a)-(b). There is only one type-1 UEP on this stability boundary implying that the pseudo-fault trajectory intersects with the stable manifold of that UEP at the exit point. Figure 6.2 (a)-(b) show that the post-switching initial point is in the stability region of the post-switching system for the stable case, whereas the post-switching initial point is outside the stability region of the post-switching system for the unstable case.

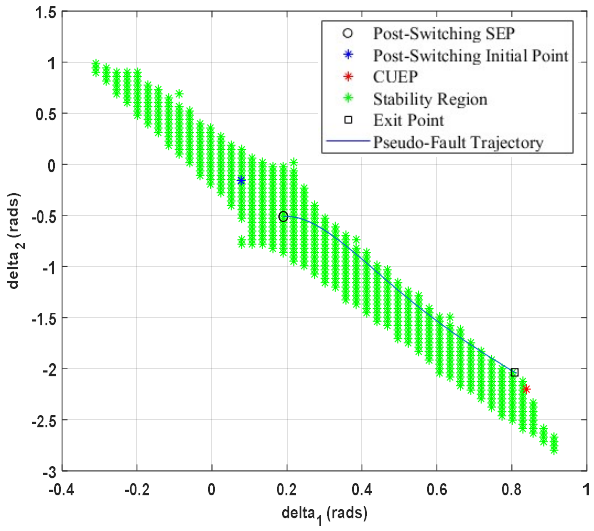

(a)

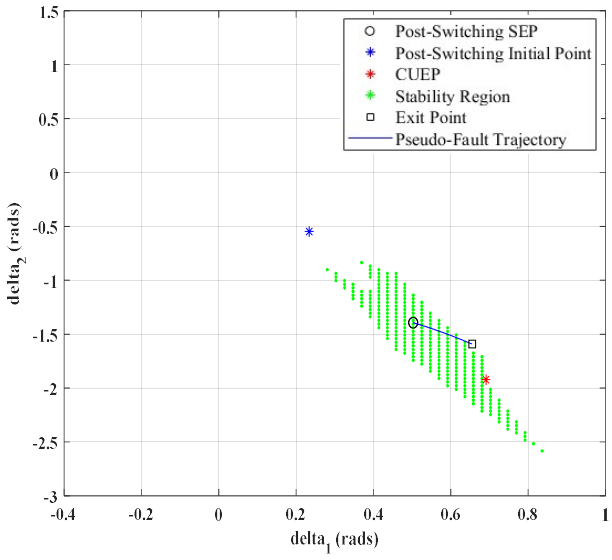

(b)

Figure 6.2 Numerical example of the proposed method applied to the WSCC 9-bus 3-machine system for a switching event, opening of line between buses 4 and 5, under two loading conditions. (a) Stable case, the system is under uniform loading condition of 200 MW. (b) Unstable case, the system is under uniform loading condition of 270.5 MW.

6.5 Numerical Simulations and Discussions

This study is performed on transmission line switching events using the same systems and structure-preserving models used in the numerical simulations in Chapter 5. The exit points were computed using the iterative method proposed in [1], and the BCU method was used for the controlling UEP computations.

Table 6.1 List of Line Switching Events for the WSCC 9-bus 3-machine System

Event Number	Switched Line	
	From Bus	To Bus
1	7	5
2	8	7
3	4	6
4	6	9
5	9	8
6	5	4

6.5.1 Numerical Example for the WSCC 9-Bus 3-Machine System

In this subsection, the method is tested on the structure-preserving model of the WSCC 9-bus 3-machine system with a classical generator model, and constant impedance load. The loading condition is set to 279.5MW real power at each load bus, with the reactive power demand kept at the same values as the base case. The test was performed on the 6 events shown in Table 6.1. The results from the proposed method are compared to the time domain simulation results and results from a brute-force implementation of the closest UEP method.

From Table 6.2, it is observed that the proposed method can detect all of the unstable switching events accurately. The table also shows that the closest UEP method can detect all of the unstable and stable switching events accurately. For switching event 2, it is observed that the proposed

method did not produce a stability assessment result because the BCU method failed to find the CUEP. This failure could be attributed to the failure of the stability boundary following procedure, where the procedure converges to the wrong local minimum, or the failure of the algebraic solver used in solving for the CUEP. In such cases, it is recommended that the contingency be tested further by detailed time domain simulation. For event 6, there is no energy margin because the post-switching SEP could not be found when computed with the post-switching initial point as the initial guess. Such contingencies will also require further detailed analysis. For contingencies 1, 3, and 4, it is observed that the closest UEP method and the proposed method have the same energy margins: the difference in energy between the critical point and the post-switching initial point. This is because the computed CUEP is the same as the closest UEP. However, for contingency 5, the closest UEP has a smaller energy margin compared to our proposed method, making the closest UEP method more conservative.

Table 6.2 Stability Results for the WSCC 9-bus 3-machine System

Contingency Number	**Time Domain Simulation Stability**	**Closest UEP Method**		**Proposed Method**	
		Stability	**Energy Margin**	**Stability**	**Energy Margin**
1	Unstable	Unstable	-0.0579	Unstable	-0.0579
2	Stable	Stable	0.3856	-	-
3	Unstable	Unstable	-0.3121	Unstable	-0.3121
4	Stable	Stable	0.3271	Stable	0.3271
5	Stable	Stable	2.2868	Stable	2.3658
6	Unstable	Unstable	-	Unstable	-

6.5.2 Numerical Example for the IEEE 145-Bus 50-Machine System

In this subsection, the method is tested on the structure-preserving model of the IEEE 145-bus 50-machine system with a classical generator model and constant impedance load. Table 6.3 shows the 10 contingencies used in the test and the corresponding simulation results. From Table 6.3, we observe compared to the time domain simulation results that the proposed method detects all the unstable and stable switching events with 100% accuracy.

Table 6.3 Stability Results for the IEEE 145-bus 50-machine System

Contingency Number	Switched Line		Proposed Method				Time Domain Simulation Stability
	From Bus	To Bus	Critical Energy	Energy at Initial Point	Energy Margin	Stability	
1	7	6	6.3247	1.7957	4.529	Stable	Stable
2	14	17	0.1322	1.2989	-1.1667	Unstable	Unstable
3	59	72	3.8657	2.01E-09	3.8657	Stable	Stable
4	115	116	100.1745	0.0114	100.1631	Stable	Stable
5	100	72	4.6176	0.000559144	4.617	Stable	Stable
6	91	75	1.9879	6.04E-05	1.9878	Stable	Stable
7	112	69	7.9669	0.0016	7.9654	Stable	Stable
8	101	73	8.674	0.000275667	8.6737	Stable	Stable
9	137	145	0.0043	0.742	-0.7376	Unstable	Unstable
10	139	145	0.0369	18.0473	-18.0105	Unstable	Unstable

6.6 Scheme for Online Transient Stability Analysis of Transmission Switching Events

The simulation results show that, despite the 3 major assumptions made in the implementation of the proposed method, the results obtained were accurate in both test systems when the underlying controlling UEP method works. It should be noted that, in some cases, the exit point of a fault trajectory cannot be computed due to the fault trajectory hitting a singular surface [39]. This is a typical challenge for energy-based direct methods that use sustained fault trajectories. These challenges were observed for some of the fault trajectories in the simulation on the heavily loaded WSCC 9-bus 3-machine system. However, in all those instances, only one out of the two fault trajectories hit a singular surface. If the fault trajectory for both buses of a switched line hits a singular surface, the switching event should be evaluated with detailed time domain simulation.

As in most applications of direct methods for online transient stability analysis, it is recommended that the proposed method be used as a screening tool, after which the unstable switching events are sent to the time domain for detailed analysis. Consequently, the following steps are proposed for the transient stability analysis of transmission switching events.

Step 1: Starting from the post-switching initial point, compute the post-switching SEP using the Newton method or other reliable and yet fast algebraic solvers. If the SEP computation fails, then the post-switching system may be unstable. Go to step 8; otherwise, continue to step 2.

Step 2: Compute the energy at the post-switching initial point.

Step 3: Starting from the post-switching SEP, determine the exit point of the sustained fault trajectories for faults applied to the buses of the switched branch in the post-switching system.

Step 4: Compute the energy at the two exit points and compare them to the energy at the post-switching initial point. If any one of them is less than the energy at the initial point, the post-switching system may be unstable. Skip to step 8 for time domain simulation.

Step 5: Find the CUEP for the exit point with the lowest energy or both exit points in the post-switching system, using the BCU method.

Step 6: Compute the critical energy at the CUEP(s). Select the CUEP with the lowest energy if you calculated both CUEPs in step 5.

Step 7: Evaluate the transient stability of the post-switching system by comparing the energy at the selected CUEP with the energy at the post-switching initial point. If the former is greater than the latter, the post-switching system is stable; otherwise, the post-switching system may be unstable.

Step 8: Evaluate the stability of the unstable and critical cases detected in steps 1, 4, and 7 using detailed time domain simulation.

This proposed scheme can be implemented by making slight changes to the implementations for the existing CUEP direct methods used for the online transient stability analysis of power systems with fault events.

6.7 Conclusion

A new method for the transient stability analysis of power system transmission switching events has been proposed. The proposed method uses the controlling UEP of a fault event closely related to the switching event being assessed, pseudo-fault, to define the stability region of the post-switching system. The numerical simulations performed on the WSCC 9-bus 3-machine, and the 145-bus 50-machine system shows that the proposed method can accurately assess the stability of a switching. Finally, a scheme for the online screening and detailed analysis of the transient stability of switching events in a power system has been presented. Extension of the proposed method to the transient stability of generator trip events, and to transient stability of power system with renewable energy sources that have low voltage ride through models will be investigated in future work.

CHAPTER 7

Towards Online Line Switching for Transient Stability Enhancement of Look-ahead Power Systems

7.1 Introduction

Operations of modern power grids are near their limits due to the lack of investment in infrastructure. There is also an increase in uncertainty in the power grid due to an increase in the penetration of intermittent energy sources. These changes have led to the need for implementing online transient stability control and enhancement schemes to ensure reliable operations. One such scheme is the use of online network topology control or transmission line switching for online look-ahead transient stability enhancement.

Transmission line switching is already used in power system responses to faults and other disturbances via automatic circuit breaker actions. The authors in [62 - 67] have also proposed some forms of operator and automatic controlled transmission switching techniques for transient stability control. In [67] the authors proposed a switching scheme for severe faults where the pre-fault system is strengthened by using transmission line switching to sectionalize the power grid and then interconnect the system after the switching event. The authors in [65] proposed the use of substation capacitor switching to reduce the impact of faults on the transmission system. In [64] the authors proposed the use of transmission switching for emergency transient stability control by using changes in transmission line susceptance to change fault-on and post-fault dynamics. The

effectiveness of transmission line switching or transmission line impedance changes in general is demonstrated by the work in [62]. In [63] a scheme for real-time transient stability control of power systems using transmission line switching after a fault event is proposed. The scheme in [63] is based on repeated offline time domain simulations to determine transmission line switching control actions for a set of pre-specified contingencies. The line switching control actions are then applied when one of the pre-specified contingencies occurs under the same network topology conditions as those that the control actions were designed to resolve. Repeated time domain simulations can be very time consuming and determining the control actions offline implies that there is a high chance the proposed control actions might not even be applicable by the time the fault occurs. The method also focuses on finding an optimal switching scheme just for individual contingencies.

In this chapter, we propose the use of transmission line switching for the preventive online look-ahead transient stability enhancement of power systems. While the authors in [62-67] focus on improving the transient stability of individual contingencies, in this work we focus on the use of transmission line switching to enhance the transient stability of multiple contingencies for look-ahead operating conditions. Our proposal is focused on the design of preventive control—applying line switching control before a fault leading to insecure conditions occurs. Thus, we propose finding an optimal pre-fault network topology via line switching that (optimally) enhances the stability of critical faults or contingencies. Generally, the combinatorial nature of optimal line switching problems makes them computationally demanding and consequently, rather challenging for online applications [51–59]. To address this challenge, we present a three-stage methodology comprising the stages of screening, ranking, and detailed analysis to identify a set of pre-fault line switching solutions that improve the stability of a selected list of critical contingencies in a look-

ahead operating condition. The three-stage strategy employs direct method, and linear sensitivity analysis to speed up the search for optimal switching options that can enhance the transient stability of critical contingencies. The three-stage strategy has been applied to address the online voltage stability enhancement [60] and small-signal stability enhancement [68] of a base/single contingency case. This work will be using the three-stage strategy to enhance the transient stability of multiple contingencies.

A conventional approach to optimal line switching for enhancing power system static security is to formulate the problem as a mixed integer nonlinear programming (MINLP) problem [51–59]. This is generally computationally demanding and will be especially so if extended to line switching applications for transient stability enhancement, since for transient stability enhancement via optimal line switching, on objective function will be constrained by a system of DAEs [63]. Thus, if the MINLP formulation is used in the transient stability enhancement problem, each iteration of the solution process would require a time domain simulation [63] or an energy-based direct method assessment of the contingency(ies) under study. This will make the already computationally demanding MINLP approach too slow for online transient stability enhancement applications, especially when several contingencies are under consideration. To speed up the search for optimal line switching, we extend the three-stage method proposed in [60] and [68] for online voltage stability and small signal stability enhancement, respectively, to the transient stability enhancement problem. The goal of the three-stage method is to quickly and reliably determine line switching solutions through the three stages: 1) the screening stage, 2) the ranking stage, and 3) the detailed analysis/selection stage.

The main contributions of this work are: 1) the proposal of an online look-ahead line switching scheme for the transient stability enhancement of multiple critical contingencies, 2) a formulation

of the look-ahead line switching problem for transient stability enhancement of multiple critical contingencies, 3) the proposal of a weighting scheme to help compare the impact of various switching control actions on the transient stability of multiple contingencies, and 4) the development and implementation of an online look-ahead methodology for enhancing the transient stability limits of a group of critical contingencies for a structure-preserving power system model.

The proposed method provides multiple line switching options (network topologies) that are stable before and after the occurrence of the contingencies under consideration. The proposed 3-stage method can also efficiently find a set of optimal line switching control actions. The goal of this work is to develop a tool to provide network operators with new options for online or look-ahead control of multiple insecure transient stability contingencies without compromising the stability of secure contingencies or the pre-fault system.

The chapter is organized as follows. In section 7.2, we present the general problem formulation for transient stability control of multiple contingencies via transmission line switching. We then present the architecture and numerical scheme for the proposed online switching methodology in section 7.3. The online line switching scheme for transient stability enhancement is then presented in section 7.4. In section 7.5, numerical examples are presented, and the conclusion is presented in section 7.6.

7.2 Problem Formulation

Given the network balance equation model of the current/base operating condition of a power system, a look-ahead operating condition of the system can be modeled by adjusting the current system model for the forecasted change in the operating condition and planned network changes.

Thus, the power system transient stability problem, due to fault disturbances, for a look-ahead system can be formulated mathematically as a parameterized system of equations comprising: a quasi-steady state pre-fault system with look-ahead parameters, a fault system, and a post-fault system, as shown in (7.1) – (7.3):

Pre-Fault System:

$$0 = g_b(y, \lambda, m, p) = g_{pre}(y, m, p) + \lambda b$$

$$0 = f_{pre}(x, y)$$

$$t < t_f \tag{7.1}$$

Fault-on System:

$$\dot{x} = f_F(x, y)$$

$$0 = g_F(x, y)$$

$$t_f \leq t < t_{cl} \tag{7.2}$$

Post-Fault System:

$$\dot{x} = f(x, y)$$

$$0 = g(x, y)$$

$$t \geq t_{cl} \tag{7.3}$$

where x and y are vectors of the dynamic state and algebraic variables (voltage magnitude and angle), respectively, and m and p are the vectors of control variables. In this case, the control

vectors correspond to network topology changes where m is the planned changes in the network topology and p is the switching action that will be used to enhance the transient stability of the look-ahead system. The differential equations in (7.2) and (7.3) describe the electromechanical and electrical dynamics of components such as generators, dynamic loads, and other associated control systems. The algebraic system of equations in (7.2) and (7.3) represent the transmission system and the static behaviors of passive power system elements like static loads [1]. In the pre-fault system, the power system is assumed to be in equilibrium. $f_{pre}(.)$ represents the portion of the equilibrium equations that corresponds to the electromechanical and electrical dynamic models of the pre-fault system, and $g_b(.)$ represents the active and reactive power flow balance equations. The value of the parameter λ determines whether the power balance equations represent the base case pre-fault system or the look-ahead pre-fault system. $\lambda = 0$ for the base case pre-fault power balance system equations and $\lambda = 1$ for the look-ahead pre-fault power system balance equations. The variation in the real and reactive power injection, load and generator, in the look-ahead pre-fault system relative to the base-case system, is represented by the vector b. During this pre-fault period, the expected changes are the changes in the power injections as we look ahead, scheduled changes in the network topology, and the change in network topology for transient stability enhancements due to switching. These expected changes are represented by the parameters λ, b, m and p in (7.1).

When a fault occurs at time t_f, there is a structural change in the power system, leading to a new system represented mathematically by the DAE in (7.2), called the fault-on system. During the fault-on period, the structure of the fault-on system can change many times as the protective mechanisms/relays of the power system react to the fault with network topology changes. These network topology changes are due to automated switching events, which are included in the

modeling of the fault event. Thus, these switching events or network topology changes do not form part of the proposed line switching-based transient stability enhancement technique presented in this chapter.

During the post-fault period, the fault has been cleared and, depending on the contingency, the network topology of the post-fault system might be different from that of the pre-fault system. The loading conditions are assumed to be the same as for the pre-fault system if there is no islanding, an assumption that applies to the rest of this chapter. In this work, we only focus on the case where the control action is applied to the pre-fault system. However, the application of the switching control action [62 – 67], including the proposed online scheme, to the post-fault system for transient stability enhancement is possible and will be considered in subsequent work.

Unlike the pre-fault system equations, the fault-on and post-fault system equations (7.2) - (7.3) do not have the power variation vector b nor the control vectors m and p. After the power system model is updated in the pre-fault system for the look-ahead operating condition and the selected line switching action is applied, the impact of the variation and control vectors in the pre-fault system will be translated to the equations of the fault-on and post-fault system, since the dynamic variables of the fault-on and post-fault systems are initialized with the pre-fault power flow equations, and the power balance equations of the fault-on and post-fault systems are derived by making changes to the network structure or the impedances of the pre-fault system.

For a set of N possible network topologies, the goal of optimal line switching schemes is to efficiently find line switching actions that result in a network topology, $\mathcal{N} \in N$, to optimize an objective function subject to power system operational constraints. The goal can be to improve power system stability, reduce the cost of operation, or address overload conditions. In this chapter,

our aim is to efficiently find a line switching action or network topology change that leads to the maximum increase in the transient stability (increases the stability margins) of a given set of critical contingencies subject to the constraint that non-critical contingencies do not become critical or unstable. Figure 7.1 shows an illustration of the goal. Here X_i^b, X_i^{LA} and X_i^{PS}, $i = 1$ to 4 correspond to the unstable equilibrium points whose stable manifold forms the stability boundary of post-fault systems of the base case, look-ahead and the post-switching systems, respectively. In Figure 7.1(a) we show that when we add the look-ahead variation to the base case system, we move the pre-fault state, X_{pre}^b, the post-fault SEP, X_{sep}^b, and post-fault initial point, X_{cl}^b, to new states X_{pre}^{LA}, X_{sep}^{LA}, and X_{cl}^{LA}, respectively. The stability margin of the post-fault system also changes from E_M^b to E_M^{LA} due to changes in the stability boundary. Figure 7.1(b) illustrates how the pre-fault state then moves to X_{pre}^{PS} after the selected line switching control action is applied to the look-ahead system. The post-fault SEP, X_{sep}^{LA}, and the post-fault initial point, X_{cl}^{LA}, also move to X_{sep}^{PS} and X_{cl}^{PS}, respectively, after the line switching control action is applied. The changes in the stability boundary due to the line switching action then lead to a change in the stability margin from E_M^{LA} to E_M^{PS}. The goal is to select a line switching action such that the sum of the changes in the stability margins of the critical contingencies $\sum_{i=1}^{n}(E_M^{PS} - E_M^{LA})$ is the largest possible value subject to the stability constraints of all the contingencies (critical and non-critical), where n is the number of critical contingencies.

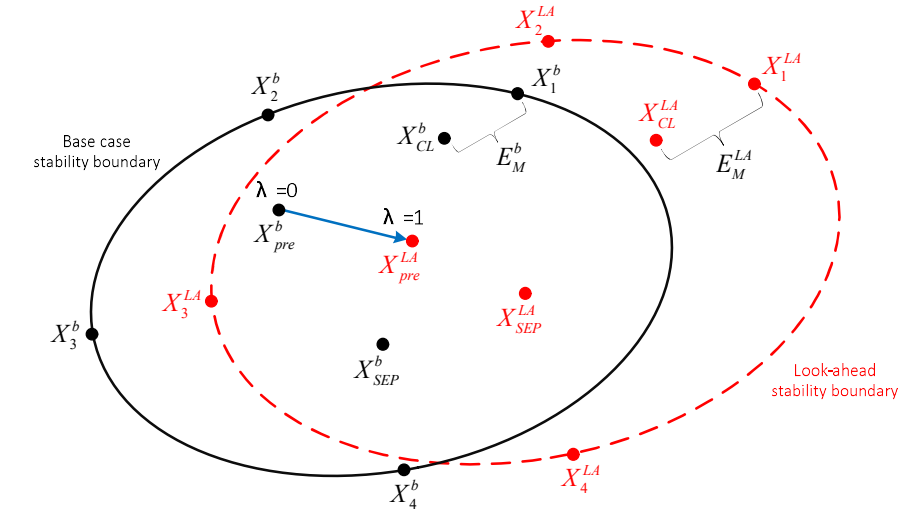

(a)

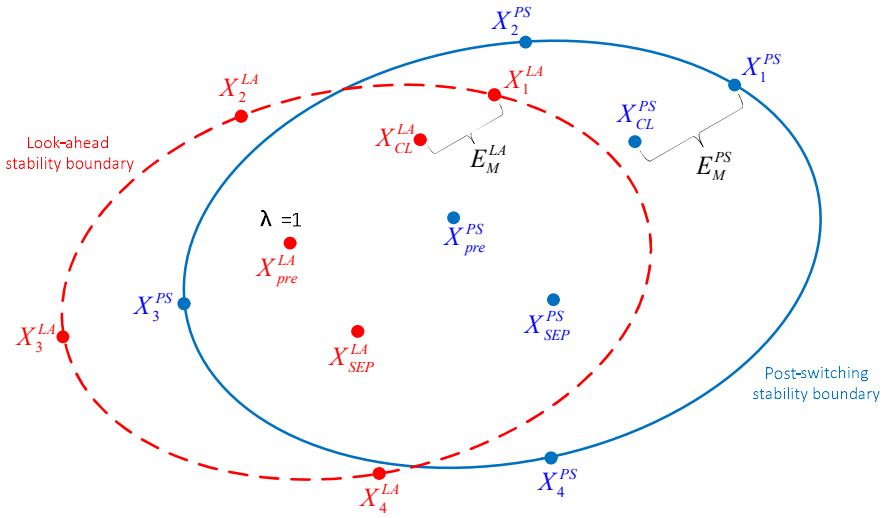

(b)

Figure 7.1 Illustration of transient stability enhancement by transmission line switching of a look-ahead system. (a) Depicts the difference in the stability region of a base case system and a look-ahead system. (b) Depicts the change in the stability region of the look-ahead system post-switching. The goal is to enlarge the stability margin of the look-ahead system for a fault by switching open a selected transmission line before the fault occurs. Thus, select a switching action that will make $E_M^{PS} > E_M^{LA}$.

To enhance the stability margin of a critical contingency, measuring the degree of stability or the stability margin is required. Currently, the stability margin can be measured by either the critical clearing time (CCT) obtained from repeated time domain simulations, or by the energy margin obtained from energy-based direct methods. The CCT approach is accurate but time consuming and it requires precise system parameters, whereas energy-based direct methods are faster and tolerant to system parameter variations but are constrained by modeling limitations.

In this work, we measure the degree of stability using the magnitude of the energy margin, E_M. The energy margin is obtained from the results of the transient stability assessment of the power system using energy-based direct methods: the larger the energy margin of a post-fault network topology, the higher the stability of the post-fault system. The accuracy of our proposed three-stage enhancement scheme is evaluated by comparing the CCTs of the critical contingencies for the look-ahead case with no switching with the CCTs of the critical contingencies of the post-switching system.

7.2.1 Objective Function with Constraints

To enhance the transient stability of multiple critical contingencies using optimal pre-fault line switching, we propose the following objective function:

$$\underset{\mathcal{N}}{\operatorname{argmax}} \sum_{i=1}^{n} E_M^i(\mathcal{N}) \tag{7.4}$$

such that, for the contingencies, $i = 1, \dots, n, \dots m$ where n is the number of critical contingencies and m is the total number of contingencies.

For each $j \in m$, the following constraints must hold:

$$E_M^{j^{\mathcal{N}}}(x, y, p) \geq C_M^j \tag{7.5}$$

Pre-Fault System:

$$0 = g_b^{j^{\mathcal{N}}}(y, \lambda, p)$$

$$0 = f_{pre}^{j^{\mathcal{N}}}(x, y)$$

$$t < t_f \tag{7.6}$$

Fault System:

$$\dot{x} = f_F^{j^{\mathcal{N}}}(x, y)$$

$$0 = g_F^{j^{\mathcal{N}}}(x, y)$$

$$t_f \leq t < t_{cl} \tag{7.7}$$

Post-Fault System:

$$\dot{x} = f^{j^{\mathcal{N}}}(x, y)$$

$$0 = g^{j^{\mathcal{N}}}(x, y)$$

$$t \geq t_{cl} \tag{7.8}$$

where C_M^j is the minimum energy margin value for contingency j below which the contingency can be classified as being critical. Thus, a critical contingency j is then defined as a contingency whose energy margin is below C_M^j. $\mathcal{N}$ is the resulting pre-fault network topology after the line switching action. $\mathcal{N} \in N$ where N is the set of possible network topologies. In this study, we

consider only single line switching candidates but multiple line switching control actions are also possible.

The objective is to find a new network topology for the pre-fault look-ahead power system that maximizes the sum of the energy margins of the critical contingencies under consideration subject to the following:

(1) the constraints requiring all contingencies to be non-critical by having energy margins greater than the energy margin threshold (7.5),

(2) the constraints of the equilibrium equations of the pre-fault system, (7.6), and

(3) the constraints of the differential algebraic equations of the fault-on (7.7) and the post-fault systems (7.8).

The constraint (7.5) can be relaxed, so it only applies to the contingencies that are not already critical. Thus, the constraint will only require that the energy margin of the non-critical contingencies remain non-critical, while those contingencies that are already critical improve.

Solving this problem using direct optimization or combinatorial techniques for online applications is rather challenging. To overcome this challenge, we propose the following three-stage methodology.

7.3 Proposed Architecture

The three-stage scheme of screening, ranking, and detailed analysis has been in use for online transient stability assessment for power systems for a while now, particularly in applications involving the use of energy-based direct methods [1]. In this work, we extend the idea of screening,

ranking, and detailed analysis to the application of online line switching for enhancement of look-ahead transient stability. The architecture of the overall process is depicted in Figure 7.2. The first component is an input phase where the current system state information (state estimation output, and network topology); the forecast data, which include the look-ahead (15-60 mins) load forecast and generation schedule or network topology changes; the list of lines that can be switched out for control; and the list of credible contingencies are collected. These inputs are then analyzed by performing a look-ahead base-case power flow and a three-stage (screening, ranking, and detailed analysis) transient stability contingency analysis in the second phase, called the analysis phase. A list of critical contingencies is then identified from the transient stability analysis results. Using the list of critical contingencies, the stability information for all the contingencies (energy margin and stability), and information on the critical unstable equilibrium point for each critical contingency from the analysis phase the online line switching can then be performed using the proposed three-stage process in the third phase, also called the identification phase.

The key outputs of this tool are a list of top line switching candidates that can enhance the transient stability of the critical contingencies without compromising the stability of the non-critical contingencies, and the stability margin of the post-switching systems after the top line switching candidates have been applied.

In implementing the online line switching phase for the look-ahead system, we observed that the combinatorial nature of the optimal transmission line switching problem makes it very challenging to find the optimal network topology that improves the transient stability of a single contingency. Extending this problem to include multiple contingencies makes it even more challenging. Coupling these challenges with the need to perform the optimal line switching task online or 30 to 60 minutes ahead makes the MINLP approach impractical for large/physical power

systems. A global optimal solution for all line switching problems usually exists but trying to find the global optimal solution online or 60 minutes ahead can be intractable. Hence, we focus on addressing the problem by the three-stage strategy that offers the advantages of speed, accuracy, and robustness.

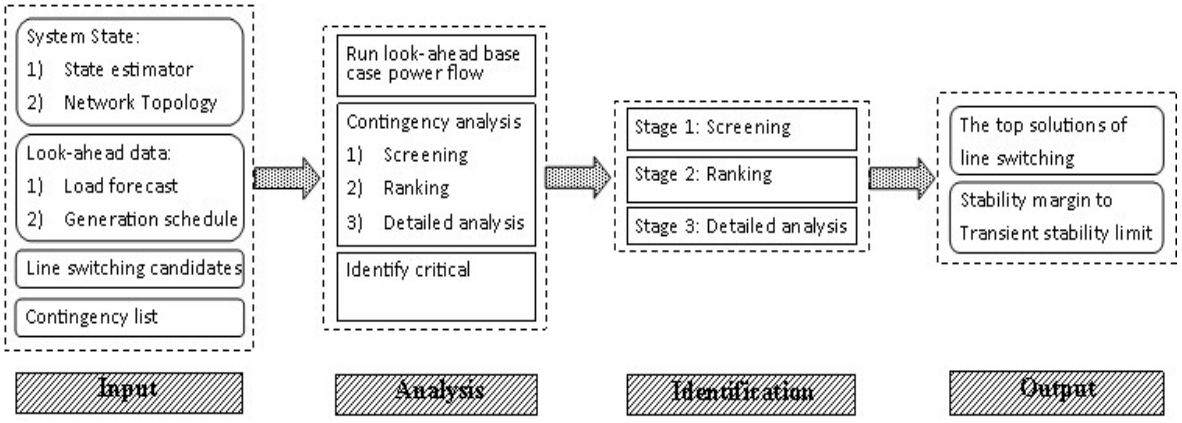

Figure 7.2 Architecture of the proposed online switching for transient stability enhancement of look-ahead power systems.

Before we present the proposed three-stage methodology, we first introduce a novel index, total weighted changes, to assess the performance of line switching candidates.

7.3.1 Total Weighted Changes

In our application of the line switching control action to improve transient stability, we consider the impact of candidate line switching on the transient stability of several critical contingencies. Since the transient stability impact of a line switching candidate will vary for different contingencies, a metric is needed to assess the total impact of a line switching candidate on multiple contingencies. To this end, we propose a total weighted change index. The advantage with this index is that it is effective and suitable for an online or look-ahead application.

For n contingencies and q switching options, let $\Lambda = [\lambda_{ij}]$ be an n-by-q matrix of energy margin sensitivities or energy margin changes where λ_{ij} is the energy margin sensitivity/energy margin change for contingency i for the switching option j.

Let $z = [z_1, \cdots, z_q]^T$, $z_j \in \{0,1\}$ be a vector of the states of the switching options where a state $z_j = 1$ implies that a control action has been taken by switching out the candidate line j. Let $\alpha = [\alpha_1, \cdots, \alpha_n]^T$ be a vector of the weights assigned to the critical contingencies where α_i is the weight assigned to contingency i based on its ranking from the transient stability contingency analysis.

We can define the q-by-1 vector h such that each element h_k of h is given by

$$h_k = [diag(\alpha) * \Lambda] * z$$

$$\sum_{j=1}^{q} z_j = 1, z_k = 1\,. \tag{7.9}$$

Each element in h_k corresponds to the total weighted change in energy margin sensitivities or energy margin changes for switching candidate k. The weights, α, are chosen such that the most critical contingencies have the highest weight, and the least critical contingency has the least weight. The selection of the weights will be based on how the network operator wants to prioritize the criticality of a contingency in selecting the switching options. The weights were chosen to be equal to the inverse of a contingency's ranking for our numerical simulations.

With (7.9), the net transient stability effect of each line switching candidate can be quantified, compared, and ranked relative to other line switching candidates.

We now present the proposed three-stage method for the online line switching for transient stability enhancement of a look-ahead power system. Given the look-ahead power flow and dynamic data, the list of switching candidates, the list of contingencies, the list of critical contingencies, and the transient stability assessment results from the analysis phase, the goal is to find the list of switching candidates that maximizes the total weighted changes in the critical contingencies without making non-critical contingencies critical or any contingency unstable.

7.3.2 Stage 1 (Screening Stage)

In this stage, a fast, energy margin sensitivity method is proposed to screen out the line switching candidates that reduce the transient stability margin, the energy margin, of the critical contingencies after the line switching. This stage reduces the line switching candidates to a smaller list of candidates that are likely to enhance the transient stability of critical contingencies. Line switching candidates with low energy margin sensitivity can also be screen out at this stage.

This stage is based on the energy margin sensitivity method [17, 62, 69, 70]. In the direct method for the transient stability analysis, the stability of a contingency is given by the energy margin. The energy margin of a fault-event or contingency, defined in Chapter 1, is given by the difference between the critical energy and the energy at the fault clearing state (see equation (7.10)) where $E_{uep}(x, y, p)$ is the energy at the critical UEP, and $E_{cl}(x, y, p)$ is the energy at the fault clearing point:

$$E_M(x, y, p) = E_{uep}(x, y, p) - E_{cl}(x, y, p). \tag{7.10}$$

The value of the energy margin, $E_M(x, y, p)$, is a measure of the degree of stability or instability of the post-fault system. Thus, an increase in the energy margin implies an improvement in stability. A change in the energy margin due to a parameter change can be expressed as (7.11).

$$\Delta E_M(x,y,p) = \Delta E_{uep}(x,y,p) - \Delta E_{cl}(x,y,p) \tag{7.11}$$

The change in the energy at the clearing point and the critical UEP with respect to parameter p can be expressed as (7.12) and (7.13), respectively. ΔW_o is the change in the energy margin at the post-fault SEP.

$$\Delta E_{uep}(x,y,p) = \frac{\partial}{\partial x}E_{uep}(x,y,p)\Delta x + \frac{\partial}{\partial y}E_{uep}(x,y,p)\Delta y + \frac{\partial}{\partial p}E_{uep}(x,y,p)\Delta p - \Delta W_o \tag{7.12}$$

$$\Delta E_{cl}(x,y,p) = \frac{\partial}{\partial x}E_{cl}(x,y,p)\Delta x + \frac{\partial}{\partial y}E_{cl}(x,y,p)\Delta y + \frac{\partial}{\partial p}E_{cl}(x,y,p)\Delta p - \Delta E_o \tag{7.13}$$

For a change in network topology, $\Delta p = \Delta Y_{bus}$ where

$$\Delta Y_{bus} = Y_{bus}^{New} - Y_{bus}^{old} \tag{7.14}$$

Y_{bus}^{New} and Y_{bus}^{old} are the matrix representation of the network admittances before and after the network topology change, respectively.

This implies that calculating the energy margin sensitivity to opening transmission line $i-j$, where i and j are the index of the from and to buses of the transmission line, is equivalent to the sum of the energy margin sensitivity to the following network parameter changes:

$$\Delta Y_{bus,ij} = \Delta G_{ij} + j\Delta B_{ij} \tag{7.15}$$

$$\Delta Y_{bus,ii} = j\Delta B_{ii} \tag{7.16}$$

$$\Delta Y_{bus,jj} = j\Delta B_{jj}\,. \tag{7.17}$$

If we neglect network losses, the energy margin sensitivity of a structure-preserving power system to each of the line parameters, series, and shunt admittances, is given by the following equations:

$$E_M^{ij}(x, y, B_{ij}) = \Delta E_{uep}^{ij}(x, y, B_{ij}) - \Delta E_{uep}^{ij}(x, y, B_{ij}) \tag{7.18}$$

$$E_M^{ii}(x, y, B_{ii}) = \Delta E_{uep}^{ii}(x, y, B_{ii}) - \Delta E_{uep}^{ii}(x, y, B_{ii}) \tag{7.19}$$

$$E_M^{jj}(x, y, B_{jj}) = \Delta E_{uep}^{jj}(x, y, B_{jj}) - \Delta E_{uep}^{ij}(x, y, B_{jj}) . \tag{7.20}$$

We can then express the energy margin sensitivity of a structure-preserving power system to network topology changes due to the opening of line $i - j$ in (7.21).

$$\Delta E_M(x, y, Y_{bus}^{ij}) = \Delta E_M^{ij}(x, y, B_{ij}) + \Delta E_M^{ii}(x, y, B_{ii}) + \Delta E_m^{jj}(x, y, B_{jj}) \tag{7.21}$$

The implementation of the complete analytical energy margin sensitivity for a structure-preserving model of the power system to a parameter will require computation of the sensitivity of the initial conditions, state variables x and algebraic variables y to the parameter. It will also include some path-dependent terms for constant impedance load models. This makes online implementation of this method challenging due to the large computational demand required to compute the path-dependent terms and the other sensitivity terms. To overcome this challenge, we employ a faster analytical approach based on some assumptions.

Analytical Energy Margin Sensitivity:

In this analytical approach, we work with the following assumptions:

1. The power system model is represented by a structure-preserving model with classical generator models.

2. Real and reactive loads are modeled as constant power and constant reactance, respectively, for the energy margin sensitivity calculation.
3. There is no governor control and damping factor is assumed to be negligible.

Under the above assumptions, the sensitivity of the energy margin to changes in shunt admittance and line reactance can be approximated by (7.22) and (7.23), respectively, if we neglect the component of the energy margin sensitivity due to the change in the machine angles and speeds at the fault clearing point [62]:

$$E_M^{ii}(\delta, \omega, V, \theta, B_{ii}) = \frac{1}{2}\left(V_{cl,ii}^2 - V_{uep,ii}^2\right) * \Delta B_{ii} \tag{7.22}$$

$$E_M^{ij}\left(\delta, \omega, V, \theta, B_{ij}\right) = \frac{1}{2}\left(I_{cl,ij}^2 - I_{uep,ij}^2\right) * \frac{\Delta B_{ij}}{B_{ij}} \tag{7.23}$$

where $\delta, \omega, V, \theta, V_{cl,ii}$, $V_{uep,ii}$, $I_{cl,ij}$ and $I_{uep,ij}$ correspond to the machine angle, machine speed, the bus voltage magnitude, the bus voltage angle, the bus voltage magnitude at bus i at the clearing point, the bus voltage at bus i at the critical UEP, current flow from bus i to bus j at the clearing point, and current flow from bus i to bus j at the critical UEP, respectively.

Thus, based on the above assumptions, the sensitivity of the energy margin to changes in the network topology due to opening the line $i - j$ is given by (7.24):

$$\Delta E_M\left(x, y, Y_{bus}^{ij}\right) = \frac{1}{2}\left(V_{cl,ii}^2 - V_{uep,ii}^2\right)\Delta B_{ii} + \frac{1}{2}\left(V_{cl,jj}^2 - V_{uep,jj}^2\right)\Delta B_{jj} + \frac{1}{2}\left(I_{cl,ij}^2 - I_{uep,ij}^2\right)\Delta B_{ij}/B_{ij} \tag{7.24}$$

Total Weighted Energy Margin Sensitivity:

If the control action is applied to only one contingency, the screening stage is a simple computation of the sensitivity using (7.24) for each line switching candidate, followed by the elimination of the line switching candidates with negative sensitivity values. However, in the case of multiple contingencies, after the energy margin sensitivity of each critical contingency is computed for each switching candidate using (7.24), the total weighted energy margin sensitivity for each switching candidate can be calculated using (7.9). Then, based on the resulting list of total weighted sensitivities from (7.9), the switching options with negative total weighted energy sensitivities can be eliminated and the rest sent to stage 2 for further assessment. Line switching candidates with low total weighted energy sensitivities can also be screen out at this stage.

7.3.3 Stage 2 (Ranking Stage)

In this stage, the effect of the shortlisted line switching candidates on the energy margins of the critical contingencies are assessed with a more accurate energy margin estimation method. Using the results from the contingency analysis step that preceded the online switching process, the energy margin of each of the critical contingencies is estimated for the shortlisted switching candidates by estimating their critical UEPs after the application of each of the remaining switching candidates. The shortlisted switching candidates are then ranked based on the total weighted change in the energy margins of the critical contingencies and then the top-ranked line switching options are sent to the next stage for further analysis and identification. The estimation of the critical UEP for each critical contingency for the switching candidates assumes that the critical UEP of the post-switching system can be traced from the critical UEP of the pre-switching system. Using this tracing concept, for each network topology change due to transmission line switching, the critical UEP of the post-fault system of each critical contingency can be quickly

computed. This is done by setting the initial value for the algebraic solver being used to compute the post-fault critical UEP of the post network topology change system equal to the critical UEP of the corresponding contingency before the network topology change. By computing the critical UEP with this initial guess, we avoid the time-consuming steps required for critical UEP computations, like the exit point and minimum gradient point computations [1].

The algorithm for estimating the energy margin of the critical contingencies for each line switching candidate is as follows. For each critical contingency:

Step 1: Compute the pre-fault look-ahead stable equilibrium point after the transmission line switching.

Step 2: Compute the post-fault equilibrium point.

Step 3: Integrate the fault-on trajectory to the fault clearing time, which is usually less than 0.1 seconds.

Step 4: Evaluate the critical UEP, using the contingency's critical UEP for the pre-switching post-fault system as the initial guess.

Step 5: Compute the energy function value at the clearing time and the critical UEP, and consequently, the energy margin for the contingency after the network topology change.

Step 6: Compute the change in energy margin for the contingency after the network topology change by comparing it to the energy margin of the pre-switching system, which can be obtained from the contingency analysis step.

The change in energy margin after the network topology change for each contingency is basically a numerical energy margin sensitivity to the change in network topology. Obviously, this

stage requires more computations for each contingency compared to the computations in stage 1, and thus, will be slower. However, due to the fewer assumptions required, the results in this stage are expected to give much more accurate energy margin change/sensitivity results. Another advantage of this step is that, during stage 3, we will already have most of the information we need to perform the complete energy-based direct method transient stability analysis for each critical contingency for the selected candidate switching candidates. We will have the post-fault equilibrium point, the integration of the fault-on trajectory to the fault clearing time, and an estimation of the critical UEP. In stage 3 during the accurate computation of the critical UEP, we can also compare the initial guess of the critical UEP (minimum gradient point) to the critical UEP obtained in the stage 2 calculation and if the norm of their difference is below a certain threshold, we can set the critical UEP for the stage 3 computation to be equal to the value of the critical UEP obtained from the numerical energy sensitivity calculation in stage 2. Thus, there is no need to compute the critical UEP in stage 3 if the approximation in stage 2 is sufficiently accurate.

Total Weighted Energy Margin Change:

If the switching control action is applied to only one contingency then the ranking stage, stage 2, is a simple estimation of the energy margin for each switching candidate. When the control action is applied to multiple contingencies, stage 2 becomes more complicated. Ideally, we want switching candidates that improve/increase the energy margins of all the contingencies. If that is not possible then we seek the switching candidates that improve most of the contingencies and do not make any contingency unstable. We use the total weighted energy margin change to address that goal by calculating the total impact of each line switching candidate on the critical

contingencies. The line switching candidates can then be ranked based on the values of their total weighted energy margin change to determine the top switching candidates.

To meet the criteria proposed above, follow the steps below:

Step 1: Compute the energy margin of each critical contingency for switching candidates.

Step 2: Remove all switching candidates that lead to a negative energy margin of any of the critical contingencies.

Step 3: Compute the change in the energy margin for each contingency for the remaining switching candidates. This change in energy margin is equivalent to the numerical energy margin sensitivity to the change in network topology resulting from the switching candidates.

Step 4: Rank the switching candidates based on the total weighted change in energy margin,and send the top tier of the switching candidates to stage 3 for more accurate and detailed identification of the top switching candidates.

7.3.4 Stage 3 (Detailed Analysis and Identification)

Finally, in stage 3, a standard CUEP-based direct method (BCU method) is used to accurately estimate the effect of each of the top-ranked candidate line switching options on the energy margin, of each critical contingency. The total weighted change in the energy margins of the critical contingencies are then used to identify and select a few top-ranked line switching control actions. To ensure accuracy, the stability of each of the non-critical contingencies is checked for the selected top-ranked line switching solutions using the CUEP-based direct method. If any of the contingencies become unstable or critical after a line switching solution, then that line switching option will be removed from the list of candidates.

The CUEP-based direct method (BCU) is used to accurately compute the energy margin of each of the top-ranked candidate line switching options for each critical contingency. As in stage 2, for each critical contingency the energy margin is computed by computing the critical UEP, i.e. controlling UEP, of the post-fault systems after the application of each of the shortlisted line switching candidates from stage 2. However, in this stage the controlling UEP computation is much more accurate. To minimize the computational burden of this stage, we exploit the fact that we already have some of the information we need to compute the controlling UEP for the critical contingencies in stage 3. From stage 2, we have the post-fault equilibrium point, the fault-on trajectory to the fault clearing time, and an estimation of the controlling UEP for each critical contingency for all the top-ranked line switching candidates. Using this information, we compute the energy margins of the critical contingencies for all the top-ranked switching candidates with the following algorithm. This algorithm is tailored for CUEP-based direct methods that use the BCU method for the computation of the controlling UEP.

For each critical contingency and line switching candidate:

Step 1: Obtain the state of the fault-on system at the clearing time from the results in stage 2 and integrate the sustained fault-on trajectory until you reach the exit point. The exit point can be determined by checking for the point of first maximum potential energy of the energy function value along the sustained fault-on trajectory or by checking the sign of the gradient along the sustained fault-on trajectory.

Step 2: Apply the ray-adjustment method to compute the minimum gradient point (MGP)/initial point of the controlling UEP.

Step 3: Compare the MGP to the controlling UEP computed in stage 2. If they are sufficiently close, use the controlling UEP from stage 2 as the initial guess or as the controlling UEP for the critical contingency in stage 3.

Step 4: Get the energy function value at the clearing time from stage 2 and compute the energy function value of the controlling UEP. Consequently, compute the energy margin.

Step 5: Compute the change in energy margin for the contingency after the network topology change by comparing it to the energy margin of the pre-switching system, which can be obtained from the analysis phase.

Again, if the switching control action is applied to only one contingency, then the final stage is a simple computation of the change in energy margin for each switching candidate. When the control action is applied to multiple contingencies, stage 3 becomes just as complicated as stage 2. Consequently, the line switching candidates can be ranked using the steps proposed to rank the switching candidates in stage 2. In summary, the total weighted change in the energy margins of the critical contingencies for each line switching candidate is computed and then used to rank and identify the top few line switching solutions to recommend to the power system operators. To ensure accuracy, the stability of the non-critical contingencies is checked for the top few line switching solutions by using the CUEP-based direct method. If any of the contingencies are unstable for a line switching solution, then that line switching option will be removed from the list of solutions. A time domain simulation is also performed for the contingencies that turn out to be critical for each of the top switching solutions. The top ranked switching candidates that are stable for all contingencies will then be reported, along with their energy margins and other transient stability information necessary for other control actions like generator rescheduling.

The resulting output is the following information, which network operators can use for transient stability enhancement:

1. A list of switching actions that improve the transient stability of the critical contingencies and doesn't make other contingencies critical or unstable.
2. The energy margin for the look-ahead post-fault system for each contingency, which can be important for other control actions like real power control.

7.4 Online Line Switching Control Methodology

A numerical implementation of the proposed three-stage line switching methodology for transient stability enhancement is presented below:

Step 1: Collect information on the current operating point and the corresponding network topology, the look-ahead (say the next 30 to 60 minutes) load forecasting and generation schedule, the dynamic data set needed for transient stability analysis, and a list of contingencies.

Step 2: Apply the TEPCO-BCU method to determine the stability/instability and energy margin of each contingency, and then rank the contingencies based on energy margins. If all the contingencies are stable, then go to step 3; otherwise, design preventive control actions for unstable contingencies before moving to step 3. The design and implementation of preventive control actions for unstable contingencies is not covered in this work.

Step 3: Create a list of critical contingencies based on a defined threshold value of the energy margin. Thus, all contingencies with energy margin less than the threshold value will be considered critical.

Step 4: Input a list of candidate lines that can be switched open. List of candidate lines that can be switched closed to enhance transient stability can also be considered.

Step 5: (Screening stage) Apply the linear sensitivity-based method presented in the previous section to identify the list of potentially effective switching candidate lines that can increase the energy margin of the critical contingencies.

Step 6: (Ranking stage) For each effective candidate line identified in step 5, estimate its impact on the energy margin of each critical contingency with the CUEP approximation technique described in stage 2. Remove candidate lines that lead to negative energy margins for any of the critical contingencies. Rank the remaining candidate lines using the total weighted energy margin change criteria, with the candidate lines with the largest positive total weighted energy margin change at the top. Send the top-ranked candidate lines to the next stage for detailed evaluation.

Step 7: (Evaluation Stage) For each top-ranked line switching candidate, compute the energy margin of each critical contingency using a CUEP-based method such as the BCU method. Remove candidate lines that lead to negative energy margins for any of the critical contingencies. For the remaining candidate lines, rank each of them according to the weighted energy margin change criteria. Examine the stability of the remaining contingencies for the top-ranked switching candidates using the CUEP-based direct method, and also check for the stability of any contingency that still remains critical using the time domain simulations. Remove any top-ranked switching candidate rendering any of the contingencies unstable.

Step 8: Output report:

1. The top line switching candidates and their effect on the energy margins of all the contingencies (critical and non-critical).
2. Time domain simulation results for critical contingencies.
3. The energy margin for the look-ahead post-fault system for each contingency.

7.5 Numerical Studies

The numerical simulations were performed on a computer with an Intel® Core™ i7-3630QM CPU @2.40GHz processor and 16GB memory. All the simulations were performed with Matlab 7.11. The simulated system is the structure-preserving model of the IEEE 145-bus 50-machine system with classical generators. The generalized list of equations for the structure-preserving model is shown in section 3.2.1 of Chapter 3.

The method is tested on the IEEE 145-bus 50-machine system to improve the transient stability of the critical contingencies in the list of contingencies in Table 7.1. The test is performed on the base-case loading condition and a look-ahead loading condition. 160 branches of the IEEE 145-bus 50-machine system are considered as candidates that can be switched open for transient stability enhancement of critical contingencies. See Appendix A for the list of line switching candidates used in this numerical study. The 160 line switching candidates were selected from the branches of the IEEE 145-bus 50-machine system by evaluating the impact of switching open each of the branches, that are not part of the contingency list, on the energy margin of contingency 1 and then selecting a subset of branches with the most positive impact on the energy margin of contingency 1, the subset of branches with the most negative impact on the energy margin of contingency 1, and a subset of branches with very little impact. Each of the faults in the

contingency list is a three-phase bus fault for a duration of 0.1 seconds, followed by a three-phase line trip.

7.5.1 Numerical Example I

Table 7.2 shows the ranking of the contingencies, based on energy margins, after performing the BCU-based contingency screening and ranking for the base-case loading condition. The contingencies are ranked in descending order of the energy margin. The top seven contingencies in Table 7.2 are selected as the critical contingencies for which their energy margins are to be improved via the line switching action. After performing the energy margin sensitivity-based screening in stage 1 of the proposed method, 40 out of 160 candidate lines (with positive energy margin sensitivities) were sent to stage 2 for ranking. The total weighted change computations used in all the stages (stages 1 to 3) used the inverse of the ranking of the contingencies in Table 7.2 as the weights.

In stage 2, the change in the energy margins of each of the critical contingencies due to the remaining 40 line switching candidates are computed using the CUEP computed with fast CUEP computation method proposed for stage 2. The 40 candidate lines were then screened to remove switching candidates that make any of the critical contingencies unstable. The remaining switching candidates were ranked based on the total weighted change in the energy margins of the critical contingencies. The top 20 of the remaining switching candidates and their corresponding total weighted change in the energy margins is shown in Table 7.3. It should be noted that the ranking of the 20 line switching candidates was in descending order of their total weighted change in the energy margins. The top 10 of the switching candidates were then sent to stage 3 for a detailed estimation of their impact on the critical contingencies using the BCU method. Table 7.4 shows the results of the detailed analysis of the top 10 switching candidates from stage 3 and their

corresponding total weighted change in the energy margins. It can be observed that the list of switching candidates shortlisted in stage 3 is the same as the top 10 candidates obtained in stage 2 in Table 7.3. The total weighted change in energy margins of the shortlisted candidates identified in stage 3 is also equal to the total weighted change in energy margins estimated in stage 2 for all the top 10 line switching candidates. This shows that the CUEP computed with the approximated initial guess in stage 2 offers a significant level of accuracy.

Table 7.1 List of Fault based Contingencies for the IEEE 145-bus 50-machine System

Contingency Number	Fault Bus	Fault Duration (secs)	Tripped Branch		
			From Bus	To Bus	Circuit
1	59	0.1	59	72	1
2	72	0.1	59	72	1
3	115	0.1	115	116	1
4	116	0.1	115	116	1
5	72	0.1	100	72	1
6	100	0.1	100	72	1
7	91	0.1	91	75	1
8	112	0.1	112	69	1
9	69	0.1	112	69	1
10	101	0.1	101	73	1
11	73	0.1	101	73	1
12	6	0.1	6	1	1
13	1	0.1	6	1	1
14	59	0.1	59	103	1
15	103	0.1	59	103	1

Table 7.2 Ranking of Contingencies for the IEEE 145-bus 50-machine System Base Case

Ranking	Contingency Number	Energy Margin
1	15	1.497994678
2	7	1.66624606
3	14	2.014115664
4	1	2.087183221
5	6	4.129883538
6	8	6.937108757
7	10	7.558672164
8	12	24.55048253
9	11	27.57557333
10	2	29.41301965
11	5	29.41558595
12	9	29.93682707
13	13	31.31396353
14	4	92.44915269
15	3	176.3239816

Figure 7.3 shows a comparison of the energy margins of the 7 critical contingencies before and after switching open the top-1 switching candidate identified in stage 3. It is observed that applying the top switching candidate from stage 3 leads to improvement in the energy margins of all 7 contingencies. The energy margin improvements were particularly significant for contingencies 14 and 1, which experience a 188.633% and 180.641% increase in energy margin, respectively. The other contingencies experience changes ranging from an increase in energy margin of 0.636% to 3.556%. Table 7.5 also shows that the critical clearing time of contingencies 14 and 1 are also improved when the top-1 switching candidate is applied. The critical clearing time for the remaining 5 contingencies did not change. The time domain simulations of all 15 contingencies were also stable after application of all of the top 10 switching candidates. The results show that by applying the proposed three-stage method for online transmission line control for transient stability enhancement of this case, we improve the energy margins and critical clearing time of

some of the critical contingencies are improved while keeping the energy margins and critical clearing time of the other critical contingencies the same. Also, all the other contingencies remain stable and non-critical.

Table 7.3 Top 20 Line Switching Candidates and their weighted changes in energy margin for the IEEE 145-bus System based on Stage 2

Switching Candidates			**Total Weighted Change in Energy Margin**
From Bus	**To Bus**	**Circuit**	
24	76	1	2.304866943
22	83	1	0.340321204
25	27	1	0.113430111
25	27	2	0.113430111
12	72	1	0.055354491
12	72	2	0.055354491
12	72	3	0.055354491
76	77	1	0.040111078
12	25	1	0.033807342
12	25	2	0.033807342
16	58	1	0.017778233
2	6	1	0.017672549
29	75	1	0.015718182
6	10	1	0.01110068
6	9	1	0.011042593
10	69	1	0.008944162
9	69	1	0.008890172
8	66	1	0.000341207
8	66	2	0.000341207
62	86	1	-8.34E-05

Table 7.4 Top 10 Line Switching Candidates and their weighted changes in energy margin for the IEEE 145-bus System based on Stage 3

Switching Candidates			Total Weighted Change in Energy Margin
From Bus	To Bus	Circuit	
24	76	1	2.304866943
22	83	1	0.340321204
25	27	1	0.113430111
25	27	2	0.113430111
12	72	1	0.055354491
12	72	2	0.055354491
12	72	3	0.055354491
76	77	1	0.040111078
12	25	1	0.033807342
12	25	2	0.033807342

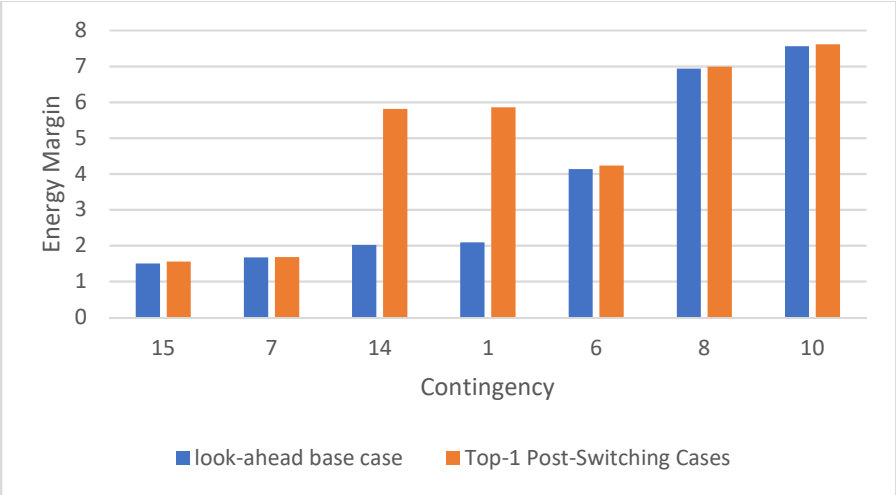

Figure 7.3 Comparison of the energy margins of the base case and the top-1 post-switching case (Line 24 -76) for the top 7 critical contingencies.

Table 7.5 Comparison of Critical Clearing Times of the Top 7 Critical Contingencies after Opening the Top-1 Line Switching Candidate (Line 24 -76) for the IEEE 145-bus 50-machine System Base Case

Contingency Number	Base Case CCT (Seconds)	Top-1 Post-Switching Case CCT (Seconds)
15	0.275	0.275
7	0.2	0.2
14	0.235	0.29
1	0.235	0.29
6	0.27	0.27
8	0.255	0.255
10	0.255	0.255

7.5.2 Numerical Example II

The proposed method is now tested on a look-ahead loading condition. The variation vector of the look-ahead system is shown in Table 7.6. The variation vector is derived from the forecasted change in load and generation. Again, 160 branches of the IEEE 145-bus 50-machine system are considered as candidates for the online transmission line switching for transient stability enhancement. The list of contingencies used in this study is the same as the list used in numerical example I, Table 7.1. Table 7.7 shows the contingency ranking based on the energy margin after performing the BCU-based contingency screening and ranking for the look-ahead loading condition. The top 7 contingencies in Table 7.7 are selected as the critical contingencies whose energy margins are to be improved via the transmission switching process. After applying the proposed three-stage method to the look-ahead case study, the list of 20 in Table 7.8 and 10 in Table 7.9, switching candidates were obtained after stages 2 and 3, respectively. It can be observed that the list of switching candidates shortlisted in stage 3 are the same as the top 10 candidates obtained in stage 2 in Table 7.8. The total weighted change in energy margins of the shortlisted candidates identified in stage 3 are also equal to the total weighted change in energy margins

estimated in stage 2 for all the top 10 line switching candidates. This shows that again the CUEP computed with the approximated initial guess in stage 2 offers a significant level of accuracy.

Table 7.6 Real Load and Generation Variation

Number	Load Bus	Increased Load Direction (MW) - ΔP_L	Generator Bus	Increased Generation Direction (MW) - ΔP_G
1	115	205.05	40	1934.950321
2	116	237.78	41	561.1787464
3	117	145.59	42	4873.493125
4	118	195.57	44	5331.667147
5	119	628.2	45	2169.19695
6	141	9839.7	46	3556.477341
7	142	5321.1	47	2293.590634
8	143	1401.6	48	492.8841748
9	144	2880.6	49	1069.166528
10	145	2751.9	50	1324.485034

Table 7.7 Ranking of Contingencies for the IEEE 145-bus 50-machine System for the Look-ahead Loading Condition

Ranking	Contingency Number	Energy Margin
1	15	1.49819718
2	7	1.673157381
3	14	1.788787203
4	1	1.858799261
5	6	4.126673723
6	8	6.921281748
7	10	7.542042949
8	12	20.35545379
9	11	23.34891502
10	2	25.1748431
11	5	25.17615697
12	9	25.69869091
13	13	27.17933242
14	4	96.68207316
15	3	170.4801402

Table 7.8 Top 20 Line Switching Candidates and their weighted changes in energy margin for the IEEE 145-bus System based on Stage 2 under the Look-ahead Loading Condition

Switching Candidates			Total Weighted Change in Energy Margin
From Bus	To Bus	Circuit	
24	76	1	2.317080274
22	83	1	0.341142659
25	27	1	0.123839554
25	27	2	0.123839554
12	72	1	0.055822747
12	72	2	0.055822747
12	72	3	0.055822747
76	77	1	0.04062853
12	25	1	0.037196973
12	25	2	0.037196973
2	6	1	0.019947549
16	58	1	0.018168975
29	75	1	0.016332646
6	10	1	0.011669654
6	9	1	0.011608392
10	69	1	0.009463728
9	69	1	0.00940638
8	66	1	0.000307873
8	66	2	0.000307873
62	86	1	-9.27E-05

Figure 7.4 shows a comparison of the energy margins of the 7 critical contingencies before and after switching open the top-1 switching candidate identified in stage 3. It is observed that applying the top switching candidate identified at stage 3 leads to improved energy margins of all 7 contingencies. Contingencies 1 and 14 experience a 213.36% and 203.67% increase in the energy margin, respectively. Table 7.10 also shows that the critical clearing time of contingencies 14 and 1 also improved when the top-1 switching candidate is applied. The critical clearing time for the remaining 5 contingencies did not change. The time domain simulations of all 15 contingencies

were also stable after application of all the top 10 switching candidates. The results show the effectiveness of the proposed method in identifying line switching candidates for transient stability enhancement of look-ahead power systems. The energy margins and critical clearing time of some critical contingencies are improved while keeping the energy margins, stability, and the critical clearing time of other critical contingencies unchanged.

Table 7.9 Top 10 Line Switching Candidates and their weighted changes in energy margin for the IEEE 145-bus System based on Stage 3 under the Look-ahead Loading Condition

Switching Candidates			**Total Weighted Change in Energy Margin**
From Bus	**To Bus**	**Circuit**	
24	76	1	2.317080274
22	83	1	0.341142659
25	27	1	0.123839554
25	27	2	0.123839554
12	72	1	0.055822747
12	72	2	0.055822747
12	72	3	0.055822747
76	77	1	0.04062853
12	25	1	0.037196973
12	25	2	0.037196973

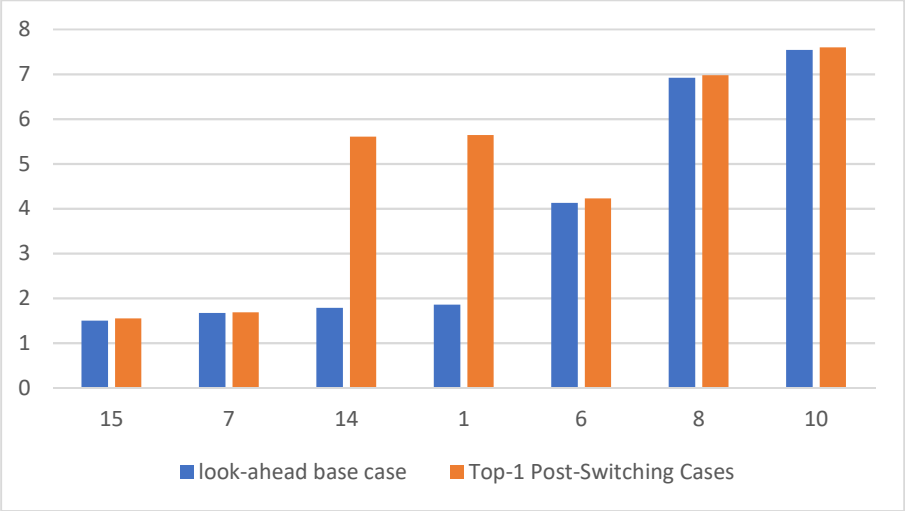

Figure 7.4 Comparison of the energy margins of the look-ahead base case and the top-1 post-switching case (line 24-76) for the top 7 critical contingencies.

Table 7.10 Comparison of Critical Clearing Time for the Top 7 Critical Contingencies After Opening the Top-1 Line Switching Candidate (Line 24 -76) for the IEEE 145-bus 50-machine System

Contingency Number	**Look-Ahead Base Case CCT(Seconds)**	**Top-1 Post-Switching Case CCT(Seconds)**
15	0.275	0.275
7	0.2	0.2
14	0.23	0.285
1	0.235	0.285
6	0.27	0.27
8	0.255	0.255
10	0.255	0.255

7.5.3 Computational Performance

To assess the computational performance of the proposed method, we compare the computation time required for the proposed three-stage method, for numerical examples I and II, to the computation time required for the direct search of the top switching candidates using the

Matlab implementation of the BCU-based direct method. Table 7.11 shows that the average total CPU time for the proposed three-stage method is significantly smaller than the CPU time required to assess the impact of all the 160 switching candidates on the top 7 contingencies using the BCU-based direct method. This is due to the significant reduction in the computational requirements from the use of linearization in stage 1, the MGP approximation in stage 2, and the use of the stability results from stage 2 in stage 3 for the scenarios where the exit-point or MGP in stage 3 is very close to the CUEP computed in stage 2. The computation time of the proposed method is approximately 9 times faster than the application of the Matlab implementation of the BCU-based direct method to all 160 switching candidates. The proposed method and the BCU-based direct method are expected to be much faster in commercial grade implementations.

Table 7.11 Average CPU Time in Minutes for the Two Numerical Examples

	Proposed Method				**Matlab Implementation of BCU Method (min)**
	Stage 1 (min)	**Stage 2 (min)**	**Stage 3 (min)**	**Total (min)**	
Numerical Example I	0.0388	23.657	22.982	46.6778	430.216
Numerical Example II	0.0407	23.633	23.34	47.0137	

7.6 Conclusion

In this chapter, a model for the look-ahead transient stability control of power systems using transmission line switching was presented. An effective transmission line switching methodology for online transient stability enhancement of look-ahead operating conditions was proposed and implemented. The proposed method used a three-stage strategy comprising screening, ranking, and identifying/detailed analysis, to reduce the computational burden inherent with the conventional approach to optimal transmission switching problems. Energy margin sensitivity, and MGP approximation is used to speed up the determination of top line switching candidates. A novel method for quantifying the impact of line switching actions on the stability of multiple contingencies was also proposed and implemented. The method was developed with a focus on speed, accuracy, and robustness. The three-stage method identifies several switching candidates that enhance the transient stability of multiple critical contingencies under look-ahead operating conditions.

It was numerically demonstrated that the proposed method finds line switching candidates that can enhance the transient stability of multiple contingencies in a look-ahead operating condition. The numerical results also show that the proposed three-stage method can fast determine effective candidate lines for look-ahead applications.

Future work on this subject will focus on an extension of the proposed three-stage method to applications where multiple line switching actions are used for the transient stability enhancement control, or applications where line switching control actions, both out and in, are combined with other controls such as real power rescheduling for further enhancing power system transient stability.

CHAPTER 8

A Method for Online Transient Stability Analysis of Look-Ahead Power Systems with Uncertainty

8.1 Introduction

The proliferation of intermittent renewable energy sources, wind and solar energy, in modern electric power systems has led to an increase in uncertainty in an already stochastic system. For the transient stability assessment of the power system, the increase in uncertainty in the power system due to the increase in penetration of intermittent renewable energy sources cannot always be efficiently and accurately handled by the existing deterministic approach, which considers only worst-case scenarios. In this chapter the uncertainty introduced by some elements of the power system, like intermittent energy sources or varying load demand, is incorporated into the transient stability assessment of power systems using CUEP-based direct methods. A dynamic model for the online look-ahead transient stability analysis of power systems with renewable/load uncertainty, considering automatic generation control (AGC) at the pre-fault stage, is formulated. A three-stage method based on direct method is then proposed for online transient stability assessment of look-ahead power systems with uncertainty. Only the uncertainty associated with load and renewable energy sources (modeled as negative load) is considered in this work. The correlations between the random variables, the forecasted load and renewable energy injection, are also considered in this work.

The uncertainty in power systems can generally be incorporated into the system analysis using

a deterministic worst-case scenario approach, a probabilistic approach [79-91] or a stochastic approach [92, 93]. The worst-case scenario approach ignores the probability of occurrence of other scenarios and focuses only on the potentially worst system scenarios. This can result in overly conservative stability assessments and control actions, leading to possible inefficient operation of power systems.

It has been shown in practical applications that the worst-case scenario for a power system is not always the scenario with the worst stability outcome [86]. The stochastic approach to power system analysis usually presents stability results in terms of expected values and their variance which might lack some required information needed for robust control actions. As a result, we adopt a probabilistic approach to the look-ahead transient stability analysis of a power system with uncertainty in this chapter. The probabilistic approach can be grouped mainly into numerical probabilistic methods [82, 85, 86, 87], analytical methods [83, 88, 89, 90, 94,112,113] or estimation methods [80, 95]. The analytical probabilistic methods generally use linearization of power system equations [94, 112, 113] coupled with convolution techniques or employ conditional probability [83, 88, 89, 90]. The linearization of the power system equations and convolution techniques in the analytical method introduces approximation errors and large computational burdens, respectively. This make these types of analytical probabilistic methods impractical for accurate online power system analysis. The conditional probability approach on the other hand requires a lot of data on the probability of individual random variables, power system parameters and events [83, 88, 89, 90]. The results from conditional probability analysis might also not be of practical importance to power system operators, as it only gives a probability of stability or instability of an event. The point estimation methods use the statistical moments of the random input variables as inputs to the non-linear model of the power system to approximate the

distribution of output random variables by their statistical moments [80, 95]. Point estimation method has the advantage of speed over numerical probabilistic methods for small and medium size power systems. However, the computational requirements can increase with increase in system size making it intractable for larger power systems.

The numerical probabilistic methods are generally based on the Monte Carlo (MC) method. The MC method incorporates uncertainty in the analysis of the power system by performing several deterministic analyses of the power system for samples/scenarios created from the probability distribution of the independent random variables or parameters in the system. The common version of the MC method is the random sampling Monte Carlo. This version of MC uses random sampling, a form of data sampling where an independent number of samples are randomly picked from a given probability distribution as representatives of the distribution. The advantages of random sampling MC is its relative simplicity, and its ability to handle nonparametric distributions and correlated random variables, a feature that is not possible in most of the analytical and approximation methods. However, random sampling MC is computationally intensive, and most times requires over 1000 repetitive deterministic runs for a good representation of the system state. Due to its speed limitation, random sampling MC is usually restricted to power system planning applications where time is not of essence.

In this chapter, we use a hybrid between random sampling and stratified sampling called the Latin Hypercube sampling (LHS) [96, 97, 110, 111] in our proposed method. This hybrid method has the advantage of requiring less samples for a full representation of the probability distribution of a random variable. A lot of work has been done on the probabilistic transient stability assessment of power systems [81-91]. Most of this work is based on either the numerical MC method [82, 85, 86, 87] or the conditional probability method [83, 88, 89, 90], and others are based

on other analytical techniques [84]. The authors in [82] use a stochastic and probabilistic approach to model the uncertainty in disturbance occurrences and the system response using an energy-based direct method. The inclusion of the uncertainty of fault clearing time in transient stability assessments is addressed in [83]. A method for estimating the real-time probabilistic critical transfer capability for contingencies using a model which includes short-term wind fluctuations was proposed in [84]. In [85] the MC method is used in the study of the effect of wind generation intermittency and volatility on power system transient stability by computing the angle difference and CCT of contingencies. Monte Carlo techniques were also used to determine the maximum penetration level of wind generation, considering power system transient stability and frequency stability in [87]. The authors in [86] applied the numerical probabilistic method to the B.C. hydro system considering load level factors, fault type, fault location, fault clearing, and automatic reclosing, as probabilistic variables. In [88] the authors incorporated uncertainties into the assessment of the risk of transient instability. The uncertainty considered are randomness in fault occurrence, fault type, fault location, fault clearing time, successful automatic reclosing, fault impedance and the output power of generators. The paper uses a combination of conditional probability, a hybrid transient stability simulation method, and the cost of transient instability in its risk assessments. Probabilistic assessment of power system transient stability considering the uncertainty in fault occurrence, fault type, fault location, fault clearing time, and operating conditions, is also performed using conditional probability in [89, 90]. The author in [90] also included uncertainty due to wind power.

While the authors in [81–91] focused on uncertainty related with both faults and the system operating condition (including uncertainty due to wind power), we will focus on only the uncertainties due to renewable energy or load (system operating condition) for look-ahead

operating conditions since we believe that that uncertainty information is easier to obtain and much more practical. We also consider the impact of the pre-fault automatic generation controls and include them in the system model and propose that the transient stability assessments with uncertainty are performed for only critical contingencies. Finally, we focus making the proposed method fast to make it more applicable to online transient stability assessment of look-ahead power systems by employing a method that requires less samples or scenarios. Thus, we employ a method that reduces the number of samples required while retaining a good representation of the input random variables. We also explore a scenario reduction technique to further reduce the number of deterministic simulations performed in the assessment. To that end, a three-stage methodology of scenario creation, scenario reduction and the transient stability analysis of the shortlisted scenarios is proposed for online look-ahead transient stability assessment of power systems with uncertainty (renewable and load) and AGC.

The main contributions of this work are:

(1). A look-ahead transient stability model considering renewable and load uncertainty, and pre-fault static AGC.

(2). Developing a new method for online look-ahead transient stability assessment of power systems with uncertainty and pre-fault AGC.

(3). Application of the AP clustering algorithm for the reduction of the number of deterministic assessments required for the proposed scenario-based online transient stability assessment of look-ahead power systems with uncertainty and pre-fault AGC.

(4). Creating uncertainty-related contingencies for the proposed scenario-based online transient stability assessment of look-ahead power systems with uncertainty and pre-fault AGC.

(5). Exploiting group properties of scenario contingencies to accelerate the numerical transient stability assessment of power systems with uncertainty and pre-fault AGC.

The proposed method provides much more relevant information for power system operators compared to probabilistic methods based on conditional probability or stochastic methods.

The chapter is organized as follows. In section 8.2, we present the general problem formulation for transient stability of a power system with uncertainty and AGC. We then present the architecture and the numerical scheme of our proposed online methodology for transient stability assessment of look-ahead power systems in section 8.3. The online scheme for transient stability assessment for power systems with uncertainty is then presented in section 8.4. In section 8.5, numerical examples are presented, and the conclusion is presented in section 8.6.

8.2 Problem Formulation

The power system transient stability problem due to fault disturbances for a look-ahead system with uncertainty can be formulated mathematically as comprising: a quasi-steady state pre-fault system with random variables and parameters, a fault system with random variables, and a post-fault system also with random variables, as shown in (8.1) – (8.3):

Look-Ahead Pre-fault System:

$$0 = \tilde{g}_b(\tilde{y}, \lambda, \tilde{u}) = g_{pre}(\tilde{y}) + \lambda \tilde{b}$$

$$0 = f_{pre}(\tilde{x}, \tilde{y}, \tilde{u})$$

$$t < t_f \tag{8.1}$$

Look-Ahead Fault-on System:

$$\dot{\tilde{x}} = f_F(\tilde{x}, \tilde{y}, \tilde{u}\,)$$

$$0 = g_F(\tilde{x}, \tilde{y}, \tilde{u})$$

$$t_f \leq t < t_{cl} \tag{8.2}$$

Look-Ahead Post-Fault System:

$$\dot{\tilde{x}} = f(\tilde{x}, \tilde{y}, \tilde{u})$$

$$0 = g(\tilde{x}, \tilde{y}, \tilde{u})$$

$$t \geq t_{cl} \tag{8.3}$$

where $\tilde{x}$ and $\tilde{y}$ are the vectors of random dynamic state and algebraic variables (voltage magnitude and angle), respectively, and $\tilde{u}$ is a random vector of control variables like real power injection, transmission line switching, and bus voltage magnitude. In the pre-fault system, (8.1), the power system is assumed to be in equilibrium, and $f_{pre}(.)$ represents the dynamic component of the equilibrium equations of the pre-fault system. $\tilde{g}_b(.)$ represent the active and reactive power flow balance equations with uncertainty. The value of the parameter λ determines whether the power balance equations represents the base case pre-fault system or the look-ahead pre-fault system. $\lambda = 0$ for the base case pre-fault power balance system equations and $\lambda = 1$ for the look-ahead pre-fault power balance equations. The variation in the real and reactive power injection due to loads and generators in the look-ahead pre-fault system relative to the base case system is

represented by the vector $\tilde{b}$. The power injection variation vector, $\tilde{b}$, contains deterministic parameters corresponding to scheduled changes in dispatchable generation units without AGC, and random parameters due to forecasted load and renewable energy changes. The vector, $\tilde{b}$, also contain random parameters corresponding to changes in generation of generators with AGC. Since the AGC generation units adjust their power injections to accommodate the real-time changes in demand due to the load and renewable uncertainties their variation parameters will have random components. The reactive load variation parameters are assumed to be constant in this work, but they can also be random. A component of the power injection variation vector corresponding to a forecasted real power load or renewable energy change, represented by a random parameter say $\Delta\tilde{p}$, can be modeled as a combination of a constant change in real power Δp_c, and an error component $\tilde{e}$, as shown in (8.4). The error $\tilde{e}$ is the independent random component of the models in (8.1) and (8.4) and can be represented by a probability distribution function (parametric), or set of data points (nonparametric). The probability distribution function of the forecast error describes the possible values of the error of the associated variation parameter and their corresponding probabilities:

$$\Delta\tilde{p} = \Delta p_c + \tilde{e}. \tag{8.4}$$

The changes in real power due to the error, $\tilde{e}$, will require unscheduled real-time changes in conventional generation (synchronous generators) to ensure the balance of power in the power grid. Since the changes due to $\tilde{e}$ are not scheduled, they can only be handled by generators with automatic generation controls (AGC). The variation in real power injection at each node in the pre-fault system can be represented by equation (8.5):

$$\Delta\tilde{p}_i = \sum_{j\in i} \Delta\tilde{p}_{g_j}^{agc} + \sum_{j\in i} \Delta p_{g_j}^{nagc} + \sum_{j\in i} \Delta\tilde{p}_j^{r} - \sum_{j\in i} \Delta\tilde{p}_j^{d} \tag{8.5}$$

where $\Delta\tilde{p}_{g\_j}^{agc}$ is the change in real power output of AGC unit j, and $\Delta p_{g\_j}^{nagc}$ is the scheduled change in real power output of non-AGC unit j. This value is not random and stays constant for all possible values of the random parameters. $\Delta\tilde{p}_j^{r}$ is the change in real power output of renewable unit j connected to node i, $\Delta\tilde{p}_j^{d}$ is the change in real power demand of load j connected to node i. $j \in i$ implies that node or element j is connected to node i. The change in real power output of a renewable unit j and the change in real power demand of load j can be represented by equations (8.6) and (8.7), respectively.

$$\Delta\tilde{p}_j^{r} = \Delta p_{c_j}^{r} + \tilde{e}\left(\Delta p_j^{r}\right) \tag{8.6}$$

$$\Delta\tilde{p}_j^{d} = \Delta p_{c_j}^{d} + \tilde{e}\left(\Delta p_j^{d}\right) \tag{8.7}$$

$\Delta p_{c\_j}^{r}$ and $\Delta p_{c\_j}^{d}$ are the constant components of the forecasted change in renewable energy and load demand of renewable unit j and load j, respectively, and $\tilde{e}\left(\Delta p_j^{r}\right)$ and $\tilde{e}\left(\Delta p_j^{d}\right)$ are random error components/functions of the forecasted change in renewable energy and load demand of renewable unit j and load j, respectively.

The forecasted change in the real power output of an AGC unit i, $\Delta\tilde{p}_{g\_i}^{agc}$, can be represented by the equation in (8.8). Changes in real power output of AGC units due to renewable generation and load uncertainties is accounted for by the affine adjustment scheme in (8.8).

$$\Delta\tilde{p}_{g\_i}^{agc} = \Delta p_{g\_i}^{agc} + \alpha_i \sum_{j=1}^{N_r} \tilde{e}\left(\Delta p_j^r\right) - \alpha_i \sum_{j=1}^{N_L} \tilde{e}\left(\Delta p_j^d\right)$$

$$\sum_{i=1}^{N_a} \alpha_i = 1 \tag{8.8}$$

where α_i is the participation factor of AGC unit i, $\Delta p_{g\_i}^{agc}$ is the scheduled change in the AGC unit i, N_r is the total number of renewable sources, N_L is the total number of nodes with a load, and N_a is the total number of AGC units.

The differential equations in (8.2) - (8.3) describe the electromechanical and electrical dynamics of components like generators, dynamic loads and their associated control systems. The algebraic system of equations in (8.2) - (8.3), represents the transmission system and the internal static behaviors of passive devices [1]. The renewable energy sources are modeled as constant load models (8.6) and so are only included in the algebraic equations in (8.2) - (8.3).

Unlike in the pre-fault system, the fault-on and post-fault systems (8.2) - (8.3) do not have power variation vectors. This is because after the power system model is updated in the pre-fault system for the look-ahead condition (including uncertainty) the impact of the variation vectors in the pre-fault system will be translated to the equations and variables of the fault-on and post-fault system, since the dynamic variables of the fault-on and post-fault systems are initialized with the

pre-fault equilibrium equations, and the power balance equations of the fault-on and post-fault systems are derived by making changes to the network structure or impedances of the pre-fault system. It is also assumed that there are no changes in the random parameters, forecasted load and renewable energy, during the pre-fault and post-fault periods, since the 5 – 30 seconds duration of time domain simulations are too short for there to be any significant changes in forecasted load and renewable energy sources. Thus, the changes that occur in the pre-fault system due to the variation vector (including the random parameters) is kept constant during the fault-on and the post-fault system for a given scenario. This also implies that once the mechanical power or torque component of the generators are updated to account for the change in their generation, both AGC and non AGC, they remain constant unless a governor model is included in the dynamic models in (8.2) - (8.3). Thus, the impact of the AGC is modeled as static.

With this model (8.1) – (8.8), a method for online transient stability assessment of look-ahead power systems with uncertainty (renewable sources and load), and AGC can be implemented using the proposed three-stage process of scenario creation, scenario reduction, and contingency analysis (screening, ranking and detailed analysis of scenario contingencies). We propose that an initial screening, ranking and detailed analysis is performed for all contingencies using the scenario where random parameters (forecasted renewable energy, load, and AGC injection) of the variation vector are set to their expected values. If there are no unstable contingencies after the initial analysis, then the critical contingencies should be further assessed with the three-stage strategy, else if there are unstable contingencies a control action should be taken, and the initial analysis should be performed again, after the control action. This step should be repeated until all unstable contingencies have been made stable. The proposed method is based on the CUEP-based direct method.

8.3 Architecture and Numerical Scheme for Proposed Method

The numerical probabilistic approach to power system transient stability analysis requires a lot of repetitive simulations which make it computationally demanding. The speed required for an online implementation for multiple contingencies makes the conventional numerical probabilistic approach impractical for online assessment of large/physical power systems. The resulting probability values presented as results from probabilistic assessments might also be impractical for power system operators. To overcome these challenges, we use a scenario contingency-based three-stage strategy built on an CUEP-based direct method that ensures celerity, accuracy of results, and robustness.

The three-stage scheme of scenario creation and scenario reduction followed by technical analysis has been proposed for probabilistic assessments of power systems (unit commitment) for a while now [98-100]. In this work, we apply a similar scheme to online transient stability assessment of look-ahead power systems with load and renewable uncertainty. The layout of the overall process excluding the control actions is depicted in Figure 8.1. It comprises of inputs consisting mainly of the current system state (state estimation output, and network topology), forecast data (including look-ahead (15-30 mins) load and renewable forecast, the generation schedule, forecast error probability distributions, and the correlation between random variables), and a list of contingencies. We will assume the network topology remains the same in the look-ahead system but forecasted changes in the network topology can easily be included as an input. These inputs are then analyzed by first performing the current standard online transient stability analysis of screening, ranking and detailed analysis using the forecasted data without uncertainties or the scenario where random parameters of the variation vector are set to their expected values. For a forecast with zero-mean error the two systems will be the same. If there are no unstable

contingencies then the critical contingencies are sent to the next stage for a detailed assessment using the proposed three-stage scheme of scenario creation, scenario reduction, and transient stability assessment of the resulting list of scenario contingencies. The transient stability assessment of the scenario contingencies is also done using: screening, ranking and detailed analysis. The main outputs are the list of stability status and stability margin of each critical contingency for different scenarios (scenario contingencies), and the stability and margins of the noncritical contingencies. If any of the original contingencies or scenario contingencies are unstable then control actions must be taken and the transient stability analysis performed again.

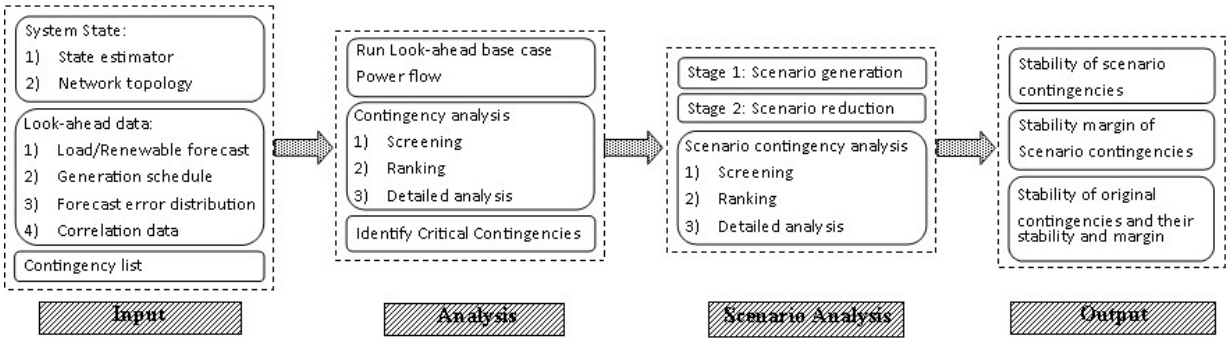

Figure 8.1 Architecture of the proposed online transient stability assessment of look-ahead power systems with load and renewable uncertainty.

To perform the transient stability of the power system with uncertainty online, using a scenario contingency approach, the following three-stage methodology is proposed.

8.3.1 Stage 1 (Scenario Creation)

The implementation of a scenario contingency energy-based method for assessing the transient stability of power systems with renewable energy requires the creation of scenarios. The common approach to creating scenarios for probabilistic or Monte Carlo assessment is to use random

sampling. As highlighted in the introduction, many samples are required for a good representation of the distribution of the random variable being sampled with the random sampling technique, a requirement which is obviously a disadvantage in applications like online assessments where speed is important.

Alternatively, scenarios can be created using stratified sampling techniques or Latin Hypercube sampling (LHS) [96, 97, 110, 111]. LHS has been shown to require less samples compared to random sampling for an equally good or better representation of the distribution of a random variable/parameter [111]. For the same number of samples LHS has also been shown to produce better estimation of the statistics of the distribution being sampled [111]. In [97] the authors observed that the computation time for LHS is comparable to that of random sampling. The Latin Hypercube sampling technique is used to create the optimal number of correlated scenarios required to represent the uncertainty in load and generation in the transient stability analysis by sampling the distribution of the forecasted changes in the look-ahead operating condition. This stage of the proposed method helps incorporate the uncertainty associated with the forecasted load and renewable energy sources in the look-ahead power system into the transient stability analysis of the system with a minimal number of scenarios.

Latin Hypercube Sampling (LHS)

LHS is a hybrid combination of random sampling and stratified sampling. In stratified sampling, the distribution of the random variable/parameter being sampled is subdivided into strata, then each stratum is randomly sampled [96, 110]. Each stratum will have a specific probability or weight to it. This scheme to sampling ensures that every portion of the distribution is sampled.

However, stratified sampling requires the determination of strata and their weights which can be complicated for large dimensions. Thus, weight calculation, and determination of strata makes the stratified sampling process a much more challenging sampling technique compared to the random sampling technique [110]. Latin Hypercube Sampling (LHS) exploits the simplicity features of random sampling while at the same time ensuring good sampling/representation of all portions of a probability distribution by using some modified form of stratified sampling. In LHS the distribution of the random variable/parameter is divided into *N* non-overlapping intervals of equal probability and one value is selected at random or at the middle of each interval [96, 97, 110, 111]. For applications where scenarios are to be created from samples of several independent random variables/parameters, the LHS method is partitioned into a sampling step and a permutation step. The permutation step can serve the purpose of either reducing or establishing correlation between the generated samples. In this work we use the permutation step to establish the correlation between the generated samples based provided correlation data.

Sampling [96, 97, 110, 111]:

If the variables $V_1, V_2, \dots, V_k$ are the random variables/parameters being sampled and (8.9) is the cumulative density function (CDF) of the random variable/parameter V_k:

$$U_k = F_k(V_k), \tag{8.9}$$

then in the sampling stage of the LHS, the CDF of each random variable/parameter is evenly divided into N (where N is the sample size) sampling intervals of equal probability and size $1/N$. In each sample interval, one value, v_k is either randomly picked or selected from the center of the interval [97]. The random selection of v_k in each interval is implemented by randomly picking a

cumulative probability value u_k in the interval and then calculating the corresponding value v_k with equation (8.10). The mid-point selection is attained by selecting the cumulative probability value u_k in the middle of the interval and calculating the corresponding value of v_k with (8.10). The mid-point approach was used in the numerical simulations performed in this chapter.

$$v_k = F_k^{-1}(u_k). \tag{8.10}$$

In this work this sampling technique is applied to the error distribution function of each random load or renewable energy parameter. The result is a well-distributed *N* samples of the random parameters and hence a good representation of their probability distribution.

The sampled random variables/parameters are then assembled in a matrix *V* of dimension *N by K* where *N* is the number of samples and *K* is the number of independent random variables/parameters sampled. The variables are permutated based on the correlation that exists between their distributions. If there is no correlation, then the permutation is done with the aim of minimizing the correlation that exists in the sampled data in V. In this application we are using a technique that applies Cholesky decomposition [96, 109, 110].

Permutation using Cholesky Decomposition (CD) [109, 110]:

In situations where several independent random variables/parameters are being sampled, the sampled variables/parameters are permutated to create scenarios before being passed as inputs to functions, in this case, the transient stability assessment tool. The permutation of sampled variables/parameters can be done randomly to reduced correlation or in a defined manner to reduce

or establish correlations between the random variables/parameters. Several permutation methods exist for increasing or decreasing the correlation between sampled variables e.g. ranked Gram-Schmidt orthogonalization, Cholesky decomposition (CD), single-switch optimization, and other meta-heuristic techniques [97,109]. The major factor to consider when choosing any of these methods is the performance and computational requirement. Of all the methods listed above, Cholesky decomposition (CD) is one of the most efficient methods for permutation of correlated independent random variables/parameters [97]. In the permutation step the goal is to rearrange the sampled data in each column of V (the sample matrix) so that the rank correlation between the samples in each row of the resulting matrix are equal/close to the rank correlation between the random variables/parameters they represent. Let the given rank correlation matrix be, C,. To attain this goal the following steps proposed in [109] are implemented.

Step 1) Construct a matrix S of the same dimension as V. Each column of S will comprise of random permutations of van der Waerden scores $\Phi^{-1}(i/(N+1)), i = 1,2,\ldots..N$, where Φ^{-1} corresponds to the inverse of the standard normal distribution function [109, 110].

Step 2) Apply Cholesky decomposition to C to get the lower triangular matrix P.

$$C = PP^T. \tag{8.11}$$

Step 3) Check the correlation E between the columns of S. If there is approximately zero correlation, that is E is close to an identity matrix, reorder the columns of S using equation (8.12) to get S^*. Then sort the columns of V in the same order of magnitude as the corresponding columns in S^* to get a new matrix V^*. V^* is the rank correlated permutation of the random variables/parameters. If E is not an identity matrix move to step 4.

$$S^* = SP^T \tag{8.12}$$

Step 4) Apply Cholesky decomposition to E to get the lower triangular matrix Q.

$$E = QQ^T \tag{8.13}$$

Step 5) Implement equation (8.14) to remove the correlation that exist between the columns of S, and then apply the desired correlation C to S to get S^*. Sort the columns of V in the same order of magnitude as the corresponding columns in S^* to get V^*. The matrix V^* is the rank correlated permutation of the random variables/parameters.

$$S^* = S(Q^{-1})^T P^T \tag{8.14}$$

The resulting rank correlation approximates the actual correlation C between the random variables/parameters and, in some instances, there might be significant differences between the correlation matrix of V^* and the desired correlation matrix C. The results in such cases can be improved by creating a new S and repeating the steps described above.

V^* containing the generated correlated scenarios is then sent to the next stage for the scenario reduction process.

8.3.2 Stage 2 (Scenario Reduction)

A traditional numerical probabilistic assessment of the transient stability of the shortlisted critical contingencies will require that for each critical contingency, transient stability assessments are performed for all the scenarios generated in the scenario generation stage. Thus, if N scenarios are created in the scenario generation stage, then the number of transient stability studies increases by a multiple of N relative to a simple deterministic study of the critical contingencies. To address this challenge, we propose a scenario reduction step using unsupervised clustering algorithms like

the affinity propagation (AP) algorithm. Clustering algorithms divide datasets into groups based on data attributes or a given metric (measure function). In this work the data set is the scenarios created in the scenario generation stage, and the data attributes/measure function is the square of the Euclidean distance between the scenarios/data points. After grouping the scenarios into clusters, the exemplar/centroid (the scenario around which the other members of a cluster are grouped), and the scenarios with data points farthest from the exemplar of a cluster are used as representatives of the cluster. For each representative scenario, each critical contingency must be assessed for transient stability. Towards this end, a new contingency list comprised of contingencies defined by a combination of the network faults and the representative scenarios is created in this stage. The clustering algorithm used in this work is the AP cluster, but other clustering algorithm could be used

AP Cluster

The affinity propagation (AP) clustering algorithm is a type of unsupervised learning algorithm that clusters data points based on the concept of message passing between data points and a center called an exemplar [101]. The messages shared between the data points can be classified as "Responsibilities" or "Availabilities". A data point indicates how suitable a candidate exemplar is for the data point by sending "Responsibilities" to candidate exemplar, and candidate exemplars on the other hand send "Availabilities" to data points to indicate the fit of a data point to the exemplar's cluster [101]. The messages are all functions of the similarity measures between data points (the negative of the square of the Euclidian distance in this application). The similarity is a measure of how well a data point with index k is suited to be the exemplar of a data point with index i [101]. After a repetitive exchange of messages, the optimal clusters that maximizes the objective function called net similarity is found. Thus, each data point is grouped into clusters such

that the combined “Responsibilities” and “Availabilities” of data points and exemplars is optimal. The AP cluster method does not need a pre-specified number of clusters; it only needs the similarities between data points to determine the number of clusters and the members in each cluster. This feature can be an advantage or disadvantage depending on how the method is being applied. The AP cluster method as per [101] has better performance in terms of speed and accuracy when compared to the k-means clustering method. See [101] for a detailed description of the algorithm. Given the forecast error distributions of the real power injection of two intermittent energy sources with zero mean, a variance of 36, and correlation of 0.5, Figure 8.2 (a) shows example of a plot of a set of 200 data points corresponding to scenarios created with the scenario generation step described in stage ,1 and Figure 8.2 (b) shows a plot of results after clustering the scenarios using AP cluster. In Figure 8.2 (b) data points of the same color belong to the same cluster and the data points with circles are the exemplars of their cluster.

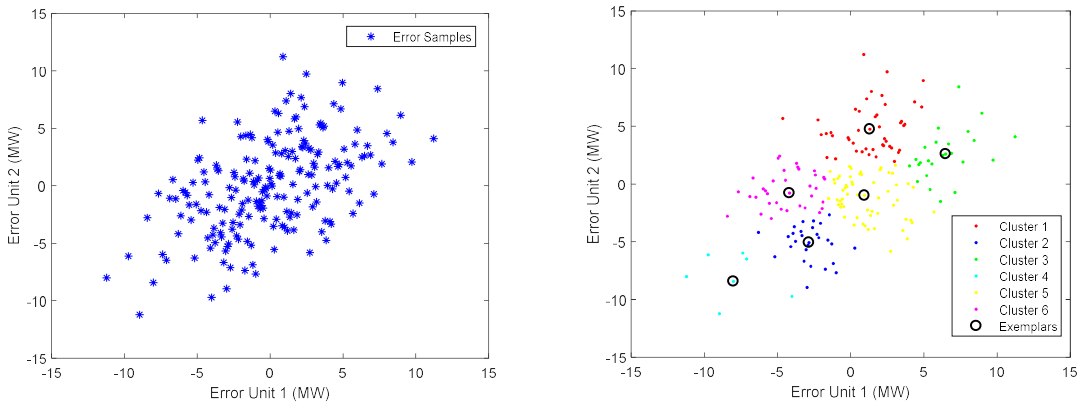

(a) (b)

Figure 8.2 Application of AP cluster to scenarios created from the forecast error of two random parameters (renewable energy generation or load). (a) Shows the original data points. (b) Shows the clusters after applying the AP cluster algorithm to the data in (a).

Scenario Contingency List

After grouping the scenarios into clusters, the exemplar and the top two scenarios farthest from the exemplar of each cluster are chosen as the representative of all the scenarios in the cluster. This assumes that all the scenarios in a cluster share a group property such that their modes of instability are the same. With this assumption, the transient stability results of the representative scenarios of a cluster can be used as the result of the other scenarios in the cluster. But the method compensates for cluster outliers by including the two farthest scenarios as representatives of a cluster. The advantage of this approach is that the number of transient stability assessments is significantly reduced. Also, by dividing the scenarios into clusters, the uncertainty, introduced by the intermittent renewable and load, are still factored into the transient stability assessment as the exemplars and cluster outliers are more likely to be different between clusters and hence, will be a good representative of the uncertainty with minimal computational requirements. Figure 8.3 shows a plot of the clustering in Figure 8.2 (b) with all the exemplars and cluster outliers represented by circles. It shows after the clustering the 200 data points/scenarios can now be represented by 18 scenarios.

The representative scenarios from the scenario reduction step are then set up as a sub-contingency for each contingency in the critical contingency list provided. Thus, a new contingency list based on the scenarios is created, which we will call the scenario contingency list, and is of size M times the number of critical contingencies, where M is the number of scenarios remaining after the scenario reduction.

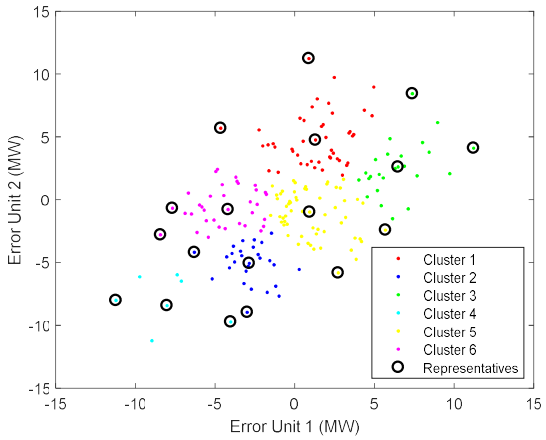

Figure 8.3 Application of AP cluster to scenarios created from the forecast error of two random parameters (renewable energy generation or load). This graph shows the clusters after applying the AP cluster method to the data points in Figure 8.2 (a) and also highlights the exemplars and outliers which are used as cluster representatives with circles.

8.3.3 Stage 3 (Contingency Screening, Ranking and Detailed Analysis)

Finally, in stage 3, a CUEP-based direct method (BCU) is used to accurately compute the energy margin and assess the stability of each of the scenario contingencies created in the screening stage. The energy margin is computed by computing the controlling UEP of the post-fault systems for each scenario contingency. To minimize the computational burden of this stage, we exploit the fact that some of the scenario contingencies belong to the same group, and hence, once we compute the critical UEP of a scenario contingency, we will have some of the information we need, the initial guess of the critical UEP, to compute the critical UEP for the other scenario contingencies in that group. Thus, we do not have to compute the initial guess for the critical UEP for other scenario contingencies in the group. A group here is defined as all the scenario contingencies that are in the same scenario cluster and are derived from the same critical contingency. Using this approach, we can compute the energy margins and consequently assess the stability of all the scenario contingencies in that group, if we have the critical UEP of one scenario in the group. To

improve the performance of the critical UEP computation of a scenario contingency i, using the critical UEP of another scenario contingency j, we will choose j such that the scenario component of scenario contingency j, is the closest to the scenario component of scenario contingency i in terms of the Euclidean distance between the data points sampled for that scenario. Thus, we are going to use the critical UEP of the scenario contingency whose scenario is closest to the scenario of the scenario contingency for which critical UEP is being computed. The grouping of the scenario contingencies can also include any group property that may exist between network contingencies used in the creation of the scenario contingencies [1]. The full algorithm for stage 3 is as presented below. This algorithm is tailored for energy-based direct methods that use the controlling UEP as the critical point.

Step 1: For each scenario from stage 2 create a dynamic assessment data file, run power flow for the look-ahead scenarios, and initialize the dynamic variables.

Step 2: For each scenario contingency, integrate the sustained fault-on trajectory until you reach the exit point if the scenario contingency is the first in its group; otherwise, integrate the fault-on trajectory up to the clearing time. The exit point can be determined by checking the derivative of the energy function value along the sustained fault-on trajectory or by checking for a change in the sign of the gradient along the sustained fault-on trajectory.

Step 3: For each scenario contingency, if the scenario contingency is the first in its group, then using BCU-method solve for the controlling UEP; otherwise, set the controlling UEP of the scenario contingency closest to the scenario contingency being studied as the MGP (Closest in the sense of the Euclidean distance between the scenarios).

Step 4: For each scenario contingency, compute the energy function value at the clearing time and the controlling UEP, and consequently, the energy margin for the scenario contingency.

Step 5: Rank the scenario contingencies based on their energy margins in ascending order.

Step 6: Perform detailed time domain analysis of the unstable or critically stable scenario contingencies to determine the exact unstable contingencies.

Step 7: If any of the scenario contingencies are unstable perform a robust control action and then perform the contingency analysis again starting with the original list of scenarios.

Step 8: Output the following results:

1. The stability of scenario contingences from the contingency screening, ranking and detailed analysis.
2. The stability margin of scenario contingencies.

8.4 Implementation of the Proposed Method

The steps required for the numerical implementation of the proposed online transient stability assessment of look-ahead power systems with uncertainty is as illustrated in the flow chart in Figure 8.4, and described as follows:

Step 1: Using the state estimation results, network topology, expected value of the look-ahead load/generation forecasting, and contingency list perform a transient stability contingency analysis. The analysis is performed using the contingency screening, ranking and detailed analysis strategy. If any of the contingencies are unstable perform control actions and then

send the new system back for another contingency analysis, else identify the critical contingencies and send them to the next step for the scenario contingency analysis.

Step 2: Using the look-ahead load/generation forecasting and correlation data, create scenarios using the LHS method. This scenario creation step is intended to help factor in the uncertainties due to errors in renewable and load forecasts. The LHS method makes it possible to fully represent the distribution of the random parameters with fewer samples compared to random sampling.

Step 3: Reduce the number of scenarios created in step 2 by clustering the scenarios with the AP clustering algorithm, and then in each cluster select the exemplar and the two farthest data points/scenarios as representative scenarios for the cluster. This helps to further reduce the number of scenarios, and hence, the number of transient stability analysis performed without losing the effect of the uncertainties.

Step 4: Create a list of scenario contingencies using the provided list of critical contingencies from step one and the representative scenarios from step three.

Step 5: Using the current operating point, the look-ahead load/generation forecasting, generation schedule, and representative scenarios, create look-ahead dynamic cases for each scenario. This will comprise of creating for each representative scenario a power flow data file with the appropriate updates to the loads, renewable energy source data, and the power injection from generators, both non AGC and AGC units, and a dynamic data file.

Step 6: Determine the stability and energy margin of the scenario contingencies using the BCU method or any other direct method, and then rank the contingencies based on their energy margins.

Step 7: Perform a detailed time domain analysis of the unstable and critical scenario contingencies. If any of the scenario contingencies are unstable or critical, perform robust control and then the perform contingency analysis again starting from step 1.

Step 8: Output the report which will comprise of the scenario contingency ranking, and their energy margins. Other results like time domain simulations are also reported in cases where it is performed in step 7.

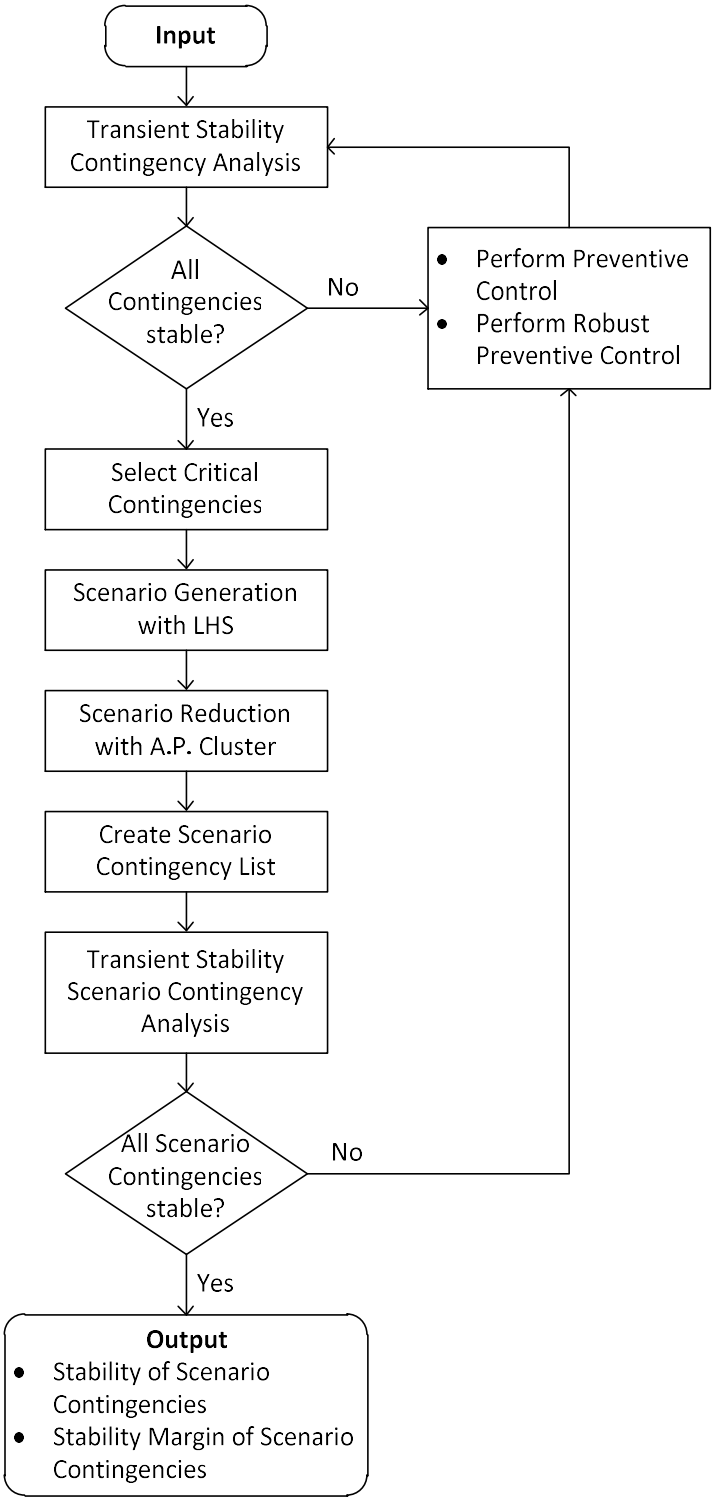

Figure 8.4 Flowchart for the implementation of the probabilistic online transient stability analysis of look-ahead power systems with uncertainty.

8.5 Numerical Studies

The numerical simulations were performed on a computer with an Intel® Core™ i7-3630QM CPU @2.40GHz processor and 16GB memory. All the simulations were performed with Matlab 7.11. The simulations were performed on the structure-preserving model of the WSCC 9-bus 3-machine system with classical generators and constant impedance load. The generalized list of equations for this structure-preserving model is shown in section 3.2.1 of Chapter 3.

The simulations were performed with the list of contingencies shown in Table 8.1 at two look-ahead conditions. Thus, two different sets of forecast errors and correlation data. The faults in the contingency list are three-phase bus faults followed by a three-phase line trip. The fault duration is set at 0.1 seconds for the first numerical test and 0.35 seconds for the second numerical test. The WSCC 9-bus 3-machine system used is shown in Figure 8.2. It is assumed that there are three intermittent renewable energy sources (Wind farms) connected to buses 5, 6 and 8.

Table 8.1 List of Network Contingencies for the WSCC 9-bus 3-machine System

Contingency Number	Fault Bus	Fault Duration	Tripped Branch		
		(secs)	From Bus	To Bus	Circuit
1	5	0.1(0.35)	7	5	1
2	7	0.1(0.35)	7	5	1
3	7	0.1(0.35)	8	7	1
4	4	0.1(0.35)	4	6	1
5	6	0.1(0.35)	4	6	1
6	6	0.1(0.35)	6	9	1
7	9	0.1(0.35)	6	9	1
8	9	0.1(0.35)	9	8	1
9	4	0.1(0.35)	5	4	1
10	5	0.1(0.35)	5	4	1

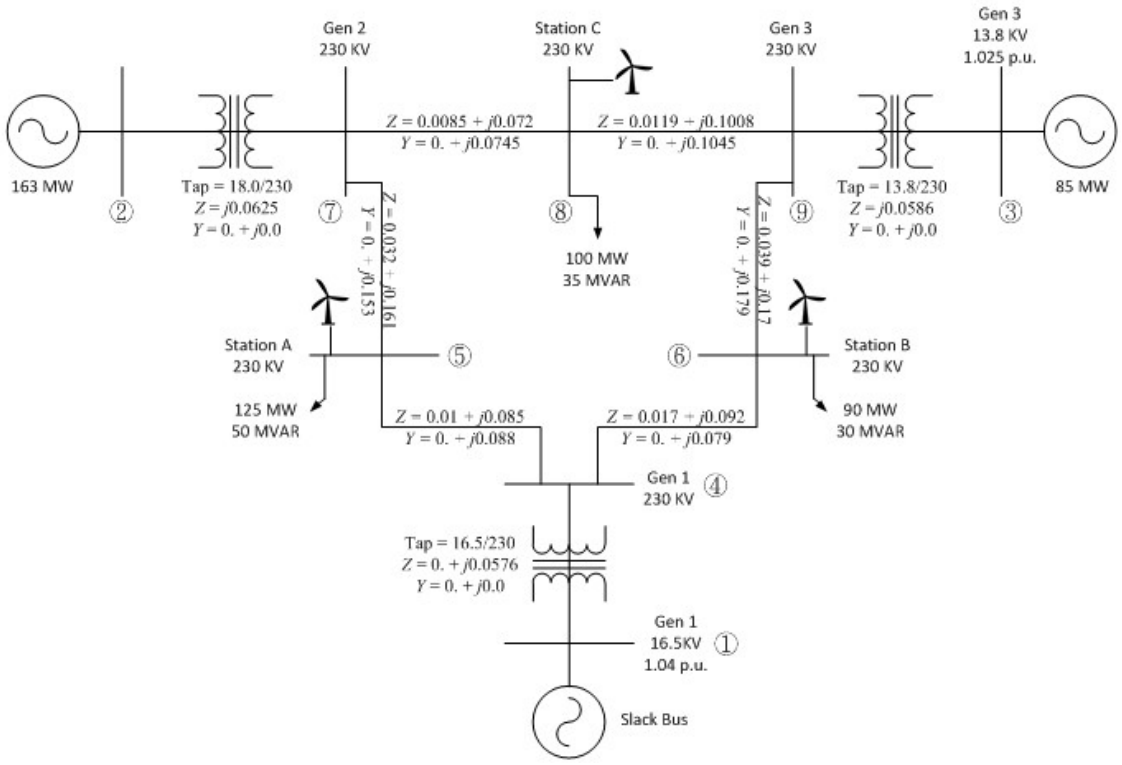

Figure 8.5 The WSCC 9-bus 3-machine system with wind generation units. The value of Y is half the line charging.

8.5.1 Numerical Example I

In this numerical example, the proposed method is tested on a look-ahead operating condition with a variation vector with the parameter values shown in Table 8.2. It is assumed that there is no change in load, see column 4 of Table 8.2. However, there is a change in the scheduled power injection from the synchronous generators at buses 2 and 3 as shown in column 2 of Table 8.2. This change can be attributed to change in generator participation due to scheduling and change due to the renewable energy changes in column 3. Thus, the forecasted renewable energy change has already been factored in the generation change in Table 8.2. Table 8.2 also shows the forecasted variation in the power injected by the renewable energy sources in column 3. It shows the mean and variance of the error associated with the forecasted change in the power injections

from the renewable energy. The error is assumed to have a normal distribution. If it is assumed that there is originally zero power injection from the renewable unit then the forecasted change in power injection from renewable energy units implies that there is a forecasted 30% renewable energy penetration in the look-ahead model. The variance associated with the forecast errors also implies that 99.7% of the absolute value of the forecast errors fall below 57% of the forecasted value. It is assumed that a rank correlation of 0.5 exist between each of the three renewable energy units. The generator at bus 1 is treated as the slack bus, the generator at bus 2 is treated as the AGC unit and the generator at bus 3 is treated as a non AGC unit. All the changes in demand due to the forecasting error are handled by the AGC unit.

Table 8.3 shows the ranking of the contingencies based on energy margin after performing the BCU-based contingency screening and ranking for the look-ahead operating condition without considering the error distribution/uncertainty in the forecasted data. Since all the contingencies are stable the top 2 contingencies in Table 8.3, contingencies 3 and 8, are selected as the critical contingencies. The stability of the critical contingencies under the look-ahead operation condition with uncertainty were then assessed using the proposed three-stage strategy of scenario creation, scenario reduction, and scenario contingency analysis.

Table 8.2 Look-ahead Variation Data – Numerical Example I

Bus Number	Δp_g (MW)	Δp^r (MW)	Δp^L (MW)	$e(\Delta p^r)$	
				Mean	Variance
1	-	-	-	-	-
2	-75.93	-	-	-	-
3	-53.06	-	-	-	-
4	-	-	-	-	-
5	-	31.5	0	0	36
6	-	31.5	0	0	36
7	-	-	-	-	-
8	-	31.5	0	0	36
9	-	-	-	-	-

Table 8.3 Ranking of Contingencies for the WSCC 9-Bus 3-Machine System for Look-ahead Operating Condition without Uncertainty for Fault Duration of 0.1 Seconds

Ranking	Contingency Number	Energy Margin
1	3	2.6568
2	8	2.8090
3	7	3.1645
4	2	3.1902
5	6	3.2224
6	1	3.2543
7	5	3.9471
8	10	4.3605
9	4	4.3667
10	9	4.5132

100 LHS samples were created in stage 1. Table 8.4 and 8.6 shows the resulting scenario contingency list based on the cluster representatives and the critical contingencies, contingency 3 and 8, after the first two stages of the proposed three-stage methodology. It is observed that there

are 60 scenario contingencies in all 30 based on each critical contingency. For each set of 30 scenario contingencies there are 10 groups with three scenario contingencies in each group, implying 10 clusters were created in stage 2. After the screening, ranking and detailed analysis of the scenario contingencies based on contingency 3 we ended up with the stability results shown in Table 8.5. Table 8.5 shows the ranking of the scenario contingencies. From the table we observe that all the scenario contingencies for contingency 3 are stable. Thus, contingency 3 is stable under the uncertainty and there is no need for robust control actions. Table 8.7 also shows the transient stability ranking of the scenario contingencies based on contingency 8. The results in Table 8.7 show that contingency 8 is also stable under uncertainty for this numerical example.

If there had been any unstable scenario contingencies, then robust control actions will be required and the contingency analysis for the 10 original contingencies will be performed again after the control action.

To check the performance of the proposed method, 100 scenario contingencies were created for each of the critical contingencies, contingency 3 and 8, using the 100 LHS samples from stage 1 of the proposed method. The transient stability assessment results for the 100 scenario contingencies corresponding to each critical contingency, contingency 3 and 8, were then compared to the stability assessment results of the corresponding 30 scenario contingencies created in stage 2 of the proposed method. It was observed that all the 100 scenario contingencies derived from contingency 3 and 8 just like the 30 scenario contingencies that were assessed in stage 3 of the proposed method were stable. See Appendix B for the simulation results for the 100 scenario contingencies. This result suggested that the proposed method had a 100% accuracy in the assessment of the transient stability of scenario contingencies. Since all the scenario contingencies for the selected critical contingencies are stable, it is assumed that the noncritical contingencies

are also stable under the look-ahead operating condition with uncertainty. It was confirmed numerically by assessing the transient stability of all the noncritical contingencies for the 100 LHS samples/scenarios created in stage 1 of the three-step process.

Table 8.4 List of Scenario Contingencies for Contingency 3 After First Two Stages – Numerical Example I

Scenario Contingency Number	Fault Bus	Fault Duration (secs)	Tripped Branch			Scenario Data (MW)			Group
			From Bus	To Bus	Circuit	Bus 5	Bus 6	Bus 8	
1	7	0.1	8	7	1	4.531806	4.942615	-3.05998	1
2	7	0.1	8	7	1	-1.44234	10.86982	-4.53181	1
3	7	0.1	8	7	1	8.23198	10.17085	-4.73443	1
4	7	0.1	8	7	1	-6.34777	-8.23198	-6.09041	2
5	7	0.1	8	7	1	-13.0186	-11.758	-15.4526	2
6	7	0.1	8	7	1	-5.8438	-13.0186	2.889925	2
7	7	0.1	8	7	1	6.617376	6.901054	5.378028	3
8	7	0.1	8	7	1	15.45264	6.090412	15.45264	3
9	7	0.1	8	7	1	4.734435	11.75801	13.01858	3
10	7	0.1	8	7	1	-3.05998	4.33422	4.33422	4
11	7	0.1	8	7	1	-4.14123	-0.37618	9.587711	4
12	7	0.1	8	7	1	-4.73443	1.911547	10.17085	4
13	7	0.1	8	7	1	-7.20107	-2.07044	-5.60669	5
14	7	0.1	8	7	1	-15.4526	-1.75398	-1.75398	5
15	7	0.1	8	7	1	-10.8698	-1.13454	-2.39277	5
16	7	0.1	8	7	1	-1.59762	-3.58602	-1.13454	6
17	7	0.1	8	7	1	-8.63588	-5.60669	3.586019	6
18	7	0.1	8	7	1	-3.95243	-3.95243	6.347771	6
19	7	0.1	8	7	1	-1.13454	1.442338	-3.40779	7
20	7	0.1	8	7	1	-1.75398	4.531806	-8.23198	7
21	7	0.1	8	7	1	-5.15693	3.952429	-3.76747	7
22	7	0.1	8	7	1	2.392769	0.678129	1.442338	8
23	7	0.1	8	7	1	1.134539	0.376184	5.156925	8
24	7	0.1	8	7	1	5.378028	1.753984	3.232528	8
25	7	0.1	8	7	1	3.407794	-5.37803	-2.2308	9
26	7	0.1	8	7	1	9.083239	-3.23253	-6.34777	9
27	7	0.1	8	7	1	0.526989	-4.33422	-6.90105	9
28	7	0.1	8	7	1	4.33422	-3.40779	4.141227	10
29	7	0.1	8	7	1	8.635885	-1.59762	7.520257	10
30	7	0.1	8	7	1	5.606689	-3.05998	8.23198	10

Table 8.5 Ranking of Scenario Contingencies for Contingency 3 – Numerical Example I

Ranking	Scenario Ctg. No.	Energy Margin	BCU Stability	Time Domain Stability
1	8	1.843616	Stable	Stable
2	9	1.990233	Stable	Stable
3	7	2.230916	Stable	Stable
4	29	2.331891	Stable	Stable
5	3	2.352595	Stable	Stable
6	30	2.413779	Stable	Stable
7	24	2.423326	Stable	Stable
8	12	2.478035	Stable	Stable
9	23	2.502467	Stable	Stable
10	1	2.513612	Stable	Stable
11	10	2.521297	Stable	Stable
12	11	2.531904	Stable	Stable
13	2	2.540869	Stable	Stable
14	28	2.544037	Stable	Stable
15	22	2.554455	Stable	Stable
16	26	2.680453	Stable	Stable
17	18	2.687915	Stable	Stable
18	19	2.728596	Stable	Stable
19	25	2.760274	Stable	Stable
20	21	2.76792	Stable	Stable
21	20	2.783881	Stable	Stable
22	16	2.80424	Stable	Stable
23	17	2.899346	Stable	Stable
24	27	2.911937	Stable	Stable
25	15	2.987557	Stable	Stable
26	13	3.003626	Stable	Stable
27	6	3.031587	Stable	Stable
28	14	3.093944	Stable	Stable
29	4	3.146154	Stable	Stable
30	5	3.631724	Stable	Stable

Table 8.6 List of Scenario Contingencies for Contingency 8 After First Two Stages - Numerical Example I

Scenario Contingency Number	Fault Bus	Fault Duration (secs)	Tripped Branch			Scenario Data (MW)			Group
			From Bus	To Bus	Circuit	Bus 5	Bus 6	Bus 8	
1	9	0.1	9	8	1	4.531806	4.942615	-3.05998	1
2	9	0.1	9	8	1	-1.44234	10.86982	-4.53181	1
3	9	0.1	9	8	1	8.23198	10.17085	-4.73443	1
4	9	0.1	9	8	1	-6.34777	-8.23198	-6.09041	2
5	9	0.1	9	8	1	-13.0186	-11.758	-15.4526	2
6	9	0.1	9	8	1	-5.8438	-13.0186	2.889925	2
7	9	0.1	9	8	1	6.617376	6.901054	5.378028	3
8	9	0.1	9	8	1	15.45264	6.090412	15.45264	3
9	9	0.1	9	8	1	4.734435	11.75801	13.01858	3
10	9	0.1	9	8	1	-3.05998	4.33422	4.33422	4
11	9	0.1	9	8	1	-4.14123	-0.37618	9.587711	4
12	9	0.1	9	8	1	-4.73443	1.911547	10.17085	4
13	9	0.1	9	8	1	-7.20107	-2.07044	-5.60669	5
14	9	0.1	9	8	1	-15.4526	-1.75398	-1.75398	5
15	9	0.1	9	8	1	-10.8698	-1.13454	-2.39277	5
16	9	0.1	9	8	1	-1.59762	-3.58602	-1.13454	6
17	9	0.1	9	8	1	-8.63588	-5.60669	3.586019	6
18	9	0.1	9	8	1	-3.95243	-3.95243	6.347771	6
19	9	0.1	9	8	1	-1.13454	1.442338	-3.40779	7
20	9	0.1	9	8	1	-1.75398	4.531806	-8.23198	7
21	9	0.1	9	8	1	-5.15693	3.952429	-3.76747	7
22	9	0.1	9	8	1	2.392769	0.678129	1.442338	8
23	9	0.1	9	8	1	1.134539	0.376184	5.156925	8
24	9	0.1	9	9	1	5.378028	1.753984	3.232528	8
25	9	0.1	9	8	1	3.407794	-5.37803	-2.2308	9
26	9	0.1	9	8	1	9.083239	-3.23253	-6.34777	9
27	9	0.1	9	8	1	0.526989	-4.33422	-6.90105	9
28	9	0.1	9	8	1	4.33422	-3.40779	4.141227	10
29	9	0.1	9	8	1	8.635885	-1.59762	7.520257	10
30	9	0.1	9	8	1	5.606689	-3.05998	8.23198	10

Table 8.7 Ranking of Scenario Contingencies for Contingency 8 – Numerical Example I

Ranking	Scenario Ctg. No.	Energy Margin	BCU Stability	Time Domain Stability
1	5	2.794832	Stable	Stable
2	4	2.803511	Stable	Stable
3	6	2.804071	Stable	Stable
4	8	2.805004	Stable	Stable
5	27	2.80568	Stable	Stable
6	26	2.805823	Stable	Stable
7	25	2.80636	Stable	Stable
8	13	2.807025	Stable	Stable
9	16	2.8076	Stable	Stable
10	29	2.807863	Stable	Stable
11	28	2.808056	Stable	Stable
12	14	2.808123	Stable	Stable
13	17	2.808139	Stable	Stable
14	30	2.808338	Stable	Stable
15	15	2.808451	Stable	Stable
16	19	2.808944	Stable	Stable
17	24	2.808977	Stable	Stable
18	20	2.808988	Stable	Stable
19	3	2.809024	Stable	Stable
20	22	2.809113	Stable	Stable
21	1	2.809182	Stable	Stable
22	18	2.809303	Stable	Stable
23	7	2.809414	Stable	Stable
24	23	2.80973	Stable	Stable
25	9	2.809769	Stable	Stable
26	21	2.810093	Stable	Stable
27	11	2.811036	Stable	Stable
28	10	2.811384	Stable	Stable
29	2	2.811404	Stable	Stable
30	12	2.81182	Stable	Stable

8.5.2 Numerical Example II

In this example the proposed method is tested on the same look-head loading condition as in example I but with a different forecast error, correlation data, and fault duration (0.35seconds). The error is assumed to have a normal distribution. It is also assumed that a rank correlation of 0.9, 0.2 and 0.5 exist between the forecasted renewable data for bus 5 and 6, bus 5 and 8, and bus 6 and 8, respectively. The generator at bus 1 is treated as the slack bus, the generator at bus 2 is treated as a non AGC unit and the generator at bus 3 is treated as the AGC unit.

Table 8.9 shows the new contingency ranking based on energy margin after performing the BCU-based contingency screening and ranking for the look-ahead operating condition without considering the error distribution/uncertainty in the forecasted data. Since all the contingencies are stable the top 1 contingency in Table 8.9, contingency 8, is selected as the critical contingency. The stability of the critical contingency under the look-ahead operating condition with uncertainty was then assessed using the proposed three-stage strategy of scenario creation, scenario reduction, and scenario contingency analysis.

Table 8.8 Look-ahead Variation Data – Numerical Example II

Bus Number	Δp_g **(MW)**	Δp^r **(MW)**	Δp^L **(MW)**	$e(\Delta p^r)$	
				Mean	**Variance**
1	-	-	-	-	-
2	-75.93	-	-	-	-
3	-53.06	-	-	-	-
4	-	-	-	-	-
5	-	31.5	0	0	144
6	-	31.5	0	0	81
7	-	-	-	-	-
8	-	31.5	0	0	100
9	-	-	-	-	-

Table 8.10 shows the resulting scenario contingency list based on contingency 8 after the first two stages of the proposed three-stage methodology. In this example we started with 200 LHS samples in stage 1. From Table 8.10 we observe that there are 36 scenario contingencies in all, with three in each group, implying 12 clusters were created in stage 2. Table 8.11 presents the ranking of the scenario contingencies that are based on contingency 8. Ten, 27.7%, of the scenario contingencies are observed to be unstable. This implies that the unstable scenario contingencies must be sent for control actions after which the whole contingency analysis is to be repeated for the resulting system. The design and implementation of the robust control is not covered in this work but will be considered in future work. The stability analysis of all the 200 samples created in stage 1 is also presented in Appendix B. It is observed that 77 of the 200 scenario contingencies are transiently unstable when assessed with the BCU-based direct method, and 28% are unstable when assessed with the conventional time domain simulation. This result show that the proposed method can capture a high percentage of the potentially unstable scenario contingencies with results almost as accurate as the time domain simulation of all contingencies.

Table 8.9 Ranking of Contingencies for the WSCC 9-Bus 3-Machine System for Look-ahead Operating Condition without Uncertainty for Fault Duration of 0.35 Seconds

Ranking	**Contingency Number**	**Energy Margin**
1	8	0.3846
2	3	0.3918
3	7	1.1377
4	2	1.3824
5	6	3.186
6	1	3.2132
7	5	3.8335
8	10	4.1803
9	4	4.2465
10	9	4.3864

Table 8.10 List of Scenario Contingencies for Contingency 8 – Numerical Example II

Scenario Contingency Number	Fault Bus	Fault Duration (secs)	Tripped Branch			Scenario Data (MW)			Group
			From Bus	To Bus	Circuit	Bus 5	Bus 6	Bus 8	
1	9	0.35	9	8	1	-15.2069	-5.04557	5.315241	1
2	9	0.35	9	8	1	-20.6655	-6.42834	20.04352	1
3	9	0.35	9	8	1	-25.2965	-13.1148	8.870126	1
4	9	0.35	9	8	1	12.82792	12.49416	9.63946	2
5	9	0.35	9	8	1	20.03209	21.88811	22.41064	2
6	9	0.35	9	8	1	23.02304	18.03917	14.57202	2
7	9	0.35	9	8	1	20.66549	15.02406	1.82715	3
8	9	0.35	9	8	1	33.67932	14.58754	-13.2532	3
9	9	0.35	9	8	1	29.18414	25.25949	8.150032	3
10	9	0.35	9	8	1	-4.06117	-1.41558	3.251901	4
11	9	0.35	9	8	1	-7.08234	-3.4067	-2.08262	4
12	9	0.35	9	8	1	-7.26214	-5.58268	-0.06266	4
13	9	0.35	9	8	1	1.735344	0.169182	6.509737	5
14	9	0.35	9	8	1	4.06117	5.998884	9.05742	5
15	9	0.35	9	8	1	3.744074	5.582681	10.04634	5
16	9	0.35	9	8	1	-19.45	-15.4991	-7.97656	6
17	9	0.35	9	8	1	-16.2733	-16.6048	-28.0661	6
18	9	0.35	9	8	1	-33.6793	-25.2595	-16.6934	6
19	9	0.35	9	8	1	12.56469	6.574753	-8.15003	7
20	9	0.35	9	8	1	25.29648	8.675514	-13.8824	7
21	9	0.35	9	8	1	14.24878	4.914121	-21.0804	7
22	9	0.35	9	8	1	-0.52648	4.271665	15.33889	8
23	9	0.35	9	8	1	7.998512	13.45002	28.0661	8
24	9	0.35	9	8	1	-8.1873	-1.64443	19.18586	8
25	9	0.35	9	8	1	4.54227	1.529885	-3.78523	9
26	9	0.35	9	8	1	-1.28061	-0.62079	-5.31524	9
27	9	0.35	9	8	1	0.677047	-2.57218	-4.32955	9
28	9	0.35	9	8	1	-2.49914	-4.39832	-10.6899	10
29	9	0.35	9	8	1	6.034479	-5.17809	-24.3201	10
30	9	0.35	9	8	1	2.807344	-3.52818	-18.4498	10
31	9	0.35	9	8	1	7.082343	6.722932	1.699872	11
32	9	0.35	9	8	1	13.09747	4.525859	1.067179	11
33	9	0.35	9	8	1	11.80904	4.020835	-1.69987	11
34	9	0.35	9	8	1	-9.16394	-8.32315	-6.05178	12
35	9	0.35	9	8	1	-11.809	-10.9184	-16.2084	12
36	9	0.35	9	8	1	-11.3303	-13.45	-12.9573	12

Table 8.11 Ranking of Scenario Contingencies for Contingency 8 – Numerical Example II

Ranking	Scenario Ctg. No.	Energy Margin	BCU Stability	Time Domain Stability
1	4	-2.525075	Unstable	Unstable
2	8	-2.517288	Unstable	Unstable
3	20	-1.629753	Unstable	Unstable
4	15	-1.537701	Unstable	Unstable
5	14	-1.517307	Unstable	Unstable
6	22	-1.50541	Unstable	Unstable
7	32	-1.492854	Unstable	Unstable
8	31	-1.207229	Unstable	Unstable
9	33	-1.085291	Unstable	Unstable
10	19	-0.791336	Unstable	Unstable
11	24	-0.568872	Unstable	Stable
12	13	-0.499394	Unstable	Stable
13	25	0.128194	Stable	Stable
14	21	0.542679	Stable	Stable
15	10	0.633094	Stable	Stable
16	18	0.696515	Stable	Stable
17	27	1.043059	Stable	Stable
18	26	1.146696	Stable	Stable
19	2	1.18661	Stable	Stable
20	5	1.589337	Stable	Stable
21	9	1.622817	Stable	Stable
22	11	1.699947	Stable	Stable
23	12	1.736024	Stable	Stable
24	6	1.744658	Stable	Stable
25	23	1.85856	Stable	Stable
26	1	1.941812	Stable	Stable
27	7	2.09221	Stable	Stable
28	17	2.131981	Stable	Stable
29	28	2.156379	Stable	Stable
30	30	2.284088	Stable	Stable
31	29	2.629675	Stable	Stable
32	34	2.655243	Stable	Stable
33	3	3.062638	Stable	Stable
34	16	3.272556	Stable	Stable
35	36	3.440265	Stable	Stable
36	35	3.482234	Stable	Stable

8.5.3 Computational Performance

To assess the computational performance of the proposed method, we compare the combined computation time required for stage 2 and 3 of the proposed three-stage method, for numerical examples I and II, to the computation time required for the direct stability assessment (BCU) of the 100 and 200 scenarios from LHS samples created in the two numerical examples. Table 8.12 shows that the average total CPU time for the last two stages of the proposed method is significantly smaller than the CPU time for direct method assessment of the 100 and 200 scenario contingencies. This is obviously due to the 70% and 82% reduction in the number of scenario contingencies obtained in numerical examples I and II, respectively, by using the proposed method. The approximation of the MGP for the controlling UEP computation also reduces the CPU time for the energy-based transient stability assessment of a scenario by 30% on the average. The computation time for stage one of the proposed method is not included in the comparison because it is a required step for both the full simulation and the proposed three stage method.

Table 8.12 Average CPU Time in Seconds for the Two Numerical Examples

	Proposed Method	**Direct Method**	**Increase in Speed (%)**
Numerical Example I	41.0024	197.0760	480.6343
Numerical Example II	49.451935	434.2827	878.1915

8.6 Conclusion

A look-ahead transient stability model for a power system with renewable and load uncertainty was presented. A scenario-based method for the online transient stability assessment of look-ahead power systems with uncertainty and AGC was proposed and implemented. The proposed method used a three-stage strategy, comprising, scenario generation, scenario reduction, and scenario contingency analysis (scenario contingency screening, ranking and detailed analysis) to speed up the transient stability assessment of look-ahead power systems with uncertainty. The Latin hypercube sampling method was employed in the scenario generation stage to reduce the number of samples required for a good representation of the probability distribution of random input parameters. In the scenario reduction stage, the AP cluster method was used to create clusters from which representative scenario contingencies, based on the exemplar and outlier cluster members, were created. The energy based direct method together with the conventional time domain method was then used to assess the transient stability of scenario contingencies created in stage 2 of the proposed method.

From the numerical examples its observed that the proposed method provides accurate transient stability results for power systems with uncertainty. The proposed three-stage method is also obviously faster compared to assessing the stability of all the scenarios generated with either LHS or random sampling techniques, as it requires less executions of the underlying deterministic transient stability assessments. This makes the proposed method more applicable in online look-ahead environments. The proposed method also provides practical information on the stability of potential scenario contingencies instead of expected values of stability for a contingency. This information and manner of presentation of the stability will give system operators a better

understanding of the potential transient instability problems due to uncertainty and will also give them the data they need to perform robust control actions.

Future work on this subject will focus on an extension to include the dynamic models of the renewable energy sources, further reduction in required scenarios, and the formulation and implementation of a robust control action for cases with unstable scenario contingencies.

CHAPTER 9

Conclusion and Future Work

9.1 Conclusion

The thesis addressed the problem of developing power system tools and solutions for fast and yet reliable online transient stability assessment and control based on the BCU method with a three-prong approach: improving the robustness of unstable equilibrium point computations; extending the model capabilities of the BCU-based controlling UEP method; and implementing novel assessment and control capabilities based on the BCU method.

In Chapter 2 and 3 we focused on the robust computation of unstable equilibrium points. We used the quotient gradient transformation to transform the unstable equilibrium point into a stable equilibrium point and effectively enlarged the convergence region of the point corresponding to the unstable equilibrium point. We then solved for the unstable equilibrium point, by computing the stable equilibrium point that resulted from the quotient gradient transformation, with the pseudo-transient continuation method. It improved the speed of the UEP computation and expanded the convergence region of the UEP compared to the convergence region of the UEP for the Newton-Raphson method and other continuous Newton methods. We improved the computational performance of the combined quotient gradient transformation and pseudo-transient continuation method by approximating the Jacobian in the implementation of the steps of the pseudo-transient continuation method. The Jacobian approximation exploited the structure of the quotient gradient system that resulted from the transformation. Approximating the Jacobian

eliminated the construction of a second Jacobian and ensured that the proposed method only converged to solutions that were equilibrium points of the original system. We studied the convergence properties of the method resulting from the proposed combination of the quotient gradient transformation and the inexact pseudo-transient continuation method. We showed that the proposed method will only converge to solutions of the original system. We also demonstrated the performance of the proposed method with numerical examples, and an integrated solution algorithm that combines the quotient gradient-based pseudo-transient continuation method with the Newton-Raphson method was proposed for reliable computation of unstable equilibrium points.

Chapter 4 explored the extension of the BCU method to power system models with nonlinear excitation system. A numerical energy function for a lossy power system model with a nonlinear excitation system was developed. The resulting energy function and the theoretical work in [1] was used to extend and implement the BCU method for the detailed power system with nonlinear excitation. The extended method was evaluated on a test system and, numerical results show that the BCU method for lossy power system models with detailed excitation models has the potential of providing fast and accurate stability assessment results if the energy function is less path dependent and the stability boundary following procedure used in the BCU method is implemented successfully.

Chapter 5 and 6 investigated the dynamics and stability of post-switching power systems and developed a novel CUEP-based direct method for the transient stability analysis of switching events. We studied the dynamics of the post-switching power system and numerically and theoretically showed that the static stability of a post-switching power system does not imply dynamic stability. Thus, the existence of a post-switching equilibrium point does not imply the

post-switching system is stable. We also showed that the frequency of occurrence of the mismatch between static and dynamic stability assessments increases with increasing loading conditions, and this increase in frequency of stability mismatches can be attributed to the decrease in the size of the stability region of the post-switching equilibrium point as the loading condition increases. Confirming work done in [114] we showed that the decrease in the size of the stability region of the post-switching power system with increase in loading condition can be attributed to the changes in the locations of the stable post-switching equilibrium point and the unstable equilibrium points on the stability boundary of the post-switching power system, and that beyond a loading condition close to the saddle node bifurcation point of a post-switching power system the changes in the size of the stability region of the post-switching power system can be attributed to the movement of the closest UEP towards the post-switching stable equilibrium point. In Chapter 6, we proposed and implemented a novel BCU-based direct method for assessing the transient stability of switching events. The proposed method uses the CUEP of a fault event, closely related to the switching event being assessed, to define the stability region of the post-switching system. A scheme based on screening, ranking and detailed analysis, using the proposed direct method, for the transient stability assessment of switching events is presented.

In Chapter 7 we proposed and implemented a tool for the fast and online determination of transmission line switching candidates that can be used to enhance the transient stability of multiple contingencies for look-ahead loading conditions of a power system. We first formulated the look-ahead line switching for transient stability enhancement of multiple critical contingencies optimization problem. We then proposed and implemented a novel weighting scheme to help compare the impact of various line switching actions on the transient stability of multiple contingencies. A three-stage strategy for the fast and online determination of line switching

candidates that can be used to enhance the transient stability of multiple critical contingencies for a look-ahead loading condition of a power system was then proposed and implemented. The three-stage strategy comprises a screening stage using energy margin sensitivity, a ranking stage using a MGP approximation technique, and an identification stage using an energy-based direct method like the BCU method.

Chapter 8 proposed and implemented a scenario-based method for online transient stability assessment of look-ahead power systems with uncertainty. We formulated the electromechanical dynamics of a look-ahead power system before, during, and after a fault-disturbance. We then proposed and implemented a three-stage strategy for the online transient stability assessment of a look-ahead power system with uncertainty and automatic governor control using a three-stage scenario contingency approach. The three-stage strategy comprised a scenario creation stage using the Latin hypercube sampling method, a scenario reduction stage using the affinity propagation clustering algorithm, and a scenario contingency analysis stage using a combination of an CUEP-based direct methods like the BCU method and time domain simulations.

9.2 Future Work

- Apply the work in Chapter 2 and 3 to improve the speed of the BCU-based controlling UEP method. This is because if the convergence region of a controlling UEP is expanded with the quotient gradient-based pseudo-transient continuation method, then the procedure for finding the minimum gradient point could be improved since the initial point for the controlling UEP can be farther away.

- Improve the performance of the work done in Chapter 4. The method should be made robust enough to work for all contingencies. The work on model extensions for the BCU method could also be extended to governor models and excitation systems with limiters.
- The novel direct method for the transient stability analysis of switching events proposed in Chapter 6 can be extended to the transient stability assessment of generator trip events, and to transient stability assessment of power systems with renewable energy sources that have low voltage ride through models.
- Future work will focus on an extension of the proposed three-stage method for transient stability enhancement of look-ahead power systems to applications where multiple line switching actions are used for the transient stability enhancement control, or applications where line switching control actions, both out and in, are combined with other controls such as real power rescheduling to enhance power system transient stability.
- The work on the online look-ahead transient stability of power systems with uncertainty in Chapter 8 can be extended to include dynamic models for the renewable energy sources. It can also be extended to include online robust control of unstable scenario contingencies.
- Future work can also focus on extending the CUEP-based method to power system transient voltage problems.

APPENDIX A

Line Switching Candidates

Table A.1. List of Line Switching Options for Power System Transient Stability Enhancement

Candidate No.	From Bus	To Bus	Circuit
1	28	75	1
2	15	58	1
3	19	59	1
4	14	17	1
5	14	17	2
6	18	59	1
7	83	89	1
8	12	14	1
9	12	14	2
10	72	98	1
11	58	98	1
12	89	103	1
13	7	66	1
14	67	124	1
15	67	69	1
16	136	141	1
17	60	94	1
18	59	89	1
19	75	108	1
20	2	6	1
21	65	97	1
22	116	118	1
23	136	143	1
24	22	30	1
25	30	78	1
26	141	117	1
27	75	96	1
28	132	133	1
29	142	130	1
30	63	116	1
31	121	122	1
32	70	112	1
33	136	117	1

Candidate No.	From Bus	To Bus	Circuit
34	67	121	1
35	10	32	1
36	32	69	1
37	9	11	1
38	11	69	1
39	82	91	1
40	91	109	1
41	73	74	1
42	119	144	1
43	121	132	1
44	142	120	1
45	74	96	1
46	130	144	1
47	33	38	1
48	117	143	1
49	97	124	1
50	128	131	1
51	142	117	1
52	115	117	1
53	139	142	1
54	8	66	1
55	8	66	2
56	136	140	1
57	109	121	1
58	134	139	1
59	142	116	1
60	142	116	1
61	61	62	1
62	61	62	2
63	61	62	3
64	142	125	1
65	123	131	1
66	143	144	1
67	116	143	1
68	14	15	1
69	47	87	1
70	14	16	1
71	48	87	1
72	91	96	1

Candidate No.	From Bus	To Bus	Circuit
73	118	132	1
74	41	42	1
75	47	48	1
76	52	53	1
77	54	55	1
78	56	57	1
79	64	65	1
80	101	112	1
81	70	71	1
82	71	73	1
83	133	143	1
84	141	132	1
85	62	86	1
86	62	86	2
87	118	131	1
88	27	28	1
89	39	84	1
90	40	84	1
91	45	85	1
92	46	85	1
93	142	133	1
94	120	130	1
95	71	74	1
96	131	133	1
97	137	140	1
98	108	109	1
99	67	132	1
100	128	130	1
101	108	121	1
102	124	131	1
103	142	132	1
104	122	143	1
105	9	69	1
106	10	69	1
107	122	132	1
108	119	129	1
109	6	9	1
110	6	10	1
111	135	95	1

Candidate No.	From Bus	To Bus	Circuit
112	120	124	1
113	68	69	1
114	73	81	1
115	98	103	1
116	119	125	1
117	29	75	1
118	25	74	1
119	12	25	1
120	12	25	2
121	16	58	1
122	121	128	1
123	60	135	1
124	59	60	1
125	124	132	1
126	59	98	1
127	12	72	1
128	12	72	2
129	12	72	3
130	119	121	1
131	119	128	1
132	25	27	1
133	25	27	2
134	94	95	1
135	94	138	1
136	120	125	1
137	131	132	1
138	98	100	1
139	117	118	1
140	14	58	1
141	79	107	1
142	60	138	1
143	59	80	1
144	60	95	1
145	139	145	1
146	120	121	1
147	59	107	1
148	79	92	1
149	59	100	1
150	76	77	1

Candidate No.	From Bus	To Bus	Circuit
151	59	92	1
152	102	117	1
153	135	138	1
154	24	77	1
155	128	129	1
156	121	125	1
157	59	79	1
158	22	83	1
159	76	89	1
160	24	76	1

APPENDIX B

Scenario Contingency Analysis Results

Table B.1. Results for 100 Scenario Contingencies for Contingency 3 – Numerical Example I

Scenario Ctg. No.	Energy Margin	BCU Stability	Time Domain Stability
1	2.319152	Stable	Stable
2	3.536486	Stable	Stable
3	2.351853	Stable	Stable
4	2.766793	Stable	Stable
5	2.65359	Stable	Stable
6	2.111943	Stable	Stable
7	2.785795	Stable	Stable
8	2.918664	Stable	Stable
9	2.76792	Stable	Stable
10	3.031587	Stable	Stable
11	2.444056	Stable	Stable
12	2.671317	Stable	Stable
13	2.454169	Stable	Stable
14	2.642857	Stable	Stable
15	3.141161	Stable	Stable
16	2.282777	Stable	Stable
17	2.661325	Stable	Stable
18	2.5776	Stable	Stable
19	1.843616	Stable	Stable
20	2.831441	Stable	Stable
21	3.148655	Stable	Stable
22	2.331891	Stable	Stable
23	2.621477	Stable	Stable
24	2.687915	Stable	Stable
25	3.004522	Stable	Stable
26	2.618288	Stable	Stable
27	3.216578	Stable	Stable
28	2.502467	Stable	Stable
29	2.899346	Stable	Stable
30	3.171084	Stable	Stable
31	1.990233	Stable	Stable
32	2.352595	Stable	Stable

Scenario Ctg. No.	Energy Margin	BCU Stability	Time Domain Stability
33	2.911937	Stable	Stable
34	2.540869	Stable	Stable
35	2.215348	Stable	Stable
36	3.631724	Stable	Stable
37	2.987557	Stable	Stable
38	2.513612	Stable	Stable
39	2.767787	Stable	Stable
40	2.385708	Stable	Stable
41	2.793449	Stable	Stable
42	2.855631	Stable	Stable
43	2.455721	Stable	Stable
44	3.146154	Stable	Stable
45	3.241768	Stable	Stable
46	2.507	Stable	Stable
47	2.062072	Stable	Stable
48	2.950597	Stable	Stable
49	2.585534	Stable	Stable
50	2.680453	Stable	Stable
51	2.705582	Stable	Stable
52	2.688991	Stable	Stable
53	2.614456	Stable	Stable
54	3.28459	Stable	Stable
55	2.58466	Stable	Stable
56	2.498904	Stable	Stable
57	2.42704	Stable	Stable
58	2.8846	Stable	Stable
59	2.83141	Stable	Stable
60	2.98999	Stable	Stable
61	2.531904	Stable	Stable
62	3.093944	Stable	Stable
63	2.230916	Stable	Stable
64	2.413779	Stable	Stable
65	2.936654	Stable	Stable
66	2.585223	Stable	Stable
67	2.168522	Stable	Stable
68	2.521297	Stable	Stable
69	2.327405	Stable	Stable
70	1.966034	Stable	Stable

Scenario Ctg. No.	Energy Margin	BCU Stability	Time Domain Stability
71	2.561931	Stable	Stable
72	2.492762	Stable	Stable
73	2.783881	Stable	Stable
74	2.715939	Stable	Stable
75	3.003626	Stable	Stable
76	2.454469	Stable	Stable
77	2.342624	Stable	Stable
78	2.860173	Stable	Stable
79	2.808217	Stable	Stable
80	2.227893	Stable	Stable
81	2.287378	Stable	Stable
82	2.755687	Stable	Stable
83	2.423326	Stable	Stable
84	2.787595	Stable	Stable
85	2.80424	Stable	Stable
86	3.055867	Stable	Stable
87	2.728596	Stable	Stable
88	2.554455	Stable	Stable
89	2.760274	Stable	Stable
90	2.478035	Stable	Stable
91	2.219488	Stable	Stable
92	2.050673	Stable	Stable
93	3.159725	Stable	Stable
94	2.297719	Stable	Stable
95	2.758827	Stable	Stable
96	2.634294	Stable	Stable
97	2.924975	Stable	Stable
98	2.777661	Stable	Stable
99	3.141867	Stable	Stable
100	2.544037	Stable	Stable

Table B.2. Results for 100 Scenario Contingencies for Contingency 8 – Numerical Example I

Scenario Ctg. No.	Energy Margin	BCU Stability	Time Domain Stability
1	2.808973	Stable	Stable
2	2.79477	Stable	Stable
3	2.811086	Stable	Stable
4	2.808132	Stable	Stable
5	2.808308	Stable	Stable
6	2.807371	Stable	Stable
7	2.806562	Stable	Stable
8	2.807928	Stable	Stable
9	2.810093	Stable	Stable
10	2.804071	Stable	Stable
11	2.811358	Stable	Stable
12	2.810283	Stable	Stable
13	2.809525	Stable	Stable
14	2.811508	Stable	Stable
15	2.803169	Stable	Stable
16	2.80983	Stable	Stable
17	2.810293	Stable	Stable
18	2.80828	Stable	Stable
19	2.805004	Stable	Stable
20	2.806269	Stable	Stable
21	2.80528	Stable	Stable
22	2.807863	Stable	Stable
23	2.808431	Stable	Stable
24	2.809303	Stable	Stable
25	2.807825	Stable	Stable
26	2.808702	Stable	Stable
27	2.802463	Stable	Stable
28	2.80973	Stable	Stable
29	2.808139	Stable	Stable
30	2.802891	Stable	Stable
31	2.809769	Stable	Stable
32	2.809024	Stable	Stable
33	2.80568	Stable	Stable
34	2.811404	Stable	Stable
35	2.80909	Stable	Stable

Scenario Ctg. No.	Energy Margin	BCU Stability	Time Domain Stability
36	2.794832	Stable	Stable
37	2.808451	Stable	Stable
38	2.809182	Stable	Stable
39	2.808742	Stable	Stable
40	2.812482	Stable	Stable
41	2.809039	Stable	Stable
42	2.805729	Stable	Stable
43	2.811546	Stable	Stable
44	2.803511	Stable	Stable
45	2.80262	Stable	Stable
46	2.809212	Stable	Stable
47	2.807826	Stable	Stable
48	2.804112	Stable	Stable
49	2.808695	Stable	Stable
50	2.805823	Stable	Stable
51	2.805916	Stable	Stable
52	2.808927	Stable	Stable
53	2.808563	Stable	Stable
54	2.803034	Stable	Stable
55	2.809634	Stable	Stable
56	2.809963	Stable	Stable
57	2.809085	Stable	Stable
58	2.808524	Stable	Stable
59	2.807245	Stable	Stable
60	2.805652	Stable	Stable
61	2.811036	Stable	Stable
62	2.808123	Stable	Stable
63	2.809414	Stable	Stable
64	2.808338	Stable	Stable
65	2.805824	Stable	Stable
66	2.809421	Stable	Stable
67	2.808316	Stable	Stable
68	2.811384	Stable	Stable
69	2.808636	Stable	Stable
70	2.807643	Stable	Stable
71	2.809847	Stable	Stable
72	2.811686	Stable	Stable
73	2.808988	Stable	Stable

Scenario Ctg. No.	Energy Margin	BCU Stability	Time Domain Stability
74	2.808316	Stable	Stable
75	2.807025	Stable	Stable
76	2.808069	Stable	Stable
77	2.811466	Stable	Stable
78	2.804822	Stable	Stable
79	2.808106	Stable	Stable
80	2.811005	Stable	Stable
81	2.810053	Stable	Stable
82	2.807392	Stable	Stable
83	2.808977	Stable	Stable
84	2.808751	Stable	Stable
85	2.8076	Stable	Stable
86	2.806729	Stable	Stable
87	2.808944	Stable	Stable
88	2.809113	Stable	Stable
89	2.80636	Stable	Stable
90	2.81182	Stable	Stable
91	2.807715	Stable	Stable
92	2.809798	Stable	Stable
93	2.804784	Stable	Stable
94	2.809864	Stable	Stable
95	2.807725	Stable	Stable
96	2.808567	Stable	Stable
97	2.80471	Stable	Stable
98	2.808093	Stable	Stable
99	2.802548	Stable	Stable
100	2.808056	Stable	Stable

Table A.3. Results for 200 Scenario Contingencies for Contingency 8 – Numerical Example II

Scenario Ctg. No.	Energy Margin	BCU Stability	Time Domain Stability
1	-0.96178	Unstable	Unstable
2	2.804667	Stable	Stable
3	1.941812	Stable	Stable
4	2.991955	Stable	Stable
5	-2.52508	Unstable	Unstable
6	2.06846	Stable	Stable
7	2.195538	Stable	Stable
8	-0.4257	Unstable	Stable
9	1.043059	Stable	Stable
10	-2.32109	Unstable	Unstable
11	-2.11478	Unstable	Unstable
12	-1.27543	Unstable	Unstable
13	3.271099	Stable	Stable
14	-1.48619	Unstable	Unstable
15	-0.09048	Unstable	Stable
16	0.629385	Stable	Stable
17	0.177973	Stable	Stable
18	3.20315	Stable	Stable
19	2.629675	Stable	Stable
20	2.934156	Stable	Stable
21	3.212837	Stable	Stable
22	-0.03313	Unstable	Stable
23	0.696515	Stable	Stable
24	1.952895	Stable	Stable
25	-1.55002	Unstable	Unstable
26	2.0786	Stable	Stable
27	2.040564	Stable	Stable
28	0.746963	Stable	Stable
29	2.189414	Stable	Stable
30	1.85856	Stable	Stable
31	-2.50406	Unstable	Unstable
32	2.09221	Stable	Stable
33	-0.4638	Unstable	Stable
34	0.239629	Stable	Stable
35	0.009515	Stable	Stable
36	0.633094	Stable	Stable
37	0.654131	Stable	Stable

Scenario Ctg. No.	Energy Margin	BCU Stability	Time Domain Stability
38	2.063312	Stable	Stable
39	-1.62975	Unstable	Unstable
40	1.622866	Stable	Stable
41	2.125112	Stable	Stable
42	-0.57149	Unstable	Stable
43	-1.62463	Unstable	Unstable
44	-0.49939	Unstable	Stable
45	-1.78502	Unstable	Unstable
46	0.729001	Stable	Stable
47	1.749133	Stable	Stable
48	1.699947	Stable	Stable
49	1.622817	Stable	Stable
50	2.618581	Stable	Stable
51	-2.54308	Unstable	Unstable
52	1.589337	Stable	Stable
53	3.272556	Stable	Stable
54	-0.92667	Unstable	Unstable
55	2.98574	Stable	Stable
56	3.062638	Stable	Stable
57	3.360314	Stable	Stable
58	-0.90554	Unstable	Unstable
59	2.131981	Stable	Stable
60	-0.32974	Unstable	Stable
61	2.096131	Stable	Stable
62	-1.38036	Unstable	Unstable
63	0.782268	Stable	Stable
64	1.633573	Stable	Stable
65	1.516259	Stable	Stable
66	1.81807	Stable	Stable
67	-2.29268	Unstable	Unstable
68	-0.79134	Unstable	Unstable
69	3.128358	Stable	Stable
70	0.041706	Stable	Stable
71	-1.69877	Unstable	Unstable
72	1.49347	Stable	Stable
73	2.712978	Stable	Stable
74	3.454384	Stable	Stable
75	2.052472	Stable	Stable

Scenario Ctg. No.	Energy Margin	BCU Stability	Time Domain Stability
76	2.486177	Stable	Stable
77	1.904619	Stable	Stable
78	2.218978	Stable	Stable
79	-1.46817	Unstable	Unstable
80	1.877492	Stable	Stable
81	2.865935	Stable	Stable
82	-0.24334	Unstable	Stable
83	-1.87546	Unstable	Unstable
84	-1.49988	Unstable	Unstable
85	-1.68118	Unstable	Unstable
86	-1.26326	Unstable	Unstable
87	-1.59635	Unstable	Unstable
88	1.909588	Stable	Stable
89	0.372672	Stable	Stable
90	-2.01529	Unstable	Unstable
91	-1.72511	Unstable	Unstable
92	-1.5377	Unstable	Unstable
93	2.859658	Stable	Stable
94	2.040274	Stable	Stable
95	-0.61076	Unstable	Unstable
96	0.876099	Stable	Stable
97	3.440265	Stable	Stable
98	0.929659	Stable	Stable
99	0.370215	Stable	Stable
100	1.923569	Stable	Stable
101	0.262062	Stable	Stable
102	2.620944	Stable	Stable
103	1.963908	Stable	Stable
104	-1.50541	Unstable	Unstable
105	-0.56448	Unstable	Stable
106	-0.6262	Unstable	Unstable
107	0.878059	Stable	Stable
108	2.485394	Stable	Stable
109	-2.54353	Unstable	Unstable
110	0.531145	Stable	Stable
111	2.284088	Stable	Stable
112	-0.68038	Unstable	Unstable
113	1.641812	Stable	Stable

Scenario Ctg. No.	Energy Margin	BCU Stability	Time Domain Stability
114	0.125502	Stable	Stable
115	-0.56887	Unstable	Stable
116	-2.04209	Unstable	Unstable
117	-1.05601	Unstable	Unstable
118	1.492105	Stable	Stable
119	1.45307	Stable	Stable
120	2.519572	Stable	Stable
121	-0.52691	Unstable	Stable
122	-0.11802	Unstable	Stable
123	-1.49285	Unstable	Unstable
124	3.077654	Stable	Stable
125	0.542679	Stable	Stable
126	3.366564	Stable	Stable
127	1.744658	Stable	Stable
128	1.736024	Stable	Stable
129	2.185118	Stable	Stable
130	-0.03795	Unstable	Stable
131	-2.17722	Unstable	Unstable
132	3.034663	Stable	Stable
133	-1.21317	Unstable	Unstable
134	2.856429	Stable	Stable
135	2.796455	Stable	Stable
136	-0.43007	Unstable	Stable
137	1.366592	Stable	Stable
138	1.18661	Stable	Stable
139	0.011456	Stable	Stable
140	2.079423	Stable	Stable
141	-1.89837	Unstable	Unstable
142	-0.55797	Unstable	Stable
143	-0.23681	Unstable	Stable
144	0.128194	Stable	Stable
145	2.156379	Stable	Stable
146	1.974314	Stable	Stable
147	-0.68596	Unstable	Unstable
148	2.569841	Stable	Stable
149	0.227659	Stable	Stable
150	-0.54819	Unstable	Stable
151	2.756321	Stable	Stable

Scenario Ctg. No.	Energy Margin	BCU Stability	Time Domain Stability
152	-0.36315	Unstable	Stable
153	0.062764	Stable	Stable
154	1.678642	Stable	Stable
155	2.791616	Stable	Stable
156	2.687046	Stable	Stable
157	3.058122	Stable	Stable
158	0.821009	Stable	Stable
159	2.088632	Stable	Stable
160	1.797088	Stable	Stable
161	1.017576	Stable	Stable
162	-1.20723	Unstable	Unstable
163	-2.25046	Unstable	Unstable
164	-0.57042	Unstable	Stable
165	1.403057	Stable	Stable
166	-0.44864	Unstable	Stable
167	-0.87147	Unstable	Unstable
168	-2.28983	Unstable	Unstable
169	-1.6088	Unstable	Unstable
170	2.967411	Stable	Stable
171	-2.54664	Unstable	Unstable
172	3.482234	Stable	Stable
173	-0.39069	Unstable	Stable
174	-1.53462	Unstable	Unstable
175	1.805858	Stable	Stable
176	-1.41302	Unstable	Unstable
177	1.146696	Stable	Stable
178	2.655243	Stable	Stable
179	1.913539	Stable	Stable
180	2.129314	Stable	Stable
181	0.462681	Stable	Stable
182	2.785642	Stable	Stable
183	2.904251	Stable	Stable
184	-1.6081	Unstable	Unstable
185	-2.10731	Unstable	Unstable
186	-0.92363	Unstable	Unstable
187	-1.89156	Unstable	Unstable
188	-1.51731	Unstable	Unstable
189	-1.10865	Unstable	Unstable

Scenario Ctg. No.	Energy Margin	BCU Stability	Time Domain Stability
190	1.19118	Stable	Stable
191	-2.50141	Unstable	Unstable
192	1.73012	Stable	Stable
193	2.337637	Stable	Stable
194	3.030446	Stable	Stable
195	1.035082	Stable	Stable
196	2.788391	Stable	Stable
197	-2.51729	Unstable	Unstable
198	1.358571	Stable	Stable
199	1.008478	Stable	Stable
200	-1.08529	Unstable	Unstable

Bibliography

[1] H.-D. Chiang, *Direct Methods for Stability Analysis of Electric Power Systems: Theoretical Foundation, BCU Methodologies, and Applications*. Hoboken, NJ, USA: John Wiley & Sons, Mar. 2011.

[2] P. Varaiya, F. F. Wu, and R. L. Chen, "Direct methods for transient stability analysis of power systems: Recent results," in *Proceedings of the IEEE*, vol. 73, no. 12, pp. 1703–1715, 1985.

[3] T. Van Cutsem and C. Vournas, *Voltage Stability of Electric Power Systems*, vol. 441, Springer, 1998.

[4] P. Kundur, *Power System Stability and Control*, New York, 1994.

[5] C. L. DeMarco and T. J. Overbye, "An energy based security measure for assessing vulnerability to voltage collapse," *Power Systems, IEEE Transactions on,* vol. 5, no. 2, pp. 419–427, 1990.

[6] T. J. Overbye and C. L. DeMarco, "Voltage security enhancement using energy based sensitivities," *Power Systems, IEEE Transactions on*, vol. 6, no. 3, pp. 1196–1202, 1991.

[7] T. J. Overbye, "Use of energy methods for on-line assessment of power system voltage security," *Power Systems, IEEE Transactions on,* vol. 8, no. 2, pp. 452–458, 1993.

[8] H.-D. Chiang, J. Tong, and Y. Tada, "On-line transient stability screening of 14,000-bus models using TEPCO-BCU: Evaluations and methods," IEEE Power and Energy Society General Meeting, 2010.

[9] W. Ma and J. Thorp, "An efficient algorithm to locate all the load flow solutions," *Power Systems, IEEE Transactions on*, vol. 8, no. 3, pp. 1077–1083, Aug. 1993.

[10] H. D. Nguyen and K. S. Turitsyn, "Appearance of multiple stable load flow solutions under power flow reversal conditions," in *IEEE Power and Energy Society General Meeting*, 2014.

[11] F. M. A. Salam, L. Ni, S. Guo, and X. Sun, "Parallel processing for the load flow of power systems: the approach and applications," in *Decision and Control, Proceedings of the 28th IEEE Conference on*, vol. 3, pp. 2173–2178, Dec. 1989.

[12] C.-W. Liu, C.-S. Chang, J.-A. Jiang, and G.-H. Yeh, "Toward a cp-flow-based algorithm to compute all the type-1 load-flow solutions in electric power systems," *Circuits and Systems I: Regular Papers, IEEE Transactions on*, vol. 52, no. 3, pp. 625–630, 2005.

[13] D. Mehta, H. D. Nguyen, and K. Turitsyn, "Numerical Polynomial Homotopy Continuation method to locate all the power flow solutions," *IET Generation, Transmission & Distribution*, vol. 10, no. 12, pp. 2972-2980, Aug. 2016.

[14] R. T. Treinen, V. Vittal, and W. Kliemann, "An Improved Technique to Determine the Controlling Unstable Equilibrium Point in a Power System," *Circuits and Systems I: Fundamental Theory and Applications, IEEE Transactions on*, vol. 43, no. 3, pp. 625–630, 2005.

[15] A.A. Fouad, V. Vittal, and T. Oh, "Critical energy for Direct Transient Stability Assessment of a Multimachine Power System," *Power Systems, IEEE Transactions on*, vol. PAS-103, pp. 2199-2206, Aug. 1984.

[16] K. Uemura, J. Matsuki, I. Yamada, and T. Tsuji, "Approximation of an Energy Function in Transient Stability Analysis of Power Systems," *Electrical Engineering in Japan*, vol. 92, no. 6, pp. 96-100, 1972.

[17] A.A. Fouad, and V. Vittal, *Power System Transient Stability Analysis Using the Transient Energy Function Method*, Prentice-Hall, Upper Saddle River, NJ, 1992.

[18] L. Chen, Y. Min, F. Xu, and K.-P. Wang, "A continuation-Based Method to compute the Relevant Unstable Equilibrium Points for Power System Transient Stability Analysis," *Power Systems, IEEE Transactions on,* vol. 24, no. 1, pp. 165–172, 2009.

[19] W. Kaipeng, Z. Yiwei, C. Lei, and M. Yong, "Computation of Unstable Equilibrium Points on the Transient Stability Boundary of Power Systems with Detailed Generator Model," *Proceedings of the 44th International UPEC Conference*, 2009.

[20] J. Mitra, M. Benidris, and N. Cai, "Use of Homotopy-based Approaches in Finding Controlling Unstable Equilibrium Points in Transient Stability Analysis," Power System Computation Conference, 2016.

[21] C.-W. Liu, and, J. S. Thorp, "A Novel Method to Compute the Closest Unstable Equilibrium Point for Transient Stability Region Estimate in Power Systems," *Circuits and Systems, IEEE Transactions on*, vol. 44, no. 7, pp. 630-635, Jul. 1997.

[22] J. Lee, "A Novel Homotopy-Based Algorithm for the Closest Unstable Equilibrium Point Method in Nonlinear Stability Analysis," *Circuits and Systems, ISCAS'03, Proceedings of the 2003 International Symposium on*, vol. 3, pp. 8-11, 2003.

[23] J. Lee, and H.-D. Chiang, "A Singular Fixed-Point Homotopy Method to Locate the Closest Unstable Equilibrium Point for Transient Stability Region Estimate," *Circuits and Systems II: Express Briefs*, vol. 51, no. 4, pp. 185-189, 2004.

[24] J. Lee, "Dynamic Gradient Approaches to Compute the Closest Unstable Equilibrium Point for Stability Region Estimate and their Computational Limitations," *Automatic Control, IEEE Transactions on*, vol. 48, no. 2, pp. 321-324, 2003.

[25] I. Luna-Lopez, J. M. Canedo, and A. Loukianov, "Dynamical Method for CUEP Detection in Power System Transient Stability Assessment," *Proceedings of the IEEE Power Engineering Society Winter Meeting Conference*, vol. 1, 2002.

[26] D. K. Molzahn, B. C. Lesieutre, and H. Chen, "Counterexample to a continuation-based algorithm for finding all power flow solutions," *Power Systems, IEEE Transactions on*, vol. 28, no. 1, pp. 564–565, 2013.

[27] B. Berggren, and G. Anderson, "On the Nature of Unstable Equilibrium Points in Power Systems," *Power Systems, IEEE Transactions on*, vol. 8, no. 2, pp. 738-745, May 1993.

[28] J. Lee, "An Optimization-Driven Framework for the Computation of the Controlling UEP in Transient Stability Analysis," *Automatic Control, IEEE Transactions on*, vol. 49, no. 1, pp. 115-119, Jan. 2004.

[29] J. Lee, and H.-D. Chiang, "A Dynamical Trajectory-Based Methodology for Systematically Computing Multiple Optimal Solutions of General Nonlinear Programming Problems," *Automatic Control, IEEE Transactions on*, vol. 49, no. 6, pp. 888-899, Jun. 2004.

[30] J. S. Thorp, and S. A. Naqavi, "Load flow fractals," *Decision and Control, Proc. of the 28th IEEE Conference on*, Dec. 1989.

[31] F. Milanno, "Continuous Newton's Method for Power Flow Analysis," *Power Systems, IEEE Transactions on*, vol. 24, no. 1, pp. 50–56, Feb. 2009.

[32] J.-J. Deng, H.-D. Chiang, and T.-Q Zhao, "Newton method and Trajectory Based-Method for Solving Power Flow Problems," *Int. J. Bifurcation and Chaos*, vol. 25, no. 6, 2015.

[33] X. Wang, H.-D. Chiang, "Application of pseudo-transient continuation method in dynamic stability analysis," IEEE PES General Meeting, Conference and Exposition, Oct. 2014.

[34] C. T. Kelley, and D. E. Keyes, "Convergence Analysis of Pseudo-Transient Continuation," *SIAM Journal on Numerical Analysis*, vol. 35, no. 2, pp. 508-523, Apr. 1998.

[35] T. S. Coffey, C. T. Kelley, and D. E. Keyes, "Pseudo-Transient Continuation and Differential-Algebraic Equations," *SIAM Journal of Scientific Computing*, vol. 25, no. 2, pp. 553-569, 2003.

[36] G. H. Golub, and C. F. Van Loan, *Matrix Computations* (3rd ed.). Baltimore: The Johns Hopkins University Press, 1996.

[37] C.C. Chu, H.-D. Chiang, "Constructing Analytical Energy Functions for Lossless Network-Reduction Power System Models: Framework and New Developments," *Circuits Systems and Signal Processing*, vol. 18, no. 1, 1999.

[38] C.C. Chu, H.-D. Chiang, "Constructing Analytical Energy Functions for Lossless Network-Preserving Power System Models," *Circuits Systems and Signal Processing*, vol. 24, no. 4, 2005.

[39] W. Suampun, "Novel BCU-Based Methods for Enhancing Power System Transient Stability," Ph.D. dissertation, ECE. Dept., Cornell. Univ., Ithaca, NY, 2013.

[40] K. R. Padiyar, and K. K. Ghosh, "Direct Stability Evaluation of Power Systems with Detailed Generator Models Using Structure-Preserving Energy Functions," *Int. J. Power & Energy Systems,* vol. 11, no. 1, pp. 47-56, 1989.

[41] P. C. Magnusson, "The Transient-Energy Method of Calculating Stability," *AIEE Trans*., vol. 66, no. 1, pp. 747–755, Jan. 1947.

[42] P. D. Aylett, "The energy-integral criterion of transient stability limits of power systems," *Proc. IEE*, vol. 105, no. 8, pp. 527-536, 1958.

[43] Y.-H. Moon, B.-H. Cho, Y.-H. Lee, H.-S. Hong, "Energy Conservation Law and Its Application for the Direct Energy Method of Power System Stability," IEEE PES Winter Meeting, 1999.

[44] N. A. Tsolas, A. Arapostathis, P. P. Varaiya, "A Structure Preserving Energy Function for Power System Transient Stability Analysis," *Circuits and Systems, IEEE Transactions on*, vol. 8, no. 2, pp. 738-745, May 1993.

[45] M. A. Pai*, Energy Function Analysis for Power System Stability*. Boston, MA: Kluwer Academic Publishers, 1989.

[46] H.-D. Chiang, "Study of the existence of energy functions for power systems with losses," *IEEE Transactions on Circuits and Systems*, vol. 36, no. 11, pp. 1423-1429, Nov. 1989.

[47] N. Kakimoto, N. Y. Ohsawa, and M. Hayashi, "Transient Stability Analysis of Electric Power System via Lure-Type Lyapunov Function," *Trans. IEE Japan*, 1978.

[48] N. Kakimoto, N. Y. Ohsawa, and M. Hayashi, "Transient Stability Analysis of Large-Scale Power Systems by Lyapunov's Direct Method," Power Appar. Syst., IEEE, PAS-103, pp. 160-167, 1984.

[49] A. G. Bakirtzis and A. P. Meliopoulos, "Incorporation of Switching Operations in Power System Corrective Control Computations," *IEEE Trans. on Power Systems*, vol. PWRS-2, no. 3, pp. 669-676, Aug. 1987.

[50] V. H. Quintana, and N. Miiller, "Overload and voltage control of power systems by line switching and generation rescheduling," *Canadian Journal Elect. & Comp. Eng*., vol. 15, no. 4, pp. 167-173, 1990.

[51] E. B. Fisher, R. P. O'Neill, and M. C. Ferris, "Optimal transmission switching," *IEEE Trans. Power Syst*., vol. 23, no. 3, pp. 1346-1355, Aug. 2008.

[52] R. P. O'Neill, R. Baldick, U. Helman, M. H. Rothkopf, and W. Stewart, "Dispatchable transmission in RTO markets," *IEEE Trans. Power Syst*., vol. 20, no. 1, pp. 171–179, Feb. 2005.

[53] K. W. Hedman, R. P. O'Neill, E. B. Fisher, and S. S. Oren, "Optimal Transmission Switching with Contingency Analysis," *IEEE Trans. Power Syst*., vol. 24, no. 3, pp. 1577–1586, 2009.

[54] A. Khodaei, and M. Shahidehpour, "Transmission Switching in Security-Constrained Unit Commitment," *IEEE Trans. Power Syst*., vol. 25, no. 4, pp. 1937–1945, Nov. 2010.

[55] S. Bruno, M. D'Aloia, G. D. Carne, and M. L. Scala, "Controlling Transient Stability through Line Switching," 28th Session, IEEE PES Innovative Smart Grid Technologies Europe, 2012, Berlin.

[56] R. A. M. Van, Amerongen, and H. P. Van Meeteren, "Security Control by Real Power Rescheduling-Network Switching and Load Shedding," 28th Session, CIGRE Report 32-02, France, 1980.

[57] H.–J. Koglin, and H. Muller, "Overload Reduction Through Corrective Switching Actions," IEE International Conference on Power System Monitoring and Control, London, 1980, pp. 159-164.

[58] J. G. Rolim, and L. J. B. Machado, "A study of the use of corrective switching in transmission systems," *IEEE Trans. Power Syst*., vol. 14, no. 1, pp. 336–341, Feb. 1999.

[59] W. Shao, and V. Vittal, "Corrective switching algorithm for relieving overloads and voltage violations," *IEEE Trans. Power Syst*., vol. 20, no. 4, pp. 1877-1885, Nov. 2005.

[60] L. Wang, and H.-D. Chiang, "Towards online line switching for increasing load margins to static stability limit," *Power Systems, IEEE Transactions on,* vol. 31, no. 3, pp. 1744-1751, May 2016.

[61] L. Chen, Y. Tada, H. Okamoto, R. Tanabe, and H. Mitsuma, "Optimal Reconfiguration of Transmission Systems with Transient Stability Constraints," POWERCON, 1998.

[62] K. N. Shubhanga, and Anil M. Kulkarni, "Application of Structure Preserving Energy Margin Sensitivity to Determine the Effectiveness of Shunt and Series FACTS Devices," *Power Systems, IEEE Transactions on*, vol. 17, no. 3, pp. 730-738, Aug. 2002.

[63] S. Bruno, M. D'Aloia, G. D. Carne and M. L. Scala, "Controlling Transient Stability through Line Switching," 2012 3rd IEEE PES Innovative Smart Grid Technologies Europe (ISGT Europe), Berlin.

[64] T. L. Vu, H.-D. Chiang, and K. Turitsyn, "Smart Transmission Network Emergency Control," 2015.

[65] D. Sutanto, and W. R. Lachs, "Improving transient stability by containing accelerating energy," Advances in Power System Control, Operation and Management, 2000. APSCOM-00. 2000 International Conference on.

[67] S. Chen, and H. Glavitsch, "Stabilizing Switching," Power Systems, IEEE Transactions on, vol. 8, no. 4, pp. 1511-1517, Nov. 1993.

[68] C. Li, H.-D. Chiang, and Z. Du, "Online Line Switching Method for Enhancing the Small-Signal Stability Margin of Power Systems," *Smart Grid, IEEE Transactions on*, Early Issue, vol. PP, no. 99, 2017.

[69] V. Chadalavada, and V. Vittal, "Transient Stability Assessment for Network Topology Changes: Application of Energy Margin Analytical Sensitivity," *IEEE Trans., Power Syst.,* vol. 9, no. 3, pp. 1658-1664, Aug. 1994.

[70] J. Tong, H.-D. Chiang, and T. P. Conneen, "A sensitivity-based BCU method for fast derivation of stability limits in electric power systems," *IEEE Transactions on Power Systems*, vol. 8, no. 4, pp. 1418–1428, 1993.

[71] J. Qiang Wu, A. Bose, J. A. Huang, A. Valette and F. Lafrance, "Parallel implementation of power system transient stability analysis," IEEE Trans. Power Systems, vol. 10, pp. 1226-1233, Aug. 1995.

[72] G. Aloisio, M. A. Bochicchio, M. La Scala and R. Sbrizzai, "A distributed computing approach for real-time transient stability analysis," *IEEE Trans. Power Systems*, vol. 12, pp. 981-987, May 1997.

[73] Y. Li, X. Zhou, Z. Wu, and Jian Guo, "Parallel algorithms for transient stability simulation on PC cluster," in P*roc. 2002 Int. Conf. on Power System Technology (POWERCON '2002)*, 13-17 Oct. 2002, vol. 3, pp. 1592-1596.

[74] N. Duan, and K. Sun, "Application of the Adomian Decomposition Method for SemiAnalytic Solutions of Power System Differential Algebraic Equations", 2015 IEEE Powertech, Eindhoven.

[75] N. Duan, and K. Sun, "Power System Simulation Using the Multistage Adomian Decomposition Method" *IEEE Trans. Power Systems*, vol. 32, pp. 430-441, Apr. 2016.

[76] C. Liu, B. Wang, and K. Sun "Fast Power System Simulation Using Semi-Analytical Solutions Based on Pade Approximants", *Proc., 2017 IEEE PES General Meeting*.

[77] E. Abreut, B. Wang, and K. Sun, "Semi-Analytical Fault-on Trajectory Simulation and Its Application in Direct Methods", *Proc., 2017 IEEE PES General Meeting*.

[78] V. Vittal, P. Sauer, S. Meliopoulos, and G. K. Stefopoulos, "On-Line Transient Stability Assessment Scoping Study," PSERC Publication 05-04, Feb. 2005.

[79] B. Borkowska, "Probabilistic load flow," *IEEE Trans. Power Apparatus and Syst*., vol. 93, no. 3, pp. 752–759, 1974.

[80] M. Fan, V. Vittal*,* G. T. Heydt, and R. Ayyanar, *"*Probabilistic Power Flow Analysis With Generation Dispatch Including Photovoltaic Resources," *IEEE Transactions on Power Systems,* vol. 28, no. 2, 1797–1805, May 2013.

[81] R. Billinton and P. R. S. Kuruganty, "A probabilistic index for transient stability," *IEEE Trans. Power App. Syst.*, vol. PAS-99, no. 1, pp. 195–206, Jan. 1980.

[82] P. M. Anderson and A. Bose, "A Probabilistic Approach to Power System Stability Analysis," *IEEE Transactions on Power Apparatus and Systems*, vol. PAS-102, no. 8, pp. 2430–2439, Aug. 1983.

[83] D. Z. Fang, L. Jing, and T. S. Chung, "Corrected transient energy function-based strategy for stability probability assessment of power systems," *IET Generation, Transmission & Distribution,* vol. 2, no. 3, pp. 424–432, May 2008.

[84] K. Hua, A. Vahidnia, Y. Mishra, and G. Ledwich, "Efficient probabilistic contingency analysis through a stability measure considering wind perturbation," *IET Generation, Transmission & Distribution,* vol. 10, no. 4, pp. 897–905, 2016.

[85] L. Shi, S. Sun, Li. Yao, Y. Ni, and M Bazargan, "Effects of wind generation intermittency and volatility on power system transient stability," *IET Renewable Power Generation*, vol. 8, no. 5, pp. 509–521, Jul. 2014.

[86] E. Vaahedi, W. Li, T. Chia, and H. Dommel, "Large Scale Probabilistic Transient Stability Assessment Using B.C. Hydro's On-Line Tool," *IEEE Transactions on Power Systems,* vol. 15, no. 2, pp. 661–667, May 2000.

[87] H. Ahmadi, and H. Ghasemi, "Maximum penetration level of wind generation considering power system security limits," *IET Generation, Transmission & Distribution*, vol. 6, no. 11, pp. 1164–1170, Nov. 2012.

[88] M. Abapour, and M. -R. Haghifam, "On-line assessment of the transient instability risk," *IET Generation, Transmission & Distribution*, vol. 7, no. 6, pp. 602–612, Jun. 2013.

[89] Y. -Y. Hsu, and C. -L. Chang, "Probabilistic Transient Stability Studies Using the Conditional Probability Approach," *IEEE Transactions on Power Systems*, vol. 3, no. 4, pp. 1565 – 1572, Nov. 1988.

[90] S.O. Faried, R. Billinton, and S. Aboreshaid, "Probabilistic evaluation of transient stability of a power system incorporating wind farms," *IET Renewable Power Generation*, vol. 4, no. 4, pp. 299–307, 2010.

[91] P. N. Papadopoulos, and J. V. Milanović, "Probabilistic Framework for Transient Stability Assessment of Power Systems With High Penetration of Renewable Generation," *IEEE Transactions on Power Systems*, vol. 32, no. 4, Jul. 2017.

[92] J. Dopazo, O. Klitin, and A. Sasson, "Stochastic load flows," *IEEE Transactions on Power Apparatus and Systems*, vol. 94, no. 2, pp. 299– 309, Mar. 1975.

[93] X. Wang, H. Chiang, J. Wang, H. Liu, and T. Wang, "Long-term stability analysis of power systems with wind power based on stochastic differential equations: Model development and foundations," *IEEE Trans. Sustain. Energy*, vol. 6, no. 4, pp. 1534–1542, Oct. 2015.

[94] R. Allan, A. Leite da Silva, and R. Burchett, "Evaluation methods and accuracy in probabilistic load flow solutions," Power Apparatus and Systems, *IEEE Transactions on, vol. PAS-100*, no. 5, pp. 2539–2546, May 1981.

[95] C.-L. Su, "Probabilistic load-flow computation using point estimate method," *Power Systems, IEEE Transactions on*, vol. 20, no. 4, pp. 1843–1851, Nov. 2005.

[96] M. D. Mckay, R. J. Beckman, and W. J. Conover, "A comparison of three methods for selecting values of input variables in the analysis of output from a computer code," *Technometrics*, vol. 21, no. 2, pp. 239–245, May 1979.

[97] H. Yu, C. Y. Chung, K. P. Wong, H. W. Lee, and J. H. Zhang, "Probabilistic Load Flow Evaluation With Hybrid Latin Hypercube Sampling and Cholesky Decomposition," *IEEE Trans. Power Systems,* vol. 24, no. 2, pp. 661-667, May 2009.

[98] E. Du, N. Zhang, C. Kang, J. Bai, L. Cheng, Y. Ding, "Impact of Wind Power Scenario Reduction Techniques on Stochastic Unit Commitment," *International Symposium on Stochastic Models in Reliability Engineering, Life Science and Operations Management*, 2016.

[99] J. Sumaili, H. Keko, V. Miranda, Z. Zhou, A. Botterud, and J. Wang, "Finding representative wind power scenarios and their probabilities for stochastic models," in *Proc. 16th Intelligent System Application to Power Systems (ISAP). Conf*., pp.1, 6, 25-28, Hersonissos. Greece, 2011.

[100] H. Keko, and V. Miranda, "Impact of Clustering-based Scenario Reduction on the Perception of Risk in Unit Commitment Problem," *Intelligent System Application to Power Systems (ISAP). Conf.*, 2015.

[101] B. J. Frey, and D. Dueck, "Clustering by Passing Messages Between Data Points," *Science*, vol. 315, no. 5814, pp. 972-976, Feb. 2007.

[102] EIA, "Energy Explained: U.S. Energy Facts: Consumption and Production" *https://www.eia.gov/energyexplained/?page=us_energy_home*, 2018.

[103] U.S. Energy Information Administration, "International Energy Outlook 2017", 2017.

[104] H. Ritchie, and M. Roser, "Energy Production and Changing Energy Sources," *https://ourworldindata.org/energy-production-and-changing-energy-sources*, 2018.

[105] Shell, "World Energy Model: A View to 2100",*https://www.shell.com/energy-and-innovation/the-energy-future/scenarios/shell-scenarios-energy-models/world-energy-model/_jcr_content/par/textimage.stream/1510344160326/d62f12b8fe88e85dc3349c38b1ca5e44cc22c5ccc6f70beed634020cfb527c82/shell-world-energy-model.pdf*, 2017.

[106] L. Wang, and H.-D. Chiang, "Toward Online Bus-Bar Splitting for Increasing Load Margins to Static Stability Limit," *Power Systems, IEEE Transactions on*, vol. 32, no. 5, pp. 3715-3725, Sep. 2017.

[107] H.-D. Chiang, and L. F. C. Alberto, *Stability Regions of Nonlinear Dynamical Systems: Theory, Estimation, and Applications*, Cambridge, UK: Cambridge University Press, Mar. 2015.

[108] P. W. Sauer, and M. A. Pai, *Power System Dynamics and Stability,* Champaign, IL, USA: Stipes Publishing L.L.C., 2006.

[109] R. L. Iman and W. J. Conover, "A Distribution-free Approach to Inducing Rank Correlation among Input Variables," *Commun. Statist.—Sim. Comput*., pp. 311–334, Jan. 1982.

[110] J. C. Helton and F. J. Davis, "Latin hypercube sampling and the propagation of uncertainty in analyses of complex systems," *Reliab. Eng. Syst. Safety*, vol. 81, pp. 23–69, 2003.

[111] T. Wang, H.-D. Chiang, and R. Tanabe, "Toward a Flexible Scenario Generation Tool for Stochastic Renewable Energy Analysis," *Proc., 2016 IEEE Power Syst. Comp. Conference.*

[112] A.M. Leite da Silva, V. L. Arienti, and R. N. Allan, "Probabilistic load Row considering dependence between input nodal powers," IEEE Trans., 1984, PAS-103, pp. 1524-1530.

[113] R. N. Allan, and A. M. Leite da Silva, "Probabilistic load flow using multilinearisations," IEE Proc., Part C: Generation, Transmission and Distribution, vol. 128, no. 5, pp 280-287, Sep. 1981.

[114] I. Dobson, and H.-D. Chiang, "Towards a theory of voltage collapse in electric power systems," Systems & Control Letters, vol. 13, no. 3, pp. 253-262, Sep. 1989.

[115] R. Owusu-Mireku, and H.-D. Chiang, "On the Dynamics and Transient Stability of Power Systems Post-Transmission Switching" *Proc., 2017 IEEE PES General Meeting*.

[116] R. Owusu-Mireku, and H.-D. Chiang, "A Direct Method for the Transient Stability Analysis of Transmission Switching Events" *Proc., 2018 IEEE PES General Meeting*.

[117] H.-D. Chiang, F. F. Wu, and P. P. Varaiya "A BCU Method for Direct Analysis of Power System Transient Stability" *Power Systems, IEEE Transactions on*, vol. 9, no. 3, pp. 1194-1208, Aug. 1994.

[118] H.-D. Chiang, M. W. Hirsch, and F. F. Wu "Stability region of nonlinear autonomous dynamical systems" *Automat. Contr., IEEE Transactions on*, vol. 33, no. 1, pp. 16-27, Jan. 1988.

[119] Siemens Power Technologies International, "PSSE 33.10: Model Library", Schenectady, NY, 2017.